Atomes froids piégés en interaction résonnante: gaz unitaire et problème à trois corps

Felix Werner

Département de Physique
École Normale Supérieure

Laboratoire Kastler Brossel

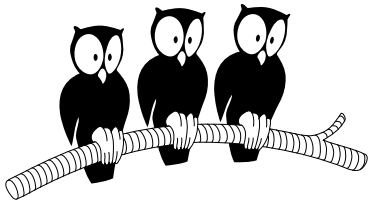

THÈSE de DOCTORAT de l'Université Paris VI

spécialité : Physique Quantique

présentée par

Félix WERNER

pour obtenir le titre de Docteur de l'Université Paris VI

ATOMES FROIDS PIÉGÉS EN INTERACTION RÉSONNANTE : GAZ UNITAIRE ET PROBLÈME À TROIS CORPS

$\sim$

TRAPPED COLD ATOMS WITH RESONANT INTERACTIONS : UNITARY GAS AND THREE-BODY PROBLEM

Soutenue le 10 juillet 2008 devant le jury composé de :

M. Alain COMTET	Président
M. Hans-Werner HAMMER	Rapporteur
M. Olivier JUILLET	Examinateur
M. Georgy SHLYAPNIKOV	Rapporteur
M. Yvan CASTIN	Directeur de thèse

Table des matières

Remerciements

Je remercie Yvan Castin d'avoir dirigé ma thèse avec autant de dynamisme, de disponibilité, de rigueur, d'enthousiasme, de persévérance, d'astuce ... J'ai beaucoup appris pendant nos nombreuses discussions. Bon nombre des idées et des résultats de cette thèse sont dus à Yvan.

Merci aux membres de la communauté pour toutes les discussions que nous avons pu avoir, qui ont parfois même orienté mes recherches. En particulier, Dmitry Petrov et Georgy Shlyapnikov m'ont introduit au sujet des pertes à 3 corps. J'ai également bénéficié de nombreuses discussions avec Ludovic Pricoupenko au début de ma thèse. Ludovic avait notamment pressenti l'existence des états universels bosoniques. Enfin, Thorsten Köhler m'a fait réfléchir à l'échelle du nanomètre. Merci également à Bernard Bernu, Eric Braaten, Frank Deuretzbacher, Antoine Georges, Kim Plassmeier, Mattia Jona-Lasinio, Paul Julienne, Pietro Massignan, Christophe Mora, Alejandro Muramatsu, Hans-Christoph Nägerl, Maxim Olshanii, Christian et Silke Ospelkaus, Achim Rosch et Christophe Salomon pour nos discussions qui ont contribué à cette thèse ; ainsi qu'aux auteurs de [1, 2, 3, 4] pour m'avoir fait parvenir leurs données.

Je remercie les membres du jury, Alain Comtet, Hans-Werner Hammer, Olivier Juillet et Georgy Shlyapnikov, de leur intérêt pour mon travail.

Merci à ceux qui m'ont donné de bonnes conditions de travail, en particulier à tous ceux qui m'ont permis de travailler dans le calme et la bonne humeur, dans notre bureau ou à la bibliothèque ; à Francis Hulin-Hubbard, Xavier Monin, Frédéric Ayrault et ... Yvan Castin, qui ont consacré une partie de leur emploi du temps chargé au bon fonctionnement de nos ordinateurs ; à tous ceux qui m'ont nourri ; à tous ceux qui administrent notre laboratoire ; à mes fournisseurs de papier et stylos ...

Plus généralement je remercie tous ceux dont l'aide et la gentillesse éclairent mes journées, et qui sont, malheureusement et heureusement, tellement nombreux que je me permets de ne pas les nommer : ma famille de Clamart, d'Ivry, de Saint-Placide et de Fribourg ; mes amis ; ceux que j'ai côtoyés à l'École Normale, au Département de Physique, au Laboratoire Kastler Brossel, à la bibliothèque, au sein du groupe atomes froids et de l'Institut Francilien des Atomes Froids ; ceux avec lesquels et auxquels j'ai eu la chance d'enseigner à l'Université Paris 6, aux Houches et dans le cadre de l'association Animath ; tous ceux avec qui j'ai eu la joie de partager mon bureau, mes déjeuners et mes discussions de couloir ; ceux qui m'ont appris à aimer la physique, les mathématiques, la musique, le hongrois ; et tous les autres.

Introduction

En 2002, grâce à l'outil des résonances de Feshbach [5, 6], les expériences sur des gaz d'atomes froids fermioniques à 2 états internes atteignent le régime d'interaction forte [7, 8, 9]. Depuis lors, les propriétés de ces gaz font l'objet de nombreux travaux expérimentaux et théoriques [10, 11, 12]. Il s'agit d'un difficile problème de fermions fortement corrélés. Cependant, il existe un petit paramètre : la portée des interaction entre atomes. Dans la limite de portée nulle, on s'attend à ce que le problème devienne universel. L'effet des interactions peut alors être décrit par un seul paramètre, la longueur de diffusion a. Le fait que les expérience soient menées avec des atomes, de ^{6}Li par exemple, avec des potentiels d'interaction complexes, peut alors être oublié. Le problème est simplement celui de N particules interagissant par un *pseudopotentiel* de portée nulle. [1] Au voisinage d'une résonance de Feshbach, $|a| \to \infty$. Dans cette limite unitaire, les interactions ne dépendent plus d'aucun paramètre ; de plus le gaz est en interaction forte.

Le pseudopotentiel est introduit dès les années 1930 par Wigner [13] puis Bethe et Peierls [14] pour étudier le problème à 2 corps proton-neutron, et est ensuite très utilisé en physique nucléaire (même s'il est une moins bonne approximation de la réalité dans ce contexte que dans le contexte des atomes froids [15]). En 1970, Efimov obtient analytiquement des solutions du problème de 3 particules interagissant *via* le pseudopotentiel, pour une longueur de diffusion $a = \infty$ [16]. Il s'agit d'une infinité d'états liés à 3 corps, dont le spectre a un point d'accumulation en zéro. Les énergies de ces états d'Efimov ne dépendent pas seulement de la longueur de diffusion. [2] En ce sens, les trimères d'Efimov peuvent être qualifiés d'états non universels. Par contre, pour des fermions à deux états internes, il n'existe pas de trimères d'Efimov et le problème à 3 corps est universel.

L'état d'équilibre d'un corps à très basse température est liquide ou solide. C'est pourquoi dans une expérience d'atomes froids, le gaz est au mieux dans un état de *quasi*-équilibre ayant durée de vie finie. Dans les premières études de résonances de Feshbach avec des atomes *bosoniques*, on observe une durée de vie dramatiquement courte [17, 18, 19, 20]. Mais avec des atomes *fermioniques*, la durée de vie du gaz à proximité de la résonance de Feshbach se révèle suffisamment longue [21, 22, 23, 24]. Cette longue durée de vie permet l'étude expérimentale des gaz de Fermi en interaction forte, en particulier de la transition BEC-BCS. Par contre, pour les gaz de Bose, la durée de vie dans le régime d'interaction forte est inférieure au temps de thermalisation [25], et l'un des sujets de recherche principaux est l'étude de la durée de vie elle-même, qui est particulièrement courte lorsqu'il existe un état lié à trois corps d'énergie nulle [2, 15, 26]. Abstraction faite du problème de la durée de vie, l'existence même d'un gaz de Bose en interaction forte est un problème théorique ouvert [27].

Dans cette thèse, nous résolvons analytiquement le problème à 3 corps unitaire dans un piège harmonique isotrope (Article III). Cette solution existe pour deux raisons. Premièrement, le problème à

1. Dans le régime non-perturbatif à 3 dimensions, ce pseudopotentiel n'est *pas* simplement proportionnel à la distribution δ de Dirac. Le pseudopotentiel porte plusieurs noms dans la littérature : "Fermi pseudopotential", "zero-range potential", "Bethe-Peierls zero-range theory", "point interaction" ...

2. Cela apparaît clairement pour $a = \infty$, car il est impossible de former une énergie à partir de la masse m et de $\hbar$.

3 corps est analytiquement soluble dans l'espace libre, comme l'a découvert Efimov. Deuxièmement, le cas du piège harmonique isotrope peut être ramené au cas de l'espace libre. Ce dernier résultat reste vrai à N corps, ce qui nous permet d'obtenir des résultats exacts pour N particules piégées à la limite unitaire (Article I). Par exemple, nous verrons que l'état fondamental pour N particules de masse m dans un piège de fréquence ω vérifie

$$\Psi(\lambda\vec{r}_1,\ldots,\lambda\vec{r}_N) = \lambda^{\left(\frac{E}{\hbar\omega}-\frac{3N}{2}\right)} e^{(1-\lambda^2)\sum_{i=1}^{N} {r_i}^2 \frac{m\omega}{2\hbar}} \Psi(\vec{r}_1,\ldots,\vec{r}_N). \quad (1)$$

Des résultats analogues existent pour tout état propre. Ces résultats sont en bon accord avec des calculs numériques [28] ce qui constitue une vérification de deux éléments fondamentaux du domaine : premièrement la précision des calculs numériques ; deuxièmement l'hypothèse mathématique que nous utilisons pour obtenir nos résultats analytiques, à savoir que la limite de portée nulle est universelle et décrite par le pseudopotentiel. Physiquement, nos résultats reposent sur l'existence d'un degré de liberté bosonique découplé, associé au mode de respiration du gaz.

Le problème à 3 corps dans un piège est accessible expérimentalement. En effet, on sait piéger un petit nombre d'atomes dans les micropuits situés aux nœuds d'un réseau optique profond, ce qui a déjà permis d'étudier expérimentalement le problème à 2 corps dans un piège ([29, 30], Article V). Les principales quantités mesurables sont le spectre et la durée de vie. En reprenant l'approche de Petrov, Salomon et Shlyapnikov, nous prédisons une durée de vie longue, non seulement pour 3 fermions, mais aussi pour *certains* états excités pour 3 bosons. Ces états sont universels. Les autres états pour 3 bosons sont des états efimoviens analogues aux trimères d'Efimov, et ont une durée de vie courte. Nous montrons ensuite que pour certains états universels bosoniques, la durée de vie est en fait beaucoup moins longue que celle obtenue par l'approche de Petrov, Salomon et Shlyapnikov. En effet ces états sont couplés aux états efimoviens, en raison de la portée non nulle des interactions. Heureusement, ce couplage reste faible, et la durée de vie reste généralement beaucoup plus longue que la période d'oscillation du piège. Il est donc possible de stabiliser 3 atomes bosoniques en interaction forte près d'une résonance de Feshbach. Pour $N \geq 4$ atomes, la question reste ouverte.

Plan du manuscrit

Le Chapitre 0 est introductif. Il illustre le caractère universel des interactions résonnantes, en allant des exemples les plus simples à 2 corps jusqu'à des résultats à 3 corps et à N corps obtenus plus récemment, en particulier dans cette thèse.

L'essentiel de nos résultats est contenu dans les Parties 1 et 2.

- La Partie 1 concerne N particules piégées en interaction résonnante.
- La Partie 2 concerne 3 particules piégées. Elle contient notamment la solution du problème à 3 corps unitaire dans un piège harmonique isotrope, ainsi qu'une étude détaillée de la durée de vie.
- Dans la Partie 3, nous revenons sur le gaz unitaire piégé avec une approche plus macroscopique.
- La Partie 4 concerne le problème à 2 corps dans un piège et son étude expérimentale.
- La Partie 5 porte sur la physique à N corps dans un réseau optique, plus particulièrement sur l'antiferromagnétisme.

Contents of the manuscript

Chapter 0 is introductory. It illustrates the universality of resonant interactions. We start from the simplest examples with 2 particles. Then we discuss some results on the 3-body and N-body problems obtained more recently, in particular in this thesis.

Our main results are contained in Parts 1 and 2.

— Part 1 concerns N trapped particles with resonant interactions.

— Part 2 concerns 3 trapped particles. In particular, it contains the solution of the unitary 3-body problem in an isotropic harmonic trap, as well as a detailed study of the 3-body loss rate.

— In Part 3, we come back to the trapped gas with a macroscopic approach.

— Part 4 concerns the 2-body problem and its experimental study.

— Part 5 concerns many-body physics and antiferromagnetism in an optical lattice.

Chapitre 0

Interactions résonnantes et universalité

Dans ce Chapitre, nous considérons des modèles simples d'interaction, et nous montrons comment, dans la limite dite de portée nulle, ces modèles tendent vers une même limite universelle.

Dans les expériences d'atomes froids, les interactions sont plus complexes que les modèles simples considérés dans ce Chapitre. Le potentiel d'interaction dépend de l'état interne des atomes, ce qui donne naissance à des résonances de Feshbach pour certaines valeurs du champ magnétique. Le point essentiel est qu'au voisinage d'une telle résonance, la limite de portée nulle est bien réalisée dans la plupart des expériences. Dans cette limite universelle, on s'attend à ce que les interactions complexes entre atomes froids deviennent équivalentes aux modèles simples considérés dans ce Chapitre. Les détails microscopiques des interactions peuvent donc être oubliés. Nous discuterons dans quelle mesure le régime universel est atteint expérimentalement au Chapitre 3 (Section 6.1 page 111) et au Chapitre 8.

1 Problème à 2 corps

1.1 Dans l'espace libre

Considérons deux particules discernables de masse m dans l'espace libre, c'est-à-dire sans potentiel extérieur. Notons $\vec{r}$ le vecteur position relative des deux particules, $r = \|\vec{r}\|$ la distance entre les particules et $V(r)$ le potentiel d'interaction. Après séparation du centre de masse, l'équation de Schrödinger pour le mouvement relatif est :

$$\left[-\frac{\hbar^2}{m}\Delta_{\vec{r}} + V(r)\right]\Psi(\vec{r}) = E\,\Psi(\vec{r}). \tag{1}$$

Un état lié à 2 corps, aussi appelé dimère ou molécule, est une solution de cette équation d'énergie $E = E_d < 0$. La fonction d'onde d'un tel dimère est normalisable : $\int |\Psi(\vec{r})|^2\, d\vec{r} = 1$.

Pour fixer les idées, prenons un potentiel d'interaction en puits carré attractif (Fig. 1) :

$$V(r) \;= \begin{cases} -v_0\,\frac{\hbar^2}{mb^2}\left(\frac{\pi}{2}\right)^2 & \text{si } r < b \\ 0 & \text{si } r > b. \end{cases} \tag{2}$$

Le calcul des dimères invariants par rotation est sans difficulté.[1] Un dimère existe pour $v_0 > 1$, et ce dimère est unique tant que $v_0 < 9$. Si v_0 n'est pas trop proche de 1, l'énergie de liaison $|E_d|$ est

1. La fonction $u(r) \equiv r\Psi(r)$ est un sinus pour $r < b$ et une exponentielle décroissante pour $r > b$. L'énergie est telle que $u'(r)/u(r)$ soit continue en $r = b$.

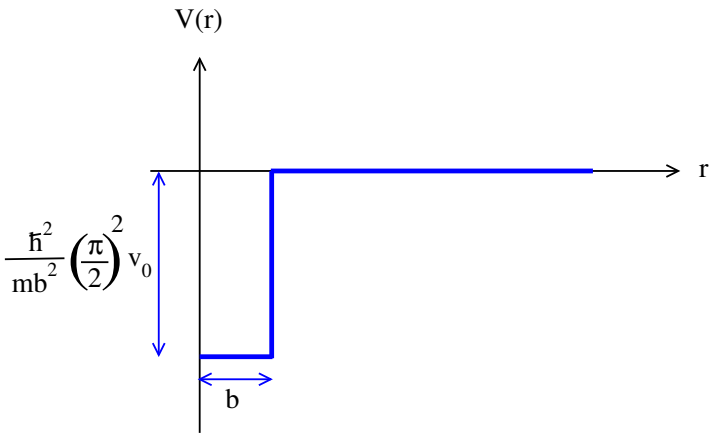

FIGURE 1 – Potentiel d'interaction en puits carré.

de l'ordre de $\hbar^2/(mb^2)$ et on parle de dimère profond. La taille du dimère, c'est-à-dire l'extension de sa fonction d'onde, est alors de l'ordre de la portée b du potentiel. Lorsque $v_0 \to 1^+$ le dimère disparaît progressivement : $|E_d| \to 0$ et on parle de dimère faiblement lié. Ceci est illustré par la Figure 2.

Considérons maintenant un état de diffusion, c'est-à-dire une solution d'énergie $E > 0$ de l'équation de Schrödinger (1) ayant le comportement asymptotique

$$\Psi(\vec{r}) \underset{r\to\infty}{\simeq} e^{i\vec{k}\cdot\vec{r}} + f_k(\vec{n})\,\frac{e^{ikr}}{r}, \tag{3}$$

où $\vec{n} = \vec{r}/r$, et $f_k(\vec{n})$ est l'amplitude de diffusion.
Pour $k \to 0$, la fonction $-f_k(\vec{n})$ tend vers une constante a , la *longueur de diffusion.*

Considérons à nouveau la limite $v_0 \to 1^+$, où l'énergie du dimère $E_d \to 0^-$. On montre aussi que

$$a/b \underset{v_0\to 1^+}{\longrightarrow} +\infty,$$

ce qui signifie que les particules de basse énergie sont fortement diffusées. L'interaction est dite résonnante. De plus, le comportement asymptotique de E_d est

$$E_d \sim -\frac{\hbar^2}{ma^2}, \tag{4}$$

et l'extension de la fonction d'onde $\langle\hat{r}\rangle \equiv \int r|\Psi(\vec{r})|^2\,d\vec{r}$ diverge comme

$$\langle\hat{r}\rangle \sim \frac{a}{2}. \tag{5}$$

Ces propriétés sont *universelles* : elles sont vraies non seulement pour l'interaction en puits carré, mais pour toute interaction (décroissant assez vite avec la distance), dans la limite où il existe un

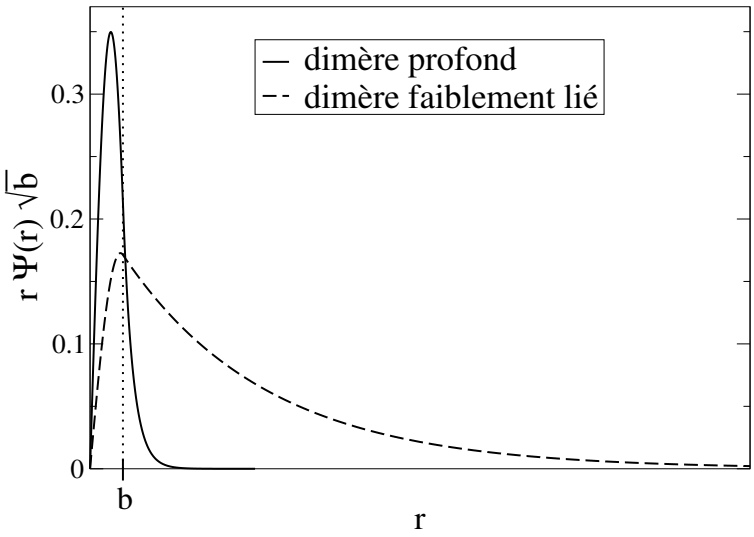

FIGURE 2 – Pour un potentiel d'interaction assez profond ($v_0 = 7$), la fonction d'onde du dimère a une extension de l'ordre de la portée b du potentiel (trait plein). Pour $v_0 \to 1^+$, l'énergie de liaison tend vers 0, et l'extension du dimère diverge. L'extension du dimère est déjà notablement plus grande que b pour $v_0 = 1.2$ (trait tireté).

dimère faiblement lié. En particulier, elles s'appliquent aux dimères formés par 2 atomes au voisinage d'une résonance de Feshbach.

La limite $|a|/b \to +\infty$ peut aussi être vue comme une *limite de portée nulle*, où la portée tend vers 0 à longueur de diffusion a fixée. Dans le cas du puits carré, nous faisons donc tendre b vers 0, tout en ajustant v_0 de telle sorte que la longueur de diffusion reste égale à une constante a. Pour $a = \infty$, il suffit de prendre $v_0 = 1$; pour une valeur finie de a il faut faire tendre v_0 vers 1, d'une façon qui dépend de a. [La profondeur du potentiel diverge donc comme $\hbar^2/(mb^2)$, et $V(r)$ ne tend *pas* vers $\delta^3(\vec{r}) \cdot constante$.] Dans le cas $a > 0$, on retrouve dans la limite $b \to 0$ un dimère faiblement lié, dont l'énergie et la fonction d'onde convergent :

$$E_d \to -\frac{\hbar^2}{ma^2} \tag{6}$$

$$\Psi(\vec{r}) \to \frac{e^{-r/a}}{r\sqrt{2\pi a}}. \tag{7}$$

Cette dernière convergence est illustrée Figure 3.

Les propriétés universelles telles que (5,6,7) peuvent s'obtenir à partir d'un modèle d'interaction de portée finie (par exemple l'interaction en puits carré) en prenant la limite de portée nulle. Mais elles s'obtiennent plus directement à partir du pseudopotentiel.

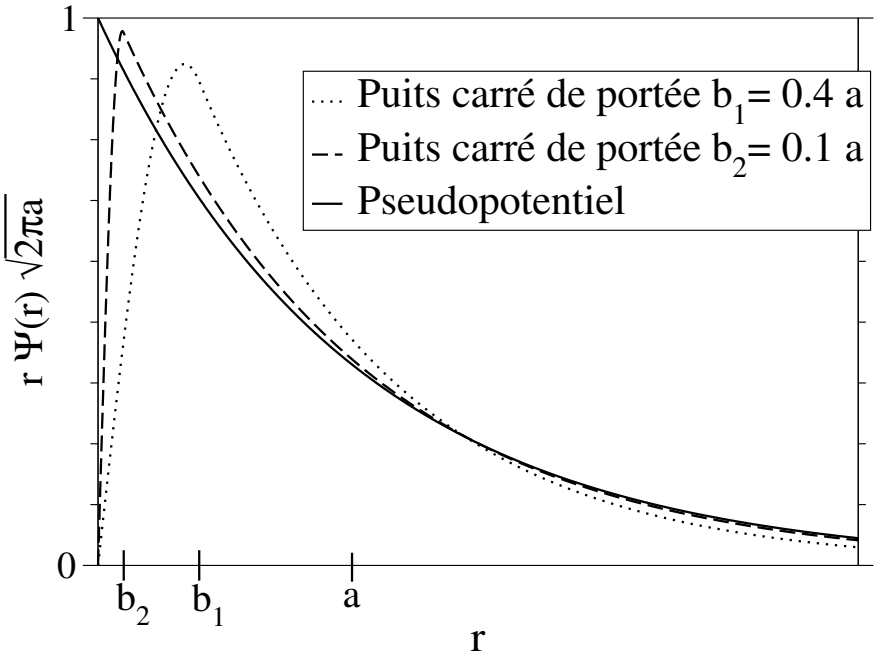

FIGURE 3 – Pour une interaction en puits carré de portée b, la fonction d'onde du dimère converge vers la solution du pseudopotentiel dans la limite $b/a \to 0$.

Le pseudopotentiel

Dans le cas présent (mouvement relatif de 2 particules dans l'espace libre), le pseudopotentiel est défini par :

$$\begin{cases} \bullet \text{ Pour } \vec{r} \neq \vec{0} : \; -\dfrac{\hbar^2}{m}\Delta_{\vec{r}}\,\Psi(\vec{r}) = E\,\Psi(\vec{r}) & (8) \\ \bullet \text{ Pour } r \to 0 : \text{ il existe } A \text{ tel que } \Psi(\vec{r}) = A \cdot \left(\dfrac{1}{r} - \dfrac{1}{a}\right) + O(r). & (9) \end{cases}$$

L'effet des interactions est contenu dans la *condition aux limites de Bethe-Peierls* (9).

Notons qu'une formulation équivalente à (8,9) est (cf. par exemple [31]) :

$$-\frac{\hbar^2}{m}\Delta_{\vec{r}}\,\Psi(\vec{r}) + \frac{4\pi\hbar^2}{m} a\,\delta^3(\vec{r})\,\frac{\partial}{\partial r}\,(r\,\Psi(\vec{r})) = E\,\Psi(\vec{r}). \tag{10}$$

Ceci montre à nouveau que le pseudopotentiel diffère d'une simple distribution de Dirac. [2]

Le pseudopotentiel a un état lié si $a > 0$, d'énergie $E = -\hbar^2/(ma^2)$, de fonction d'onde

$$\Psi(\vec{r}) = \frac{e^{-r/a}}{r\sqrt{2\pi a}}. \tag{11}$$

Les états de diffusion du pseudopotentiel sont :

$$\Psi(\vec{r}) = e^{i\vec{k}\cdot\vec{r}} + f_k\,\frac{e^{ikr}}{r}, \tag{12}$$

2. Ce n'est que dans le cadre d'un traitement perturbatif en a que l'on peut remplacer $\partial(r\,\Psi)/\partial r$ par Ψ dans (10).

avec l'amplitude de diffusion :

$$f_k = \frac{-1}{\frac{1}{a} + ik}. \tag{13}$$

On a donc bien

$$f_k \underset{k\to 0}{\longrightarrow} -a, \tag{14}$$

en accord avec la définition générale de la longueur de diffusion.

La *limite unitaire* correspond à $a = \infty$ (i. e. $\frac{1}{a} = 0$). $|f_k|$ atteint alors la limite supérieure imposée par le théorème optique [32].

1.2 Dans un piège harmonique

Supposons maintenant que les deux particules sont soumises à un potentiel de piégeage harmonique isotrope

$$U(r) = \frac{1}{2} m\omega^2 r^2. \tag{15}$$

L'échelle de longueur associée est la taille de l'état fondamental à une particule :

$$a_{\text{ho}} \equiv \sqrt{\frac{\hbar}{m\omega}}. \tag{16}$$

Le centre de masse est séparable (Appendice A) et le mouvement relatif est décrit par :

$$\left[-\frac{\hbar^2}{m}\Delta_{\vec{r}} + V(r) + \frac{1}{4} m\omega^2 r^2 \right] \Psi(\vec{r}) = E\, \Psi(\vec{r}). \tag{17}$$

Restreignons-nous aux états invariants par rotation. Prenons encore l'interaction $V(r)$ en puits carré définie par l'équation (2). Plaçons nous à résonance : $v_0 = 1$ et $a = \infty$. Le calcul numérique du spectre est sans difficulté (Chapitre 6, Section 3) . L'énergie $E(b)$ des deux premiers états est tracée Figure 4. On constate une convergence dans la limite de portée nulle : pour $b \to 0$, $E(b)$ tend vers une limite E_{PP}.

Les E_{PP} sont aussi les énergies propres du pseudopotentiel. Dans le cas présent (mouvement relatif de 2 particules dans un piège harmonique), le pseudopotentiel est défini par :

$$\begin{cases} \bullet \text{ Pour } \vec{r} \neq \vec{0} : \left[-\dfrac{\hbar^2}{m}\Delta_{\vec{r}} + \dfrac{1}{4} m\omega^2 r^2 \right] \Psi_{\text{PP}}(\vec{r}) = E_{\text{PP}}\, \Psi_{\text{PP}}(\vec{r}) & (18) \\ \bullet \text{ Pour } r \to 0 : \text{ il existe } A \text{ tel que} \quad \Psi_{\text{PP}}(\vec{r}) = A\left(\dfrac{1}{r} - \dfrac{1}{a}\right) + O(r). & (19) \end{cases}$$

Ce problème est exactement soluble ([33] ; Chap. 6, Section 1). Le spectre pour $a = \infty$ est :

$$E_{\text{PP}} = \left(2n + \frac{1}{2}\right) \hbar\omega, \ n \in \mathbb{N}. \tag{20}$$

Ces énergies sont abaissées par rapport au cas sans interaction d'une quantité $\hbar\omega$. Le fait qu'elles soient abaissées est évident car l'interaction en puits carré considérée précédemment est attractive.

En résumé, dans la limite de portée nulle, le problème à 2 corps a une limite universelle, décrite exactement par le pseudopotentiel. Ce principe a été confirmé par plusieurs résultats mathématiques [34].

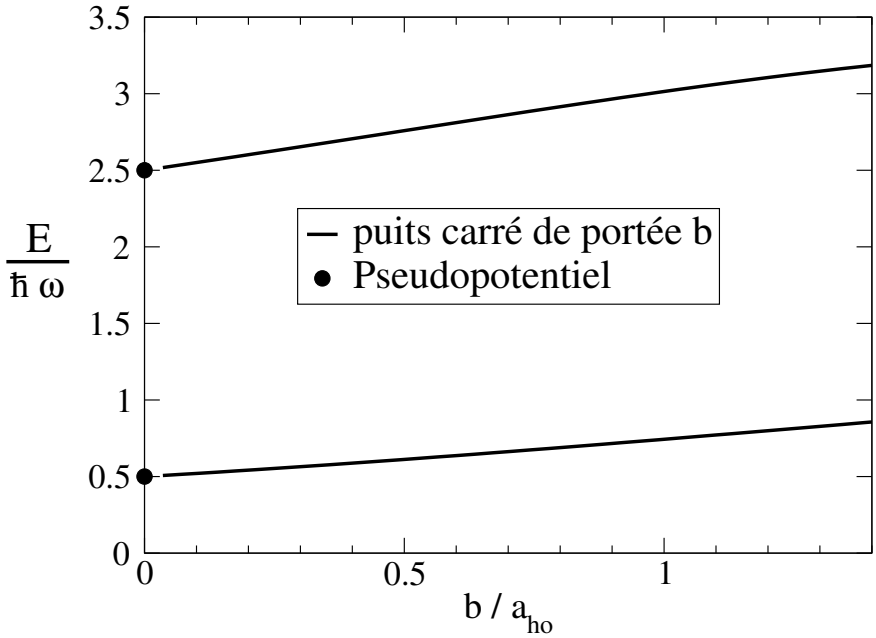

FIGURE 4 – Pour 2 particules piégées à la limite unitaire, le spectre pour une interaction en puits carré de portée b converge vers le spectre pour une interaction via le pseudopotentiel lorsque $b/a_{\rm ho} \to 0$. [$a_{\rm ho} \equiv \sqrt{\hbar/(m\omega)}$.]

Notons que dans toute cette thèse, nous excluons la possibilité que plusieurs dimères apparaissent simultanément, ce qui conduirait, en plus de la résonance "en onde s" considérée ici, à des résonances dans des ondes partielle d'ordre supérieur. De telles résonances peuvent bien sur se produire et ont été observées avec des atomes froids (cf. [35] et les références dans cet article), mais la probabilité qu'elles se produisent exactement au même point qu'une résonance en onde s est pour ainsi dire nulle.

2 Fermions à la limite unitaire

Il est généralement admis que l'universalité dans la limite de portée nulle, discutée ci-dessus dans le cas de 2 particules, reste vraie pour N particules *fermioniques de même masse à* 2 *états internes.*

2.1 Spin et symétrie

Plus précisément, considérons N fermions, chaque fermion ayant 2 états internes, notés $|\uparrow\rangle$ et $|\downarrow\rangle$. L'état interne peut donc être vu comme un spin $\frac{1}{2}$ (pour la signification physique de ce "spin" dans le cas des atomes froids, voir l'Appendice E de la Partie 4). Prenons un Hamiltonien de la forme :

$$\mathcal{H} = \sum_{i=1}^{N} \left[-\frac{\hbar^2}{2m} \Delta_{\vec{r}_i} + U(\hat{\vec{r}}_i) \right] + \sum_{i<j} \hat{V}_{ij}, \tag{21}$$

où $U(\vec{r})$ est un potentiel de piégeage et $\hat{\hat{V}}_{ij}$ est l'interaction entre les particules i et j. Supposons que l'interaction ne change pas l'état interne, i.e. :

$$\hat{\hat{V}}_{ij}\left(|\sigma_i,\sigma_j\rangle\otimes|\phi\rangle\right)=|\sigma_i,\sigma_j\rangle\otimes\left(\hat{V}_{ij}^{\sigma_i,\sigma_j}|\phi\rangle\right) \tag{22}$$

où $\sigma_i,\sigma_j\in\{\uparrow,\downarrow\}$ sont les états internes et $\phi(\vec{r}_i,\vec{r}_j)$ la fonction d'onde orbitale des particules i et j. On peut alors se placer dans le sous-espace correspondant à un nombre $N_\uparrow$ fixé de particules ayant un spin $|\uparrow\rangle$, et un nombre $N_\downarrow$ fixé de particules ayant un spin $|\downarrow\rangle$. Définissons un hamiltonien orbital H par :

$$\mathcal{H}\left(|\uparrow\rangle^{\otimes N_\uparrow}|\downarrow\rangle^{\otimes N_\downarrow}\otimes|\Phi\rangle\right)=|\uparrow\rangle^{\otimes N_\uparrow}|\downarrow\rangle^{\otimes N_\downarrow}\otimes\left(H|\Phi\rangle\right), \tag{23}$$

où $|\uparrow\rangle^{\otimes N_\uparrow}$ représente le produit tensoriel de $N_\uparrow$ facteurs $|\uparrow\rangle$. Restreignons-nous au cas où il n'y a pas d'interaction entre particules de même spin :

$$\hat{V}_{ij}^{\sigma_i,\sigma_j}=\begin{cases}0 & \text{si } \sigma_i=\sigma_j\\ \hat{V}_{ij} & \text{si } \sigma_i\neq\sigma_j.\end{cases} \tag{24}$$

Dans ce cas H est simplement :

$$H=\sum_{i=1}^{N}\left[-\frac{\hbar^2}{2m}\Delta_{\vec{r}_i}+U(\hat{\vec{r}}_i)\right]+\sum_{\substack{1\le i\le N_\uparrow\\ N_\uparrow+1\le j\le N}}\hat{V}_{ij}. \tag{25}$$

On montre que les états $|\psi\rangle=\hat{A}\left(|\uparrow\rangle^{\otimes N_\uparrow}|\downarrow\rangle^{\otimes N_\downarrow}\otimes|\Phi\rangle\right)$ forment une base d'états propres , où $\hat{A}$ est l'opérateur antisymétriseur, et $\Phi(\vec{r}_1,\ldots,\vec{r}_N)$ est un état propre de H, antisymétrique pour l'échange des particules 1 à $N_\uparrow$ et antisymétrique pour l'échange des particules $N_\uparrow+1$ à N :

$$\forall(i,j)\in\{1,\ldots,N_\uparrow\}^2\cup\{N_\uparrow+1,\ldots,N\}^2,\Phi(\ldots,\vec{r}_i,\ldots,\vec{r}_j,\ldots)=-\Phi(\ldots,\vec{r}_j,\ldots,\vec{r}_i,\ldots). \tag{26}$$

Notons que

$$\Phi(\vec{r}_1,\ldots,\vec{r}_N)\propto\left(\langle\uparrow|^{\otimes N_\uparrow}\langle\downarrow|^{\otimes N_\downarrow}\otimes\langle\vec{r}_1,\ldots,\vec{r}_N|\right)|\psi\rangle. \tag{27}$$

Dans la suite nous ne parlerons plus que de la fonction d'onde $\Phi(\vec{r}_1,\ldots,\vec{r}_N)$, qui satisfait l'équation de Schrödinger :

$$\left[\sum_{i=1}^{N}\left[-\frac{\hbar^2}{2m}\Delta_{\vec{r}_i}+U(\vec{r}_i)\right]+\sum_{\substack{1\le i\le N_\uparrow\\ N_\uparrow+1\le j\le N}}\hat{V}_{ij}\right]\Phi(\vec{r}_1,\ldots,\vec{r}_N)=E\ \Phi(\vec{r}_1,\ldots,\vec{r}_N). \tag{28}$$

2.2 Le pseudopotentiel

Dans la suite de ce Chapitre, restreignons-nous au cas d'une longueur de diffusion $a=\infty$. Nous serons amenés à considérer différents modèles, chacun étant caractérisé par une "portée" b. Le concept d'universalité signifie que, pour $b\to 0$, les énergies propres et les états propres convergent vers une limite indépendante du modèle ; et que ces limites sont aussi les énergies propres et les états propres du pseudopotentiel.

Le pseudopotentiel est défini de la façon suivante : il n'y a pas de terme d'interaction dans le hamiltonien ($\hat{V}_{ij} = 0$) de sorte que l'équation de Schrödinger se réduit à

$$\sum_{i=1}^{N} \left[-\frac{\hbar^2}{2m} \Delta_{\vec{r}_i} + U(\vec{r}_i) \right] \Phi(\vec{r}_1, \ldots, \vec{r}_N) = E\, \Phi(\vec{r}_1, \ldots, \vec{r}_N). \tag{29}$$

Les interactions sont modélisées comme suit. L'équation de Schrödinger n'est imposée que lorsque la distance $r_{ij} = \|\vec{r}_j - \vec{r}_i\|$ entre les particules i et j est non nulle pour toute paire de particules (i, j). Pour $r_{ij} \to 0$ on impose les conditions aux limites suivantes sur la fonction d'onde :[3] il existe une fonction A_{ij} telle que

$$\Phi(\vec{r}_1, \ldots, \vec{r}_N) \underset{r_{ij} \to 0}{=} \left(\frac{1}{r_{ij}} - \frac{1}{a} \right) \cdot A_{ij} \left(\vec{R}_{ij}, (\vec{r}_k)_{k \notin \{i,j\}} \right) + O(r_{ij}) \tag{30}$$

où $\vec{R}_{ij} = (\vec{r}_i + \vec{r}_j)/2$ est la position du centre de masse des particules i et j, et $(\vec{r}_k)_{k \notin \{i,j\}}$ sont les positions des autres particules. La limite $r_{ij} \to 0$ est prise pour $\vec{R}_{ij}$ et $(\vec{r}_k)_{k \notin \{i,j\}}$ fixés. On n'impose cette condition que lorsque $\vec{R}_{ij} \notin \{\vec{r}_k, k \notin \{i, j\}\}$, et lorsque tous les $\vec{r}_k$ sont distincts.

Pour le cas $N_\uparrow = N_\downarrow = 1$, aucune contrainte de symétrie n'est imposée à la fonction d'onde par l'équation (26), et on est ramené au cas de 2 particules discernables étudié dans la Section 1.

Pour 2 particules de même spin, la fonction d'onde est antisymétrique [cf. équation (26)]. La condition aux limites (30) ne peut alors être satisfaite que pour $A_{12} = 0$. On est ramené au cas sans interaction. Plus généralement, deux fermions de même spin n'interagissent pas via le pseudopotentiel.[4]

2.3 Trois fermions piégés

Pour $N = 3$, le cas intéressant est donc celui où les 3 particules n'ont pas le même spin, par exemple $N_\uparrow = 2$ et $N_\downarrow = 1$.
Restreignons-nous dans la suite à la limite unitaire :

$$\frac{1}{a} = 0. \tag{31}$$

Pour un piège harmonique isotrope [$U(r) = \frac{1}{2} m\omega^2 r^2$], ce problème est exactement soluble (cf. Partie 2). Nous trouvons que l'état fondamental a un moment cinétique total $l = 1$, et que son énergie est

$$E_0 = \left(s + \frac{5}{2} \right) \hbar\omega = 4.27272\ldots\, \hbar\omega \tag{32}$$

où s est la plus petite solution strictement positive de l'équation transcendante

$$(1 - s^2) \sin\left(s\frac{\pi}{2} \right) + (1 - s)\frac{4}{\sqrt{3}} \cos\left(s\frac{\pi}{6} \right) - \frac{8}{\sqrt{3}} \sin\left[(1 - s)\frac{\pi}{6} \right] = 0. \tag{33}$$

Revenons à une interaction entre particules de spin opposé décrite par un potentiel $V(r)$:

$$\hat{V}_{ij} = V(\|\hat{\vec{r}}_i - \hat{\vec{r}}_j\|). \tag{34}$$

3. Mathématiquement ces conditions aux limites définissent le domaine du hamiltonien [36, 34].

4. On s'attend donc à ce que, même si on incluait une interaction de portée b entre particules de même spin [contrairement à ce que nous faisons dans l'équation (24)], l'effet de cette interaction disparaîtrait dans la limite $b \to 0$. Plus généralement, deux fermions de même spin n'interagissent pas dans la limite des basse énergies. Rappelons que nous excluons le cas peu probable où une résonance dans une onde partielle d'ordre supérieur se produirait simultanément à celle dans l'onde s.

Reprenons, pour fixer les idées, l'exemple du puits carré :

$$V(r) = \begin{cases} -V_0 & \text{si } r < b \\ 0 & \text{si } r > b. \end{cases} \tag{35}$$

avec

$$V_0 = \frac{\hbar^2}{mb^2}\left(\frac{\pi}{2}\right)^2, \tag{36}$$

i.e. au seuil d'apparition du premier dimère, où $a = \infty$. Pour $N = 2$, nous avons vu dans la Section 1 que les energies propres de ce modèle tendent vers celles du pseudopotentiel pour $b \to 0$. On pense que cela reste vrai pour $N = 3$. Un calcul par diagonalisation numérique [28], effectué non pas précisément pour un puits carré, mais pour un puits gaussien de portée assez faible [$V(r) \propto e^{-r^2/(2b^2)}$ avec $b = 0.01\sqrt{\hbar/(m\omega)}$], donne $E_0 = 4.275\,\hbar\omega$, en bon accord avec la valeur (32) du pseudopotentiel.

Les modèles d'interaction en puits attractif sont également utilisés dans les calculs Monte-Carlo à nœuds fixés. Cette méthode variationnelle semble souvent être une bonne approximation. L'idée est de minimiser l'énergie, en maintenant fixée la surface nodale de la fonction d'onde (i.e. l'ensemble des points où la fonction d'onde s'annule). Pour $N = 3$ fermions dans un piège harmonique isotrope, les valeurs $E_0 = 4.281(4)$ [28] et $E_0 = 4.28(4)$ [37] obtenues par cette méthode sont en bon accord avec celle du pseudopotentiel (32).

Considérons maintenant un autre modèle d'interaction, appelé potentiel séparable, défini par :

$$\langle \vec{r}_i, \vec{r}_j | \hat{V}_{ij} | \vec{r}_i^{\,'}, \vec{r}_j^{\,'} \rangle = g_0\ \zeta(r_{ij})\,\zeta(r'_{ij})\,\delta^3(\vec{R}_{ij} - \vec{R}_{ij}^{\,'}) \tag{37}$$

où $r_{ij} = \|\vec{r}_j - \vec{r}_i\|$, $\vec{R}_{ij} = (\vec{r}_i + \vec{r}_j)/2$, et nous choisissons pour ζ une gaussienne normalisée de portée b :

$$\zeta(r) = e^{-\frac{r^2}{2b^2}}\ (2\pi b^2)^{-3/2}. \tag{38}$$

De tels modèles sont couramment utilisés en physique [5] [38].

Un unique dimère existe pour $g_0 > g_{0,c}$ où

$$g_{0,c} = -4\pi^{3/2}\frac{\hbar^2}{m}b. \tag{39}$$

Nous prenons donc $g_0 = g_{0,c}$ de façon à avoir une longueur de diffusion infinie.

Un avantage du potentiel séparable est que le problème à 3 corps se ramène à une équation intégrale à une variable, qui peut être résolue numériquement (cf. Partie 2, Appendice C). Nous avons ainsi pu vérifier la convergence vers le pseudopotentiel dans la limite de portée nulle (Figure 5).

2.4 Le gaz unitaire homogène

Un problème célèbre est le calcul de l'énergie du gaz homogène (i. e. sans potentiel de piégeage et avec des conditions aux limites périodiques dans un cube de volume V) à la limite unitaire (i. e. pour une longueur de diffusion infinie et dans la limite de portée nulle) dans le cas équilibré en spin ($N_\uparrow = N_\downarrow$). D'après l'hypothèse d'universalité et par analyse dimensionnelle, l'énergie E_{unitaire} de ce gaz unitaire doit être, dans la limite thermodynamique, proportionnelle à l'énergie E_{parfait} d'un gaz parfait de même densité :

$$E_{\text{unitaire}} \underset{N\to\infty}{\sim} \eta\ E_{\text{parfait}}. \tag{40}$$

5. Notons que $\zeta(r) \underset{b\to 0}{\to} \delta^3(\vec{r})$. Le potentiel séparable est donc simplement une façon de régulariser l'interaction en $\delta^3(\vec{r})$, qui équivaut d'ailleurs à introduire une fonction de coupure dans l'espace de Fourier.

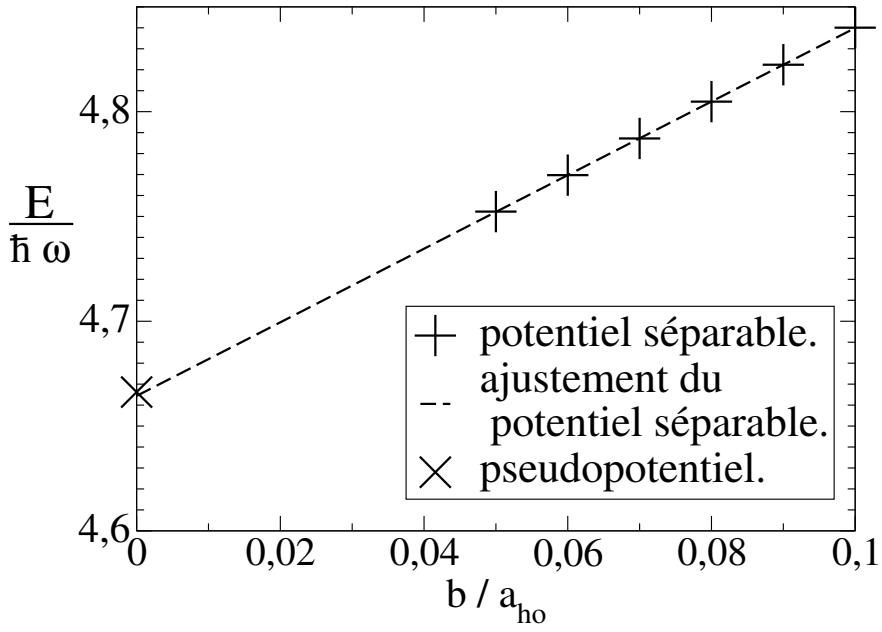

FIGURE 5 – Pour 3 fermions à la limite unitaire, dans un piège harmonique, les valeurs de l'énergie de l'état fondamental (dans le secteur de moment cinétique total nul) obtenues numériquement pour un potentiel d'interaction séparable pour différentes valeurs de la portée b (+) sont bien ajustées par la droite $E/(\hbar\omega) = 4.6644 + 1.7553\ b/a_{\rm ho}$ (trait pointillé), qui tend vers une valeur en bon accord avec la valeur $E = 4.6662\ldots$ obtenue analytiquement pour le pseudopotentiel (×). [$a_{\rm ho} \equiv \sqrt{\hbar/(m\omega)}$.]

Rappelons que

$$E_{\text{parfait}} \underset{N\to\infty}{\sim} N\,\frac{3}{5}\frac{\hbar^2 k_F^2}{2m} \tag{41}$$

où

$$k_F = \left(3\pi^2 \frac{N}{V}\right)^{\frac{1}{3}} \tag{42}$$

est le vecteur d'onde de Fermi.

Les calculs Monte-Carlo à nœuds fixés donnent $\eta = 0.44(1)$ [39] et $\eta = 0.42(1)$ [40]. Ces valeurs sont par construction inférieures à la borne supérieure donnée par la théorie BCS [41, 39], $\eta \leq 0.59\ldots$. L'interaction en puits carré est utilisée dans [40], avec $N = 66$ particules, et une portée $b = 0.3/k_F$, jugée suffisamment petite pour avoir atteint la limite de portée nulle. Il existe également des calculs Monte-Carlo sans biais (c'est-à-dire numériquement exacts), qui obtiennent $\eta = 0.449(9)$ [42] et $\eta = 0.25(3)$ [43] (le dernier résultat étant en net désaccord avec les trois précédants). Ces deux derniers calculs utilisent des modèles sur réseau de type Hubbard (voir ci-après). Les résultats expérimentaux obtenus avec des atomes de ^{6}Li sont : $\eta = 0.27^{+0.09}_{-0.12}$ [44], $\eta = 0.41(15)$ [45], $\eta = 0.51(4)$ [46], $\eta = 0.46(5)$ [47], et avec des atomes de ^{40}K : $\eta = 0.46^{+0.12}_{-0.05}$ [48].

Mais pour ce modèle en puits carré, on rencontre la difficulté suivante : il existe une valeur critique N_c telle que pour $N \geq N_c$, l'énergie de l'état fondamental tend vers $-\infty$ pour $b \to 0$. Cet effet est bien connu, et est probablement présent pour tout potentiel purement attractif [49, 50, 51]. Donnons-en une dérivation dans le cas du puits carré. Considérons $N = N_\uparrow + N_\downarrow$ fermions, avec $N_\uparrow = N_\downarrow$, dans l'espace libre, avec l'interaction en puits carré résonnant (35,36). Montrons que pour N assez grand, il existe un état lié à N corps dont l'énergie tend vers $-\infty$ pour $b \to 0$. Prenons l'Ansatz variationnel suivant : une mer de Fermi (i. e. l'état fondamental sans interaction) dans une boîte cubique (fictive) de côté $b/\sqrt{3}$, avec des murs infinis (i. e. la fonction d'onde s'annule au bord de la boîte). L'énergie cinétique est celle du gaz parfait dans un volume $V = (b/\sqrt{3})^3$, soit d'après (41,42) :

$$E_{\text{cin}} \underset{N\to\infty}{\sim} \frac{\hbar^2}{mb^2}\, N^{\frac{5}{3}}\, \frac{\pi^{\frac{4}{3}} 3^{\frac{8}{3}}}{2\cdot 5}. \tag{43}$$

La distance entre particules dans notre boîte étant toujours inférieure à b, l'énergie d'interaction moyenne est simplement

$$E_{\text{int}} = -V_0 \left(\frac{N}{2}\right)^2. \tag{44}$$

Donc

$$\frac{|E_{\text{int}}|}{E_{\text{cin}}} \underset{N\to\infty}{\sim} \left(\frac{N}{\tilde{N}_c}\right)^{\frac{1}{3}} \tag{45}$$

avec

$$\tilde{N}_c = \frac{3^8\, 2^9}{\pi^2\, 5^3} \simeq 2723. \tag{46}$$

Par analyse dimensionnelle, l'énergie totale moyenne $E = E_{\text{cin}} + E_{\text{int}}$ est de la forme

$$E = \frac{\hbar^2}{mb^2}\, C_N \tag{47}$$

où C_N est sans dimension. De (45) on déduit que $C_N \underset{N\to\infty}{\to} -\infty$. Par conséquent, il existe N_c tel que, pour $N \geq N_c$, on ait $C_N < 0$ et donc $E \underset{b\to 0}{\to} -\infty$. De plus, $N_c \simeq \tilde{N}_c \simeq 2723$. En conclusion, pour $N \gtrsim 2723$, il existe un état lié à N corps dont l'énergie tend vers $-\infty$ pour $b \to 0$. Le N critique exact est bien sûr inférieur à la valeur 2723 obtenue variationnellement.

Si les N utilisés dans les calculs Monte-Carlo à nœuds fixés dépassent ce N critique, on peut s'inquiéter sur leur validité. Cela étant, un état tel que l'état variationnel ci-dessus ayant une extension de l'ordre de b a une surface nodale très différente de celles des fonctions d'onde d'essai utilisées (telles que la fonction d'onde BCS) et on s'attend donc à ce qu'il n'influence pas le résultat des calculs [49, 12]. Les auteurs des calculs à nœuds fixés pensent donc qu'ils obtiendraient une borne supérieure pour le paramètre universel η même s'ils dépassaient le N critique. D'un point de vue plus fondamental, on s'attend à ce que, même dans un cas où l'état fondamental ne converge pas pour $b \to 0$, il existe des états excités qui soient proches des états propres du pseudopotentiel lorsque $b \to 0$.

Notons à ce propos qu'expérimentalement, les états gazeux universels ne sont que des états excités, puisque même pour 2 atomes, il existe de nombreux états liés profonds. L'existence de ces états profonds, ajoutée au fait que le potentiel de piégeage a une profondeur finie, conduit à une durée de vie finie du gaz. Pour les fermions, cette durée de vie est généralement plus longue que les autres échelles de temps, de sorte que tout se passe comme si le gaz était dans son état fondamental [23].

Décrivons brièvement une dernière classe de modèles : les modèles sur réseau (voir [32] pour plus de détails). Les modèles sur réseau (et plus généralement les modèles de potentiel séparable) présentent deux avantages importants. Premièrement, ils sont souvent moins difficiles à résoudre numériquement. Deuxièmement, pour autant que l'on sache, *tous* leurs états propres convergent pour $b \to 0$. En particulier, le paramètre η peut être obtenu directement par un calcul exact de l'énergie de l'état fondamental [42].

Les vecteurs positions ont alors des coordonnées égales à un nombre entier fois le pas b du réseau, et deux particules n'interagissent que si leurs positions sont égales. Ainsi, la limite de portée nulle $b \to 0$ coïncide avec la limite continue.

Il y a plusieurs choix possibles pour le Laplacien discret définissant l'énergie cinétique du modèle sur réseau. Un premier choix conduit au modèle de Hubbard,

$$H = -t \sum_{\substack{\vec{i},\vec{j} \in \mathbb{Z}^3 \\ \|\vec{i}-\vec{j}\|=1 \\ \sigma=\uparrow,\downarrow}} c^\dagger_{\vec{i}\sigma}\, c_{\vec{j}\sigma} + C + \mathcal{U} \sum_{\vec{i}} n_{\vec{i}\uparrow} n_{\vec{i}\downarrow} + \sum_{\vec{i}\sigma} U\left(b\vec{i}\right) n_{\vec{i}\sigma}, \tag{48}$$

où l'on prend $t = \hbar^2/(2mb^2)$ et $C = 6t\hat{N}$ afin de retrouver, dans la limite $b \to 0$, la relation de dispersion $\epsilon_{\vec{k}} = \hbar^2 k^2/(2m)$ d'une particule libre dans l'espace continu. Le modèle de Hubbard est très utilisé en physique de la matière condensée, avec des nombres de particules par site d'ordre unité. Mais pour réaliser la limite unitaire, il faut :

— prendre $\mathcal{U}/t = -7.914\ldots$, où la longueur de diffusion diverge, et où le premier dimère apparaît [52, 32]

— faire tendre $k_F\, b$ vers 0, autrement dit, faire tendre le nombre de particules par site vers 0.

Ce modèle a été utilisé dans des calculs Monte-Carlo [52, 53, 54, 55]. La valeur de la température critique pour la transition vers l'état superfluide obtenue par le groupe de Amherst [52] est

$$T_c = 0.152(7) E_F \tag{49}$$

où $E_F = \hbar^2 k_F^2/(2m)$ est l'énergie de Fermi.

Un autre choix pour le Laplacien discret consiste à imposer une relation de dispersion exactement égale à la relation de dispersion dans l'espace continu [i. e. $\epsilon_k = \hbar^2 k^2/(2m)$] [56, 57]. Pour $N \leq 3$ fermions dans une boîte, la convergence du spectre de ce modèle sur réseau vers celui du

pseudopotentiel dans la limite de portée nulle a été vérifiée par une étude analytique et numérique détaillée [58]. Ce modèle a également été utilisé dans les calcul Monte-Carlo de η et du gap d'Olivier Juillet [42]. [6]

2.5 N fermions piégés

Nous donnons maintenant un résultat qui est dérivé dans le Chapitre 1 et l'Article I. Nous reproduisons ensuite la comparaison effectuée par Blume, von Stecher et Greene [28] entre ce résultat analytique et leurs résultats numériques. Cette comparaison constitue une vérification supplémentaire de l'universalité, non seulement pour le spectre mais aussi pour les fonctions d'ondes.

Notons

$$\vec{C} = \frac{1}{N}\sum_{i=1}^{N} \vec{r}_i \tag{50}$$

le centre de masse des N particules.

Une quantité essentielle ici est l'hyperrayon R, défini par

$$R = \sqrt{\sum_{i=1}^{N} \left(\vec{r}_i - \vec{C}\right)^2} = \sqrt{\frac{1}{N}\sum_{i<j} {r_{ij}}^2}. \tag{51}$$

L'hyperrayon est une mesure de la taille globale du système, il est petit si toutes les N particules sont proches.
Pour chaque état propre, notons $P(R)$ la densité de probabilité de l'hyperrayon. [7]

Considérons l'état fondamental, d'énergie E. Définissons le réel s par

$$E = \left(s + \frac{5}{2}\right)\hbar\omega. \tag{52}$$

Pour le pseudopotentiel, on a alors (Chapitre 1, Article I, [59]) :

$$P(R) = \frac{2}{\Gamma(s+1)}\left(\frac{R}{a_{ho}}\right)^{2s+1} e^{-\left(\frac{R}{a_{ho}}\right)^2}. \tag{53}$$

De plus, on sait depuis [31] qu'il existe un état excité d'énergie $E + 2\hbar\omega$. Pour cet état on a (Chapitre 1, Article I) :

$$P(R) = \frac{2}{\Gamma(s+2)}\left(\frac{R}{a_{ho}}\right)^{2s+1} e^{-\left(\frac{R}{a_{ho}}\right)^2}\left[\left(\frac{R}{a_{ho}}\right)^2 - (s+1)\right]^2. \tag{54}$$

Venons-en à la comparaison avec les résultats numériques publiés dans [28], dont les fichiers nous ont été envoyés par J. von Stecher.

Pour $N = 4$, l'énergie obtenue numériquement est : $E = 5.028\,\hbar\omega$ [28]. [8] L'équation (52) donne alors $s = 2.528$, ce qui permet de tracer $P(R)$ pour l'état fondamental d'après la formule analytique (53). L'accord avec le $P(R)$ calculé numériquement est excellent (Figure 6). Nous avons

6. Pour 3 particules dans un piège, la méthode Monte-Carlo de [42] est d'ailleurs en bon accord avec la valeur (32) du pseudopotentiel.

7. La probabilité pour que $A < R < B$ est donc $\int_A^B dR\, P(R)$,
et $P(R') = \int |\Phi(\vec{r}_1, \ldots, \vec{r}_N)|^2\, \delta(R' - R)\, d\vec{r}_1 \ldots d\vec{r}_N$ où R est donné par l'équation (51).

8. Ces calculs sont restreints au sous-espace de moment cinétique total $L = 0$. Cet état est donc l'état fondamental dans ce sous-espace, mais pas nécessairement l'état fondamental absolu. Les résultats analytiques (52,53,54) restent applicables dans ce cas.

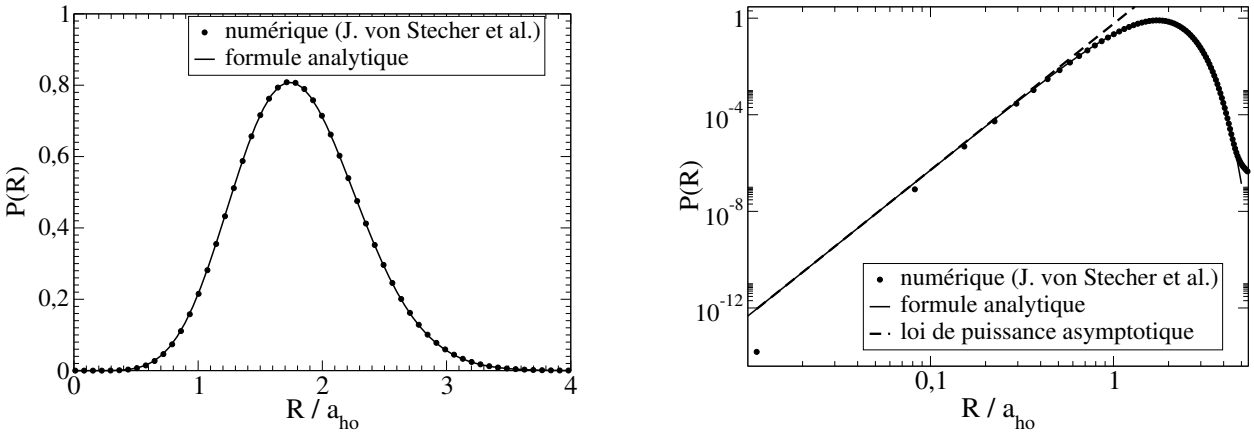

FIGURE 6 – Pour $N = 4$ fermions piégés, distribution de probabilité $P(R)$ de l'hyperrayon, dans l'état fondamental du secteur $l = 0$. Trait plein : formule analytique obtenue pour le pseudopotentiel, pour la valeur de l'énergie $E = 5.028\,\hbar\omega$ calculée numériquement [28]. Points : résultats numériques [28]. Dans le graphe de droite en échelle logarithmique, la droite tiretée est la loi de puissance équivalente pour $R \to 0$ à la formule analytique.

également tracé le résultat en échelle logarithmique (graphe de droite de la Figure), avec la loi de puissance équivalente pour $R \ll a_{\rm ho}$ à la formule analytique (53) :

$$P(R) \underset{R\to 0}{\sim} R^{2s+1}\,\frac{2}{\Gamma(s+1)}. \tag{55}$$

La formule analytique (53) est exacte pour le pseudopotentiel. Pour un modèle de portée finie b, on s'attend à ce qu'elle soit valable pour $R \gg b$. La formule (55) doit donc s'appliquer pour $b \ll R \ll a_{\rm ho}$. C'est bien ce que l'on observe sur le graphe de droite de la Figure 6, les calculs numériques étant effectués pour un potentiel d'interaction gaussien $V(r) \propto e^{-r^2/(2b^2)}$ de portée $b = 0.01\ a_{\rm ho}$.

Numériquement on trouve qu'il existe un état excité d'énergie E', telle que $E' - E = 2.003\,\hbar\omega$, ce qui est proche du résultat exact $2\hbar\omega$ valable pour le pseudopotentiel. La distribution de probabilité de l'hyperrayon $P(R)$ pour cet état est en bon accord avec la formule (54), cf. Figure 7.

Pour un nombre de particules plus grand, D. Blume *et al.* ont effectué des calculs numérique par une méthode Monte-Carlo à nœuds fixés. L'accord avec la formule analytique (53) est satisfaisant pour l'état fondamental à $N = 17$ particules, cf. Figure 8. On peut en déduire que le biais résultant du choix de la surface nodale ainsi que l'effet de la portée finie des interactions sont assez faibles. Cela constitue une vérification assez précise de l'hypothèse d'universalité.

3 Trois bosons pour $|a| = \infty$.

Considérons maintenant N particules bosoniques identiques sans spin, de fonction d'onde $\Phi(\vec{r}_1, \ldots, \vec{r}_N)$ symétrique. Pour $N = 2$ particules, toute la Section 1 s'applique [il faut simplement symétriser les états de diffusion ayant le comportement asymptotique (3) pour obtenir les états de diffusion physiques]. Mais dans le cas $N = 3$ considéré dans la suite, la situation change dramatiquement.

Dans cette Section la longueur de diffusion est infinie.

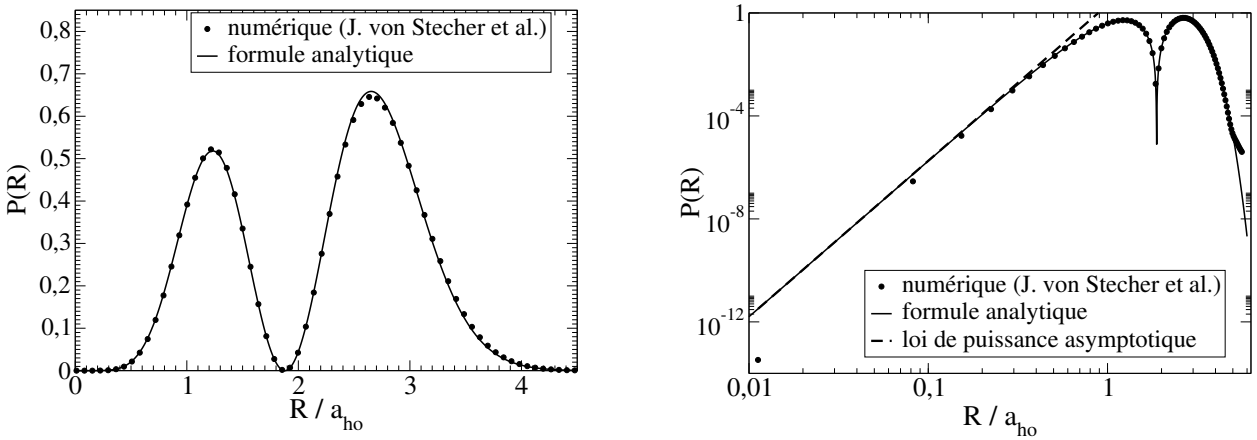

FIGURE 7 – Mêmes quantités que la Figure 6, pour un état *excité* à $N = 4$ particules, dont l'énergie calculée numériquement [28] vaut $E' = E + 2.003\hbar\omega$, conformément au résultat analytique $E' = E + 2\hbar\omega$ valable pour le pseudopotentiel.

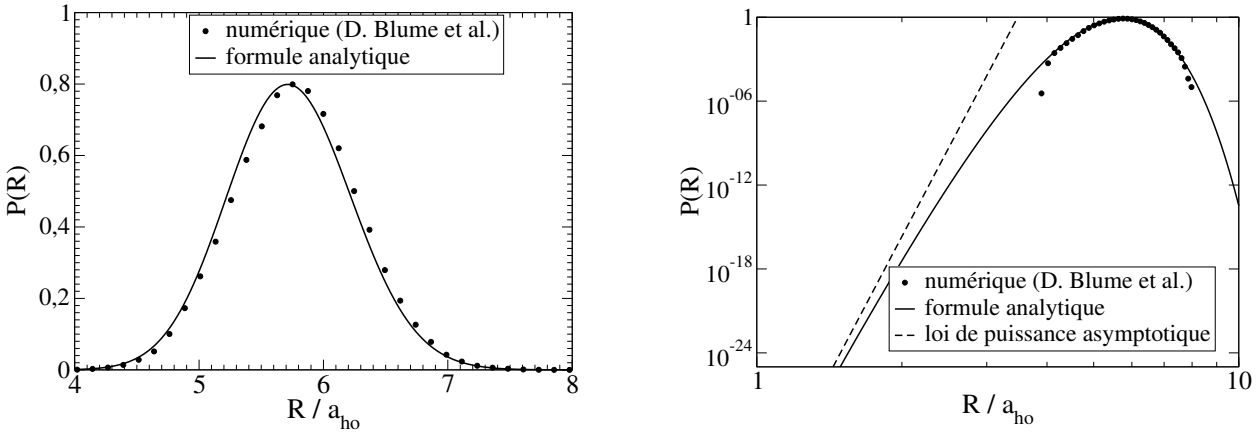

FIGURE 8 – Mêmes quantités que la Figure 6, pour l'état fondamental à $N = 17$ particules. Les valeurs numériques sont obtenues par une méthode Monte-Carlo à nœuds fixés, l'énergie obtenue étant $E = 34.64(12)\hbar\omega$ [28].

3.1 Trimères dans l'espace libre

Commençons par nous placer dans l'espace libre.

3.1.a Effet de Thomas

De façon générale, il existe alors des trimères (i.e. des états propres d'énergie négative). Pour un modèle d'interaction donné de portée b, l'énergie d'un trimère doit, par analyse dimensionnelle, être égale à une constante négative fois $\hbar^2/(mb^2)$, et donc tendre vers $-\infty$ lorsque $b \to 0$. Ceci est appelé effet de Thomas. Le travail original publié par L. H. Thomas en 1935 [60] concerne un potentiel d'interaction général de longueur de diffusion positive, et démontre l'existence d'un trimère en utilisant une fonction d'onde variationnelle non triviale, remarquablement semblable à la fonction d'onde d'Efimov. Mais si l'on considère un modèle donné d'interaction, une fonction d'onde variationnelle simple suffit souvent à conclure.

Un cas particulièrement simple est celui d'un modèle sur réseau, où l'on peut prendre un Ansatz où les N bosons sont localisés sur le même site du réseau ([58], note 10). Pour la version bosonique du modèle de Hubbard,

$$H = -t \sum_{\substack{\vec{i},\vec{j} \in \mathbb{Z}^3 \\ \|\vec{i}-\vec{j}\|=1}} c_{\vec{i}}^\dagger c_{\vec{j}} + 6t\hat{N} + \frac{\mathcal{U}}{2} \sum_{\vec{i}} n_{\vec{i}}(n_{\vec{i}} - 1), \tag{56}$$

avec comme dans le cas fermionique présenté ci-dessus, $t = \frac{\hbar^2}{2mb^2}$ et $\mathcal{U}/t = -7.914\ldots$, on trouve ainsi une énergie variationnelle par particule

$$\frac{E}{N} = \frac{\hbar^2}{2mb^2}\left(6 - \frac{N-1}{2}\left|\frac{\mathcal{U}}{t}\right|\right) \underset{b\to 0}{\to} -\infty \tag{57}$$

pour $N \geq 3$.

Dans le cas d'un potentiel d'interaction attractif, l'Ansatz suivant permet souvent d'obtenir une énergie négative [61, 50] :

$$\Phi(\vec{r}_1, \vec{r}_2, \vec{r}_3) = \mathcal{N} \exp\left(-\frac{\sum_{i<j} r_{ij}^2}{2(yb)^2}\right), \tag{58}$$

où y est un paramètre variationnel et $\mathcal{N}$ est la normalisation. Pour le puits carré

$$V(r) = \begin{cases} -\frac{\hbar^2}{mb^2}\left(\frac{\pi}{2}\right)^2 & \text{si } r < b \\ 0 & \text{si } r > b, \end{cases} \tag{59}$$

nous trouvons que l'énergie moyenne E est minimale pour $y = 1.197\ldots$ et vaut

$$E = \frac{\hbar^2}{mb^2}(-0.1668\ldots) \underset{b\to 0}{\to} -\infty. \tag{60}$$

3.1.b États d'Efimov

En 1970, Efimov montra qu'il existe *une infinité* d'états liés à 3 corps, dont les énergies E_n tendent vers 0 comme une série géométrique :

$$\frac{E_n}{E_{n+1}} \underset{n\to\infty}{\longrightarrow} e^{2\pi/|s_0|} \simeq 515.04, \tag{61}$$

où $s_0 = i \cdot 1.00624\ldots$ est la solution imaginaire de l'équation transcendante :

$$-s\cos\left(s\frac{\pi}{2}\right) + \frac{8}{\sqrt{3}}\sin\left(s\frac{\pi}{6}\right) = 0. \tag{62}$$

Afin d'illustrer cet effet, considérons d'abord un modèle particulier d'interaction entre particules, le potentiel séparable de portée b défini par (37,38). Ce modèle présente l'avantage que le problème à 3 corps est soluble numériquement, le calcul du spectre dans l'espace libre étant particulièrement aisé (cf. Appendice C). Pour les trois premiers états nous obtenons :

$$\begin{aligned} E_1^{\rm sep} &= -0.090475\frac{\hbar^2}{mb^2} \\ E_2^{\rm sep} &= -1.6506\cdot 10^{-4}\,\frac{\hbar^2}{mb^2} \\ E_3^{\rm sep} &= -3.199\cdot 10^{-7}\,\frac{\hbar^2}{mb^2}. \end{aligned} \tag{63}$$

Le rapport

$$\frac{E_2^{\rm sep}}{E_3^{\rm sep}} = 516.0\ldots \tag{64}$$

est déjà proche de la valeur limite attendue (61).
Même le rapport

$$\frac{E_1^{\rm sep}}{E_2^{\rm sep}} \simeq 548 \tag{65}$$

est relativement proche de (61), ce qui est probablement une particularité du modèle de potentiel séparable.

3.1.c Pseudopotentiel et paramètre à 3 corps

Pour obtenir le résultat analytique (61), Efimov a utilisé le pseudopotentiel, défini comme pour les fermions par l'équation de Schrödinger (29) et la condition aux limites de Bethe-Peierls (30). Cependant, pour 3 bosons, pour que le pseudopotentiel soit auto-adjoint, il faut et il suffit d'ajouter une condition aux limites supplémentaire dans la limite où les 3 particules sont proches, i. e. lorsque l'hyperrayon R défini en (51) tend vers 0. Ce fait a été découvert par Danilov [62]. Cette condition aux limites dépend d'un *paramètre à 3 corps* R_t et s'écrit :

$$\Phi(\vec{r}_1,\vec{r}_2,\vec{r}_3) \underset{R\to 0}{\sim} R^{-2}\sin\left[|s_0|\ln\left(\frac{R}{R_t}\right)\right]\cdot A, \tag{66}$$

où la limite $R \to 0$ est prise en gardant fixés les vecteurs $(\vec{r}_i - \vec{C})/R$ et le centre de masse $\vec{C} = (\vec{r}_1+\vec{r}_2+\vec{r}_3)/3$, et où A est une fonction arbitraire des vecteurs $(\vec{r}_i-\vec{C})/R$ et de $\vec{C}$. Les interactions étant modélisées par le pseudopotentiel et la condition aux limites à la Danilov (66), la solution d'Efimov du problème à 3 corps conduit au spectre ([16],Chap. 3) :

$$E_q^{\rm PP} = -\frac{2\hbar^2}{mR_t^2}\exp\left(-q\frac{2\pi}{|s_0|} + \frac{2}{|s_0|}\arg\Gamma(1+s_0)\right),\ q\in\mathbb{Z}. \tag{67}$$

Ce spectre est une série géométrique. Notons que R_t est définit à une transformation $R_t \mapsto R_t e^{\pi/|s_0|}$ près, puisque cette transformation ne change pas la condition aux limites (66) et le spectre (67). Nous prenons par convention $1 \le R_t < e^{\pi/|s_0|} \simeq 22.7$.

Ce spectre est non borné inférieurement, ce qui paraît choquant au premier abord. Le fait que le spectre est non borné inférieurement a été découvert par Minlos et Faddeev [63], et ils pensaient que cela "discrédite quelque peu" le modèle du pseudopotentiel avec la condition aux limites à la Danilov [64]. Cependant, Efimov [16] comprit que ce modèle est bien correct, à condition de ne l'utiliser que dans son domaine de validité $|E| \ll \hbar^2/(mb^2)$, i. e. pour les états assez excités. Le résultat du pseudopotentiel (67) ne prédit donc rien sur l'état fondamental (pour lequel $|E| \sim \hbar^2/(mb^2)$), mais devient asymptotiquement exact pour les états très excités, ce qui implique (61).

Pour tout modèle de portée b, le spectre dans la limite $|E| \ll \hbar^2/(mb^2)$, i. e. $E \to 0^-$, coïncide donc exactement avec le spectre (67) du pseudopotentiel, et ce pour une valeur de R_t qui dépend du modèle. Par analyse dimensionnelle on a

$$R_t = c \cdot b \tag{68}$$

où c est une constante sans dimensions dépendante du modèle.

Pour le potentiel séparable, les conditions

$$\exists q / E_q^{\mathrm{PP}} \simeq E_3^{\mathrm{sep}} \tag{69}$$

et

$$\exists q / E_q^{\mathrm{PP}} \simeq E_2^{\mathrm{sep}} \tag{70}$$

donnent toutes les deux :

$$c \simeq 3.60. \tag{71}$$

3.1.d Cycle limite

Il existe une façon alternative de voir les choses, reposant sur la notion de cycle limite. Pour illustrer ceci, sur la Figure 9, les énergies E_i^{sep} donnés par (63) sont représentées en fonction de la portée b en traits pointillés. Les traits pleins sont la prédiction du pseudopotentiel (67), avec $R_t = c\,b$ et $c = 3.6$ (cf. ci-dessus). La prédiction du pseudopotentiel est exactement invariante par la transformation $b \mapsto b/e^{\pi/|s_0|}$, i. e. par une translation $-\ln b \mapsto -\ln b + \pi/|s_0|$. Le spectre du potentiel séparable est approximativement invariant par cette même transformation, comme on le voit clairement sur l'agrandissement de la partie (b) de la Figure ; plus précisément, si l'on considère l'ensemble du spectre du potentiel séparable dans des fenêtres

$$\begin{array}{rcl} b_0 e^{-n\pi/|s_0|} & > b > & b_0 e^{-(n+1)\pi/|s_0|} \\ E_{\min} & < E < & E_{\max} \end{array} \tag{72}$$

avec n entier, alors l'image contenue dans cette fenêtre converge dans la limite $n \to +\infty$ (la Fig. 9 (b) montre deux telles fenêtres successives). L'image limite ainsi obtenue est décrite exactement par le pseudopotentiel (avec $R_t = c\,b$, et $c \simeq 3.6$ pour le potentiel séparable). Ceci découle d'ailleurs de l'éq. (61). Contrairement au cas des fermions discuté dans la Section précédente, on n'a donc pas une convergence dans la limite de portée nulle $b \to 0$, mais on a un phénomène de *cycle limite* : le spectre, restreint à une fenêtre en énergie (72), devient log-périodique dans la limite $b \to 0$.

Sur le plan mathématique, l'effet d'Efimov a fait l'objet de plusieurs travaux, et est donc bien établi, même si de nombreux points, comme (61), n'ont pas à ce jour reçu de démonstration rigoureuse (cf. [65, 66, 67, 68] et les articles cités dans ces références).

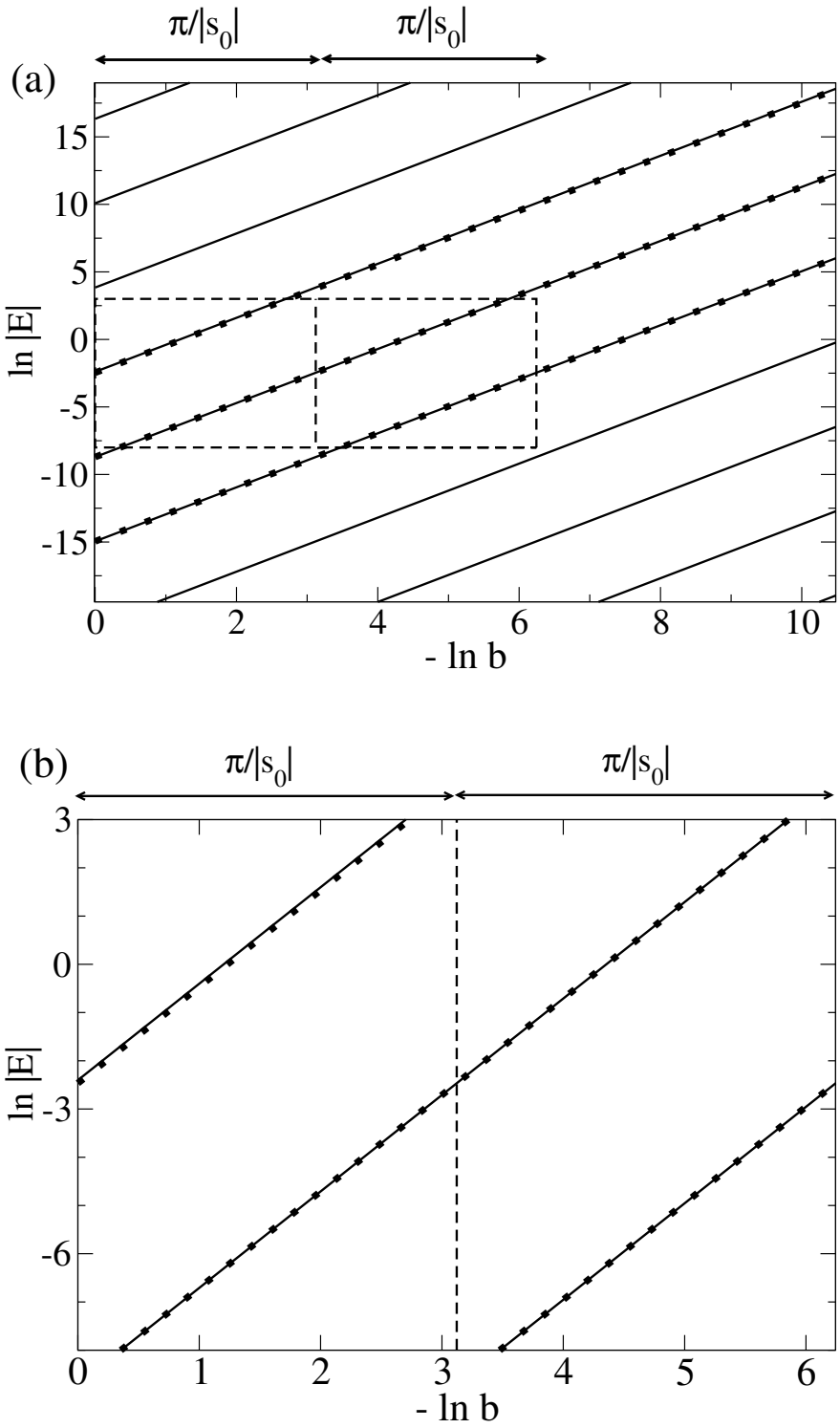

FIGURE 9 – énergies E des états liés à 3 bosons en fonction de la portée b. Lignes pointillées : les trois premiers états obtenus numériquement pour le potentiel d'interaction séparable. Lignes continues : prédiction analytique du pseudopotentiel pour un paramètre à trois corps R_t relié à b par $R_t = c \cdot b$, où nous avons choisi $c = 3.60$ pour reproduire au mieux les états excités du potentiel séparable. La prédiction du pseudopotentiel est périodique, celle du potentiel séparable est asymptotiquement périodique dans la limite $b \to 0$, si l'on se restreint à une fenêtre bornée en énergie. [Dans cette figure $\hbar = m = 1$, et E et b sont exprimés dans des unités E_u et b_u reliées par $E_u = (b_u)^{-2}$.]

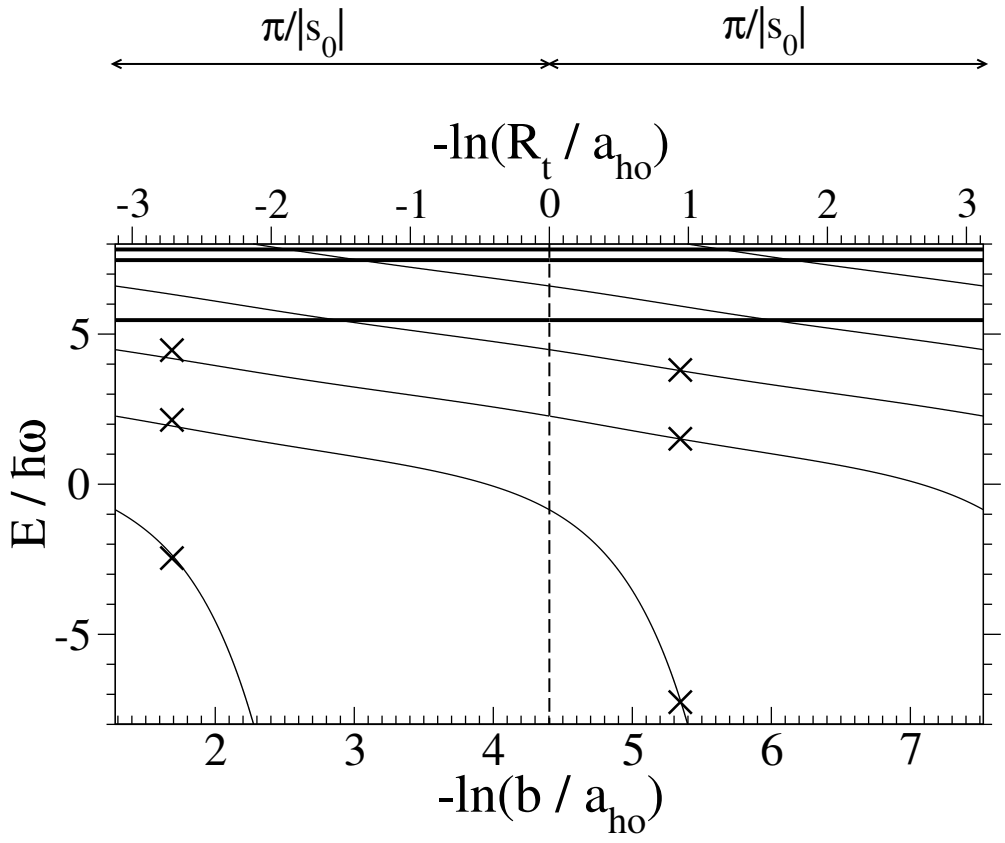

FIGURE 10 – Spectre pour 3 bosons piégés. Lignes continues : solution analytique du pseudopotentiel : états efimoviens en fonction du paramètre à 3 corps R_t (lignes fines) et états universels (lignes épaisses horizontales). Croix : quelques états propres du potentiel séparable, obtenus numériquement par Köhler et Stoll [1], en fonction de la portée b. Nous avons pris $R_t = 3.60\,b$, comme dans l'espace libre. Le potentiel séparable se rapproche du pseudopotentiel lorsque l'on passe de la fenêtre de gauche à la fenêtre de droite, c'est-à-dire lorsque b est divisé par $e^{\pi/|s_0|}$. Cela confirme l'existence d'un cycle limite.

3.2 Trois bosons piégés

Dans un piège harmonique isotrope, le problème de 3 bosons interagissant via le pseudopotentiel est exactement soluble (Article III, Chap. 3, [69]). Il existe deux types d'états propres : les états efimoviens qui dépendent du paramètre à 3 corps R_t, et les états universels qui n'en dépendent pas. Ces états sont représentés sur la Figure 10, où nous montrons également quelques états propres pour le potentiel séparable en fonction de la portée b, en prenant $R_t = 3.60\,b$ comme dans la Section précédente. On observe que les deux modèles se rapprochent lorsque $b \to 0$, ce qui indique que le phénomène de cycle limite se produit non seulement dans l'espace libre, mais aussi dans un piège.

Partie 1 : Le problème à N corps

Dans cette Partie, nous présentons des résultats exacts pour N particules en interaction résonnante dans un potentiel extérieur. Excepté dans l'Article II qui présente des théorèmes du viriel très généraux, nous supposerons que le potentiel extérieur est harmonique isotrope, et que les interactions sont à la limite unitaire, c'est-à-dire de longueur de diffusion infinie et de portée nulle.

Le Chapitre 1 contient une dérivation alternative très directe des résultats principaux de l'Article I.

Le Chapitre 2 contient des développements non publiés sur le cas où il existe, en plus de la résonance à 2 corps qui rend la longueur de diffusion infinie, une résonance à N corps.

L'Appendice B traite en détail du problème d'une particule dans un potentiel proportionnel à $1/r^2$, dont la compréhension est utile à celle du problème à N corps, des résonances à N corps, et du problème à 3 corps qui sera traité dans la Partie 2.

Chapitre 1

N particules à la limite unitaire dans un piège harmonique isotrope

1 Problème considéré

Considérons N particules de masses m_1, m_2, …, m_N.
Notons $P = \{(i,j); 1 \leq i < j \leq N\}$ l'ensemble des paires de particules.
Soit $I \subset P$.
Pour $(i,j) \notin I$, supposons qu'il n'y a pas d'interactions entre les particules i et j.
Pour $(i,j) \in I$, supposons que l'interaction entre les particules i et j est à la limite unitaire, i. e. de longueur de diffusion infinie et de portée nulle ; l'interaction est donc décrite exactement par le pseudopotentiel.
Notons que les résultats de ce Chapitre restent vrais en l'abscence d'interaction, i.e. pour $I = \{\}$.
Supposons de plus que les particules sont piégées dans un potentiel harmonique isotrope de pulsation ω.

Un état stationnaire d'énergie E_{tot} satisfait donc :

$$\begin{cases} \bullet\ H_{\text{tot}}\Phi(\vec{r}_1,\ldots,\vec{r}_N) = E_{\text{tot}}\,\Phi(\vec{r}_1,\ldots,\vec{r}_N) & (1.1) \\ \bullet\ \left.\dfrac{\partial(r_{ij}\Phi)}{\partial r_{ij}}\right|_{r_{ij}=0} = 0, & (1.2) \end{cases}$$

où

$$H_{\text{tot}} = \sum_{i=1}^{N}\left[-\frac{\hbar^2}{m_i}\Delta_{\vec{r}_i} + \frac{1}{2}m\omega^2\,{r_i}^2\right].$$

L'équation de Schrödinger (1.1) n'est valable que si aucun des r_{ij} n'est nul.
La condition aux limites de Bethe-Peierls (1.2) est valable pour $(i,j) \in I$ (i. e. si les particules i et j interagissent). La dérivée par rapport à r_{ij} est prise pour $\vec{R}_{ij} = (m_i\vec{r}_i + m_j\vec{r}_j)/(m_i+m_j)$ fixé, $\hat{r}_{ij} = \vec{r}_{ij}/r_{ij}$ fixé, et $(\vec{r}_k)_{k\notin\{i,j\}}$ fixé. On n'impose cette condition que lorsque $\vec{R}_{ij} \notin \{\vec{r}_k, k \notin \{i,j\}\}$, et lorsque tous les $\vec{r}_k$ sont distincts. [1]

Les particules peuvent obéir à une statistique arbitraire. Par exemple :

1. Une forme équivalente de cette condition aux limites est : $\exists A_{ij} / \Phi(\vec{r}_1,\ldots,\vec{r}_N) \underset{r_{ij}\to 0}{=} \frac{1}{r_{ij}}A_{ij}\left(\vec{R}_{ij},(\vec{r}_k)_{k\notin\{i,j\}}\right) + O(r_{ij})$, la limite $r_{ij}\to 0$ étant prise pour $\vec{R}_{ij}$ et $(\vec{r}_k)_{k\notin\{i,j\}}$ fixés. L'équivalence est vraie si Φ est assez régulier, ce qui devrait être le cas des lors que Φ satisfait l'équation de Schrödinger (1.1).

— Pour $N_\uparrow$ fermions de spin $\uparrow$ et $N_\downarrow$ fermions de spin $\downarrow$ (comme nous l'avons vu au Chapitre 0, Section 2) :

$$P_{ij}\,\Phi = -\Phi, \quad \forall (i,j) \in \{1,\dots,N_\uparrow\}^2 \cup \{N_\uparrow+1,\dots,N_\uparrow+N_\downarrow\}^2 \tag{1.3}$$

où P_{ij} est l'opérateur échangeant les particules i et j.

— Pour N bosons dans le même état de spin,

$$P_{ij}\,\Phi = \Phi, \quad \forall (i,j). \tag{1.4}$$

— Pour N_B bosons dans le même état de spin et N_F fermions dans le même état de spin,

$$\begin{cases} P_{ij}\,\Phi = \Phi & \forall (i,j) \in \{1,\dots,N_B\}^2 \quad (1.5) \\ P_{ij}\,\Phi = -\Phi & \forall (i,j) \in \{N_B+1,\dots,N_B+N_F\}^2. \quad (1.6) \end{cases}$$

— Pour N particules discernables, aucune contrainte n'est imposée.

Le choix de la statistique doit être compatible avec le choix de l'ensemble I des paires interagissantes. Par exemple, pour N bosons sans spin, toutes les paires interagissent ($I = \{1,\dots,N\}^2$) ou bien aucune paire n'interagit ($I = \{\,\}$) .

Comme toujours en mécanique quantique, on souhaite que le hamiltonien soit autoadjoint, i. e. que les états stationnaires forment une base orthonormée. Nous conservons la définition usuelle du produit scalaire dans $L^2(\mathbb{R}^{3N})$,

$$\langle \Phi_1 | \Phi_2 \rangle = \int d\vec{r}_1 \dots d\vec{r}_N \; \Phi_1(\vec{r}_1,\dots,\vec{r}_N)^* \; \Phi_2(\vec{r}_1,\dots,\vec{r}_N). \tag{1.7}$$

En effet, nous souhaitons décrire les états propres universels du pseudopotentiel, qui sont les limites de portée nulle des états propres d'un modèle de portée finie, et ces derniers sont orthogonaux pour le produit scalaire usuel. [2]

Remarque : L'équation de Schrödinger (1.1), la condition aux limites de Bethe-Peierls (1.2) et un choix de statistique tel que (1.3) suffisent-ils à définir un problème autoadjoint pour le produit scalaire usuel ?

La réponse dépend de la statistique, de l'ensemble I des paires interagissantes, et des rapports de masses m_i/m_j.

— *Cas 1* : Le problème est automatiquement autoadjoint, dès lors que l'on se limite aux états tels que $\langle \Phi | \Phi \rangle < \infty$. On pense notamment que c'est le cas pour des fermions de spin 1/2 de même masse. Pour $N = 3$, nous avons vérifié analytiquement, en nous restreignant au sous-espace de moment cinétique nul, que les états propres $|\Phi_n\rangle$ que nous avons obtenus sont orthogonaux, et nous avons vérifié pour un choix particulier de $|\Psi\rangle$ que la relation de fermeture $\sum_n \langle \Psi | \Phi_n \rangle \langle \Phi_n | \Psi \rangle = 1$ est satisfaite, cf. Chap. 3.

— *Cas 2* : Oui, à condition d'éliminer les résonances à p corps, $3 \le p \le N$. Pour ce faire, on se limite aux états propres suffisamment réguliers lorsque p particules sont proches. Plus précisément on impose que pour tout ensemble de particules $J \subset \{1,\dots,N\}$ comprenant p particules,

$$\Phi \underset{R_J \to 0}{=} O\left(\frac{1}{(R_J)^{\frac{3p-5}{2}}} \right) \tag{1.8}$$

2. Il existe des variantes du pseudopotentiel, non considérées ici, pour lesquelles le produit scalaire diffère du produit scalaire usuel. Ces modèles interviennent dans le contexte des résonances étroites [70, 71, 32, 72] ou des résonances dans l'onde p [73].

où $R_J \equiv \sqrt{\sum_{i,j\in J}(r_{ij})^2}$ est l'hyperrayon associé à l'ensemble de particules J. Ce "filtrage" est nécessaire dans le cas de mélanges de 2 espèces fermioniques sans spin (comprenant N_1 fermions de masse m_1 et N_2 fermions de masse m_2) si le rapport des masses $m_1/m_2 \in]8.62\ldots;13.6\ldots[$. Ceci résulte de la solution du problème à 3 corps obtenue par Efimov [74], ainsi que de la discussion du Chap. 2, où nous reviendrons sur ce problème des résonances à p corps et où nous montrerons comment les inclure dans le formalisme du pseudopotentiel.

— *Cas 3* : Il existe un effet d'Efimov. C'est le cas pour 3 bosons, 3 particules discernables ou encore pour 2 fermions de masse m_1 et une troisième particule de masse m_2 lorsque $m_1/m_2 > 13.6\ldots$. Dans ce cas, le problème ne devient autoadjoint que si l'on impose une condition aux limites supplémentaire pour $R \to 0$, qui fait intervenir un paramètre à 3 corps (cf. Partie 2), ce qui brise l'universalité et invalide les résultats de ce Chapitre. Cependant, les résultats de ce Chapitre sont valables si l'on se restreint au sous-espace des états universels ; on est alors ramené aux Cas 1 et 2. Par exemple, pour 3 bosons de même masse, le sous-espace des états universels appartient au Cas 1 (cf. Partie 2).

2 Séparation du centre de masse

Commençons par séparer le centre de masse. Notons qu'il existe également une variante de nos résultats où l'on ne sépare pas le centre de masse (cf. Article I). Dans ce Chapitre nous présentons la variante avec séparation du centre de masse, qui présente l'avantage d'être directement applicable au problème à 3 corps.

Rappelons que le problème considéré s'écrit :

$$\bullet H_{\rm tot}\Phi = E_{\rm tot}\Phi \tag{1.9}$$

$$\bullet \left.\frac{\partial(r_{ij}\Phi)}{\partial r_{ij}}\right|_{r_{ij}=0} = 0,\ \forall (i,j)\in I. \tag{1.10}$$

Comme dans l'Appendice A (page 63), posons

$$M = \sum_{i=1}^{N} m_i \tag{1.11}$$

$$\vec{C} = \frac{1}{M}\sum_{i=1}^{N} m_i\,\vec{r}_i \tag{1.12}$$

$$M_j = \sum_{i=1}^{j} m_i \tag{1.13}$$

$$\vec{C}_j = \frac{1}{M_j}\sum_{i=1}^{j} m_i\,\vec{r}_i \tag{1.14}$$

$$\mu_j = \frac{m_j M_{j-1}}{m_j + M_{j-1}} = \frac{m_j M_{j-1}}{M_j}, \tag{1.15}$$

et introduisons les coordonnées de type Jacobi :

$$\vec{\eta}_j = \vec{r}_j - \vec{C}_{j-1}, \tag{1.16}$$

en particulier

$$\vec{\eta}_2 = \vec{r}_2 - \vec{r}_1. \tag{1.17}$$

Soit la masse moyenne

$$m = M/N. \tag{1.18}$$

Définissons un vecteur $\vec{R} \in \mathbb{R}^{3N-3}$ regroupant les positions relatives des N particules :

$$\boxed{\vec{R} = \frac{1}{\sqrt{m}} \left(\sqrt{\mu_2}\,\vec{\eta}_2, \ldots, \sqrt{\mu_N}\,\vec{\eta}_N\right).} \tag{1.19}$$

Ainsi nous disposons de la bijection $(\vec{r}_1, \ldots, \vec{r}_N) \mapsto (\vec{R}, \vec{C})$.
On a alors [Appendice A, éq. (A.7)] :

$$H_{\text{tot}} = H_{\text{int}} + H_{\text{CM}} \tag{1.20}$$

avec

$$H_{\text{CM}} = -\frac{\hbar^2}{2M}\Delta_{\vec{C}} + \frac{1}{2}M\omega^2 C^2, \tag{1.21}$$

$$H_{\text{int}} = -\frac{\hbar^2}{2m}\Delta_{\vec{R}} + \frac{1}{2}m\omega^2 R^2. \tag{1.22}$$

La séparation du centre de masse consiste à prendre l'Ansatz :

$$\Phi(\vec{R}, \vec{C}) = \Psi_{\text{int}}(\vec{R})\Psi_{\text{CM}}(\vec{C}). \tag{1.23}$$

L'équation de Schrödinger (1.9) est satisfaite dès lors que :

$$E_{\text{tot}} = E_{\text{int}} + E_{\text{CM}}, \tag{1.24}$$

$$H_{\text{CM}}\Psi_{\text{CM}}(\vec{C}) = E_{\text{CM}}\Psi_{\text{CM}}(\vec{C}), \tag{1.25}$$

$$H_{\text{int}}\Psi_{\text{int}}(\vec{R}) = E_{\text{int}}\Psi_{\text{int}}(\vec{R}). \tag{1.26}$$

La condition aux limites de Bethe-Peierls (1.10) devient :

$$\left.\frac{\partial\left(r_{ij}\Psi_{\text{int}}(\vec{R})\right)}{\partial r_{ij}}\right|_{r_{ij}=0} = 0,\ \forall (i,j) \in I. \tag{1.27}$$

Le problème du centre de masse (1.25) est simplement un oscillateur harmonique tridimensionnel, de spectre $E_{\text{CM}} \in (3/2 + \mathbb{N})\hbar\omega$, de base propre bien connue.
Nous sommes donc ramenés à l'étude du problème interne (1.26,1.27) décrivant le mouvement relatif des N particules.
Une base d'états $\Phi(\vec{r}_1, \ldots, \vec{r}_N)$ complète dans $L^2(\mathbb{R}^{3N})$ est obtenue dès lors que l'on dispose d'une base d'états $\Psi_{\text{int}}(\vec{R})$ complète dans $L^2(\mathbb{R}^{3N-3})$.[3]

3 Coordonnées hypersphériques

Définissons l'hyperrayon par :

$$R = \|\vec{R}\|, \tag{1.28}$$

i.e.

$$R^2 = \sum_{i=1}^{N}\left(\vec{r}_i - \vec{C}\right)^2 = \frac{1}{N}\sum_{i<j} {r_{ij}}^2. \tag{1.29}$$

3. Cf. Eq. (A.10) p. 64.

Posons

$$\vec{\Omega} = \vec{R}/R. \tag{1.30}$$

Ce vecteur unitaire de $\mathbb{R}^{3N-3}$ peut être paramétré par $3N-4$ hyperangles :

$$\vec{\Omega} \mapsto (\alpha_2, \ldots, \alpha_{N-1}, \hat{\eta}_2, \ldots, \hat{\eta}_N)\,, \tag{1.31}$$

où $\hat{\eta}_i = \vec{\eta}_i/\eta_i$ et les $\alpha_i \in [0; \pi/2]$ sont définis par :

$$\begin{cases} \eta_2 \sqrt{\frac{\mu_2}{m}} = R \sin\alpha_2 \\ \eta_3 \sqrt{\frac{\mu_3}{m}} = R \cos\alpha_2 \sin\alpha_3 \\ \vdots \\ \eta_{N-1} \sqrt{\frac{\mu_{N-1}}{m}} = R \cos\alpha_2 \cos\alpha_3 \ldots \cos\alpha_{N-2} \sin\alpha_{N-1} \\ \eta_N \sqrt{\frac{\mu_N}{m}} = R \cos\alpha_2 \cos\alpha_3 \ldots \cos\alpha_{N-2} \cos\alpha_{N-1}. \end{cases} \tag{1.32}$$

Dans ces coordonnées hypersphériques $(R, \vec{\Omega})$, le hamiltonien interne s'écrit

$$H_{\text{int}} = -\frac{\hbar^2}{2m}\left(\frac{\partial^2}{\partial R^2} + \frac{3N-4}{R}\,\frac{\partial}{\partial R} + \frac{1}{R^2} T_{\vec{\Omega}}\right) + \frac{1}{2} m\omega^2 R^2, \tag{1.33}$$

où $T_{\vec{\Omega}}$ est un opérateur différentiel agissant sur $\vec{\Omega}$, appelé Laplacien sur l'hypersphère.

4 Séparabilité en coordonnées hypershpériques

L'invariance par changement d'échelle des conditions aux limites de Bethe-Peierls pour $a = \infty$ motive l'Ansatz :

$$\Psi_{\text{int}}(\vec{R}) = G(R)\,\phi(\vec{\Omega}). \tag{1.34}$$

L'équation de Schrödinger interne (1.26) se sépare en :

$$T_{\vec{\Omega}}\ \phi(\vec{\Omega}) = -\Lambda\,\phi(\vec{\Omega}), \tag{1.35}$$

$$\left[-\frac{\hbar^2}{2m}\left(\frac{d^2}{dR^2} + \frac{3N-4}{R}\,\frac{d}{dR} - \frac{\Lambda}{R^2}\right) + \frac{1}{2} m\omega^2 R^2\right] G(R) = E_{\text{int}}\, G(R). \tag{1.36}$$

Ici Λ est une constante, que l'on peut supposer réelle, car on peut prendre toutes les fonctions d'ondes réelles.

Supposons $N \geq 3$. La séparation est achevée en remarquant que les conditions aux limites de Bethe-Peierls ne portent que sur les hyperangles. Elles donnent donc lieu à des conditions aux limites sur la fonction $\phi(\vec{\Omega})$, et n'imposent aucune contrainte sur $G(R)$. [4]
Il suffit de vérifier ce fait pour la paire de particules $(i, j) = (1, 2)$, les autres cas s'en déduisant par renumérotation des particules. On vérifie d'abord que

$$\left.\frac{\partial}{\partial \alpha_2}\right|_{\alpha_2=0} = R\ \left.\frac{\partial}{\partial \eta_2}\right|_{\eta_2=0}, \tag{1.37}$$

4. À cet égard, le cas $N = 2$ est pathologique, car la condition de Bethe-Peierls est alors une condition aux limites pour $R \to 0$. Il s'agit d'un cas particulier des résonances à N corps traitées au Chapitre 2.

où la dérivée par rapport à α_2 est prise à $\alpha_3, \ldots, \alpha_N, \hat{\eta}_2, \ldots, \hat{\eta}_N$ fixés, et la dérivée par rapport à $\eta_2 = r_{12}$ est prise à $\eta_3, \ldots, \eta_N, \hat{\eta}_2, \ldots, \hat{\eta}_N$ fixés. On en déduit que la condition aux limites de Bethe-Peierls (1.27) pour $(i, j) = (1, 2)$ équivaut à :

$$\frac{\partial}{\partial \alpha_2} \left(\sin \alpha_2 \, \phi(\vec{\Omega}) \right)_{\alpha_2 = 0} = 0. \tag{1.38}$$

On s'est ramené à la résolution de deux problèmes séparés : le problème hyperradial (1.36), et le problème hyperangulaire défini par (1.35) et par une condition aux limites du type (1.38) pour chaque paire de particules interagissante.

5 Problème hyperangulaire

Le problème hyperangulaire a pour vecteurs propres les fonctions $\phi(\vec{\Omega})$ et pour valeurs propres les réels Λ. Les Λ forment un spectre discret. L'équation aux valeurs propres est (1.35), avec une condition aux limites du type (1.38) pour chaque paire $(i, j) \in I$ [plus précisément, pour chaque $(i, j) \in I$, la condition aux limites est obtenue à partir de (1.38) par la renumérotation $(1, 2) \mapsto (i, j)$].

Pour $N = 3$ particules, le problème hyperangulaire a été résolu analytiquement par Efimov [16, 74] (cf. Partie 3 pour une étude détaillée).

Pour $N \geq 4$ le problème n'a pas à ce jour été résolu analytiquement. Cependant, le spectre des Λ est relié très simplement au spectre des énergies propres du problème à N corps dans le piège, comme nous le verrons dans la Section suivante. On peut donc obtenir des informations sur les Λ grâce aux calculs numériques effectués dans un piège [28]. Pour $N \gg 1$, on peut utiliser l'approximation de densité locale pour exprimer le Λ minimal en fonction de l'énergie du gaz homogène, comme nous le verrons au Chapitre 4.

Remarque : Pour obtenir un problème autoadjoint, il est dans certains cas nécessaire d'exclure les résonances à p corps en imposant la condition (1.8). Pour $p < N$, cette condition peut se réécrire comme une condition aux limites sur les hyperangles, et ne concerne donc que le problème hyperangulaire. Pour $p = N$, cette condition ne concerne que le problème hyperradial, discuté ci-dessous.

6 Solution du problème hyperradial

Le problème hyperradial est donné par l'équation de Schrödinger hyperradiale (1.36). Les vecteurs propres sont les fonctions $G(R)$. Les valeurs propres sont les E_{int}, qui sont aussi les énergies propres du problème à N corps interne. Le problème hyperradial dépend du paramètre Λ, qui est une valeur propre du problème hyperangulaire.
On constante que le problème hyperradial est équivalent au problème d'une particule fictive se déplaçant en dimension $3N - 3$ dans un potentiel effectif

$$V_{\text{eff}}(R) = \frac{\hbar^2}{2m} \frac{\Lambda}{R^2} + \frac{1}{2} m \omega^2 R^2. \tag{1.39}$$

La masse de la particule fictive est m, la norme de son vecteur position est R, sa fonction d'onde, invariante par rotation, est $G(R)$, et son énergie est E_{int}.

Ce problème est résolu dans l'Appendice B. Comme dans la Partie 1 de l'Appendice B, ramenons-nous à 2 dimensions en posant :

$$G(R) = R^{-\frac{3N-5}{2}} F(R). \tag{1.40}$$

Le problème devient :

$$-\frac{\hbar^2}{2m}\left(F''(R) + \frac{1}{R}F'(R)\right) + \left(\frac{\hbar^2}{2m}\frac{s^2}{R^2} + \frac{1}{2}m\omega^2 R^2\right) F(R) = E_{\rm int}\, F(R), \tag{1.41}$$

avec

$$s^2 \equiv \Lambda + \left(\frac{3N-5}{2}\right)^2. \tag{1.42}$$

L'éq. (1.41) est l'équation de Schödinger pour une particule fictive se déplaçant en dimension 2 dans un potentiel effectif

$$U_{\rm eff}(R) = \frac{\hbar^2}{2m}\frac{s^2}{R^2} + \frac{1}{2}m\omega^2 R^2. \tag{1.43}$$

Notons que l'orthogonalité des états propres $\Phi(\vec{r}_1, \ldots, \vec{r}_N)$ du problème à N corps pour le produit scalaire usuel (1.7) implique l'orthogonalité des états propres $F(R)$ pour le produit scalaire

$$\{F_1|F_2\} = \int_0^\infty dR\, R\, F_1(R)\, F_2(R), \tag{1.44}$$

ce qui justifie l'hypothèse faite dans l'Appendice B.

Résumons la discussion de l'Appendice B. Pour simplifier la discussion nous supposons $s \neq 0$, le cas particulier $s = 0$ pouvant se traiter de façon analogue. On vérifie aisément que les fonctions R^s et R^{-s} sont des solutions de l'équation de Schrödinger (1.41) dans la limite où $R \to 0$. Une solution $F(R)$ de l'équation de Schrödinger satisfait donc

$$F(R) \underset{R\to 0}{\simeq} \alpha R^{-s} + \beta R^s. \tag{1.45}$$

La nature du problème dépend fortement du signe de s^2. Nous prenons la détermination suivante du signe de s :

$$\begin{cases} s \in \mathbb{R}_+ & \text{si } s^2 \in \mathbb{R}_+ \quad (1.46) \\ s \in i\,\mathbb{R}_+ & \text{si } s^2 \in \mathbb{R}_- \ . \quad (1.47) \end{cases}$$

Dans ce chapitre nous supposons $s \in \mathbb{R}_+$. Pour exclure les résonances à N corps, nous imposons que $F(R) \propto R^s$ pour $R \to 0$, ce qui signifie que $\alpha = 0$ dans (1.45), que $F(R)$ est bornée, et que $\Phi = O(1/R^{(3N-5)/2})$. Dans le cas où $s \geq 1$, cette condition est automatiquement satisfaite dès lors que l'on impose que $\langle\Phi|\Phi\rangle < \infty$, i. e. que $\{F|F\} < \infty$; en effet, R^{-s} est alors non normalisable au voisinage de $R = 0$ pour la norme $\{\}$. Dans le cas où $0 < s < 1$, R^{-s} est normalisable, mais nous imposons dans ce Chapitre que $\alpha = 0$ dans (1.45) ; en effet, autoriser $\alpha \neq 0$ reviendrait à considérer le cas d'une résonance à N corps, ce que nous ferons au Chap. 2.

Mentionnons que le cas $s^2 < 0$ survient pour $N = 3$ corps lorsqu'il existe un effet d'Efimov. L'exemple le plus simple est celui de 3 bosons, où il existe une valeur négative de s^2, $s^2 \simeq -(1.00624\ldots)^2$. Mais il existe également une infinité de valeurs positives de s^2 (rappelons que chaque valeur de s correspond à une solution du problème hyperangulaire). Les résultats qui suivent s'appliquent pour ces valeurs positives de s, correspondant au sous-espace des états universels. Une discussion complète du problème à 3 corps incluant les états d'Efimov fera l'objet du Chapitre 3.

Considérons le cas piégé : $\omega > 0$. La solution de l'équation de Schrödinger (1.41), dans le cas $s^2 \geq 0$ et avec la condition que F est bornée, est la suivante (cf. Appendice B, Tableau page 70,

lignes 1,2,6).
Pour chaque valeur de s, le spectre est

$$E_{\rm int} = (s+1+2q)\hbar\,\omega,\ q \in \mathbb{N}. \tag{1.48}$$

Le fait que le spectre comporte des niveaux équidistant de $2\hbar\omega$ peut aussi être obtenu à partir de l'existence d'une solution par changement d'échelle dans un piège harmonique dépendant du temps ([31],Article I).
Les fonctions d'ondes hyperradiales sont :

$$F_{s,q}(R) = \left(\frac{R}{a_{ho}}\right)^s e^{-\left(\frac{R}{a_{ho}}\right)^2/2} L_q^{(s)}\left(\left(\frac{R}{a_{ho}}\right)^2\right), \tag{1.49}$$

où $L_q^{(s)}$ désigne un polynôme de Laguerre généralisé de degré q [75, 76], et $a_{\rm ho} = \sqrt{\hbar/(m\omega)}$.
Les résultats (1.48,1.49) ont été obtenus indépendamment et avant nous par Shina Tan dans le cas particulier $q = 0$ [59].
Ces fonctions d'ondes satisfont la relation d'orthogonalité [75, 76] :

$$\{F_{s,q}\,|\,F_{s,q'}\} = (a_{ho})^2\,\delta_{q,q'}\,\frac{\Gamma(s+1+q)}{2\cdot q!}. \tag{1.50}$$

En résumé, les énergies propres sont de la forme

$$\boxed{E_{\rm tot} = (s+1+2q)\hbar\,\omega + E_{\rm CM}} \tag{1.51}$$

avec $q \in \mathbb{N}$. Les états propres sont de la forme

$$\boxed{\Phi(\vec{r}_1,\ldots,\vec{r}_N) = F(R)\,R^{-\frac{3N-5}{2}}\,\phi(\vec{\Omega})\,\Psi_{\rm CM}(\vec{C}),} \tag{1.52}$$

avec

$$\boxed{F(R) = \left(\frac{R}{a_{ho}}\right)^s e^{-\left(\frac{R}{a_{ho}}\right)^2/2} L_q^{(s)}\left(\left(\frac{R}{a_{ho}}\right)^2\right).} \tag{1.53}$$

Les résultats utilisés pour la comparaison avec les résultats numériques de la page 24 découlent du fait que la densité de probabilité de l'hyperrayon dans l'état (1.52) est

$$P(R) = \frac{R\,F(R)^2}{\int_0^\infty dR' R' F(R')^2}.$$

7 Lien avec le problème à N corps dans l'espace libre

Ci-dessus nous avons considéré le cas piégé : nous avons supposé que $\omega > 0$. Que se passe-t-il dans l'espace libre, i. e. pour $\omega = 0$? Tout ce qui précède l'éq. (1.48) reste valable, et la fonction d'onde pour le mouvement relatif reste séparable en coordonnées hypersphériques :

$$\Psi_{\rm int}(R,\vec{\Omega}) = F(R)\,R^{-\frac{3N-5}{2}}\,\phi(\vec{\Omega}). \tag{1.54}$$

Le problème hyperangulaire est indépendant de ω. On a donc les mêmes s et $\phi(\vec{\Omega})$ que dans le cas piégé.

Dans le problème hyperradial, le potentiel effectif vu par la particule fictive se déplaçant à 2 dimensions (1.43) se réduit à

$$U_{\text{eff}}(R) = \frac{\hbar^2}{2m}\frac{s^2}{R^2}. \tag{1.55}$$

Comme nous prenons la condition aux limites $F(R)$ bornée, il n'y a pas d'état lié pour la particule fictive, i. e. pas d'état lié à N corps (ceci peut changer dans le cas d'une résonance à N corps, cf. Chapitre 2). L'absence d'état lié peut d'ailleurs être justifiée plus simplement : l'énergie d'un état lié universel devrait être une fonction de $\hbar$ et m seulement, ce qui est impossible par analyse dimensionnelle.
On a donc un spectre continu, $E_{\text{int}} \in [0; +\infty[$.
Pour une énergie $E_{\text{int}} = 0$, la solution de l'équation de Schrödinger radiale (1.41) est :

$$F(R) = R^s. \tag{1.56}$$

[On peut d'ailleurs retrouver cette forme à partir de la solution du cas piégé (1.49) en prenant la limite $\omega \to 0$, i. e. $a_{\text{ho}} \to \infty$.]
On a donc un lien très simple entre les fonctions d'onde dans le piège et dans l'espace libre, d'après les éq. (1.53,1.56,1.54) :

$$F^{\text{piege}}(R)/F^{\text{espace libre}}(R) = \Psi_{\text{int}}^{\text{piege}}(R,\vec{\Omega})/\Psi_{\text{int}}^{\text{espace libre}}(R,\vec{\Omega}) = e^{-\left(\frac{R}{a_{ho}}\right)^2/2} L_q^{(s)}\left(\left(\frac{R}{a_{ho}}\right)^2\right). \tag{1.57}$$

On peut ainsi construire explicitement les états propres dans le cas piégé à partir des états propres d'énergie nulle dans l'espace libre, cf. Article I.
Pour $N = 3$, cela est une méthode possible pour construire les états propres dans le piège [77], les états propres dans l'espace libre étant connus depuis Efimov [16, 74].

8 Moments de l'énergie potentielle de piégeage

L'énergie potentielle de piégeage est définie par :

$$\hat{H}_{\text{trap}} = \frac{1}{2}m\omega^2 \sum_{i=1}^{N} {r_i}^2. \tag{1.58}$$

La relation

$$\hat{H}_{\text{trap}} = \frac{1}{2}m\omega^2(R^2 + NC^2), \tag{1.59}$$

permet de relier la densité de probabilité de H_{trap} à celles de R et de C, dont la forme est connue. Cela permet d'obtenir les relations suivantes sur les moments de H_{trap}, cf. Article I : [5]

— Pour l'état fondamental,

$$\langle (H_{\text{trap}})^n \rangle = E_0\big(E_0 + \hbar\omega\big)\ldots\big(E_0 + (n-1)\hbar\omega\big)/2^n, \tag{1.60}$$

où E_0 est l'énergie de l'état fondamental. [6]
En particulier, pour $n = 1$,

$$\langle H_{\text{trap}} \rangle = \langle H \rangle/2. \tag{1.61}$$

5. Ces relations s'obtiennent plus directement dans l'approche de l'Article I, où l'on ne sépare *pas* le centre de masse.

6. Cette relation est vraie non seulement pour l'état fondamental, mais aussi pour tout état propre d'énergie E_0 tel qu'il n'existe pas d'état propre d'énergie $E_0 - 2\hbar\omega$, i. e. pour un état situé en bas d'une échelle.

Cette relation est le théorème du viriel pour le gaz unitaire. Il est généralisé dans l'Article II, notamment au cas d'une longueur de diffusion finie et d'un piège non harmonique.

— à température non nulle, le théorème du viriel [éq. (1.61)] reste vrai, car il est vrai pour tout état propre.

Il existe également des relations sur les moments d'ordre supérieur de $H_{\rm trap}$. Pour le second moment, nous obtenons :

$$\langle (H_{\rm trap})^2 \rangle = \left[\langle H^2 \rangle + \langle H \rangle \hbar\omega \cdot \operatorname{cotanh}\left(\frac{\hbar\omega}{k_B T} \right) \right] /4. \tag{1.62}$$

Physiquement, cette relation décrit les fluctuations thermiques du mode de respiration du gaz, comme discuté au Chapitre 5.

Chapitre 2

Résonances à N corps

Dans ce Chapitre nous développons quelques idées sur la description des résonances à N corps, i. e. des situations où un état lié à N corps est sur le point d'apparaître ou de disparaître. [1]

1 Le cas $N = 2$

Commençons par le cas bien connu d'une résonance à 2 corps pour un système de 2 particules. Ce cas est décrit par le pseudopotentiel.

Dans un piège harmonique, le problème est alors défini par :
• La condition aux limites de Bethe-Peierls : il existe une fonction A telle que

$$\Phi(\vec{r}_1, \vec{r}_2) \underset{r\to 0}{=} A(\vec{C}) \left(\frac{1}{r_{12}} - \frac{1}{a} \right) + O(r), \tag{2.1}$$

la limite $r_{12} \to 0$ étant prise pour une position fixée du centre de masse $\vec{C}$ des deux particules.
• L'équation de Schrödinger, pour $r_{12} \neq 0$:

$$\sum_{i=1}^{2} \left[-\frac{\hbar^2}{m_i} \Delta_{\vec{r}_i} + \frac{1}{2} m\omega^2 \, r_i^2 \right] \Phi(\vec{r}_1, \vec{r}_2) = E_{\rm tot} \, \Phi(\vec{r}_1, \vec{r}_2). \tag{2.2}$$

Nous résolvons ce problème très directement dans le Chapitre 6, mais nous utilisons ici un formalisme légèrement différent, qui nous permettra ensuite de généraliser à $N \geq 3$.

Tout le formalisme du Chapitre 1, Sections 2, 3 et 4 reste applicable jusqu'à l'équation (1.36). Pour $N = 2$, les grandeurs introduites au Chap. 1 se réduisent à :

$$\mu_2 = \mu = \frac{m_1 m_2}{m_1 + m_2}, \tag{2.3}$$

$$m = \frac{m_1 + m_2}{2}, \tag{2.4}$$

$$\vec{\eta}_2 = \vec{r}_2 - \vec{r}_1 = \vec{r}, \tag{2.5}$$

$$\vec{R} = \sqrt{\frac{\mu}{m}} \, \vec{r}. \tag{2.6}$$

1. Ces idées sont également exposées brièvement dans la note 43 de l'Article I.

Le hyperangles sont simplement

$$\vec{\Omega} = \hat{r}, \tag{2.7}$$

et peuvent être paramétrés par les coordonnées sphériques

$$\vec{\Omega} \mapsto (\theta, \varphi). \tag{2.8}$$

Le centre de masse étant séparable,

$$\Phi(\vec{r}_1, \vec{r}_2) = \Psi_{\mathrm{CM}}(\vec{C})\Psi_{\mathrm{int}}(\vec{R}). \tag{2.9}$$

Ensuite, la nouveauté est que la condition de Bethe-Peierls ne porte que sur l'hyperrayon (alors qu'elle ne portait que sur les hyperangles dans le cas $N \geq 3$ et $a = \infty$ considéré dans la suite du Chap. 1).
On a donc toujours séparabilité en coordonnées hypersphériques :

$$\Psi_{\mathrm{int}}(\vec{R}) = G(R)\phi(\vec{\Omega}). \tag{2.10}$$

Le problème angulaire est :

$$T_{\vec{\Omega}}\phi(\vec{\Omega}) = -\Lambda\phi(\vec{\Omega}). \tag{2.11}$$

Pour $N = 2$, on a

$$T_{\vec{\Omega}} = -\hat{\vec{L}}^2, \tag{2.12}$$

où $\hat{\vec{L}} = \hat{\vec{r}} \times \hat{\vec{p}}$ et $\hat{\vec{p}} = \frac{\hbar}{i}\vec{\bigtriangledown}_{\vec{r}}$.
Les fonctions propres angulaires sont donc les harmoniques sphériques

$$\phi(\vec{\Omega}) = Y_L^m(\theta, \varphi) \tag{2.13}$$

avec $L \in \mathbb{N}$ et $m \in \{-L, \ldots, L\}$; et les valeurs propres associées sont

$$\Lambda = L(L+1). \tag{2.14}$$

Posant

$$G(R) = R^{-\frac{1}{2}}F(R), \tag{2.15}$$

le problème radial s'écrit :

$$-\frac{\hbar^2}{2m}\left(F''(R) + \frac{1}{R}F'(R)\right) + \left(\frac{\hbar^2}{2m}\frac{s^2}{R^2} + \frac{1}{2}m\omega^2R^2\right)F(R) = E_{\mathrm{int}}\,F(R), \tag{2.16}$$

avec

$$s = L + \frac{1}{2}. \tag{2.17}$$

Si l'on pose $m = \hbar = 1$, on retrouve le problème étudié au Chapitre B et résumé dans le tableau page 70. Il faut alors choisir l'une des conditions aux limites de la 2$^{\mathrm{e}}$ colonne du tableau, de façon à satisfaire la condition de Bethe-Peierls (2.1) qui peut se réécrire comme :

$$\exists A \in \mathbb{R}/\ F(R) \underset{R\to 0}{=} A \cdot \left(R^{-\frac{1}{2}} - \frac{1}{a}\sqrt{\frac{m}{\mu}}R^{\frac{1}{2}}\right) + O\left(R^{\frac{3}{2}}\right). \tag{2.18}$$

Pour $L \geq 1$, on a $s > 1$ et la seule condition aux limites possible (i. e. conduisant à une fonction d'onde normalisable) est :

$$F(R) \underset{R\to 0}{=} O(R^s) = O(R^{L+\frac{1}{2}}) = O(R^{\frac{3}{2}}), \tag{2.19}$$

ce qui satisfait automatiquement (2.18). On retrouve le fait que le pseudopotentiel n'a pas d'effet dans les ondes partielles $L \geq 1$.
Pour $L = 0$, on a $s = \frac{1}{2}$. La condition de Bethe-Peierls (2.18) est alors équivalente à la condition aux limites

$$\exists A \in \mathbb{R}/\ F(R) \underset{R\to 0}{=} A \cdot \left(R^{-s} - \frac{\epsilon}{l^{2s}} R^s\right) + O\left(R^{s+2}\right) \tag{2.20}$$

du tableau page 70, ligne 4 ; avec

$$\epsilon = \text{signe}(a), \tag{2.21}$$

$$l = |a|\sqrt{\mu/m}. \tag{2.22}$$

Dans l'espace libre, le tableau nous redonne les résultats bien connu : il existe un état lié si $a > 0$, et son énergie est

$$E = -\frac{\hbar^2}{2ml^2} = -\frac{\hbar^2}{2\mu a^2}. \tag{2.23}$$

Dans le piège on retrouve le spectre de Busch *et al.* [33], cf. éq. (6.3).

2 Généralisation à $N \geq 3$

Considérons maintenant le cas de $N \geq 3$ particules. Nous considérons le même problème qu'au Chap. 1, à savoir N particules dans un piège harmonique, chaque paire de particules ayant soit aucune interaction, soit une interaction à la limite unitaire décrite par le pseudopotentiel. Tout le formalisme du Chap. 1 s'applique jusqu'à l'éq. (1.47).
Au Chap. 1, nous prenions ensuite la condition aux limites $F(R) \underset{R\to 0}{=} O(1)$.
Pour tenir compte d'une résonance à N corps, prenons la condition aux limites (Tableau page 70, ligne 4) :

$$\exists A \in \mathbb{R}/\ F(R) \underset{R\to 0}{=} A \cdot \left(R^{-s} - \frac{\epsilon}{l^{2s}} R^s\right) + O\left(R^{s+2}\right). \tag{2.24}$$

Ceci généralise la condition de Bethe-Peierls à $N \geq 3$.
Cette approche n'est possible que si la fonction d'onde reste de carré sommable, i. e. si

$$0 \leq s < 1, \tag{2.25}$$

ce que nous supposons dans la suite. Une telle valeur de s est par exemple réalisée pour $N = 3$, avec 2 fermions de masse m_1 et une troisième particule de masse m_2, lorsque $m_1/m_2 \in]8.62\ldots; 13.6\ldots]$ [74].
On peut alors utiliser les résultats du tableau page 70 pour obtenir immédiatement, en fonction du paramètre l, l'énergie et la partie hyperradiale de la fonction d'onde pour l'état lié à N corps dans l'espace libre (s'il existe) et pour les états propres à N particules dans un piège harmonique isotrope. Ainsi, pour $0 < s < 1$, on obtient :

— Pour l'état lié à N corps, qui existe si $\epsilon = +1$:

$$E = -\frac{2\hbar^2}{m\, l^2}\left[\frac{\Gamma(1+s)}{\Gamma(1-s)}\right]^{\frac{1}{s}}, \tag{2.26}$$

$$F(R) = K_s\left(R\sqrt{-2E\frac{m}{\hbar^2}}\right). \tag{2.27}$$

— Pour les états propres dans un piège :

$$E \text{ est solution de : } \quad -\epsilon \cdot \left(\frac{\hbar}{m\omega\, l^2}\right)^s = \frac{\Gamma\left(\frac{1+s-E/(\hbar\omega)}{2}\right)\Gamma(-s)}{\Gamma\left(\frac{1-s-E/(\hbar\omega)}{2}\right)\Gamma(s)}, \tag{2.28}$$

$$F(R) = \frac{1}{R} W_{\frac{E}{2\hbar\omega}, \frac{s}{2}} \left(R^2 \frac{m\omega}{\hbar} \right). \tag{2.29}$$

En particulier, pour $l = \infty$, on est exactement sur la résonance à N corps, puisque l'énergie de l'état lié à N corps s'annule. Le spectre dans le piège est alors

$$E = (-s + 1 + 2q)\hbar\omega. \tag{2.30}$$

3 Perspectives

Notons que, bien souvent, on a $s \geq 1$, et dans ce cas il faudrait utiliser une approche similaire à celle développée par Ludovic Pricoupenko pour le cas des résonances à 2 corps en onde partielle non nulle, et introduire un produit scalaire modifié [73, 71].
Il serait également intéressant de vérifier que la présente théorie est bien la limite de portée nulle d'un modèle de portée finie. Cela n'a été vérifié que pour $N = 2$ [cf. Chap. 0] où la présente théorie est équivalente au pseudopotentiel.

Article I

Unitary gas in an isotropic harmonic trap : Symmetry properties and applications

PHYSICAL REVIEW A **74**, 053604 (2006)

Unitary gas in an isotropic harmonic trap: Symmetry properties and applications

Félix Werner and Yvan Castin
Laboratoire Kastler Brossel, École Normale Supérieure, 24 rue Lhomond, 75231 Paris Cedex 05, France
(Received 31 July 2006; revised manuscript received 15 September 2006; published 6 November 2006)

We consider N atoms trapped in an isotropic harmonic potential, with s-wave interactions of infinite scattering length. In the zero-range limit, we obtain several exact analytical results: mapping between the trapped problem and the free-space zero-energy problem, separability in hyperspherical coordinates, SO(2,1) hidden symmetry, existence of a decoupled bosonic degree of freedom, and relations between the moments of the trapping potential energy and the moments of the total energy.

DOI: 10.1103/PhysRevA.74.053604 PACS number(s): 03.75.Ss, 05.30.Jp

I. INTRODUCTION

Strongly interacting degenerate Fermi gases with two spin components are studied in present experiments with ultracold atoms [1]: by tuning the interaction strength between the atoms of different spin states *via* a Feshbach resonance, one can even reach the so-called unitary limit [2] where the interaction strength in the s-wave channel reaches the maximal amplitude allowed by quantum mechanics in a gas. More precisely, this means that the s-wave scattering amplitude between two particles reaches the value

$$f_k = -\frac{1}{ik} \tag{1}$$

for the relative momenta k that are relevant in the gas, in particular for k of the order of the Fermi momentum k_F of the particles. This implies that the s-wave scattering length a is set to infinity (which is done in practice by tuning an external magnetic field). This also implies that $k|r_e| \ll 1$, where r_e is the effective range of the interaction potential, a condition well satisfied in present experiments on broad Feshbach resonances.

The maximally interacting gas defined by these conditions is called the unitary gas [2]. It has universal properties since all the details of the interaction have dropped out of the problem. Theoretically, for spin-1/2 fermions with equal populations in the two spin states, equilibrium properties have been calculated in the thermodynamical limit in the spatially homogeneous case using Monte Carlo methods; at finite temperature [3–5], and at zero temperature with a fixed node approximation [6,7] or with a quantum Monte Carlo technique [8]. In practice, the unitary gases produced experimentally are stored in essentially harmonic traps, which raises the question of the effect of such an external potential. In this paper, we consider a specific aspect of this question: restricting to perfectly isotropic harmonic traps, but with no constraint on the relative spin populations, we show that the unitary quantum gas admits interesting symmetry properties that have measurable consequences on its spectrum and on the many-body wave functions. These properties imply that there is a mapping between the N-body eigenfunctions in a trap and the zero-energy N-body eigenfunctions in free space; the N-body problem is separable in hyperspherical coordinates; and there exist relations between the moments of the trapping potential energy and those of the total energy at thermal equilibrium.

A unitary Bose gas was not produced yet. This is related to the Efimov effect [9]: when three bosons interact with a short-range potential of infinite scattering length, an effective three-body attraction takes place, leading in free space to the existence of weakly bound trimers. This effective attraction generates high values of k so that the unitarity condition Eq. (1) is violated. It also gives a short lifetime to the gas by activating three-body losses due to the formation of deeply bound molecules [10–12]. In an isotropic harmonic trap, for three bosons, there exist Efimovian states [13,14], but there also exist eigenstates not experiencing the Efimov effect [13,15]. These last states are universal (in the sense that they depend only on $\hbar$, the mass m, and the oscillation frequency ω of an atom in the trap) and they are predicted to be long-lived [15]. The results of the present paper apply to all universal states, fermionic or bosonic, but do not apply to the Efimovian states. For spin-1/2 fermions, all states are expected to be universal [1–8,15,16].

II. OUR MODEL FOR THE UNITARY GAS

The physical system considered in this paper is a set of N particles of equal mass m (an extension to different masses is given in Appendix A). The particles are of arbitrary spin and follow arbitrary statistics; the Hamiltonian is supposed to be spin-independent so that the N-body wave function ψ that we shall consider corresponds to a given spin configuration [17]. The particles are trapped by the same isotropic harmonic potential and have a common oscillation frequency ω. We collect all the positions $\vec{r}_i$ of the particles in a single $3N$ component vector:

$$\vec{X} \equiv (\vec{r}_1, \ldots, \vec{r}_N). \tag{2}$$

Its norm

$$X = \|\vec{X}\| = \sqrt{\sum_{i=1}^{N} r_i^2} \tag{3}$$

is called the hyperradius. We will also use the unit vector

$$\vec{n} \equiv \vec{X}/X \tag{4}$$

(which may be parametrized by $3N-1$ hyperangles). The coordinates $(X, \vec{n})$ are called hyperspherical coordinates [18].

The total trapping potential energy simply writes

$$H_{\text{trap}} = \frac{1}{2} m\omega^2 X^2. \tag{5}$$

The interaction between the particles is assumed to be at the unitary limit defined in Eq. (1); one can then replace the interaction by contact conditions on the N-body wave function (this is a well established procedure, see, e.g., [16,19,20] and references therein): when the distance $r_{ij}=\|\vec{r}_j-\vec{r}_i\|$ between particles i and j tends to zero, there exists a function A such that

$$\psi(\vec{X}) \underset{r_{ij}\to 0}{=} \frac{\mathcal{A}(\vec{R}_{ij},\{\vec{r}_k:k\neq i,j\})}{r_{ij}} + O(r_{ij}), \tag{6}$$

where $\vec{R}_{ij}=(\vec{r}_i+\vec{r}_j)/2$ is the fixed center-of-mass position of particles i and j, and $\{\vec{r}_k:k\neq i,j\}$ are the positions of the other particles. In these contact conditions it is assumed that $\vec{R}_{ij}$ differs from all the $\vec{r}_k$'s, $k\neq i,j$, and that none of these $\vec{r}_k$'s coincide.

When none of the particle positions coincide, the stationary wave function ψ solves Schrödinger's equation, $H\psi=E\psi$, with the Hamiltonian

$$H = -\frac{\hbar^2}{2m}\Delta_{\vec{X}} + \frac{1}{2} m\omega^2 X^2. \tag{7}$$

At first sight, the eigenvalue problem $H\psi=E\psi$ is straightforward, since H takes the same expression as the Hamiltonian of a noninteracting gas. However, the mathematical difficulty and the physical effect of the interactions are contained in the contact conditions Eq. (6). Technically, this means that the domain of our Hamiltonian differs from the one of the ideal gas problem.

This model is expected to be exact for universal states in the limit of a zero range of the interaction potential [19]. To be more explicit, let us consider equal mass fermions of spin 1/2, interacting *via* a separable potential, in continuous space [14] or in a Hubbard-type lattice model [3–5,21], with an infinite scattering length. It is then believed that in the limit of a vanishing range of the interaction all the eigenenergies and eigenvectors converge to a well-defined limit, independent of the specific details of the model (hence the concept of universality), and that the values of the limits are given by the solutions of the above zero-range model. In this frame, it is natural to assume that the zero-range model defines a Hermitian Hamiltonian problem [22], a fact that may be checked explicitly for $N=3$ from the analytical solution [15].

III. SCALING PROPERTIES OF THE TRAPPED UNITARY GAS

A. What is scale invariance?

A fundamental property of the contact conditions Eq. (6) is their invariance by a rescaling of the spatial coordinates. More precisely, we define a rescaled wave function ψ_λ by

$$\psi_\lambda(\vec{X}) \equiv \psi(\vec{X}/\lambda), \tag{8}$$

where $\lambda>0$ is the scaling factor. Then, if ψ obeys the contact conditions, so does ψ_λ for any λ. Note that this property holds only because the scattering length is infinite (for a finite value of a, $1/r_{ij}$ in Eq. (6) would be replaced by $1/r_{ij}-1/a$, which breaks scale invariance). Since we are interested in universal states only, we assume that the domain of the Hamiltonian is also invariant by a spatial rescaling.

In free space (that is for $\omega=0$), this scale invariance implies the following property: if ψ is an eigenstate of energy E, then ψ_λ is an eigenstate of energy E/λ^2 for any λ [23]. This implies the absence of bound states in free space: otherwise the scaling transform would generate a continuum of states which are square integrable (after elimination of the center-of-mass variables), and this is forbidden for a Hermitian problem [24].

When $E=0$, one finds (see Appendix B) that the free space eigenstates can be assumed to be scale-invariant, i.e., there exists an exponent ν such that

$$\psi_\lambda(\vec{X}) = \lambda^{-\nu}\psi(\vec{X}). \tag{9}$$

Taking the derivative of this relation with respect to λ in $\lambda=1$, this shows that ψ is an eigenstate of the dilatation operator,

$$\hat{D} \equiv \vec{X}\cdot\partial_{\vec{X}}, \tag{10}$$

with the eigenvalue ν. This result is interesting for Sec. IV.

The presence of a harmonic trap introduces the harmonic oscillator length scale $a_{\text{ho}}=\sqrt{\hbar/m\omega}$, so that the eigenstates cannot be scale-invariant as in Eq. (9). However, if ψ obeys the contact condition, so do the ψ_λ's: as we shall see, this allows us to identify general properties of the eigenstates in the trap.

B. Scaling solution in a time dependent trap

We now assume that the curvature of the isotropic trap, while keeping a fixed value for all times $t\leqslant 0$, has an arbitrary time dependence at positive times. We call $\omega(t)$ the resulting time-dependent oscillation frequency of an atom in the trap.

Let us assume that, at $t\leqslant 0$, the system is in a stationary state of energy E. Then at positive times the wave function of the system will be deduced from the $t=0$ wave function by the combination of gauge and scaling transform [25]:

$$\psi(\vec{X},t) = \frac{e^{-iE\tau(t)/\hbar}}{\lambda(t)^{3N/2}} e^{imX^2\dot{\lambda}(t)/2\hbar\lambda(t)} \psi(\vec{X}/\lambda(t),0), \tag{11}$$

where the time-dependent scaling parameter obeys the Newton-like equation

$$\ddot{\lambda} = \frac{\omega^2(0)}{\lambda^3} - \omega^2(t)\lambda \tag{12}$$

with the initial conditions $\lambda(0)=1$, $\dot{\lambda}(0)=0$. We also introduced an effective time τ given by

$$\tau(t) = \int_0^t \frac{dt'}{\lambda^2(t')}. \tag{13}$$

This result may be extended to an arbitrary initial state as follows:

$$\psi(\vec{X},t) = \frac{1}{\lambda(t)^{3N/2}} e^{imX^2\dot{\lambda}(t)/2\hbar\lambda(t)} \tilde{\psi}(\vec{X}/\lambda(t), \tau(t)), \tag{14}$$

where $\tilde{\psi}$ evolves with the $t<0$ Hamiltonian [i.e., in the unperturbed trap with an oscillation frequency $\omega(0)$].

As shown by Rosch and Pitaevskii [26], the existence of such a scaling and gauge time-dependent solution is related to a SO(2,1) hidden symmetry of the problem. This we rederive in the two next subsections.

C. Existence of an undamped breathing mode

We consider the following gedanken experiment: one perturbs the gas in an infinitesimal way by modifying the trap frequency in a time interval $0<t<t_f$. After the excitation period ($t>t_f$), the trap frequency assumes its initial value $\omega(0)$. The scaling parameter then slightly deviates from unity, $\lambda(t)=1+\delta\lambda(t)$ with $|\delta\lambda| \ll 1$. Linearizing the equation of motion Eq. (12) in $\delta\lambda$, one finds that $\delta\lambda$ oscillates as

$$\delta\lambda(t) = \epsilon e^{-2i\omega t} + \epsilon^* e^{2i\omega t} + O(\epsilon^2), \tag{15}$$

where we set $\omega=\omega(0)$ to simplify the notation. The gedanken experiment has therefore excited an undamped breathing mode of frequency 2ω [26].

D. Raising and lowering operators, and SO(2,1) hidden symmetry

We now interpret the above undamped oscillation in terms of a property of the N-body spectrum of the system. Expanding Eq. (11) to first order in $\delta\lambda(t)$ leads to

$$\psi(\vec{X},t) = e^{i\alpha}[e^{-iEt/\hbar} - \epsilon e^{-i(E+2\hbar\omega)t/\hbar} L_+ + \epsilon^* e^{-i(E-2\hbar\omega)t/\hbar} L_-]\psi(\vec{X},0) + O(\epsilon^2) \tag{16}$$

(the phase α depends on the details of the excitation procedure). This reveals that the initial stationary state E was coupled by the excitation procedure to other stationary states of energies $E\pm 2\hbar\omega$. Remarkably, the wave function of these other states can be obtained from the initial one by the action of raising and lowering operators:

$$L_+ = +\frac{3N}{2} + \hat{D} + \frac{H}{\hbar\omega} - m\omega X^2/\hbar, \tag{17}$$

$$L_- = -\frac{3N}{2} - \hat{D} + \frac{H}{\hbar\omega} - m\omega X^2/\hbar. \tag{18}$$

Repeated action of L_+ and L_- will thus generate a ladder of eigenstates with regular energy spacing $2\hbar\omega$.

The hidden SO(2,1) symmetry of the problem then results from the fact that H, L_+, and L_- have commutation relations equal (up to numerical factors) to the ones of the Lie algebra of the SO(2,1) group, as was checked in [26]:

$$[H,L_+] = 2\hbar\omega L_+, \tag{19}$$

$$[H,L_-] = -2\hbar\omega L_-, \tag{20}$$

$$[L_+,L_-] = -4\frac{H}{\hbar\omega}. \tag{21}$$

Note that these commutation relations by themselves do not imply the existence of the hidden SO(2,1) symmetry. One has also to check that the operators L_+ and L_- preserve the domain of the Hamiltonian, that is, here the contact conditions Eq. (6) defining the unitary gas. The contact conditions are indeed preserved here [27].

From the general theory of Lie algebras, one may form the so-called Casimir operator which commutes with all the elements of the algebra, that is, with H and $L_\pm$; it is given by [26]

$$\hat{\mathcal{C}} = H^2 - \frac{1}{2}(\hbar\omega)^2(L_+L_- + L_-L_+). \tag{22}$$

Consider a ladder of eigenstates; as we will show later, the Hermiticity of H implies that the energy of a universal state is bounded from below, see Eq. (31), so that this ladder has a ground energy step, of value E_g. Within this ladder, the Casimir invariant assumes a constant value,

$$\mathcal{C} = E_g(E_g - 2\hbar\omega). \tag{23}$$

This allows us to express in an elegant way the operator H_g giving the ground-state energy of each ladder [28]:

$$H_g = \hbar\omega + [\hat{\mathcal{C}} + (\hbar\omega)^2]^{1/2}. \tag{24}$$

E. Existence of a bosonic degree of freedom

A physical interpretation of the SO(2,1) hidden symmetry is the following. Using the notations of the previous subsection, we define the operators b and $b^\dagger$ by

$$b = \left[\frac{\hbar\omega}{2(H+H_g)}\right]^{1/2} L_-, \tag{25}$$

$$b^\dagger = L_+\left[\frac{\hbar\omega}{2(H+H_g)}\right]^{1/2}. \tag{26}$$

Using the commutation relations of the SO(2,1) algebra and the expression of the Casimir operator, one may check that b and $b^\dagger$ obey a bosonic commutation relation:

$$[b,b^\dagger] = 1 \tag{27}$$

so that they may be interpreted as annihilation and creation operators for a bosonic degree of freedom of the unitary gas. Furthermore, the N-body Hamiltonian may be split as a sum of two commuting terms:

$$H = H_g + 2\hbar\omega b^\dagger b. \tag{28}$$

Excitation of this bosonic degree of freedom corresponds to an excitation of the breathing mode identified in Sec. III C.

In practice, this excitation may be due to an external change of the curvature of the trap (as in Sec. III C), but may also have a more intrinsic, thermal origin, as considered in Sec. V.

F. Virial theorem

Another application of the existence of raising and lowering operators is the virial theorem for the unitary gas. For a given eigenstate of H of energy E and real wave function ψ, $L_-|\psi\rangle$ is either zero (if ψ is the ground step of a ladder) or an eigenstate of H with a different energy. Assuming that H is Hermitian, this implies $\langle\psi|L_-|\psi\rangle=0$, and leads to [29,30]

$$\langle\psi|H|\psi\rangle = 2\langle\psi|H_{\text{trap}}|\psi\rangle. \tag{29}$$

At thermodynamical equilibrium, one thus has

$$\langle H\rangle = 2\langle H_{\text{trap}}\rangle, \tag{30}$$

that is, the total energy is twice the mean trapping potential energy. A direct consequence of this virial theorem is that the eigenenergy of a universal state is positive:

$$E \geqslant 0 \tag{31}$$

since the trapping potential energy is positive. Slightly better lower bounds are derived in Appendix C, see Eqs. (C7) and (C16) for $N>2$.

This virial theorem is actually also valid for an anisotropic harmonic trap (this result is due to Frédéric Chevy). One uses the Ritz theorem, stating that an eigenstate of a Hermitian Hamiltonian is a stationary point of the mean energy. As a consequence, the function of λ

$$E(\lambda) \equiv \frac{\langle\psi_\lambda|H|\psi_\lambda\rangle}{\langle\psi_\lambda|\psi_\lambda\rangle} = \lambda^{-2}\langle\psi|H-H_{\text{trap}}|\psi\rangle + \lambda^2\langle\psi|H_{\text{trap}}|\psi\rangle \tag{32}$$

satisfies $(dE/d\lambda)(\lambda=1)=0$, which leads to the virial theorem. This relies simply on the scaling properties of the harmonic potential, irrespective of its isotropy.

The proportionality between $\langle H\rangle$ and $\langle H_{\text{trap}}\rangle$ resulting from the virial theorem was checked experimentally [31].

IV. MAPPING TO ZERO-ENERGY FREE-SPACE EIGENSTATES

Usually, the presence of a harmonic trap in the experiment makes the theoretical analysis more difficult than in homogeneous systems. Here we show that, remarkably, the case of an isotropic trap for the unitary gas can be mapped exactly to the zero-energy free-space problem (which remains, of course, an unsolved many-body problem) [32].

More precisely, all the universal N-body eigenstates can be put in the unnormalized form:

$$|\psi_{\nu,q}\rangle = (L_+)^q e^{-\hat{X}^2/2a_{\text{ho}}^2}|\psi_\nu^0\rangle \tag{33}$$

and have an energy

$$E_{\nu,q} = (\nu+2q+3N/2)\hbar\omega, \tag{34}$$

where q is a non-negative integer, L_+ is the raising operator defined in Eq. (17), and ψ_ν^0 is a zero-energy eigenstate of the free-space problem which is scale-invariant:

$$\psi_\nu^0(\vec{X}/\lambda) = \psi_\nu^0(\vec{X})/\lambda^\nu \tag{35}$$

for all real scaling parameter λ, ν being the real scaling exponent [33].

We also show that the reciprocal is true, that is each zero-energy free-space eigenstate which is scale-invariant with a real exponent ν generates a semi-infinite ladder of eigenstates in the trap, according to Eqs. (33) and (34).

We note that Eq. (34) generalizes to excited states a relation obtained in [34] for the many-body ground state.

A. From a trap eigenstate to a free-space eigenstate

We start with an arbitrary eigenstate in the trap. By repeated action of L_- on this eigenstate, we produce a sequence of eigenstates of decreasing energies. According to the virial theorem Eq. (29), the total energy of a universal state is positive, see Eq. (31). This means that the sequence produced above terminates. We call ψ the last nonzero wave function of the sequence, an eigenstate of H with energy E that satisfies $L_-|\psi\rangle=0$. To integrate this equation, we use the hyperspherical coordinates $(X,\vec{n})$ defined in Eqs. (3) and (4). Noting that the dilatation operator is simply $\hat{D}=X\partial_X$ in hyperspherical coordinates, we obtain

$$\psi(\vec{X}) = e^{-X^2/2a_{\text{ho}}^2}X^{E/(\hbar\omega)-3N/2}f(\vec{n}). \tag{36}$$

Then one defines

$$\psi^0(\vec{X}) \equiv e^{X^2/2a_{\text{ho}}^2}\psi(\vec{X}). \tag{37}$$

One checks that this wave function obeys the contact conditions Eq. (6), since X^2 varies quadratically with r_{ij} at fixed R_{ij} and $\{\vec{r}_k, k\neq i,j\}$. ψ^0 is then found to be a zero-energy eigenstate in free space, by direct insertion into Schrödinger's equation. But one has also from Eqs. (36) and (37)

$$\psi^0(\vec{X}) = X^{E/(\hbar\omega)-3N/2}f(\vec{n}), \tag{38}$$

so that ψ^0 is scale-invariant, with a real exponent ν related to the energy E by Eq. (34). This demonstrates Eqs. (33) and (34) for $q=0$, that is, for the ground step of each ladder.

One just has to apply a repeated action of the raising operator L_+ on the ground step wave function to generate a semi-infinite ladder of eigenstates: this corresponds to $q>0$ in Eqs. (33) and (34). Note that the repeated action of L_+ cannot terminate since $L_+|\psi\rangle=0$ for a nonzero ψ implies that ψ is not square-integrable.

B. From a free-space eigenstate to a trap eigenstate

The reciprocal of the previous subsection is also true: starting from an arbitrary zero-energy free-space eigenstate that is scale-invariant, one multiplies it by the Gaussian factor $\exp(-X^2/2a_{\text{ho}}^2)$, and one checks that the resulting wave function is an eigenstate of the Hamiltonian of the trapped system, obeying the contact conditions [35]. Applying L_+ then generates the other trap eigenstates of a ladder.

C. Separability in hyperspherical coordinates

Let us reformulate the previous mapping using the hyperspherical coordinates $(X,\vec{n})$ defined in Eqs. (3) and (4). A

free-space scale-invariant zero-energy eigenstate takes the form $\psi^0(\vec{X})=X^\nu f_\nu(\vec{n})$, and the universal eigenstates in the trap have an unnormalized wave function

$$\psi_{\nu,q}(\vec{X}) = X^\nu e^{-X^2/2a_{\rm ho}^2} L_q^{(\nu-1+3N/2)}(X^2/a_{\rm ho}^2) f_\nu(\vec{n}), \qquad (39)$$

where $L_q^{(\cdot)}$ is the generalized Laguerre polynomial of degree q. This is obtained from the repeated action of L_+ in Eq. (33) and from the recurrence relation obeyed by the Laguerre polynomials:

$$(q+1)L_{q+1}^{(s)}(u) - (2q+s+1-u)L_q^{(s)}(u) + (q+s)L_{q-1}^{(s)}(u) = 0. \qquad (40)$$

We have thus separated out the hyperradius X and the hyperangles $\vec{n}$. The hyperangular wave functions $f_\nu(\vec{n})$ and the exponents ν are not known for $N\geqslant 4$. However, we have obtained the hyperradial wave functions, i.e., the X dependent part of the many-body wave function. A more refined version of these separability results can be obtained by first separating out the center of mass (see Appendix C), but this is not useful for the next section.

V. MOMENTS OF THE TRAPPING POTENTIAL ENERGY

A. Exact relations

As an application of the above results, we now obtain the following exact relations on the statistical properties of the trapping potential energy, relating its moments to the moments of the full energy, when the gas is at thermal equilibrium [36]. For the definition of the trapping potential energy, see Eq. (5).

At zero temperature, its moments as a function of the ground-state energy E_0 are given by

$$\langle (H_{\rm trap})^n \rangle = E_0(E_0+\hbar\omega)\cdots(E_0+(n-1)\hbar\omega)/2^n. \qquad (41)$$

At finite temperature T, the first moment is given by the virial theorem

$$\langle H_{\rm trap} \rangle = \langle H \rangle /2 \qquad (42)$$

and the second moment by

$$\langle (H_{\rm trap})^2 \rangle = \left[\langle H^2 \rangle + \langle H \rangle \hbar\omega \,\mathrm{cotanh}\left(\frac{\hbar\omega}{k_B T}\right)\right]/4. \qquad (43)$$

B. Derivation from the separability

The zero temperature result Eq. (41) follows directly from Eq. (39): for $q=0$, the Laguerre polynomial is constant so that the probability distribution of X is a power law times a Gaussian; the moments are then given by integrals that can be expressed in terms of the Γ function.

For finite T, the idea of our derivation is the following: the hyperradial part of the N-body wave function $\psi_{\nu,q}$ is known from Eq. (39); and thus the probability distribution of X in the state $|\psi_{\nu,q}\rangle$ is known, in terms of ν,q. While the thermal distribution of q is simple, the one of ν is not, but ν is related to the total energy by Eq. (34).

We will need the intermediate quantities

$$B_{n,p}(q,s) \equiv \frac{\int_0^\infty du\, e^{-u} u^{s+n} L_{q+p}^{(s)}(u) L_q^{(s)}(u)}{\int_0^\infty du\, e^{-u} u^s [L_q^{(s)}(u)]^2}, \qquad (44)$$

where $s\geqslant 0$; n, q are non-negative integers; and p is an integer of arbitrary sign. These quantities can be calculated with the $n=0$ "initial" condition $B_{0,p}=\delta_{0,p}$ and the recurrence relation

$$B_{n+1,p} = -(q+p+1)B_{n,p+1} + [2(q+p)+s+1]B_{n,p} - (q+p+s)B_{n,p-1} \qquad (45)$$

which follows from the recurrence relation Eq. (40) on Laguerre polynomials.

This allows us to calculate the moments of the trapping energy in the step q of a ladder of exponent ν, using Eq. (39):

$$\frac{\langle \psi_{\nu,q}|X^{2n}|\psi_{\nu,q}\rangle}{\langle \psi_{\nu,q}|\psi_{\nu,q}\rangle} = B_{n,0}(q,s) a_{\rm ho}^{2n}. \qquad (46)$$

Here we have set

$$s = \nu - 1 + 3N/2 \qquad (47)$$

in accordance with Eq. (39). We shall need the values of $B_{n,0}$ for $n\leqslant 2$:

$$B_{1,0}(q,s) = s + 2q + 1, \qquad (48)$$

$$B_{2,0}(q,s) = s^2 + s(6q+3) + 6q^2 + 6q + 2. \qquad (49)$$

Assuming thermal equilibrium in the canonical ensemble, the thermal average can be performed over the statistically independent variables q and s. The moments of q are easy to calculate, because of the ladder structure with equidistant steps:

$$\langle q^n \rangle = \frac{\sum_{q=0}^{+\infty} q^n e^{-2q\hbar\omega/k_B T}}{\sum_{q=0}^{+\infty} e^{-2q\hbar\omega/k_B T}}. \qquad (50)$$

The moments of s are not known exactly but they can be eliminated in terms of the moments of the total energy E and of the moments of q using the relation $E=(s+1+2q)\hbar\omega$. This leads to the exact relations (42) and (43). This method in principle allows us to calculate relations for moments of arbitrary given order, but the algebra becomes cumbersome.

C. Derivation from the existence of a bosonic degree of freedom

The relations Eqs. (42) and (43) may also be derived in a purely algebraic way by using the bosonic creation and annihilation operators of Sec. III E. Taking the sum of Eqs. (17) and (18) one expresses $H_{\rm trap}$ in terms of $L_\pm$ and H:

$$H_{\mathrm{trap}} = \frac{1}{2}H - \frac{\hbar\omega}{4}(L_+ + L_-). \tag{51}$$

Then from Eqs. (25) and (26) and Eq. (28) one can express $L_\pm$ and H as functions of the ladder ground energy operator H_g and $b, b^\dagger$. We finally obtain

$$H_{\mathrm{trap}} = \frac{1}{2}\hbar\omega A^\dagger A \quad \text{with} \quad A = \sqrt{\frac{H_g}{\hbar\omega} + b^\dagger b} - b. \tag{52}$$

In the calculation of the thermal averages $\langle H_{\mathrm{trap}}\rangle$ and $\langle (H_{\mathrm{trap}})^2\rangle$ it remains to take the expectation value over H_g and the bosonic degree of freedom, that may be considered as independent variables in the sense that, e.g.,

$$\langle H_g b^\dagger b\rangle = \langle H_g\rangle\langle b^\dagger b\rangle. \tag{53}$$

The calculation is simplified by the observation that the expectation value of the obtained terms with odd powers of b or $b^\dagger$ is exactly zero. One can use Wick's theorem to calculate the expectation value of $(b^\dagger b)^2$. One also eliminates the expectation value of H_g using Eq. (28). One obtains Eq. (42) for the first moment. For the second moment

$$4\langle (H_{\mathrm{trap}})^2\rangle = \langle H^2\rangle + \langle H\rangle\hbar\omega[2\langle b^\dagger b\rangle + 1]. \tag{54}$$

The Bose formula giving $\langle b^\dagger b\rangle$ finally leads to Eq. (43). This nicely shows how the last term of Eq. (43) originates from the thermal fluctuations of the bosonic degree of freedom, that is, of the breathing mode of the unitary gas.

VI. CONCLUSION

In this paper we have derived several exact properties of the unitary gas in an isotropic harmonic trap. The spectrum is formed of ladders; the steps of a ladder are spaced by an energy $2\hbar\omega$, and linked by raising and lowering operators. This property may be interpreted in terms of a hidden SO(2,1) symmetry [26] or in terms of the existence of a bosonic degree of freedom. This allows us to map the trapped problem to the free-space one. A lower bound on the energy of the universal states was derived, showing that the ladders are actually semi-infinite ladders. A related property is that the problem is separable in hyperspherical coordinates. The hyperradial part of the stationary state wave functions is thus known. This allows us to derive exact relations between the moments of the trapping potential energy and the moments of the total energy. The relation between the first moments is the virial theorem; the relation between the second moments may be useful for thermometry, as will be studied elsewhere.

ACKNOWLEDGMENTS

We thank F. Chevy, J. Dalibard, S. Nascimbène, L. Pricoupenko, J. Thomas, and C.-F. Vergu for very useful discussions. L.K.B. is a *Unité de Recherche de l'ENS et de l'Université Paris 6, associated with* CNRS. Our research group is a member of IFRAF.

APPENDIX A: EXTENSION TO PARTICLES WITH DIFFERENT MASSES

All our results remain valid if the particles have different masses $m_1, \ldots, m_N$; provided that the oscillation frequency ω remains the same for all the particles. We define a mean mass:

$$m \equiv \frac{m_1 + \cdots + m_N}{N}. \tag{A1}$$

The definition of $\vec{X}$ and X, given by Eqs. (2) and (3) for equal masses, has to be generalized to

$$\vec{X} \equiv \left(\sqrt{\frac{m_1}{m}}\vec{r}_1, \ldots, \sqrt{\frac{m_N}{m}}\vec{r}_N\right), \tag{A2}$$

$$X \equiv \|\vec{X}\| = \sqrt{\sum_{i=1}^{N}\frac{m_i}{m}r_i^2}. \tag{A3}$$

With this new definition of X, the trapping potential energy is still given by Eq. (5).

In the definition of the zero-range model, the contact conditions Eq. (6) remain unchanged, except that the fixed center-of-mass position of particles i and j is now $\vec{R}_{ij} \equiv (m_i\vec{r}_i + m_j\vec{r}_j)/(m_i + m_j)$.

In Appendix C, the center-of-mass position has to be redefined as

$$\vec{C} = \frac{(m_1\vec{r}_1 + \cdots + m_N\vec{r}_N)}{(m_1 + \cdots + m_N)} \tag{A4}$$

and the internal hyperangular coordinates become

$$R = \sqrt{\sum_{i=1}^{N}\frac{m_i}{m}(\vec{r}_i - \vec{C})^2}, \tag{A5}$$

$$\vec{\Omega} = \left(\sqrt{\frac{m_1}{m}}\frac{\vec{r}_1 - \vec{C}}{R}, \ldots, \sqrt{\frac{m_N}{m}}\frac{\vec{r}_N - \vec{C}}{R}\right). \tag{A6}$$

With these modified definitions, all the results of this paper remain valid.

APPENDIX B: SCALE INVARIANCE OF THE ZERO-ENERGY FREE-SPACE EIGENSTATES

In this Appendix, we show that the zero-energy free-space eigenstates of the Hamiltonian may be chosen as being scale-invariant, that is as, eigenstates of the dilatation operator $\hat{D}$, under conditions ensuring the Hermiticity of the Hamiltonian.

Consider the zero-energy eigensubspace of the free-space Hamiltonian. This subspace is stable under the action of $\hat{D}$. If one assumes that $\hat{D}$ is diagonalizable within this subspace, the corresponding eigenvectors form a complete family of scale invariant zero-energy states. If $\hat{D}$ is not diagonalizable, we introduce the Jordan normal form of $\hat{D}$.

Let us start with the case of a Jordan normal form of dimension 2, written as

$$\mathrm{Mat}(\hat{D}) = \begin{pmatrix} \nu & 1 \\ 0 & \nu \end{pmatrix}, \tag{B1}$$

in the sub-basis $|e_1\rangle, |e_2\rangle$. The ket $|e_1\rangle$ is an eigenstate of $\hat{D}$ with the eigenvalue ν. We assume that the center-of-mass motion is at rest, with no loss of generality since it is separable in free space. Using the internal hyperspherical coordinates $(R, \vec{\Omega})$ defined in Appendix C, we find that $\hat{D}$ reduces to the operator $R\partial_R$. Integrating $R\partial_R e_1 = \nu e_1$ leads to

$$e_1(\vec{X}) = R^\nu \phi_1(\vec{\Omega}). \tag{B2}$$

The ket $|e_2\rangle$ is not an eigenstate of $\hat{D}$ but obeys $R\partial_R e_2 = \nu e_2 + e_1$, which, after integration, gives

$$e_2(\vec{X}) = R^\nu \ln R \phi_1(\vec{\Omega}) + R^\nu \phi_2(\vec{\Omega}). \tag{B3}$$

One can assume that ϕ_1 and ϕ_2 are orthogonal on the unit sphere (by redefining e_2 and ϕ_2). It remains to use the fact that both e_1 and e_2 are zero-energy free-space eigenstates. From the form of the Laplacian in hyperspherical coordinates in $d=3N-3$ dimensions, see Eq. (C5), the condition $\Delta_{\vec{X}} e_1 = 0$ leads to

$$T_{\vec{\Omega}} \phi_1 = -\nu(\nu + d - 2)\phi_1. \tag{B4}$$

The condition $\Delta_{\vec{X}} e_2 = 0$ then gives $T_{\vec{\Omega}} \phi_2 = -\nu(\nu+d-2)\phi_2 - (2\nu+d-2)\phi_1$, which leads to the constraint [37]

$$\nu = 1 - d/2. \tag{B5}$$

At this stage, for this "magic" value of ν, it seems that there may exist non-scale-invariant zero-energy eigenstates.

To proceed further, one has to check for the Hermiticity of the free-space Hamiltonian. This requires a reasoning at arbitrary, nonzero energy. We use the fact that the following wave function obeys the contact conditions:

$$\psi(\vec{X}) = u(R) R^\nu \phi_1(\vec{n}), \tag{B6}$$

where $u(R)$ is a function with no singularity, except maybe in $R=0$ [38]. Using again the expression of the Laplacian in internal hyperspherical coordinates, one finds that ψ is an eigenstate of the free-space Hamiltonian if $u(R)$ is an eigenstate of

$$\hat{h} = -\frac{\hbar^2}{2m}(\partial_R^2 + R^{-1}\partial_R). \tag{B7}$$

One checks that Hermiticity of the free-space Hamiltonian for the wave function ψ implies Hermiticity of $\hat{h}$ for the wave function $u(R)$. Note that $\hat{h}$ is simply the free-space Hamiltonian for 2D isotropic wave functions. It is Hermitian over the domain of wave functions $u(R)$ with a noninfinite limit in $R=0$. Including the ket $|e_2\rangle$ in the domain of the N-body free-space Hamiltonian amounts to allowing for wave functions $u(R)$ that diverge as $\ln R$ for $R \to 0$: this breaks the Hermiticity of $\hat{h}$, since this leads to a (negative energy) continuum of square integrable eigenstates of $\hat{h}$,

$$u_\kappa(R) = K_0(\kappa R) \tag{B8}$$

with eigenenergy $-\hbar^2\kappa^2/2m$, for all $\kappa > 0$. Here $K_0(x)$ is a modified Bessel function of the second kind. Hermiticity may be restored by a filtering of this continuum [40], adding the extra contact condition $u(R) = \ln(R/l) + o(1)$ for $R \to 0$, but the introduction of the fixed length l breaks the universality of the problem and is beyond the scope of this paper (see [43] for a more detailed discussion). We thus exclude e_2 from the domain of the Hamiltonian.

This discussion may be extended to Jordan forms of higher order. For example, a Jordan form of dimension 3 generates a ket $|e_3\rangle$ such that $(\hat{D} - \nu)e_3 = e_2$. But e_2 must be excluded from the domain of the Hamiltonian by the above reasoning. Since we want the domain to be stable under $\hat{D}$, e_3 must be excluded as well.

As a conclusion, to have a free-space N-body Hamiltonian that is both Hermitian and universal (i.e., with a scale-invariant domain) forces us to reject the non-scale-invariant zero-energy eigenstates, of the form Eq. (B3).

APPENDIX C: SEPARABILITY IN INTERNAL HYPERSPHERICAL COORDINATES

We develop here a refined version of the separability introduced in Sec. IV C. First, we separate out the center-of-mass coordinates. Then we obtain the separability in hyperspherical coordinates relative to the internal variables of the gas, which allows us to derive an effective repulsive $N-1$ force and to get a lower bound on the energy slightly better than the one $E \geqslant 0$ ensuing from the virial theorem.

Let us introduce the following set of coordinates:

$$\vec{C} = \sum_{i=1}^{N} \vec{r}_i / N \tag{C1}$$

is the position of the center of mass (CM);

$$R = \sqrt{\sum_{i=1}^{N} (\vec{r}_i - \vec{C})^2} \tag{C2}$$

is the internal hyperradius; and

$$\vec{\Omega} = \left(\frac{\vec{r}_1 - \vec{C}}{R}, \ldots, \frac{\vec{r}_N - \vec{C}}{R} \right) \tag{C3}$$

is a set of dimensionless internal coordinates that can be parametrized by $3N-4$ internal hyperangles. In these coordinates, the Hamiltonian decouples as $H = H_{CM} + H_{\mathrm{int}}$ with

$$H_{CM} = -\frac{\hbar^2}{2Nm}\Delta_{\vec{C}} + \frac{1}{2}Nm\omega^2 C^2, \tag{C4}$$

$$H_{\mathrm{int}} = -\frac{\hbar^2}{2m}\left[\partial_R^2 + \frac{3N-4}{R}\partial_R + \frac{1}{R^2} T_{\vec{\Omega}} \right] + \frac{1}{2}m\omega^2 R^2, \tag{C5}$$

where $T_{\vec{\Omega}}$ is the Laplacian on the unit sphere of dimension $3N-4$. The contact conditions do not break the separability of the center of mass valid in a harmonic trap, so that the

stationary state wave function may be taken of the form

$$\psi(\vec{X}) = \psi_{CM}(\vec{C})\psi_{\text{int}}(R,\vec{\Omega}). \tag{C6}$$

At this point, this separability of the center of mass, combined with the virial theorem of Eq. (29), already gives an improved lower bound on the energy of a universal state [41]:

$$E \geqslant \frac{3}{2}\hbar\omega. \tag{C7}$$

To proceed further, one can show [42] that there is separability in internal hyperspherical coordinates:

$$\psi_{\text{int}}(R,\vec{\Omega}) = \Phi(R)\phi(\vec{\Omega}). \tag{C8}$$

This form may be injected into the internal Schrödinger equation

$$H_{\text{int}}\psi_{\text{int}} = E_{\text{int}}\psi_{\text{int}}. \tag{C9}$$

One finds that $\phi(\vec{\Omega})$ is an eigenstate of $T_{\vec{\Omega}}$ with an eigenvalue that we call $-\Lambda$. Note that the contact conditions Eq. (6) put a constraint on $\phi(\vec{\Omega})$ only [38]. The equation for $\Phi(R)$ reads

$$-\frac{\hbar^2}{2m}\left(\partial_R^2 + \frac{3N-4}{R}\partial_R\right)\Phi + \left(\frac{\hbar^2\Lambda}{2mR^2} + \frac{1}{2}m\omega^2R^2\right)\Phi = E_{\text{int}}\Phi. \tag{C10}$$

A useful transformation of this equation is obtained by the change of variable

$$\Phi(R) \equiv R^{(5-3N)/2}F(R), \tag{C11}$$

resulting in

$$-\frac{\hbar^2}{2m}\left(\partial_R^2 + \frac{1}{R}\partial_R\right)F + \left(\frac{\hbar^2 s_R^2}{2mR^2} + \frac{1}{2}m\omega^2R^2\right)F = E_{\text{int}}F(R), \tag{C12}$$

where s_R is such that

$$s_R^2 = \Lambda + \left(\frac{3N-5}{2}\right)^2. \tag{C13}$$

Formally, the equation for F is Schrödinger's equation for a particle of zero angular momentum moving in two dimensions in a harmonic potential plus a potential $\propto s_R^2/R^2$.

For $s_R^2 \geqslant 0$, one can choose $s_R \geqslant 0$. Assuming that there is no N-body resonance, $F(R)$ is bounded for $R \to 0$ [43]. The eigenfunctions of Eq. (C12) can then be expressed in terms of the generalized Laguerre polynomials:

$$F(R) = R^{s_R}L_q^{s_R}[R^2/a_{\text{ho}}^2]e^{-R^2/2a_{\text{ho}}^2} \tag{C14}$$

with the spectrum

$$E_{\text{int}} = (s_R + 1 + 2q)\hbar\omega. \tag{C15}$$

This gives a lower bound on the energy of any universal N-body eigenstate:

$$E \geqslant \frac{5}{2}\hbar\omega \tag{C16}$$

for $N > 2$ and in the absence of a N-body resonance.

For a complex s_R^2, the effective two-dimensional (2D) Hamiltonian is not Hermitian and this case has to be discarded. For $s_R^2 < 0$, Whittaker functions are square integrable solutions of the effective 2D problem for all values E_{int} so that, again, the problem is not Hermitian. One may add extra boundary conditions to filter out an orthonormal discrete subset (as was done for $N=3$ bosons [9,13,15,45]) but this breaks the scaling invariance of the domain and generates nonuniversal states beyond the scope of the present paper.

To make the link with the approach of Sec. IV, we note that

$$F(R) = R^{s_R} \tag{C17}$$

is a solution of the effective 2D problem (C12) for $\omega=0$, $E_{\text{int}}=0$. Thus a solution of the internal problem Eq. (C9) at zero energy in free space is given by

$$\psi_{\text{int}}(R,\Omega) = R^{(5-3N)/2+s_R}\phi(\vec{\Omega}). \tag{C18}$$

Multiplying this expression by $C^l Y_l^m(\vec{C}/C)$, one recovers the ψ_ν^0's of Sec. IV, with

$$\nu = \frac{5-3N}{2} + s_R + l. \tag{C19}$$

[1] K. M. O'Hara, S. L. Hemmer, M. E. Gehm, S. R. Granade, and J. E. Thomas, Science **298**, 2179 (2002); C. A. Regal, C. Ticknor, J. L. Bohn, and D. S. Jin, Nature (London) **424**, 47 (2003); T. Bourdel, J. Cubizolles, L. Khaykovich, K. M. F. Magalhães, S. J. J. M. F. Kokkelmans, G. V. Shlyapnikov, and C. Salomon, Phys. Rev. Lett. **91**, 020402 (2003); C. A. Regal, M. Greiner, and D. S. Jin, *ibid.* **92**, 040403 (2004); M. W. Zwierlein, C. A. Stan, C. H. Schunck, S. M. F. Raupach, A. J. Kerman, and W. Ketterle, *ibid.* **92**, 120403 (2004); M. Bartenstein, A. Altmeyer, S. Riedl, S. Jochim, C. Chin, J. Hecker Denschlag, and R. Grimm, *ibid.* **92**, 120401 (2004); T. Bourdel, L. Khaykovich, J. Cubizolles, J. Zhang, F. Chevy, M. Teichmann, L. Tarruell, S. J. J. M. F. Kokkelmans, and C. Salomon, *ibid.* **93**, 050401 (2004); C. Chin, M. Bartenstein, A. Altmeyer, S. Riedl, S. Jochim, J. Hecker Denschlag, and R. Grimm, Science **305**, 1128 (2004); G. B. Partridge, K. E. Strecker, R. I. Kamar, M. W. Jack, and R. G. Hulet, Phys. Rev. Lett. **95**, 020404 (2005); J. Kinast, A. Turlapov, J. E. Thomas, Q. Chen, J. Stajic, and K. Levin, Science **307**, 1296 (2005); M. W. Zwierlein, J. R. Abo-Shaeer, A. Schirotzek, C. H. Schunck, and W. Ketterle, Nature (London) **435**, 1047 (2005); Q. Chen, C. A. Regal, M. Greiner, D. S. Jin, and K. Levin,

Phys. Rev. A **73**, 041601(R) (2006); J. Kinast, S. L. Hemmer, M. E. Gehm, A. Turlapov, and J. E. Thomas, Phys. Rev. Lett. **92**, 150402 (2004); M. Bartenstein, A. Altmeyer, S. Riedl, S. Jochim, C. Chin, J. Hecker Denschlag, and R. Grimm, *ibid.* **92**, 203201 (2004); J. Kinast, A. Turlapov, and J. E. Thomas, Phys. Rev. A **70**, 051401 (2004); J. Kinast, A. Turlapov, and J. E. Thomas, Phys. Rev. Lett. **94**, 170404 (2005); M. W. Zwierlein, A. Schirotzek, C. H. Schunck, and W. Ketterle, Science **311**, 492 (2006); G. B. Partridge, W. Li, R. I. Kamar, Y. Liao, and R. G. Hulet, *ibid.* **311**, 503 (2006).

[2] H. Heiselberg, Phys. Rev. A **63**, 043606 (2001); T.-L. Ho and E. J. Mueller, Phys. Rev. Lett. **92**, 160404 (2004); L. Pricoupenko and Y. Castin, Phys. Rev. A **69**, 051601(R) (2004).

[3] E. Burovski, N. Prokof'ev, B. Svistunov, and M. Troyer, Phys. Rev. Lett. **96**, 160402 (2006); New J. Phys. **8**, 153 (2006).

[4] A. Bulgac, J. E. Drut, and P. Magierski, Phys. Rev. Lett. **96**, 090404 (2006).

[5] D. Lee and T. Schafer, Phys. Rev. C **73**, 015202 (2006).

[6] J. Carlson, S.-Y. Chang, V. R. Pandharipande, and K. E. Schmidt, Phys. Rev. Lett. **91**, 050401 (2003); S. Y. Chang, V. R. Pandharipande, J. Carlson, and K. E. Schmidt, Phys. Rev. A **70**, 043602 (2004); S. Y. Chang and V. R. Pandharipande, Phys. Rev. Lett. **95**, 080402 (2005).

[7] G. E. Astrakharchik, J. Boronat, J. Casulleras, and S. Giorgini, Phys. Rev. Lett. **93**, 200404 (2004); G. E. Astrakharchik, J. Boronat, J. Casulleras, and S. Giorgini, *ibid.* **95**, 230405 (2005).

[8] Dean Lee, Phys. Rev. B **73**, 115112 (2006); O. Juillet, cond-mat/0609063.

[9] V. N. Efimov, Yad. Fiz. **12**, 1080 (1970), [Sov. Phys. J. **12**, 589 (1971)].

[10] J. Stenger, S. Inouye, M. R. Andrews, H.-J. Miesner, D. M. Stamper-Kurn, and W. Ketterle, Phys. Rev. Lett. **82**, 2422 (1999); J. L. Roberts, N. R. Claussen, S. L. Cornish, and C. E. Wieman, *ibid.* **85**, 728 (2000); A. Marte, T. Volz, J. Schuster, S. Dürr, G. Rempe, E. G. M. van Kempen, and B. J. Verhaar, *ibid.* **89**, 283202 (2002); T. Weber, J. Herbig, M. Mark, H.-C. Nägerl, and R. Grimm, *ibid.* **91**, 123201 (2003).

[11] T. Kraemer, M. Mark, P. Waldburger, J. G. Danzl, C. Chin, B. Engeser, A. D. Lange, K. Pilch, A. Jaakkola, H.-C. Naegerl, and R. Grimm, Nature (London) **440**, 315 (2006).

[12] E. Braaten and H.-W. Hammer, Phys. Rev. Lett. **87**, 160407 (2001); Phys. Rep. **428**, 259 (2006).

[13] S. Jonsell, H. Heiselberg, and C. J. Pethick, Phys. Rev. Lett. **89**, 250401 (2002).

[14] M. Stoll and T. Köhler, Phys. Rev. A **72**, 022714 (2005).

[15] F. Werner and Y. Castin, Phys. Rev. Lett. **97**, 150401 (2006).

[16] D. S. Petrov, C. Salomon, and G. V. Shlyapnikov, Phys. Rev. A **71**, 012708 (2005); Phys. Rev. Lett. **93**, 090404 (2004); D. S. Petrov, Phys. Rev. A **67**, 010703(R) (2003).

[17] For N spin-1/2 fermions, the spin configuration can be chosen as $|\uparrow\rangle^{\otimes N_\uparrow}\otimes|\downarrow\rangle^{\otimes N_\downarrow}$ where the first $N_\uparrow$ factors of the tensorial product are the spin-up state and the $N_\downarrow=N-N_\uparrow$ remaining factors are the spin-down state. In this case, the wave function $\psi(\mathbf{r}_1,\ldots,\mathbf{r}_N)$ is antisymmetric for the permutation of the positions of the $N_\uparrow$ first particles and also antisymmetric for the permutation of the last $N_\downarrow$ particles.

[18] In the context of cold atoms, hyperspherical coordinates were used, e.g., in J. L. Bohn, B. D. Esry, and C. H. Greene, Phys. Rev. A **58**, 584 (1998); O. Sørensen, D. V. Fedorov, and A. S. Jensen, *ibid.* **66**, 032507 (2002).

[19] M. Olshanii and L. Pricoupenko, Phys. Rev. Lett. **88**, 010402 (2002).

[20] S. Albeverio, F. Gesztesy, R. Hoegh-Krohn, and H. Holden, *Solvable Models in Quantum Mechanics* (Springer-Verlag, Berlin, 1988).

[21] C. Mora and Y. Castin, Phys. Rev. A **67**, 053615 (2003); Y. Castin, J. Phys. IV **116**, 89 (2004).

[22] Since the eigenvectors are orthonormal for a finite range, their zero range limits are also orthonormal.

[23] For three bosons, this holds only in the subspace of universal states.

[24] This can be seen using the Hellmann-Feynman theorem, valid for Hermitian Hamiltonians: taking the derivative with respect to λ of $\langle\psi_\lambda|H|\psi_\lambda\rangle=E/\lambda^2$, one gets $-2E/\lambda^3=\langle\psi_\lambda|(dH/d\lambda)|\psi_\lambda\rangle=0$, in contradiction with $E<0$.

[25] Y. Castin, C. R. Phys. **5**, 407 (2004); e-print cond-mat/0406020.

[26] L. P. Pitaevskii and A. Rosch, Phys. Rev. A **55**, R853 (1997).

[27] Another example where the hidden SO(2,1) symmetry holds is the ideal gas. Therefore all the results derived in this paper, being a consequence of the SO(2,1) hidden symmetry, also apply to the ideal gas. An example where the SO(2,1) symmetry does not hold is the zero-range model with a finite value of the scattering length a.

[28] Note that E_g is larger than $\hbar\omega$, according to a lower bound on the energy derived in Appendix C: as a consequence, E_g is a univocal function of $\mathcal{C}$.

[29] Here the scalar product is the usual $3N$-uple integral restricted to the manifold of positions $\vec{r}_i\neq\vec{r}_j$ for all $i\neq j$. As a consequence, one does not have to introduce the Dirac distributions originating from the action of the Laplacian on the $1/r_{ij}$ divergencies imposed by the contact conditions.

[30] For a real ψ normalized to unity, one finds $\langle\psi|\hat{D}|\psi\rangle=-3N/2$, from the identity $\psi\vec{X}\cdot\partial_{\vec{X}}\psi=\mathrm{div}\left(\frac{1}{2}\vec{X}\psi^2\right)-\frac{3N}{2}\psi^2$ and Ostrogradsky's theorem.

[31] J. E. Thomas, J. Kinast, and A. Turlapov, Phys. Rev. Lett. **95**, 120402 (2005).

[32] F. Werner, Y. Castin, e-print cond-mat/0507399 (version 1).

[33] There are in general several zero-energy free-space eigenstates with the same exponent ν, so that our notation ψ_ν^0 is abusive.

[34] S. Tan, e-print cond-mat/0412764.

[35] This holds also when the exponent ν of the free-space eigenstate is not real, in which case the Hamiltonian is not Hermitian since the resulting eigenenergy in the trap is complex. This happens for the Efimov states of three bosons, which can be written as a sum of scale-invariant states with complex conjugate exponents. This exemplifies the fact that the present algebra is meaningful for universal states only.

[36] Strictly speaking, the system cannot thermalize, as can be realized in several ways: the breathing mode is undamped (see Sec. III C), the Casimir operator is a constant of motion (see Sec. III D), the bosonic degree of freedom is decoupled [see Eq. (28) in Sec. III E]. However, in practice the trapping potential is not perfectly isotropic, and the range of the interaction is not stricly zero. This leads to a weak coupling between the bosonic degree of freedom associated with the breathing mode and the other degrees of freedom. Therefore the system can thermalize.

[37] To obtain Eq. (B5), consider $\psi_2\equiv R^\nu u(R)\phi_2(\vec{\Omega})$. This wave

function satisfies the contact conditions [38]. It thus belongs to the domain of H [for an appropriate $u(R)$]. Since $He_1=0$, Hermiticity of H implies $\langle e_1, H\psi_2\rangle=0$; which leads to the result.

[38] To establish this fact, one needs the following lemma: if $\psi(\vec{X})$ obeys the contact conditions, so does $u(R)\psi(\vec{X})$, where $u(R)$ is a function with no singularity, except maybe in $R=0$. This lemma results from the fact that $R^2=R_0^2+O(r_{ij}^2)$, where R_0^2 is a nonzero constant in the $r_{ij}\to 0$ limit [39], so that $u(R)=u(R_0)+O(r_{ij}^2)$.

[39] We assume here $N>2$; in this case, R_0 is different from zero since the contact conditions apply for $\vec{R}_{ij}\neq\vec{r}_k$, whatever $k\neq i,j$.

[40] P. M. Morse and H. Feshbach, *Methods of Theoretical Physics* (McGraw-Hill, New York, 1953), Part II, p. 1665.

[41] Indeed, one has $\langle H\rangle=2\langle H_{\text{trap}}\rangle\geqslant\langle NmC^2\rangle=\langle H_{CM}\rangle\geqslant 3/2\hbar\omega$.

[42] The whole algebra of Sec. IV may be reproduced for the internal problem, with the modified raising and lowering operators: $\mathcal{L}_\pm\equiv\pm\left(\frac{3N-3}{2}+R\partial_R\right)+\frac{H_{\text{int}}}{\hbar\omega}-\frac{m\omega}{\hbar}R^2$.

[43] The absence of N-body resonance corresponds to the simple boundary condition: (i) $F(R)$ bounded for $R\to 0$. For $0<s_R<1$, N-body resonances can be taken into account by the modified boundary condition: (ii) $F(R)=AR^{s_R}[R^{-2s_R}-\epsilon l^{-2s_R}]+O(R^{-s_R+2})$, where $l\in]0,+\infty]$ and $\epsilon=\pm 1$ are fixed. If one is not exactly on the N-body resonance, one has $l<\infty$, which breaks scale invariance, thus invalidating the results of this paper. Exactly on the N-body resonance (e.g., when the energy of the N-body bound state in free space vanishes), one has $l=\infty$, which preserves scale invariance: all the results of this paper remain valid; one must only replace s_R by $-s_R$ in Eqs. (C14), (C15), and (C17)–(C19), and Eq. (C16) becomes $E\geqslant 3/2\hbar\omega$. For $s_R=0$, N-body resonances can be taken into account by the modified boundary condition (iii) $F(R)=A\ln(R/l)+o(1)$, where $l\in]0,+\infty[$ is fixed. If one is not exactly on the N-body resonance, one has $l<\infty$, which breaks scale invariance, thus invalidating the results of this paper. Being exactly on the N-body resonance corresponds to taking the limit $l\to\infty$ in (iii), which is equivalent to (i): the results of this paper then remain valid. For $s_R\geqslant 1$, the wave function $F(R)=R^{-s_R}$ is not square integrable near $R=0$ in two dimensions, so that the description of N-body resonances becomes more complicated (see [44] for the case $N=2$).

[44] L. Pricoupenko, Phys. Rev. A **73**, 012701 (2006); Phys. Rev. Lett. **96**, 050401 (2006).

[45] G. S. Danilov, Zh. Eksp. Teor. Fiz., **40**, 498 (1961) [Sov. Phys. JETP, **13**, 349 (1961)].

Article II

Virial theorems for trapped quantum gases

PHYSICAL REVIEW A **78**, 025601 (2008)

Virial theorems for trapped cold atoms

Félix Werner
Laboratoire Kastler Brossel, École Normale Supérieure, Université Pierre et Marie Curie-Paris 6, CNRS, 24 rue Lhomond, 75231 Paris Cedex 05, France

(Received 22 March 2008; revised manuscript received 16 June 2008; published 1 August 2008)

We present a general virial theorem for quantum particles with arbitrary zero-range or finite-range interactions in an arbitrary external potential. We deduce virial theorems for several situations relevant to trapped cold atoms: zero-range interactions with and without Efimov effect, hard spheres, narrow Feshbach resonances, and finite-range interactions. If the scattering length a is varied adiabatically in a two-component Fermi gas, we find that the trapping potential energy as a function of $1/a$ has an inflexion point at unitarity.

DOI: 10.1103/PhysRevA.78.025601 PACS number(s): 03.75.Ss, 05.30.Jp, 03.65.−w

I. INTRODUCTION

In quantum mechanics, zero-range interactions can be expressed as boundary conditions on the many-body wave function in the limit of vanishing interparticle distance [1]. These boundary conditions define the *domain* of the Hamiltonian, i.e., the set of wave functions on which the Hamiltonian is allowed to act. The Hamiltonian of a zero-range model differs from the noninteracting Hamiltonian only by its domain. In three dimensions (3D), the zero-range model has a long history in nuclear physics going back to the work of Wigner, Bethe, and Peierls on the two-nucleon problem [2].

Zero-range interactions provide an accurate description of cold atom experiments [3–5]. In particular, two-component fermionic atoms in 3D at a broad Feshbach resonance are well described by zero-range interactions of scattering length $a=\infty$. This so-called unitary limit is completely universal, e.g., the superfluid transition temperature is a universal number times the Fermi energy [6–8].

A new ingredient in cold atomic systems with respect to nuclear physics is the external trapping potential. For the unitary Fermi gas in a harmonic trap, the virial theorem

$$E = 2E_{\mathrm{tr}} \tag{1}$$

was recently shown theoretically and experimentally [9–12]. Here E is the total energy and E_{tr} is the trapping potential energy.

On the other hand, the traditional virial theorem does not concern zero-range interactions, but more usual interactions described by a potential energy $U(\mathbf{r}_1,\ldots,\mathbf{r}_N)$, where the domain is simply a set of smooth functions. It states that the kinetic energy T is one half of the virial,

$$\langle T\rangle = \frac{1}{2}\left\langle \sum_{i=1}^{N} \mathbf{r_i}\cdot\boldsymbol{\nabla}_{\mathbf{r_i}} U \right\rangle \tag{2}$$

for any eigenstate; implying $\langle T\rangle = n/2\langle U\rangle$ if U is a homogeneous function of degree n. This theorem is as old as many-particle quantum mechanics [13], and is used, e.g., to understand the properties of many-electron atoms [14].

In this paper, we present a general virial theorem for a Hamiltonian with an arbitrary domain. In the particular case where the domain does not depend on any length scale, we recover the virial theorem for the unitary gas (1) and the traditional virial theorem (2). By considering the case of a more general domain, we find virial theorems for several interactions relevant to cold atoms: zero-range interactions of arbitrary scattering length with or without Efimov effect, hard spheres, narrow Feshbach resonances, and finite-range interactions. Our theorems hold for any trapping potential, in any space dimension. They are valid not only for each eigenstate, but also at thermal equilibrium provided the entropy S is kept constant. For zero-range interactions without Efimov effect, the virial theorem implies that for any S, the function $E_{\mathrm{tr}}(1/a,S)$ has an inflexion point at the unitary limit $1/a=0$.

II. GENERAL VIRIAL THEOREM

Let us consider a quantum problem of N particles, with arbitrary statistics and dispersion relations. The position $\mathbf{r_i}$ of particle i is a vector of arbitrary dimension, with continuous or discrete coordinates. We consider a general Hamiltonian

$$H = H' + U(\mathbf{r_1},\ldots,\mathbf{r_N}) \tag{3}$$

where (i) H' and its domain depend on p parameters $l_1,\ldots,l_p$ which have the dimension of a length, on $\hbar$, and on some arbitrary fixed mass m and (ii) $U(\mathbf{r_1},\ldots,\mathbf{r_N})$ is an arbitrary function, which is sufficiently regular so that the domains of H and H' coincide.

Then, as shown below,

$$E = \left\langle U + \frac{1}{2}\sum_{i=1}^{N} \mathbf{r_i}\cdot\boldsymbol{\nabla}_{\mathbf{r_i}} U \right\rangle - \frac{1}{2}\sum_{q=1}^{p} l_q \frac{\partial E}{\partial l_q} \tag{4}$$

for any stationary state of energy E, the partial derivatives $\partial E/\partial l_q$ being taken for a fixed function U.

To derive the above theorem, we use dimensional analysis to rewrite U as

$$U(\mathbf{r}_1,\ldots,\mathbf{r_N}) = \frac{\hbar^2\lambda^2}{m} f(\lambda\mathbf{r_1},\ldots,\lambda\mathbf{r_N}), \tag{5}$$

where λ has the dimension of the inverse of a length, and f is a dimensionless function. The theorem then follows from the following two relations:

$$\lambda\frac{\partial E}{\partial\lambda} = \left\langle 2U + \sum_{i=1}^{N} \mathbf{r_i}\cdot\boldsymbol{\nabla}_{\mathbf{r_i}} U \right\rangle, \tag{6}$$

$$\lambda\frac{\partial E}{\partial\lambda}=2E+\sum_{q=1}^{p}l_q\frac{\partial E}{\partial l_q}. \tag{7}$$

Here the partial derivatives with respect to λ are taken for a fixed function f and for fixed $l_1,\ldots,l_p$.

Equation (6) follows from the Hellmann-Feynman theorem [15] and from Eq. (5). The Hellmann-Feynman theorem holds if the derivative $\partial|\psi\rangle/\partial\lambda$ of the considered eigenstate belongs to the domain of H. We expect this to be true in all situations considered in this paper.

Equation (7) follows from the fact that, by dimensional analysis, the energy is written as

$$E(l_1,\ldots,l_p,[U])=\frac{\hbar^2\lambda^2}{m}F(\lambda l_1,\ldots,\lambda l_p,[f]), \tag{8}$$

where F is a dimensionless functional.

The traditional virial theorem (2) is recovered by applying the general virial theorem to the case where (i) the operator H' in Eq. (3) reduces to the kinetic energy

$$T=-\sum_{i=1}^{N}\frac{\hbar^2}{2m_i}\Delta_{\mathbf{r_i}}, \tag{9}$$

m_i being the mass of particle i; and (ii) the domain is simply a set of wave functions which are smooth when particles approach each other. Since this domain does not depend on any length scale, the second term on the right-hand side of Eq. (4) vanishes, and the desired Eq. (2) follows.

III. VIRIAL THEOREMS FOR TRAPPED COLD ATOMS

In what follows we restrict ourselves to the experimentally relevant case where U is a sum of trapping potentials,

$$U(\mathbf{r_1},\ldots,\mathbf{r_N})=\sum_{i=1}^{N}U_i(\mathbf{r_i}), \tag{10}$$

and we rewrite the general virial theorem, Eq. (4), as

$$E=2\tilde{E}_{\mathrm{tr}}-\frac{1}{2}\sum_{i=1}^{p}l_i\frac{\partial E}{\partial l_i}, \tag{11}$$

where

$$\tilde{E}_{\mathrm{tr}}\equiv\frac{1}{2}\sum_{i=1}^{N}\left\langle U_i(\mathbf{r_i})+\frac{1}{2}\mathbf{r_i}\cdot\boldsymbol{\nabla}U_i(\mathbf{r_i})\right\rangle. \tag{12}$$

If each U_i is a harmonic trap, then $\tilde{E}_{\mathrm{tr}}$ reduces to the trapping potential energy $\tilde{E}_{\mathrm{tr}}=\Sigma_{i=1}^{N}\langle U_i(\mathbf{r_i})\rangle=E_{\mathrm{tr}}$.

A. Zero-range interactions

We now assume that each pair of particles either interacts *via* a zero-range interaction of scattering length a, or does not interact. Zero-range interactions are well known in 1D [16,17], 2D [18], and 3D [2,12,19–23].

1. Universal states

We call *universal state* a stationary state of the zero-range model which depends only on the scattering length. All eigenstates are believed to be universal in 1D and 2D ([16,17,24] and references therein) and in 3D for fermions with two components of equal masses [3–12,19–21,23,25–36] or unequal masses with a mass ratio not to far from one [5,36]. For three bosons in 3D there are both nonuniversal Efimovian states and universal states [22,23].

In the Hilbert space generated by universal states, the domain of the Hamiltonian depends only on the scattering length. Thus Eq. (11) gives for any universal state

$$E=2\tilde{E}_{\mathrm{tr}}-\frac{1}{2}a\frac{\partial E}{\partial a}, \tag{13}$$

or equivalently,

$$E=2\tilde{E}_{\mathrm{tr}}+\frac{1}{2a}\frac{\partial E}{\partial(1/a)}. \tag{14}$$

This result generalizes the virial theorem, Eq. (1), to an arbitrary scattering length, trapping potential and space dimension. Thus it also applies to quantum gases in low dimensions ([37–40] and references therein). For the case of two-component fermions in three dimensions and power-law traps, this result is also contained in two recently submitted works: it was found independently by Tan in [41] and rederived using a method similar to ours in [42].

For $a=\infty$ (which is the unitary limit in 3D and the noninteracting limit in 1D and 2D), Eq. (14) becomes

$$E=2\tilde{E}_{\mathrm{tr}}. \tag{15}$$

This generalization of Eq. (1) to an arbitrary trap was obtained by Castin [43] and is also contained in the recent independent work of Thomas [44]. Of course it also holds for $a=0$ (which is the Tonks-Girardeau limit in 1D and the noninteracting limit in 2D and 3D) in accordance with Eq. (13).

Taking the second derivative of Eq. (14) we obtain

$$\left.\frac{\partial^2\tilde{E}_{\mathrm{tr}}}{\partial(1/a)^2}\right|_{a=\infty}=0, \tag{16}$$

which means that generically the curve $\tilde{E}_{\mathrm{tr}}(1/a)$ has an inflexion point exactly at the unitary limit $1/a=0$.

We can also rewrite Eq. (14) in an integral form,

$$a_2{}^2E(a_2)-a_1{}^2E(a_1)=-4\int_{1/a_1}^{1/a_2}a^3\tilde{E}_{\mathrm{tr}}(a)d(1/a), \tag{17}$$

which is likely to have a better signal-to-noise ratio than Eq. (14) when applied to experiments or numerics.

2. Efimovian states

The boundary condition in the limit where two particles approach each other is called Bethe-Peierls boundary condition (BPBC). For three bosonic or distinguishable particles, there exists Efimov bound states [19], and the domain of the zero-range model is defined not only by the BPBC in the limit where two particles approach each other, but also by an additional boundary condition in the limit where all three particles approach each other. While the BPBC depends on the scattering length a, this additional boundary condition depends on a three-body parameter which we call R_t and has the dimensions of a length [23,45]. The resulting two-parameter model is known to be self-adjoint and physically meaningful for $N=3$ particles [19,20,22,23,45]. The case $N\geqslant 4$ is still controversial [46].

For this model, the general virial theorem, Eq. (11), gives

$$E=2\tilde{E}_{\mathrm{tr}}+\frac{1}{2}\left[\frac{1}{a}\frac{\partial E}{\partial(1/a)}-R_t\frac{\partial E}{\partial R_t}\right]. \tag{18}$$

For $a=\infty$ this reduces to

$$E = 2\tilde{E}_{\rm tr} - \frac{R_t}{2}\frac{\partial E}{\partial R_t}. \tag{19}$$

We now apply this to the unitary three-boson problem in an isotropic harmonic trap, which is exactly solvable [22,23]. The spectrum of Efimovian states is $E=E_{\rm CM}+\mathcal{E}\hbar\omega$ where $E_{\rm CM}$ is the energy of the center of mass and $\mathcal{E}$ solves

$$\arg\Gamma\left(\frac{1+s-\mathcal{E}}{2}\right) = -|s|\ln R_t + \arg\Gamma(1+s) \bmod \pi, \tag{20}$$

$s\simeq 1.00624\ i$ being the only solution $s\in(0;+\infty)\ i$ of the equation: $s\cos(s\pi/2)-8/\sqrt{3}\sin(s\pi/6)=0$. This allows to calculate $\partial\mathcal{E}/\partial R_t$, and Eq. (19) then gives [47]

$$E_{\rm tr} = \frac{1}{2}\left(E + \frac{|s|}{\mathrm{Im}\,\psi\left(\frac{1+s-\mathcal{E}}{2}\right)}\right) \tag{21}$$

where ψ is the digamma function. But we can also express $E_{\rm tr}$ using the wave function, which has a simple expression in terms of the Whittaker W function [23]; the result agrees with Eq. (21) provided that [47]

$$\int_0^\infty dx[W_{\mathcal{E}/2,s/2}(x)]^2 = 2\pi\left[\mathcal{E}\,\mathrm{Im}\,\psi\left(\frac{1+s-\mathcal{E}}{2}\right) + |s|\right] \times\left[\sinh(|s|\pi)\left|\Gamma\left(\frac{1+s-\mathcal{E}}{2}\right)\right|^2\right]^{-1}. \tag{22}$$

Numerical checks confirm this relation.

B. Hard sphere interactions

Here the domain is defined by the condition that the wave function vanishes if any interparticle distance is smaller than a. Applying the general virial theorem with a single length scale gives

$$E = 2\tilde{E}_{\rm tr} - \frac{1}{2}a\frac{\partial E}{\partial a}. \tag{23}$$

Again, it can be useful to rewrite Eq. (23) in an integral form

$$E(a) = \frac{4}{a^2}\int_0^a a'\tilde{E}_{\rm tr}(a')da'. \tag{24}$$

Within the three-dimensional Gross-Pitaevskii theory, $a\partial E/\partial a$ is the interaction energy, so that Eq. (23) agrees with the virial theorem of [48].

C. Finite-range interactions

We now consider models with two parameters, the scattering length a and a range l. Popular examples are the square-well interaction potential [28], separable potentials [23], and Hubbard-like lattice models where the lattice spacing l plays the role of the interaction range [7,26,29]. For such two-parameter models the general virial theorem gives

$$E = 2\tilde{E}_{\rm tr} + \frac{1}{2}\left[\frac{1}{a}\frac{\partial E}{\partial(1/a)} - l\frac{\partial E}{\partial l}\right], \tag{25}$$

and for $a=\infty$,

$$E = 2\tilde{E}_{\rm tr} - \frac{l}{2}\frac{\partial E}{\partial l}. \tag{26}$$

Setting $E_0=\lim_{l\to 0}E(l)$, Eq. (26) implies

$$E_0 = 3E - 4\tilde{E}_{\rm tr} + O(l^2), \tag{27}$$

which can be used to compute numerically E_0. This method is simpler than the usual one, where one computes E for several values of l and extrapolates linearly to $l=0$ [23,26,36].

D. Effective range model and narrow resonances

The effective range model has two parameters, the scattering length a and the effective range r_e. For $r_e<0$, the model describes a narrow Feshbach resonance [4,49–52]. For $r_e\to 0^-$, the model has a limit cycle described by the zero-range model of Sec. III A 2, with $R_t=Cr_e$, where the constant C was obtained numerically [49] and analytically [51]. The model is expected to be Hermitian for a modified scalar product, for two particles [53] and three particles [50]. Thus the Hellmann-Feynman theorem can be used and the general virial theorem holds, implying

$$E = 2\tilde{E}_{\rm tr} + \frac{1}{2}\left[\frac{1}{a}\frac{\partial E}{\partial(1/a)} - r_e\frac{\partial E}{\partial r_e}\right]. \tag{28}$$

For $r_e>0$, the effective range model is well defined if r_e is treated perturbatively [45], and Eq. (28) then holds, in agreement with Eq. (25).

IV. AT FINITE TEMPERATURE

We will show that the above results remain true at finite temperature, provided one considers adiabatic transformations. For concreteness we restrict ourselves to zero-range interactions in the universal case. We consider that each eigenstate n has an occupation probability p_n. We set $\bar{E}=\Sigma_n E_n p_n$ and $\overline{\tilde{E}_{\rm tr}}=\Sigma_n(\tilde{E}_{\rm tr})_n p_n$.

Let us first recall the reasoning of Tan [41,54]: for a finite system, in the limit where a is varied infinitely slowly, the adiabatic theorem implies that the p_n's remain constant, so that

$$\sum_n \frac{\partial E_n}{\partial(1/a)}p_n = \frac{\partial}{\partial(1/a)}\sum_n E_n p_n. \tag{29}$$

Tan concludes that E and $\tilde{E}_{\rm tr}$ can be replaced by their average values $\bar{E}$ and $\overline{\tilde{E}_{\rm tr}}$ in the virial theorem Eq. (14).

Alternatively, let us assume that the p_n's are given by the canonical distribution $p_n\propto e^{-E_n(a)/(k_BT)}$, where the temperature T varies with a in such a way that the entropy $S=-k_B\Sigma_n p_n\ln p_n$ remains constant. According to the principles of thermodynamics, this assumption is a good effective description of adiabatic sweep experiments where a is changed at a rate much smaller than thermalization rates and much larger than the heating and evaporation rates [8,30,35,55,56]. Under this assumption Eq. (29) also holds [57]. Thus

$$\bar{E} = 2\overline{\tilde{E}_{\rm tr}} + \frac{1}{2a}\left(\frac{\partial\bar{E}}{\partial(1/a)}\right)_S. \tag{30}$$

This result is physically consistent with Tan's conclusion. Moreover it implies

$$\frac{\partial^2\overline{\tilde{E}_{\rm tr}}}{\partial(1/a)^2}\left(\frac{1}{a}=0,S\right) = 0, \tag{31}$$

$$a_2{}^2\bar{E}(a_2,S) - a_1{}^2\bar{E}(a_1,S) = -4\int_{1/a_1}^{1/a_2} a^3\overline{\tilde{E}_{\rm tr}}(a,S)d(1/a). \tag{32}$$

V. EXPERIMENTAL CONSIDERATIONS

Both E and $\tilde{E}_{\rm tr}$ are measurable. Indeed, $\tilde{E}_{\rm tr}$ and the trapping potential energy $E_{\rm tr}$ can be deduced from an *in situ* image of the density profile [32,34,35,58], and the released energy $E-E_{\rm tr}$ from a time-of-flight image [33,38,59,60]. By measuring $\bar{E}$ and $\tilde{E}_{\rm tr}$, and using the virial theorem, Eq. (30), one could deduce the quantity $[\partial\bar{E}/\partial(1/a)]_S$ [62]. This quantity is also related to the large-momentum tail of the momentum distribution [54] and to the total energy [63].

Moreover, Eqs. (30)–(32) can be directly checked by measuring $E(a)$ and $\tilde{E}_{\rm tr}(a)$ in an adiabatic sweep experiment.

I am grateful to S. Tan and J. Thomas for drawing my attention to Refs. [41,42,44], and to M. Antezza, S. Biermann, E. Braaten, Y. Castin, M. Cheneau, F. Chevy, J. Dalibard, B. Derrida, W. Krauth, F. Laloë, S. Nascimbène, M. Olshanii, A. Ridinger, B. Roulet, C. Salomon, R. Sheshko, S. Tan, L. Tarruell, and J. Thomas for discussions and comments. Laboratoire Kastler Brossel is a *Unité Mixte de Recherche* of ENS, Université Paris 6, and CNRS. Our group is a member of IFRAF.

[1] Zero-range interactions can only be represented by an interaction potential proportional to the Dirac distribution in one dimension (1D), or in perturbative approaches in 2D and 3D.
[2] E. Wigner, Z. Phys. **83**, 253 (1933); H. Bethe and R. Peierls, Proc. R. Soc. London, Ser. A **148**, 146 (1935).
[3] *Ultra-cold Fermi Gases*, Proceedings of the International School of Physics "Enrico Fermi," Course CLXIV, 2006, edited by M. Inguscio, W. Ketterle, and C. Salomon (Società Italiana di Fisica, Bologna, 2007).
[4] Y. Castin, in *Ultra-cold Fermi Gases* [3].
[5] D. S. Petrov, C. Salomon, and G. V. Shlyapnikov, in *Ultra-cold Fermi Gases* [3].
[6] J. Kinast *et al.*, Science **307**, 1296 (2005).
[7] E. Burovski *et al.*, Phys. Rev. Lett. **96**, 160402 (2006); New J. Phys. **8**, 153 (2006).
[8] L. Luo *et al.*, Phys. Rev. Lett. **98**, 080402 (2007).
[9] F. Chevy (unpublished), reported in [10,12].
[10] Y. Castin, talk at KITP (UCSB), 2004, http://online.itp.ucsb.edu/online/gases04/castin
[11] J. E. Thomas *et al.*, Phys. Rev. Lett. **95**, 120402 (2005).
[12] F. Werner and Y. Castin, Phys. Rev. A **74**, 053604 (2006).
[13] M. Born *et al.*, Z. Phys. **35**, 557 (1926).
[14] K. Hongo *et al.*, J. Chem. Phys. **121**, 7144 (2004).
[15] See also D. T. Son, arXiv:0707.1851v1.
[16] E. H. Lieb and W. Liniger, Phys. Rev. **130**, 1605 (1963).
[17] M. Gaudin, *La Fonction d'onde de Bethe* (Masson, Paris, 1983).
[18] D. S. Petrov and G. V. Shlyapnikov, Phys. Rev. A **64**, 012706 (2001); L. Pricoupenko and M. Olshanii, J. Phys. B **40**, 2065 (2007).
[19] V. N. Efimov, Yad. Fiz. **12**, 1080 (1970) [Sov. J. Nucl. Phys. **12**, 589 (1971)].
[20] S. Albeverio *et al.*, Phys. Lett. **83A**, 105 (1981).
[21] D. S. Petrov *et al.*, Phys. Rev. Lett. **93**, 090404 (2004).
[22] S. Jonsell *et al.*, Phys. Rev. Lett. **89**, 250401 (2002).
[23] F. Werner and Y. Castin, Phys. Rev. Lett. **97**, 150401 (2006).
[24] I. V. Brodsky *et al.*, Phys. Rev. A **73**, 032724 (2006).
[25] D. Blume *et al.*, Phys. Rev. Lett. **99**, 233201 (2007).
[26] L. Pricoupenko and Y. Castin, J. Phys. A **40**, 12863 (2007).
[27] J. Carlson *et al.*, Phys. Rev. Lett. **91**, 050401 (2003).
[28] G. E. Astrakharchik *et al.*, Phys. Rev. Lett. **93**, 200404 (2004).
[29] O. Juillet, New J. Phys. **9**, 163 (2007).
[30] R. Grimm, in *Ultra-cold Fermi Gases* [3].
[31] L. Tarruell *et al.*, in *Ultra-cold Fermi Gases* [3].
[32] M. Bartenstein *et al.*, Phys. Rev. Lett. **92**, 120401 (2004).
[33] T. Bourdel *et al.*, Phys. Rev. Lett. **93**, 050401 (2004).
[34] G. B. Partridge *et al.*, Science **311**, 503 (2006).
[35] J. T. Stewart *et al.*, Phys. Rev. Lett. **97**, 220406 (2006).
[36] J. von Stecher *et al.*, Phys. Rev. A **77** 043619 (2008).
[37] I. Bloch *et al.*, arXiv:0704.3011v2, Rev. Mod. Phys. (to be published).
[38] T. Kinoshita *et al.*, Science **305**, 1125 (2004).
[39] Z. Hadzibabic *et al.*, New J. Phys. **10**, 045006 (2008).
[40] M. Holzmann *et al.*, Europhys. Lett. **82**, 30001 (2008).
[41] S. Tan, arXiv:0803.0841v1.
[42] E. Braaten and L. Platter, Phys. Rev. Lett. **100**, 205301 (2008).
[43] Y. Castin (unpublished).
[44] J. E. Thomas, arXiv:0803.1647v1.
[45] F. Werner, Ph.D. thesis, University Paris 6, 2008, Chap. 3, and references therein (http://tel.archives-ouvertes.fr/tel-00285587).
[46] L. Platter *et al.*, Phys. Rev. A **70**, 052101 (2004); M. T. Yamashita *et al.*, Europhys. Lett. **75**, 555 (2006).
[47] For details, see F. Werner, e-print arXiv:0803.3277v1.
[48] F. Dalfovo *et al.*, Rev. Mod. Phys. **71**, 463 (1999).
[49] D. S. Petrov, Phys. Rev. Lett. **93**, 143201 (2004).
[50] M. Jona-Lasinio and L. Pricoupenko (unpublished).
[51] A. O. Gogolin *et al.*, Phys. Rev. Lett. **100**, 140404 (2008).
[52] E. Braaten *et al.*, arXiv:0709.0499v2.
[53] L. Pricoupenko, Phys. Rev. A **73**, 012701 (2006).
[54] S. Tan, arXiv:cond-mat/0508320.
[55] L. D. Carr *et al.*, Phys. Rev. Lett. **92**, 150404 (2004).
[56] In low dimensions there is a caveat: the thermalization time may diverge with the system size, see A. Polkovnikov and V. Gritsev, Nat. Phys. **4**, 477 (2008).
[57] N. N. Bogoliubov, *Lectures on quantum statistics* (Gordon & Breach, New York, 1967), Vol. 1.
[58] Y. Shin *et al.*, Phys. Rev. Lett. **97**, 030401 (2006).
[59] K. M. O'Hara *et al.*, Science **298**, 2179 (2002).
[60] If the expansion dynamics is known theoretically, then other experimental methods become available: energy can be precisely added to the gas [6,11], and $E_{\rm tr}$ and $\tilde{E}_{\rm tr}$ can be deduced from a time-of-flight image [8,11]. The expansion dynamics is known if hydrodynamics [6,11] or exact scaling solutions [61] are applicable.
[61] Y. Castin, C. R. Phys. **5**, 407 (2004); C. Lobo and S. D. Gensemer, arXiv:cond-mat/0702313v1.
[62] However this method breaks down at unitarity, where $E-2\tilde{E}_{\rm tr}\to 0$.
[63] S. Tan, arXiv:cond-mat/0505200.

Appendice A

Coordonnées de Jacobi

1 Hamiltonien en coordonnées de Jacobi

Le hamiltonien d'une particule de masse m, de position $\vec{r}$, dans un piège harmonique de pulsation ω est :

$$\boxed{\hat{h}(m,\vec{r}) \equiv -\frac{\hbar^2}{2m}\Delta_{\vec{r}} + \frac{1}{2}m\omega^2\, r^2.} \tag{A.1}$$

Dans la suite nous considérons N particules de masses m_1, ..., m_N et de positions $\vec{r}_1$, ..., $\vec{r}_N$. Définissons la masse totale

$$M = \sum_{i=1}^{N} m_i, \tag{A.2}$$

et la position du centre de masse

$$\vec{C} = \frac{1}{M}\sum_{i=1}^{N} m_i\,\vec{r}_i. \tag{A.3}$$

Plus généralement, posons

$$M_j = \sum_{i=1}^{j} m_i; \quad \vec{C}_j = \frac{1}{M_j}\sum_{i=1}^{j} m_i\,\vec{r}_i. \tag{A.4}$$

Définissons pour $2 \leq j \leq N$ les coordonnées de Jacobi :

$$\vec{\eta}_j = \vec{r}_j - \vec{C}_{j-1}, \tag{A.5}$$

et les masses réduites :

$$\mu_j = \frac{m_j M_{j-1}}{m_j + M_{j-1}}. \tag{A.6}$$

On a alors la relation :

$$\boxed{\sum_{i=1}^{N} \hat{h}(m_i,\vec{r}_i) = \hat{h}(M,\vec{C}) + \sum_{j=2}^{N} \hat{h}(\mu_j,\vec{\eta}_j).} \tag{A.7}$$

Cette relation se démontre aisément par récurrence sur N. Pour $N = 2$, on la vérifie explicitement en effectuant le changement de variables $(\vec{r}_1,\vec{r}_2) \to (\vec{\eta}_2,\vec{C}_2)$. Pour passer de $N-1$ à N, on applique d'abord l'hypothèse de récurrence, puis on applique la relation pour $N = 2$ aux deux particules fictives $(m_N,\vec{r}_N)$ et $(M_{N-1},\vec{C}_{N-1})$.

2 Séparabilité du centre de masse

Une conséquence directe de la relation précédente est que le centre de masse est séparable pour un hamiltonien générique

$$H = \sum_{i=1}^{N} \hat{h}(m_i, \vec{r}_i) + \hat{V}, \tag{A.8}$$

où le hamiltonien d'interaction $\hat{V}$ n'agit que sur les coordonnées relatives. En effet, on peut alors chercher les états propres de H sous la forme

$$\Phi(\vec{r}_1, \ldots, \vec{r}_N) = \Psi_{\mathrm{CM}}(\vec{C})\, \Psi_{\mathrm{rel}} \tag{A.9}$$

où Ψ_{rel} ne dépend que des coordonnées relatives [un choix possible de coordonnées relatives étant $(\vec{\eta}_2, \ldots, \vec{\eta}_N)$] et est un état propre de $\sum_{j=2}^{N} \hat{h}(\mu_j, \vec{\eta}_j) + \hat{V}$, et $\Psi_{\mathrm{CM}}(\vec{C})$ est un état propre de $\hat{h}(M, \vec{C})$.

Cette séparabilité reste vraie pour le pseudopotentiel. On peut le vérifier en considérant un hamiltonien d'interaction $\hat{V}$ qui tend vers le pseudopotentiel dans la limite de portée nulle, ou bien directement dans le cadre du pseudopotentiel (cf. Chap. 1 Section 2).

3 Jacobien

Soit une fonction quelconque $F = F(\vec{r}_1, \ldots, \vec{r}_N) = F(\vec{\eta}_2, \ldots, \vec{\eta}_N, \vec{C})$. On a :

$$\int_{\mathbb{R}^{3N}} d\vec{r}_1 \ldots d\vec{r}_N \; F = \int_{\mathbb{R}^{3N}} d\vec{\eta}_2 \ldots d\vec{\eta}_N \, d\vec{C} \; F. \tag{A.10}$$

Cela se démontre par récurrence de la même façon que pour la relation (A.7).

4 Le cas $N = 3$

Il est utile pour le Chap. 3 de considérer le cas particulier de $N = 3$ particules de même masse m. Les coordonnées de Jacobi sont alors :

$$\vec{\eta}_2 = \vec{r}_2 - \vec{r}_1, \tag{A.11}$$

$$\vec{\eta}_3 = \vec{r}_3 - \frac{\vec{r}_1 + \vec{r}_2}{2}. \tag{A.12}$$

Il est commode de redéfinir des coordonnées de Jacobi $(\vec{r}, \vec{\rho})$ par :

$$\vec{r} \equiv \vec{\eta}_2, \tag{A.13}$$

$$\vec{\rho} \equiv \frac{2}{\sqrt{3}} \vec{\eta}_3. \tag{A.14}$$

L'équation (A.7) devient alors :

$$\boxed{\sum_{i=1}^{3} \hat{h}(m_i, \vec{r}_i) = \hat{h}(M, \vec{C}) - \frac{\hbar^2}{m} \left(\Delta_{\vec{r}} + \Delta_{\vec{\rho}} \right) + \frac{1}{4} m\omega^2 \left(r^2 + \rho^2 \right).} \tag{A.15}$$

Appendice B

Une particule dans un potentiel $A_1/R^2 + A_2R^2$

Ce chapitre est essentiellement formel, mais les résultats obtenus sont utiles pour résoudre plusieurs problèmes physiques rencontrés dans cette thèse.

Considérons une particule de masse μ. Notons $\vec{R} \in \mathbb{R}^d$ son vecteur position et d la dimension de l'espace. Supposons que la particule est soumise à un potentiel

$$\frac{\hbar^2}{2\mu}\frac{C}{R^2} + \frac{1}{2}\mu\omega^2 R^2$$

où C est une constante sans dimension.
Notons $G(\vec{R}) = G(R)$ la fonction d'onde de la particule, supposée invariante par rotation et réelle. L'équation de Schrödinger s'écrit :

$$-\frac{\hbar^2}{2\mu}\Delta_{\vec{R}}G(R) + \left(\frac{\hbar^2}{2\mu}\frac{C}{R^2} + \frac{1}{2}\mu\omega^2 R^2\right) G(R) = E\, G(R). \tag{B.1}$$

Remarquons que

$$\Delta_{\vec{R}}G(R) = \left(\frac{d^2}{dR^2} + \frac{d-1}{R}\,\frac{d}{dR}\right) G(R). \tag{B.2}$$

1 Comment se ramener à 2 dimensions

Posons

$$\begin{cases} \alpha = \dfrac{d}{2} - 1 & \text{(B.3)} \\ G(R) = R^{-\alpha}F(R). & \text{(B.4)} \end{cases}$$

L'équation de Schrödinger devient :

$$-\frac{\hbar^2}{2\mu}\left(F''(R) + \frac{1}{R}F'(R)\right) + \left(\frac{\hbar^2}{2\mu}\frac{s^2}{R^2} + \frac{1}{2}\mu\omega^2 R^2\right) F(R) = E\, F(R), \tag{B.5}$$

avec

$$s^2 \equiv C + \alpha^2.$$

Nous prenons la détermination suivante du signe de s :

$$\begin{cases} s \in \mathbb{R}_+ & \text{si } s^2 \in \mathbb{R}_+ \quad (B.6) \\ s \in i\,\mathbb{R}_+ & \text{si } s^2 \in \mathbb{R}_- \ . \quad (B.7) \end{cases}$$

Notons que pour $d = 2$, on a $\alpha = 0$, $G(R) = F(R)$ et $C = s^2$; les équations (B.1) et (B.5) sont alors identiques. Nous nous sommes donc ramenés au cas $d = 2$.

Les produits scalaires

$$\langle G_1 | G_2 \rangle := \int d^d\vec{R}\; G_1(R)\, G_2(R) \quad (B.8)$$

$$\{F_1 | F_2\} := \int_0^\infty dR\, R\, F_1(R)\, F_2(R) \quad (B.9)$$

sont reliés par

$$\langle G_1 | G_2 \rangle = c_d\, \{F_1 | F_2\}$$

où c_d est tel que $d^d\vec{R} = c_d\, R\, dR$ ($c_1 = 1$, $c_2 = 2\pi$, $c_3 = 4\pi$, ...).

Pour alléger les notations, prenons des unités où

$$\hbar = 1 \text{ et } \mu = 1.$$

Dans la suite nous étudions donc l'équation de Schrödinger :

$$-F''(R) - \frac{1}{R}F'(R) + \left(\frac{s^2}{R^2} + \omega^2 R^2\right) F(R) = 2E\, F(R). \quad (B.10)$$

2 Quelle condition aux limites pour $R \to 0$?

Afin de simplifier la discussion, restreignons-nous au cas $\omega > 0$, et prenons

$$\omega = 1. \quad (B.11)$$

Nous admettrons que le cas $\omega = 0$, qui soulève les difficultés mathématiques habituelles dans le cas des fonctions d'ondes non normalisables à l'infini, conduit à des résultats analogues.

Pour chaque $E \in \mathbb{R}$, il existe une unique solution $F_E(R)$ de l'équation (B.10) qui tend vers 0 pour $R \to \infty$. On ne peut pas considérer *tous* les F_E comme des états propres du Hamiltonien, car on aurait alors un spectre S égal à $\mathbb{R}$ tout entier.

Résolvons ce problème par la prescription que le Hamiltonien

$$H = \frac{1}{2}\left[-\frac{d^2}{dR^2} - \frac{1}{R}\frac{d}{dR} + \frac{s^2}{R^2} + \omega^2 R^2\right]$$

doit être hermitien pour le produit scalaire $\{\ ,\ \} = \{\ |\ \}$. Cela signifie que pour tout E appartenant au spectre S, l'état propre F_E doit être de norme finie

$$\forall E \in S,\ \{F_E, F_E\} < \infty, \quad (B.12)$$

et que de plus :

$$\forall E, E' \in S,\ E \neq E' \Rightarrow\ \{F_E,\, HF_{E'}\} = \{HF_E,\, F_{E'}\}\,. \quad (B.13)$$

Nous imposons de plus que S soit une famille *maximale* vérifiant (B.13). En effet nous souhaitons que les états propres $(F_E)_{E\in S}$ forment non seulement une famille orthogonale, mais aussi complète.

Cette prescription est physiquement justifiée dans chacun des cas où nous utilisons les résultats de cette Appendice. Notons que l'idée de cette prescription semble avoir été introduite par von Neumann dans un travail non publié, et a été reprise ensuite par Wigner dans son article fondateur sur le pseudopotentiel [13], puis dans [78, 79] et dans bien d'autre travaux, notamment dans le contexte du problème à 3 bosons (cf. Chap. 0, Section 3). Notons également qu'une autre façon de traiter le problème est de considérer que la divergence en $1/R^2$ du potentiel est coupée à une courte distance $R = R_c$, par exemple par un mur infini ([80] § 35) ; cette approche conduit à des calculs plus lourds, mais devient équivalente à celle que nous utilisons dans la limite $R_c \to 0$. Notons enfin qu'il est possible de généraliser la présente discussion en considérant des produits scalaires modifiés [73, 71].

Il nous faut donc déterminer toutes les sous-familles maximales S de $\mathbb{R}$ vérifiant (B.13). On peut remarquer que, compte tenu de $HF_E = EF_E$ et $HF_{E'} = E'F_{E'}$, (B.13) équivaut à :

$$\forall E, E' \in S,\ E \neq E' \Rightarrow\ \{F_E, F_{E'}\} = 0. \tag{B.14}$$

Il nous faut donc déterminer toutes les sous-familles maximales *orthogonales* $(F_E)_{E\in S}$ de $(F_E)_{E\in\mathbb{R}}$.

Le résultat est que chaque telle famille S peut être définie par une condition aux limites sur $F(R)$ pour $R \to 0$. Ces conditions aux limites sont listées dans le tableau page 70. Pour $s^2 \geq 0$, certaines de ces conditions aux limites dépendent d'un paramètre noté l. Pour $s^2 < 0$, la condition aux limites dépend d'un paramètre noté R_t.

Pour justifier ce résultat, notre raisonnement, inspiré de Morse et Feshbach [79], est le suivant. On remarque d'abord que, en vertu du théorème d'Ostrogradski, la condition

$$\{F_E,\, HF_{E'}\} - \{HF_E,\, F_{E'}\} = 0 \tag{B.15}$$

équivaut à :

$$\lim_{R\to 0} R \cdot \left(F_E \frac{dF_{E'}}{dR} - F_{E'} \frac{dF_E}{dR} \right) = 0. \tag{B.16}$$

Nous cherchons donc les sous-familles maximales S de $\mathbb{R}$ vérifiant

$$\forall E, E' \in S,\ E \neq E' \Rightarrow\ \lim_{R\to 0} R \cdot \left(F_E \frac{dF_{E'}}{dR} - F_{E'} \frac{dF_E}{dR} \right) = 0. \tag{B.17}$$

Dans la suite nous supposons $s \neq 0$, mais le cas $s = 0$ se traite de façon analogue. Un point clé est que pour tout E, il existe α_E et β_E tels que :

$$F_E(R) \underset{R\to 0}{=} \alpha_E \left(R^{-s} + O(R^{-s+2}) \right) + \beta_E \left(R^s + O(R^{s+2}) \right). \tag{B.18}$$

En effet, $F(R) = R^{\pm s}$ sont des solutions des l'équation de Schrödinger (B.10) dans la limite $R \to 0$. Plus précisément, on a

$$F_E(R) = \frac{1}{R} W_{\frac{E}{2},\frac{s}{2}} \left(R^2 \right) \tag{B.19}$$

où W est un fonction de Whittaker, qui tend gaussiennement vers 0 pour $R \to \infty$, et qui vérifie [75] :

$$F_E(R) \underset{R\to 0}{=} \frac{\Gamma(s)}{\Gamma\left(\frac{1+s-E}{2}\right)} \left(R^{-s} + O(R^{-s+2}) \right) + \frac{\Gamma(-s)}{\Gamma\left(\frac{1-s-E}{2}\right)} \left(R^s + O(R^{s+2}) \right). \tag{B.20}$$

Considérons d'abord le cas $s \in [1, +\infty[$. Dans ce cas, la fonction R^{-s} n'est pas normalisable au voisinage de $R = 0$ pour la norme $\{|\}$. Or pour tout E appartenant au spectre S, F_E doit être normalisable [cf. (B.12)]. Cela impose de prendre $\alpha_E = 0$ dans (B.18), ce qui équivaut à la condition aux limites :

$$\exists A/\ F(R) \underset{R\to 0}{=} A\ R^s + O(R^{s+2}) \tag{B.21}$$

ou encore à la simple condition que $F(R)$ soit bornée pour $R \to 0$. Réciproquement, on vérifie aisément que pour toutes fonctions F_E et $F_{E'}$ vérifiant (B.21), la condition (B.16) est satisfaite. En conclusion, le seul choix possible pour S est celui défini par la condition aux limites (B.21).

Passons au cas $s \in]0;1[$ ou $s \in i\mathbb{R}$. L'éq. (B.18) devient alors

$$F_E(R) \underset{R\to 0}{=} \alpha_E R^{-s} + \beta_E R^s + O(R^{-s+2}). \tag{B.22}$$

En reportant ce développement dans (B.16), on montre que la condition (B.16) équivaut à :

$$\alpha_E \beta_{E'} - \alpha_{E'} \beta_E = 0. \tag{B.23}$$

La condition (B.17) peut donc se réécrire comme :

$$\forall E, E' \in S,\ E \neq E' \Rightarrow\ \alpha_E \beta_{E'} - \alpha_{E'} \beta_E = 0. \tag{B.24}$$

Montrons donc que les familles S maximales vérifiant (B.24) sont les familles S définies par une des conditions aux limites du Tableau de la page 70. Pour ce faire, il suffit de montrer que :
(i) : Si S est définie par une des conditions aux limites du Tableau, alors S satisfait (B.24).
(ii) : Si S vérifie (B.24), alors il existe une des conditions aux limites du Tableau qui est vérifiée par tout F_E avec $E \in S$.

La démonstration de (i) est sans difficulté.

Pour montrer (ii), considérons une famille S vérifiant (B.24) et fixons un E appartenant à S.

— Pour $s \in]0;1[$:
Distinguons deux cas :
  — Si $\alpha_E = 0$: alors d'après (B.18), F_E vérifie la condition aux limites (B.21). Considérons ensuite un E' dans S distinct de E. On montre grâce à (B.20) que $\beta_E \neq 0$, et donc (B.23) implique : $\alpha_{E'} = 0$. Donc la condition aux limites (B.21) est non seulement satisfaite par F_E, mais aussi par $F_{E'}$, et donc par tout les $F_{\mathcal{E}}$ avec $\mathcal{E} \in S$.
  — Si $\alpha_E \neq 0$: définissons $\epsilon \in \{+1;-1\}$ et $l \in]0;+\infty]$ tels que

$$\frac{\beta_E}{\alpha_E} = -\frac{\epsilon}{l^{2s}}. \tag{B.25}$$

  En particulier, nous prenons $l = +\infty$ dans le cas où $\beta_E = 0$. D'après (B.22), F_E satisfait alors la condition aux limites :

$$\exists A/\ F(R) \underset{R\to 0}{=} A\left[R^{-s} - \frac{\epsilon}{l^{2s}} R^s\right] + O(R^{-s+2}). \tag{B.26}$$

  Considérons ensuite un E' dans S distinct de E. On peut supposer $\alpha_{E'} \neq 0$, sans quoi on se ramène au cas $\alpha_E = 0$ en échangeant les rôles de E et E'. Les équations (B.23,B.25) donnent alors :

$$\frac{\beta_{E'}}{\alpha_{E'}} = -\frac{\epsilon}{l^{2s}}, \tag{B.27}$$

  et donc $F_{E'}$ satisfait (B.26).
— Pour $s \in i\mathbb{R}$:
D'après (B.20) on a

$$\alpha_E = (\beta_E)^* \neq 0. \tag{B.28}$$

On peut donc définir $R_t \in [1; e^{\pi/|s|}[$ par

$$\frac{\beta_E}{\alpha_E} = -\frac{1}{(R_t)^{2s}}. \tag{B.29}$$

Alors d'après (B.18) F_E satisfait la condition aux limites

$$\exists A/\ F(R) \underset{R\to 0}{\sim} A \sin\left[|s| \ln\left(\frac{R}{R_t}\right)\right]. \tag{B.30}$$

Pour $E' \in S$ tel que $E' \neq E$, on a d'après (B.23,B.29)

$$\frac{\beta_{E'}}{\alpha_{E'}} = -\frac{1}{(R_t)^{2s}}, \tag{B.31}$$

et donc $F_{E'}$ satisfait (B.30).

Ceci achève la démonstration.

3 Tableau récapitulatif

Les principaux résultats de cet Appendice sont résumés dans le tableau de la page suivante. Mentionnons que les spectres donnés dans le tableau se déduisent des propriétés suivantes des fonctions de Bessel K et des fonctions de Whittaker W :

$$K_s(z) \underset{z\to 0}{=} \frac{\pi}{2\sin(s\pi)} \left\{ \left(\frac{z}{2}\right)^{-s} \left[\frac{1}{\Gamma(-s+1)} + O(z^2)\right] - \left(\frac{z}{2}\right)^{s} \left[\frac{1}{\Gamma(s+1)} + O(z^2)\right] \right\} \tag{B.32}$$

$$\frac{1}{R} W_{\frac{E}{2},\frac{s}{2}}(R^2) \underset{R\to 0}{=} \frac{\Gamma(-s)}{\Gamma(\frac{1-s-E}{2})} R^s \left(1 + O(R^2)\right) + \frac{\Gamma(s)}{\Gamma(\frac{1+s-E}{2})} R^{-s} \left(1 + O(R^2)\right). \tag{B.33}$$

	Condition aux limites : $\exists A,\ F(R) =_{R\to 0} \ldots$	états liés dans l'espace libre ($\omega = 0$)			états propres dans un piège ($\omega = 1$)		
		E	$F(R)$	$\{F\|F\}$	E	$F(R)$	$\{F\|F\}$
$s \in [1, \infty[$	$A \cdot R^s + O(R^{s+2})$				$s+1+2q,$ $q \in \mathbb{N}$	$e^{-\frac{R^2}{2}} R^s L_q^{(s)}(R^2)$	$\frac{\Gamma(s+1+q)}{2\cdot q!}$
$s \in]0, 1[$	$A \cdot R^s + O(R^{s+2})$				$s+1+2q,$ $q \in \mathbb{N}$	$e^{-\frac{R^2}{2}} R^s L_q^{(s)}(R^2)$	$\frac{\Gamma(s+1+q)}{2\cdot q!}$
	$A \cdot R^{-s} + O(R^{-s+2})$				$-s+1+2q,$ $q \in \mathbb{N}$	$e^{-\frac{R^2}{2}} R^{-s} L_q^{(-s)}(R^2)$	$\frac{\Gamma(-s+1+q)}{2\cdot q!}$
	$A \cdot [R^{-s} - \frac{\epsilon}{l^{2s}} R^s]$ $+O(R^{-s+2})$	Seulement si $\epsilon = +1$ $-\frac{2}{l^2}\left[\frac{\Gamma(1+s)}{\Gamma(1-s)}\right]^{\frac{1}{s}}$	$K_s(R\sqrt{-2E})$	$\frac{\pi\|s\|}{4\|E\|\sinh(\pi\|s\|)}$	$-\frac{\epsilon}{l^{2s}} =$ $\frac{\Gamma\left(\frac{1+s-E}{2}\right)\Gamma(-s)}{\Gamma\left(\frac{1-s-E}{2}\right)\Gamma(s)}$	$\frac{1}{R} W_{\frac{E}{2},\frac{s}{2}}(R^2)$	$\left(\frac{\pi}{2\sin(\pi s)}\right) \times$ $\left[\frac{\psi\left(\frac{1+s-E}{2}\right) - \psi\left(\frac{1-s-E}{2}\right)}{\Gamma\left(\frac{1+s-E}{2}\right)\Gamma\left(\frac{1-s-E}{2}\right)}\right]$
$s \in i\mathbb{R}_+^*$	$A \sin\left[\|s\| \ln\left(\frac{R}{R_t}\right)\right]$ $+o(1)$	$-\frac{2}{R_t^2} e^{n2\pi/\|s\|}$ $\times e^{\frac{2}{\|s\|}\arg\Gamma(1+s)},$ $n \in \mathbb{Z}$	$K_s(R\sqrt{-2E})$	$\frac{\pi\|s\|}{4\|E\|\sinh(\pi\|s\|)}$	$\arg\Gamma\left(\frac{1+s-E}{2}\right)$ $\equiv^{[\pi]} -\|s\|\ln R_t$ $+\arg\Gamma(1+s)$	$\frac{1}{R} W_{\frac{E}{2},\frac{s}{2}}(R^2)$	$\frac{\pi \cdot \mathrm{Im}\,\psi\left(\frac{1-E+s}{2}\right)}{\sinh(\|s\|\pi) \cdot \left\|\Gamma\left(\frac{1-E+s}{2}\right)\right\|^2}$
$s = 0$	$O(1)$				$1+2q,$ $q \in \mathbb{N}$	$e^{-\frac{R^2}{2}} L_q^{(0)}(R^2)$	$\frac{1}{2}$
	$A \ln\left(\frac{R}{l}\right) + o(1)$	$-\frac{2}{l^2 e^{2\gamma}}$	$K_0(R\sqrt{-2E})$	$\frac{1}{4\|E\|}$	$\psi\left(\frac{1-E}{2}\right) =$ $-2(\ln l + \gamma)$	$\frac{1}{R} W_{\frac{E}{2},\frac{s}{2}}(R^2)$	$\frac{\psi'\left(\frac{1-E}{2}\right)}{2\left[\Gamma\left(\frac{1-E}{2}\right)\right]^2}$

TABLE B.1 – Solution de l'équation $-F''(R) - \frac{1}{R}F'(R) + \left(\frac{s^2}{R^2} + \omega^2 R^2\right) F(R) = 2EF(R)$. Pour chaque valeur de s, il faut et il suffit de choisir l'une des conditions aux limite indiquées afin que le problème soit hermitien pour le produit scalaire $\{F_1|F_2\} = \int_0^\infty dR\, R\, F_1(R)^*\, F_2(R)$. La condition aux limites peut contenir des paramètres fixés ($l \in \mathbb{R}_+^*$, $\epsilon = \pm 1$; $R_t \in \mathbb{R}_+^*$). On obtient alors 0, 1 ou une infinité d'états liés (i. e. de solutions d'énergie $E < 0$) dans l'espace libre (i.e. pour $\omega = 0$) ; et une famille d'états propres dans un piège (i.e. pour $\omega > 0$, ou pour un choix convenable des unités, $\omega = 1$). $L_q^{(.)}$ désigne un polynôme de Laguerre généralisé de degré q, K une fonction de Bessel modifiée, W une fonction de Whittaker , et $\psi = \Gamma'/\Gamma$ la fonction digamma [75, 76].

Partie 2 : Le problème à 3 corps

Dans la partie précédente, nous avons vu que le problème à N corps unitaire dans un piège harmonique isotrope est équivalent au même problème dans l'espace libre. Or le problème à 3 corps dans l'espace libre a été résolu analytiquement par Efimov [16]. Nous pouvons ainsi résoudre le problème à 3 corps unitaire dans un piège. Le cas de particules bosoniques est particulièrement intéressant, car il existe deux types d'états propres, que nous appelons états efimoviens et états universels. Les états efimoviens sont la version piégée des célèbres trimères découverts par Efimov dans l'espace libre, et dépendent d'un paramètre à 3 corps. Les états universels sont indépendants du paramètre à 3 corps, et ressemblent aux états propres fermioniques. Cette différence s'explique par l'existence d'un potentiel d'interaction à trois corps effectif, qui diverge rapidement lorsque les 3 particules sont proches. Dans le cas efimovien, ce potentiel est attractif, et il y a une forte probabilité que les 3 particules soient proches, avec des grands vecteurs d'onde, et leur interaction n'est plus décrite par la seule longueur de diffusion. Ceci implique également que les états efimoviens ont une forte probabilité de se désintégrer en un dimère fortement lié et un atome libre. Dans le cas universel, le potentiel effectif est répulsif, et les 3 particules ne sont jamais trop proches. Les états universels sont ainsi immunisés contre l'effet d'Efimov, et ont une longue durée de vie.

Article III

Unitary Three-Body Problem in a Harmonic Trap

PRL 97, 150401 (2006) PHYSICAL REVIEW LETTERS week ending 13 OCTOBER 2006

Unitary Quantum Three-Body Problem in a Harmonic Trap

Félix Werner and Yvan Castin

Laboratoire Kastler Brossel, École Normale Supérieure, 24 rue Lhomond, 75231 Paris Cedex 05, France

(Received 18 July 2005; published 10 October 2006)

We consider either 3 spinless bosons or 3 equal mass spin-1/2 fermions, interacting *via* a short-range potential of infinite scattering length and trapped in an isotropic harmonic potential. For a zero-range model, we obtain analytically the exact spectrum and eigenfunctions: for fermions all the states are universal; for bosons there is a coexistence of decoupled universal and efimovian states. All the universal states, even the *bosonic* ones, have a tiny 3-body loss rate. For a finite range model, we numerically find for bosons a coupling between zero angular momentum universal and efimovian states; the coupling is so weak that, for realistic values of the interaction range, these bosonic universal states remain long-lived and observable.

DOI: 10.1103/PhysRevLett.97.150401 PACS numbers: 03.75.Ss, 05.30.Jp

With a Feshbach resonance, it is now possible to produce a stable quantum gas of fermionic atoms in the unitary limit, i.e., with an interaction of negligible range and scattering length $a = \infty$ [1]. The properties of this gas, including its superfluidity, are under active experimental investigation [2]. They have the remarkable feature of being universal, as was tested, in particular, for the zero temperature equation of state of the gas [3]. In contrast, experiments with Bose gases at a Feshbach resonance suffer from high loss rates [4–6], and even the existence of a unitary Bose gas phase is a very open subject [7].

In this context, fully understanding the few-body unitary problem is a crucial step. In free space, the unitary 3-boson problem has an infinite number of weakly bound states, the so-called Efimov states [8]. In a trap, it has efimovian states [9,10] but also universal states whose energy depends only on the trapping frequency [9]. Several experimental groups are currently trapping a few particles at a node of an optical lattice [11] and are controlling the interaction strength *via* a Feshbach resonance. Results have already been obtained for two particles per lattice node [12], a case that was solved analytically [13]. Anticipating experiments with 3 atoms per node, we derive in this Letter exact expressions for *all* universal and efimovian eigenstates of the 3-body problem for bosons (generalizing [9] to a nonzero angular momentum) and for equal mass fermions in a trap. We also show the long lifetime of the universal states and their observability in a real experiment, extending to universal states the numerical study of [10].

If the effective range and the true range of the interaction potential are negligible as compared to the de Broglie wavelength of the 3 particles, the interaction potential can be replaced by the Bethe-Peierls contact conditions on the wave function ψ: it exists a function A such that

$$\psi(\mathbf{r}_1, \mathbf{r}_2, \mathbf{r}_3) = \left(\frac{1}{r_{ij}} - \frac{1}{a}\right) A(\mathbf{R}_{ij}, \mathbf{r}_k) + O(r_{ij}) \qquad (1)$$

in the limit $r_{ij} \equiv |\mathbf{r}_i - \mathbf{r}_j| \to 0$ taken for fixed positions of the other particle k and of the center of mass $\mathbf{R}_{ij}$ of i and j.

In the unitary limit considered in this Letter, $a = \infty$. When all the r_{ij} are nonzero, the wave function ψ obeys the noninteracting Schrödinger equation

$$\sum_{i=1}^{3}\left[-\frac{\hbar^2}{2m}\Delta_{\mathbf{r}_i} + \frac{1}{2}m\omega^2 r_i^2\right]\psi = E\psi. \qquad (2)$$

ω is the oscillation frequency and m the mass of an atom.

To solve this problem, we extend the approach of Efimov [8,14] to the trapped case, and obtain the form

$$\psi(\mathbf{r}_1, \mathbf{r}_2, \mathbf{r}_3) = \psi_{\text{c.m.}}(\mathbf{C}) F(R)(1 + \hat{Q})\frac{1}{r\rho}\varphi(\alpha) Y_l^m(\boldsymbol{\rho}/\rho). \qquad (3)$$

Since the center of mass is separable for a harmonic trapping, we have singled out the wave function $\psi_{\text{c.m.}}(\mathbf{C})$ of its stationary state of energy $E_{\text{c.m.}}$, with $\mathbf{C} = (\mathbf{r}_1 + \mathbf{r}_2 + \mathbf{r}_3)/3$. The operator $\hat{Q}$ ensures the correct exchange symmetry of ψ: for spinless bosons, $\hat{Q} = \hat{P}_{13} + \hat{P}_{23}$, where $\hat{P}_{ij}$ transposes particles i and j; for spin-1/2 fermions, we assume a spin state $\uparrow\downarrow\uparrow$ so that $\hat{Q} = -\hat{P}_{13}$. The Jacobi coordinates are $\mathbf{r} = \mathbf{r}_2 - \mathbf{r}_1$ and $\boldsymbol{\rho} = (2\mathbf{r}_3 - \mathbf{r}_1 - \mathbf{r}_2)/\sqrt{3}$. Y_l^m is a spherical harmonic, l being the total internal angular momentum of the system. The function $\varphi(\alpha)$, where $\alpha = \arctan(r/\rho)$, solves the eigenvalue problem

$$-\varphi''(\alpha) + \frac{l(l+1)}{\cos^2\alpha}\varphi(\alpha) = s^2\varphi(\alpha) \qquad (4)$$

$$\varphi(\pi/2) = 0 \qquad (5)$$

$$\varphi'(0) + \eta(-1)^l\frac{4}{\sqrt{3}}\varphi(\pi/3) = 0 \qquad (6)$$

with $\eta = -1$ for fermions, $\eta = 2$ for bosons. An analytical expression can be obtained for $\varphi(\alpha)$ [15], which leads to the transcendental equation for s [16]:

$$\left\{i^l\sum_{k=0}^{l}\frac{(-l)_k(l+1)_k}{k!}\frac{(1-s)_l}{(1-s)_k}\left[2^{-k}i(k-s)e^{is(\pi/2)} + \eta(-1)^l\frac{4}{\sqrt{3}}e^{i(\pi/6)(2k+s)}\right]\right\} - \{i \leftrightarrow -i\} = 0, \qquad (7)$$

with the notation $(x)_n \equiv x(x+1)\dots(x+n-1)$. This equation is readily solved numerically: for each l, the solutions form an infinite sequence $(s_{l,n})_{n\geq 0}$, see Fig. 1. As we show below, all solutions are real, except for bosons in the $l=0$ channel, where a single purely imaginary solution exists, $s_{l=0,n=0} \equiv s_0 \simeq i \times 1.00624$, the well-known Efimov solution. Finally, the function $F(R)$, where the hyperradius is $R = \sqrt{(r^2+\rho^2)/2}$, solves the problem:

$$\left[-\frac{\hbar^2}{2m}\left(\frac{d^2}{dR^2}+\frac{1}{R}\frac{d}{dR}\right)+U(R)\right]F(R) = (E-E_{\text{c.m.}})F(R), \tag{8}$$

where $U(R) = \hbar^2 s^2/(2mR^2) + m\omega^2 R^2/2$, s being one of the $s_{l,n}$. This is the Schrödinger equation for a fictitious particle of zero angular momentum moving in two dimensions in the potential $U(R)$.

When $s^2 > 0$, one takes $s > 0$ and the solution is

$$F(R) = R^s e^{-R^2/2a_{\text{ho}}^2} L_q^{(s)}(R^2/a_{\text{ho}}^2) \tag{9}$$

where $a_{\text{ho}} = (\hbar/m\omega)^{1/2}$ is the harmonic oscillator length, $L_q^{(\cdot)}$ is the generalized Laguerre polynomial of degree q, q being an arbitrary non-negative integer. The resulting spectrum for the 3-body problem is

$$E = E_{\text{c.m.}} + (s_{l,n} + 1 + 2q)\hbar\omega. \tag{10}$$

The quantum number q leads to a semi-infinite ladder structure of the spectrum with a regular spacing $2\hbar\omega$. This is related to the existence of a scaling solution for the trapped unitary gas [17] and the subsequent embedding of the Hamiltonian in a $SO(2,1)$ algebra [18], leading to an exact mapping between trapped and free space universal states [19].

When $s^2 < 0$, as is the case in the $l = n = 0$ channel for bosons, the Schrödinger equation [Eq. (8)] does not define

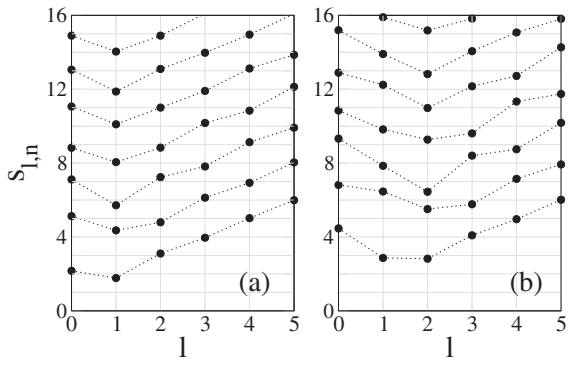

FIG. 1. The constants $s_{l,n}$ for (a) 3 equal mass fermions and (b) 3 bosons, obtained by numerical solution of the transcendental equation [Eq. (7)]. We have not represented the $s_{l=0,n=0}$ solution for bosons, which is purely imaginary. According to Eq. (10), each real $s_{l,n}$ gives rise to a semi-infinite ladder of universal states. Note that the ground universal state has a total angular momentum $l = 1$ for fermions ($E \simeq 4.27\hbar\omega$) and $l = 2$ for bosons ($E \simeq 5.32\hbar\omega$).

by itself a Hermitian problem and has to be supplemented by a boundary condition for $R \to 0$ [20,21]:

$$F(R) \propto \text{Im}\left[\left(\frac{R}{R_t}\right)^{s_0}\right], \tag{11}$$

where R_t is an additional 3-body parameter. For the resulting efimovian states, the function F is given by

$$F(R) = R^{-1} W_{(E-E_{\text{c.m.}})/2\hbar\omega, s_0/2}(R^2/a_{\text{ho}}^2), \tag{12}$$

where W is a Whittaker function, and the energy solves:

$$\arg\Gamma\left[\frac{1+s_0-(E-E_{\text{c.m.}})/\hbar\omega}{2}\right] = -|s_0|\ln(R_t/a_{\text{ho}}) + \arg\Gamma(1+s_0) \bmod \pi. \tag{13}$$

We did not yet obtain all the 3-body eigenstates [22]. Indeed, all the above states satisfy the contact condition (1) with a *nonzero* function A. But there are wave functions of the unitary gas which *vanish* when two particles are at the same point; these are also eigenstates of the noninteracting case. An example is the Laughlin state of the fractional quantum Hall effect [23]:

$$\psi = e^{-\sum_{i=1}^3 r_i^2/2a_{\text{ho}}^2} \prod_{1\leq n<m\leq 3} [(x_n + iy_n) - (x_m + iy_m)]^{|\eta|}. \tag{14}$$

In the limit of high energies $E \gg \hbar\omega$, there are actually many of these $A \equiv 0$ states: their density of states (DOS) is almost as high as the DOS of the noninteracting case:

$$\frac{\rho_{A\equiv 0}(E)}{\rho_{\text{noninter}}(E)} \underset{E\to\infty}{=} 1 - O\left(\left(\frac{\hbar\omega}{E}\right)^2\right). \tag{15}$$

In contrast, the DOS of the $A \neq 0$ states is only

$$\frac{\rho_{A\neq 0}(E)}{\rho_{\text{noninter}}(E)} \underset{E\to\infty}{=} O\left(\left(\frac{\hbar\omega}{E}\right)^3\right). \tag{16}$$

Equation (16) is a consequence of Eq. (17) given below. We found Eq. (15) by applying the rank theorem to the operator $\psi_0(\mathbf{r}_1,\mathbf{r}_2,\mathbf{r}_3) \mapsto (\psi_0(\mathbf{r}_1,\mathbf{r}_1,\mathbf{r}_3), \psi_0(\mathbf{r}_1,\mathbf{r}_2,\mathbf{r}_1), \psi_0(\mathbf{r}_1,\mathbf{r}_2,\mathbf{r}_2))$ which associates, to each noninteracting eigenstate ψ_0 of energy E, 3 functions of 2 atomic positions, and whose kernel is the space of $A \equiv 0$ states of energy E [24].

This completes our derivation of *all* eigenstates of the unitary 3-body problem in a trap. Three types of states are obtained in general: universal eigenstates common to the noninteracting case, universal interacting states, and efimovian states depending on a 3-body parameter.

We now prove that the Efimov effect is absent for 3 equal mass fermions. This fact is known but to our knowledge not demonstrated. Numerically one can only check the absence of imaginary solution of the transcendental equation in some finite interval of s and l. Here we prove that for any l and any imaginary s, there is no solution to the

PRL 97, 150401 (2006) PHYSICAL REVIEW LETTERS week ending 13 OCTOBER 2006

problem (4)–(6). Let us assume that $s^2 \leq l(l+1)$, and that (4) and (5) are satisfied. We will show that the quantity $Q(l, s^2) \equiv \varphi'(0) - (-1)^l(4/\sqrt{3})\varphi(\pi/3)$ is nonzero, which is incompatible with (6). We rewrite (4) as $\varphi''(\alpha) = u(\alpha)\varphi(\alpha)$. This is Newton's equation, α being the time and φ the position of a fictitious particle subject to an *expelling* harmonic force with time dependent spring constant $u(\alpha; l, s^2) = \frac{l(l+1)}{\cos^2\alpha} - s^2 \geq 0$. Equation (5) imposes that this particle reaches the origin at "time" $\pi/2$. The particle then should not reach the origin earlier, otherwise the expelling force would prevent it from turning back to $\varphi = 0$. We thus can take the normalization $\varphi(0) = 1$, which implies $\varphi'(0) < 0$ and $\varphi(\alpha) > 0$ for $0 \leq \alpha < \pi/2$. Thus, $Q(l, s^2) < 0$ for l even. For l odd, one needs two intermediate results: (i) $Q(l = 1, s^2 = 2) < 0$ (which we check by explicit calculation); (ii) if φ_1, φ_2 are two solutions with $u_2 \geq u_1$, then $\varphi_2 \leq \varphi_1$, and $Q_2 \leq Q_1$: because the spring constant for particle 2 is larger, particle 2 has to start faster and walk constantly ahead of particle 1 in the race towards the origin to satisfy Eq. (5). Now the assumption $s^2 \leq l(l+1)$ implies $u(\alpha; l, s^2) \geq u(\alpha; l = 1, s^2 = 2)$. One concludes that: $Q(l, s^2) \leq Q(l = 1, s^2 = 2) < 0$. For bosons, we proved similarly that all the s^2 are positive, except for the well-known $s_{n=0,l=0} \simeq i \times 1.00624$.

It appears clearly in Fig. 1 that $s_{l,n}$ gets close to an integer value $\bar{s}_{l,n}$ as soon as l or n increases, with

$$\begin{aligned} \bar{s}_{l,n} &= l + 1 + 2n \quad \text{for } l \geq |\eta| \\ \bar{s}_{l,n} &= 2n - l + (2\eta + 11)/3 \quad \text{for } l < |\eta| \end{aligned} . \tag{17}$$

To check this analytically, the transcendental equation is not useful. We rather applied semiclassical WKB techniques to the problem (4)–(6), and obtained [25]:

$$s_{l,0} - \bar{s}_{l,0} \sim_{l\to\infty} \eta(-1)^{l+1}2^{1-l}/\sqrt{3\pi l} \tag{18}$$

$$s_{l,n} - \bar{s}_{l,n} \sim_{n\to\infty} \eta \cos\left[\frac{\pi}{3}(l + 1 - n)\right] \frac{(-1)^{l+n+1}4}{\pi\sqrt{3}n} \tag{19}$$

$$\max_n |s_{l,n} - \bar{s}_{l,n}| \sim_{l\to\infty} |\eta| \frac{4\mathrm{Ai}_{\max}}{3^{7/12}\pi^{1/2}} l^{-5/6} \tag{20}$$

with $\mathrm{Ai}_{\max} \simeq 0.5357$ the maximum of the Airy function.

We now discuss the lifetime of the 3-body states found here in the trap, due to 3-body recombination to a deeply bound molecular state. The recombination rate is commonly estimated as $\Gamma_{\mathrm{loss}} \propto P\hbar/(m\sigma^2)$, where σ is the range of the interaction potential, and P is the probability that $R < \sigma$ [26]. Evaluating P from the 3-body wave functions obtained above for the zero-range model, this gives for E not much larger than $\hbar\omega$:

$$\Gamma_{\mathrm{loss}}^{\mathrm{univ}} \propto \omega\left(\frac{\sigma}{a_{\mathrm{ho}}}\right)^{2s} \tag{21}$$

for a universal state with exponent s, and $\Gamma_{\mathrm{loss}}^{\mathrm{efim}} \propto \omega$ for an efimovian state. Since $s \geq 1.77$ for fermions and $s \geq 2.82$ for bosons (Fig. 1), Eq. (21) indicates that the lifetime of universal states is $\gg 1/\omega$ for $\sigma \ll a_{\mathrm{ho}}$.

The existence of long-lived bosonic states is an unexpected feature that we now investigate in a more realistic way. The unitary three-body problem in an isotropic harmonic trap may be realized experimentally by trapping 3 atoms at a site of a deep optical lattice, and using a Feshbach resonance. For a broad Feshbach resonance, the effective range is of the order of the van der Waals length, which is roughly 1 order of magnitude smaller than a_{ho} for a usual lattice spacing of $\sim$0.5 μm and a lattice depth of $\sim$50 recoil energies. This experimental situation is not deeply in the asymptotic regime of a zero-range potential. Moreover, in the zero-range model, there are energy crossings between universal and efimovian states as a function of R_t/a_{ho} [see solid lines in Fig. 2(a)]; as we shall see, for a finite range, there is a coupling between $l = 0$ universal and efimovian states, leading to avoided crossings [27], and to an additional contribution to the loss rate of $l = 0$ universal states not included in Eq. (21).

We therefore solve a finite interaction range model, the Gaussian separable potential of range σ [10], defined as

$$\langle \mathbf{r}_1, \mathbf{r}_2|V|\mathbf{r}_1', \mathbf{r}_2'\rangle = -\frac{\hbar^2}{2\pi^{3/2}m\sigma^5} e^{-(r_{12}^2 + r_{12}'^2)/2\sigma^2} \delta(\mathbf{R}_{12} - \mathbf{R}_{12}'). \tag{22}$$

This leads to an integral equation that we solve numerically. In Fig. 2(a), we show two $l = 0$ energy branches as a

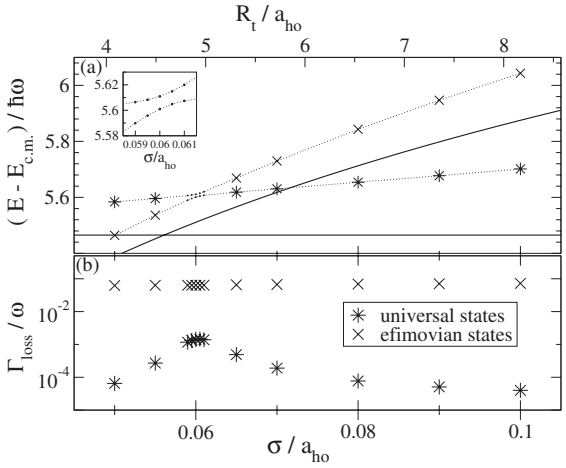

FIG. 2. Numerical solution of the separable potential model: (a) 3-body eigenenergies and (b) predicted 3-body loss rates (for the case of ^{133}Cs, see text), as a function of the potential range σ (lower axis) and the 3-body parameter R_t (upper axis) [29]. (a) The lowest energy universal branch ($*$) and an efimovian branch ($\times$) have a very weak avoided crossing (inset). The analytical predictions of the zero-range model (solid lines) are in good agreement with the numerics (except for the avoided crossing); a linear extrapolation of the stars to $\sigma = 0$ matches the zero-range result at the 10^{-3} level. (b) The universal states have a loss rate much smaller than ω.

function of σ, corresponding in the zero-range model to the lowest $l = 0$ universal state and to an efimovian branch. The smallness of the avoided crossing between the two branches shows that the coupling due to the finite range of the interaction is weak: the energy splitting at the avoided crossing is $\hbar\Omega \simeq 0.01\hbar\omega$, see inset of Fig. 2(a).

We now revisit the calculation of the 3-body loss rate for bosons, since Eq. (21) neglects the contamination of the universal state by the efimovian state. To account for the losses we add to the Hamiltonian $H_{\rm sep}$ of the separable potential model an anti-Hermitian part leading to the effective Hamiltonian in second quantized form

$$H_{\rm eff} = H_{\rm sep} - iB_3 \frac{\hbar^2\sigma^4}{12m} \int [\psi^\dagger(\vec{r})]^3 [\psi(\vec{r})]^3 d\vec{r}, \qquad (23)$$

where B_3 is a numerical factor, whose actual value depends on short-range atomic and molecular physics. Specializing to ^{133}Cs, we adjust the parameters of our model to $B_3 = 25$ and $\sigma = 6.5$ nm in order to reproduce the three-body loss rate measured in a noncondensed gas for several negative values of a in [5]. To obtain the loss rates shown in Fig. 2(b), we restricted $H_{\rm eff}$ to the two branches of Fig. 2(a): the eigenvalues of the resulting 2×2 matrix have complex parts $-i\hbar\Gamma_{\rm loss}/2$. For the efimovian states, $\Gamma_{\rm loss} \simeq 0.07\omega$. For the universal states $\Gamma_{\rm loss}$ is several orders of magnitude smaller; this remains true on the avoided crossing, because the coupling $\Omega/2$ of the universal state to the efimovian state is much smaller than the decay rate of the efimovian state [28].

Experimentally, if one starts with the noninteracting ground state, a superposition of 3-body unitary eigenstates can be prepared by switching suddenly the scattering length from zero to infinity. The Bohr frequencies in the subsequent evolution of an observable would give information on the 3-body spectrum. For bosons, there will be a finite fraction of the sites where the three atoms have a long lifetime. This fraction is equal to the probability of having populated a universal state, which we calculate to be $\simeq$0.174, a value dominated by the contribution ($\simeq$0.105) of the lowest $l = 0$ universal state.

In summary, we obtained the complete analytical solution of a zero-range unitary 3-body problem in a trap. For bosons, there are efimovian and universal states, while for equal mass fermions we proved that all states are universal. All universal states are stable in the zero-range limit with respect to 3-body losses, not only for fermions, but also for bosons. From the numerical solution of a finite range model, we find that, although the bosonic universal states of zero angular momentum slightly mix with the efimovian states, their lifetime remains much larger than the oscillation period in the trap.

We thank L. Pricoupenko, D. Petrov, T. Köhler, A. Bulgac, and D. Bauer for very useful discussions and T. Krämer *et al.* for their data. LKB is a Unité de Recherche de l'ENS et de l'Université Paris 6, associée au CNRS. Our research group is a member of IFRAF.

[1] K. M. O'Hara *et al.*, Science **298**, 2179 (2002); C. A. Regal *et al.*, Nature (London) **424**, 47 (2003); T. Bourdel *et al.*, Phys. Rev. Lett. **91**, 020402 (2003).
[2] C. A. Regal *et al.*, Phys. Rev. Lett. **92**, 040403 (2004); M. W. Zwierlein *et al.*, *ibid.* **92**, 120403 (2004); M. Bartenstein *et al.*, *ibid.* **92**, 120401 (2004); T. Bourdel *et al.*, *ibid.* **93**, 050401 (2004); G. B. Partridge *et al.*, *ibid.* **95**, 020404 (2005); C. Chin *et al.*, Science **305**, 1128 (2004); J. Kinast *et al.*, Science **307**, 1296 (2005); M. W. Zwierlein *et al.*, Nature (London) **435**, 1047 (2005).
[3] J. Carlson *et al.*, Phys. Rev. Lett. **91**, 050401 (2003); G. E. Astrakharchik *et al.*, *ibid.* **93**, 200404 (2004).
[4] J. Stenger *et al.*, Phys. Rev. Lett. **82**, 2422 (1999); J. L. Roberts *et al.*, *ibid.* **85**, 728 (2000); A. Marte *et al.*, *ibid.* **89**, 283202 (2002); T. Weber *et al.*, *ibid.* **91**, 123201 (2003).
[5] T. Kraemer *et al.*, Nature (London) **440**, 315 (2006).
[6] E. Braaten and H.-W. Hammer, Phys. Rep. **428**, 259 (2006).
[7] E. Braaten *et al.*, Phys. Rev. Lett. **88**, 040401 (2002).
[8] V. N. Efimov, Sov. J. Nucl. Phys. **12**, 589 (1971).
[9] S. Jonsell, H. Heiselberg, and C. J. Pethick, Phys. Rev. Lett. **89**, 250401 (2002).
[10] M. Stoll and T. Köhler, Phys. Rev. A **72**, 022714 (2005).
[11] M. Greiner *et al.*, Nature (London) **415**, 39 (2002).
[12] M. Köhl *et al.*, Phys. Rev. Lett. **94**, 080403 (2005).
[13] T. Busch *et al.*, Found. Phys. **28**, 549 (1998).
[14] V. Efimov, Nucl. Phys. **A210**, 157 (1973).
[15] $$\varphi(\alpha) = \left[i^l \sum_{k=0}^{l} \frac{(-l)_k (l+1)_k}{k! 2^k} \frac{(1-s)_l}{(1-s)_k} (1 + i\tan\alpha)^k e^{is[(\pi/2)-\alpha]} \right] - [i \leftrightarrow -i].$$
[16] The integer solutions must be eliminated ($l = 0$, $s = 2$ for fermions; $l = 0$, $s = 4$ and $l = 1$, $s = 3$ for bosons).
[17] Y. Castin, C.R. Physique **5**, 407 (2004).
[18] L. P. Pitaevskii and A. Rosch, Phys. Rev. A **55**, R853 (1997).
[19] S. Tan, cond-mat/0412764; F. Werner and Y. Castin, cond-mat/0507399; cond-mat/0607821.
[20] P. Morse and H. Feshbach, *Methods of Theoretical Physics* (McGraw-Hill, New York, 1953), Vol. II, p. 1665.
[21] G. S. Danilov, Sov. Phys. JETP **13**, 349 (1961).
[22] The above solution is based on a sequence of ansatz, which misses some of the eigenstates.
[23] R. B. Laughlin, Phys. Rev. Lett. **50**, 1395 (1983).
[24] The rank theorem is, for an operator T acting on a finite dimensional space $\mathcal{E}$, $\dim\mathcal{E} = \dim(\mathrm{Ker}T) + \dim(\mathrm{Im}T)$. An upper bound on $\dim(\mathrm{Im}T)$ then leads to the result.
[25] For (18) we used $\partial_{s^2}\varphi'(0) = \int_0^{\pi/2} \varphi^2(\alpha)$, where φ solves (4) and (5) with the normalization $\varphi(0) = 1$.
[26] D. S. Petrov *et al.*, Phys. Rev. Lett. **93**, 090404 (2004); E. Nielsen *et al.*, Phys. Rev. A **66**, 012705 (2002).
[27] Avoided crossings also occur for 3 bosons in a box [L. Pricoupenko (private communication)].
[28] A similar effect occurs in atomic physics, for an atomic ground state coupled via a weak laser field to an excited state: C. Cohen-Tannoudji, J. Dupont-Roc, and G. Grynberg, *Atom-Photon Interactions* §C_I.3*b* (Wiley, New York, 1992).
[29] We find $\ln(R_t/\sigma) \simeq 4.40\pi/|s_0|$ for the separable potential from the free space Efimov states energies.

Chapter 3

Three trapped atoms with resonant interactions

1 Introduction

This Chapter is an extended version of Article III. As further explained in Sec. 2, we consider 3 particles, following either bosonic or fermionic statistics, with short-range interactions of large scattering length, in an external harmonic potential. Experimentally, this corresponds to 3 atoms near a Feshbach resonance, trapped in a well of a deep optical lattice. We use two models for the interactions, the zero-range model and the separable potential model. The zero-range model depends on the scattering length, and also on a 3-body parameter if the Efimov effect occurs. The separable potential depends on the scattering length and on a range parameter b. As further discussed in Subsec. 2.4, the separable potential model converges to the zero-range model in the zero-range limit $b \to 0$. More generally, any model is expected to converge to the zero-range model in the zero-range limit. Thus, any experiment which is sufficiently deep in the zero-range limit is expected to be described accurately by the zero-range model.

In Section 3 we present the exact solution which exists for the zero-range model when the scattering length is infinite and the trap is isotropic. We find three types of eigenstates : eigenstates which are common to the non-interacting problem, truly interacting universal states, and, for bosons, also efimovian states which are the trapped version of the free space Efimov trimers. We also obtain expressions for the normalization of eigenstates, and check analytically that the eigenstates are an orthonormal basis. Finally we study the spectrum and the density of states in the high energy limit. Section 4 concerns various types of deviations from the exactly solvable case. When the scattering length is finite, we compute analytically the energy shifts to first order in $1/a$, for all states with zero angular momentum, including the free space Efimov trimers. We also compute the first order effective range corrections for bosonic universal states of zero angular momentum, and find good agreement with the separable potential model, which indicates that this effective range correction is model-independent. The separable potential model is solved numerically, as discussed in Appendix C.

Experimentally, when 3 alkali atoms approach each other, two of them tend to recombine into a dimer with a large binding energy. Near a Feshbach resonance, these 3-body losses are typically large for bosonic atoms [17, 18, 19, 20], so that relatively strong interactions were only reached in a local equilibrium situation [25]. Losses are even more enhanced when there exists a trimer of zero energy [15, 26, 81], as was observed in Innsbruck [2]. On the contrary, losses are small for fermionic

atoms [21, 22, 23, 24], which makes it possible to study the many-body physics in the BEC-BCS crossover region [10, 11, 12]. For 3 trapped atoms, we will see in Section 5 that the loss rate is small for all universal states, both fermionic and bosonic. Thus it is possible to stabilize 3 bosons with strong resonant interactions.

2 Models and notations

2.1 Trap and units

In this Chapter we consider 3 particles of positions $\vec{r}_1, \vec{r}_2, \vec{r}_3$ and of equal mass m.[1] We assume an isotropic harmonic trapping potential

$$U(r_i) = \frac{1}{2} m\omega^2 {r_i}^2. \tag{3.1}$$

We will often alleviate notations by taking m as the unit of mass and $\hbar$ as the unit of action. Moreover, when $\omega > 0$, we will take ω as the unit of frequency, so that the unit of energy is $\hbar\omega$ and the unit of length is the harmonic oscillator length

$$a_{\rm ho} = \sqrt{\frac{\hbar}{m\omega}}. \tag{3.2}$$

2.2 Statistics

For the symmetry of the wavefunction $\Phi(\vec{r}_1, \vec{r}_2, \vec{r}_3)$ we consider 2 cases :

— *Bosons :* the 3 particles are identical bosons in the same internal state, and the wavefunction is completely symmetric.

— *Fermions :* the 3 particles are identical fermions, with two particles in an internal state $\uparrow$ and one particle in another internal state $\downarrow$. Then one can take a total wavefunction of the form $\hat{A}\left(|\uparrow\downarrow\uparrow\rangle \otimes |\Phi\rangle\right)$, where $\hat{A}$ antisymmetrizes with respect to all particles, and $\Phi(\vec{r}_1, \vec{r}_2, \vec{r}_3) = -\Phi(\vec{r}_3, \vec{r}_2, \vec{r}_1)$. Thus one can consider that particles 1 and 3 are in state $\uparrow$ and particle 2 is in state $\downarrow$.

2.3 Zero-range model

In most of this Chapter we describe interactions between particles by the zero-range model. This model can be defined in terms a regularized δ pseudopotential (see e. g. [31]). Here we use the equivalent formulation in terms of Bethe-Peierls boundary conditions on the wavefunction Φ : for any pair of particles (i, j), there exists a function A_{ij} such that

$$\Phi(\vec{r}_1, \vec{r}_2, \vec{r}_3) = \left(\frac{1}{r_{ij}} - \frac{1}{a}\right) A_{ij}(\vec{R}_{ij}, \vec{r}_k) + O(r_{ij}) \tag{3.3}$$

in the limit $r_{ij} \equiv |\vec{r}_i - \vec{r}_j| \to 0$ taken for fixed positions of the other particle k and of the center of mass $\vec{R}_{ij}$ of i and j. This condition is only imposed for $\vec{r}_k \neq \vec{R}_{ij}$. We will restrict to the unitary limit where the scattering length is $a = \infty$, except in Sec. 4.1 where we will treat $1/a$ as a small

1. The case of unequal masses can be included without difficulty provided the trapping frequency ω remains identical for all particles, by using the free space solution for unequal masses given by Efimov [74].

perturbation. For fermions, antisymmetry imposes $A_{13} = 0$ in Eq. (3.3), i. e. particles with the same spin do not interact.

When all the r_{ij}'s are non zero, the wavefunction Φ obeys the non-interacting Schrödinger equation

$$\sum_{i=1}^{3} \left[-\frac{\hbar^2}{2m} \Delta_{\vec{r}_i} + \frac{1}{2} m\omega^2 r_i^2 \right] \Phi = E_{\rm tot} \Phi. \tag{3.4}$$

For fermions, Eqs. (3.3,3.4) are almost sufficient to define a self-adjoint model with a complete orthogonal family of eigenstates : one just needs to add the condition that the wavefunction is not too singular when all 3 particles become close [Eq. (3.43)].

For bosons, the Efimov effect occurs, and one needs to add a boundary condition which depends on a 3-body parameter R_t [Eq. (3.46)]. The necessity of a 3-body parameter was overlooked in the pioneering work of Skorniakov and Ter-Martirosian [82]. The 3-body parameter was first introduced by Danilov [62]. There are several equivalent conventions for the 3-body parameter. [2]

2.4 Link with finite-range models

In reality, interactions have a non-zero range. There is a precise mathematical link between finite-range models and the zero-range model. In brief, any finite-range model converges to the zero-range model in the zero-range limit. More precisely, let us consider, to fix ideas, that the interactions are given by the square-well potential :

$$V(r) \ = \begin{cases} -V_0 & \text{if } r < b \\ 0 & \text{if } r > b. \end{cases} \tag{3.5}$$

In order to have a scattering length $a = \infty$, we adjust V_0 to the value where the first 2-body bound state appears :

$$V_0 = \frac{\hbar^2}{m b^2} \left(\frac{\pi}{2} \right)^2. \tag{3.6}$$

We consider 3 particles interacting *via* this square-well potential, with the trapping potential and the statistics of Sections 2.1 and 2.2. We then take the zero-range limit :

$$b/a_{\rm ho} \to 0, \tag{3.7}$$

e. g. by keeping fixed the interaction potential and taking the limit $a_{\rm ho} \to \infty$ (i. e. $\omega \to 0$). What happens to the 3-body spectrum ?

For 3 fermions, the spectrum simply converges to the spectrum of the zero-range model. This is expected to hold for any finite range model. This has been checked for a lattice model by combining analytics and numerics [58]. It was also checked numerically for the separable potential model of Sec. 4.3 (Chap. 0, Fig. 5, p. 21), for a gaussian potential [28], for the square-well potential of Eq. (3.5) using a fixed-node Monte-Carlo method [28, 37], and for more elaborated renormalized interactions [84, 85]. For multi-channel models, which provide the best microscopic description of atomic Feshbach resonances [38], the same universality is expected in the limit where the range and the effective range are much smaller than $a_{\rm ho}$ [32]. This means that, in a Gedankenexperiment

2. Our 3-body parameter R_t is related to the 3-body parameter r_0 of [83] through $r_0 = \sqrt{3/2} R_t$, to the 3-body parameter κ_* of [15, 26] through $\ln(\kappa_* R_t) = \ln\sqrt{2} + \arg\Gamma(1+s_0)/|s_0| \bmod \pi/|s_0|$ where s_0 is defined in Eq. (3.41), and to the angular 3-body parameter θ of [69] through $\theta = -|s_0| \ln(R_t/a_{\rm ho})$. Values of R_t which differ by multiplication by an integer power of $\exp(\pi/|s_0|) \simeq 22.7$ are equivalent.

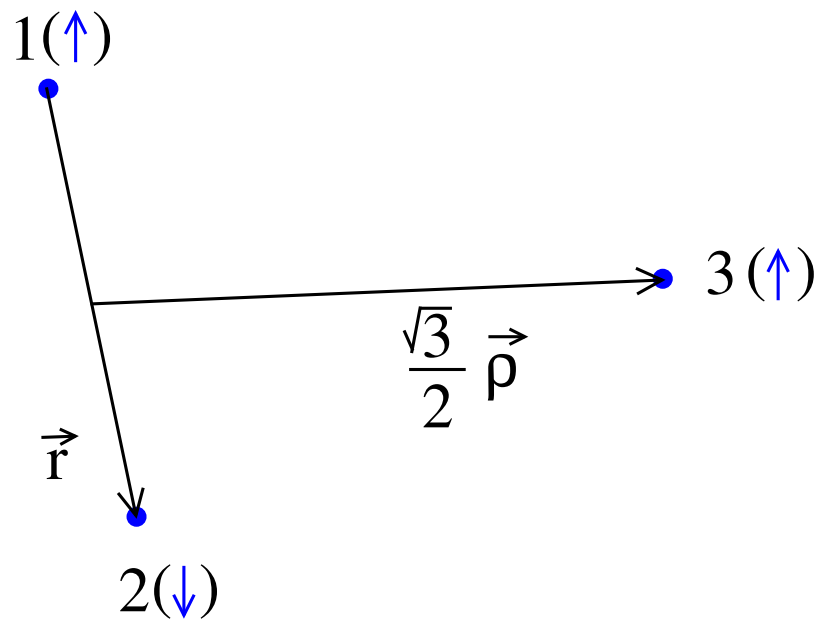

FIGURE 3.1 – Our conventions for the Jacobi coordinates $(\vec{r}, \vec{\rho})$ [Eq. (3.10,3.11)] and for the spins in the fermionic case.

where the magnetic field is exactly at the position of the Feshbach resonance so that the scattering length is infinite, if one measures $E/\hbar\omega$ for some eigenstate for different trapping frequencies ω and extrapolates to $\omega \to 0$, then the result is exactly given by the universal prediction of the zero-range model.

In contrast, for 3 bosons, the ground state energy, in units of $\hbar\omega$, tends to $-\infty$ in the zero-range limit, as a consequence of the Thomas effect ([60] ; Chap. 0, Sec. 3.1.a, p. 27). However, if one restricts to a certain window $e_{\min} < E/(\hbar\omega) < e_{\max}$, $e_{\min}$ and $e_{\max}$ being arbitrary fixed numbers, the spectrum becomes a periodic function of $\ln(b/a_{\rm ho})$ in the zero-range limit. The limiting periodic dependence of the spectrum on b is given by the zero-range model, with a 3-body parameter R_t related to b by

$$R_t = c\, b \tag{3.8}$$

where c is a model-dependent dimensionless number. We give numerical evidence for this limit-cycle behavior in a trap in Sec. 4.3, Fig. 3.6, p. 100.

For Efimov trimers in free space, such a limit-cycle behavior is well established (see Chap. 0 Sec. 3.1.d, [67, 68] and refs. therein). [3]

For bosonic *universal* states, which are independent of R_t, the situation is the same as for fermions : the separable potential simply tends to the zero-range model, without any limit cycle (Fig. 3.5, p. 98).

3 Exact solution at unitarity in an isotropic harmonic trap

3.1 Spectrum and wavefunctions

3.1.a Jacobi coordinates and separation of the center of mass

The center of mass coordinate is

$$\vec{C} = (\vec{r}_1 + \vec{r}_2 + \vec{r}_3)/3. \tag{3.9}$$

The relative motion is conveniently described by the Jacobi coordinates (see Fig. 3.1) :

$$\vec{r} = \vec{r}_2 - \vec{r}_1 \tag{3.10}$$

$$\vec{\rho} = \frac{2}{\sqrt{3}}\left(\vec{r}_3 - \frac{\vec{r}_1 + \vec{r}_2}{2}\right). \tag{3.11}$$

The center of mass can then be separated by taking the Ansatz :

$$\Phi(\vec{r}_1, \vec{r}_2, \vec{r}_3) = \psi(\vec{r}, \vec{\rho})\, \psi_{\rm CM}(\vec{C}) \tag{3.12}$$

$$E_{\rm tot} = E + E_{\rm CM}. \tag{3.13}$$

Note that in this Chapter, E and ψ stand for the energy and wavefunction of the *relative* motion.

The center of mass motion is the one of a harmonically trapped particle of mass $M = 3m$,

$$\left[-\frac{\hbar^2}{2M}\Delta_{\vec{C}} + \frac{1}{2}M\omega^2 C^2\right]\psi_{\rm CM}(\vec{C}) = E_{\rm CM}\psi_{\rm CM}(\vec{C}), \tag{3.14}$$

with the well-known spectrum $E_{\rm CM} \in (\frac{3}{2} + \mathbb{N})\hbar\omega$.

The relative motion is described by the Schrödinger equation

$$\left[-\frac{\hbar^2}{m}\left(\Delta_{\vec{r}} + \Delta_{\vec{\rho}}\right) + \frac{1}{4}m\omega^2(r^2 + \rho^2)\right]\psi(\vec{r}, \vec{\rho}) = E\,\psi(\vec{r}, \vec{\rho}) \tag{3.15}$$

when none of the particles have the same position (i. e. when $r \neq 0$ and $\pm\vec{r}/2 + (\sqrt{3}/2)\vec{\rho} \neq \vec{0}$), and by the Bethe-Peierls boundary condition for the pair of particles $(1, 2)$: there exists a function A such that

$$\psi(\vec{r}, \vec{\rho}) \underset{r\to 0}{=} \frac{1}{r}A(\vec{\rho}) + O(r). \tag{3.16}$$

The Bethe-Peierls boundary conditions for the other pairs of particles are then automatically satisfied by symmetry.

Before solving Equations (3.15,3.16), let us switch to the natural units defined in Sec. 2.1, and rewrite them as :

$$\left(-\Delta_{\vec{r}} - \Delta_{\vec{\rho}} + \omega^2\frac{r^2 + \rho^2}{4}\right)\psi(\vec{r}, \vec{\rho}) = E\,\psi(\vec{r}, \vec{\rho}) \tag{3.17}$$

$$\left.\frac{\partial\,(r\psi)}{\partial r}\right|_{r=0} = 0. \tag{3.18}$$

3. There exists a different way of reaching the same zero-range limit, where a 3-body interaction is introduced in the Hamiltonian [15].

3.1.b Efimov's Ansatz

Let us change from the Jacobi coordinates $(\vec{r}, \vec{\rho})$ to the hyperspherical coordinates $(R, \vec{\Omega})$, which are defined as follows. The hyperradius R is [4] :

$$R = \sqrt{\frac{r^2 + \rho^2}{2}}. \tag{3.19}$$

For the hyperangles we choose :

$$\vec{\Omega} = (\alpha, \hat{r}, \hat{\rho}\,) \tag{3.20}$$

with

$$\alpha = \arctan\left(\frac{r}{\rho}\right) \tag{3.21}$$

$$\hat{r} = \vec{r}/r \tag{3.22}$$

$$\hat{\rho} = \vec{\rho}/\rho. \tag{3.23}$$

Extending Efimov's approach [16, 74] to the trapped case, we are led to the Ansatz

$$\psi(R, \vec{\Omega}) = \frac{F(R)}{R^2}\,\phi(\vec{\Omega}), \tag{3.24}$$

with

$$\phi(\vec{\Omega}) = (1 + \hat{Q})\frac{\varphi(\alpha)}{\sin(2\alpha)}\,Y_l^m(\hat{\rho}\,). \tag{3.25}$$

Here the operator $\hat{Q}$ ensures the correct exchange symmetry :

$$\hat{Q} = \begin{cases} \hat{P}_{13} + \hat{P}_{23} & \text{for bosons} \\ -\hat{P}_{13} & \text{for fermions} \end{cases} \tag{3.26}$$

where $\hat{P}_{ij}$ transposes particles i and j.

The separability in hyperspherical coordinates Eq. (3.24) holds because the trap is isotropic, so that the trapping potential $\omega^2 R^2/2$ is independent of the hyperangles. This separability remains true for universal eigenstates of the N-body problem ([59], Article I), and is related to a $SO(2,1)$ dynamical symmetry ([31], Article I).

The presence of the spherical harmonic Y_l^m implies that ψ is an eigenstate of the total relative angular momentum of the 3 particles with the quantum numbers l and m. [5]

The above Ansatz solves the 3-body problem (3.17,3.18) provided the functions $F(R)$ and $\varphi(\alpha)$ respectively solve the following hyperradial and hyperangular problems.

3.1.c Hyperangular problem

The hyperangular problem is the following : there exists an eigenvalue $s^2 \in \mathbb{R}$ such that

$$-\varphi''(\alpha) + \frac{l(l+1)}{\cos^2\alpha}\,\varphi(\alpha) = s^2\,\varphi(\alpha), \tag{3.27}$$

4. This definition of R differs by a factor $\sqrt{2}$ from Efimov's one [16, 74] but agrees with the one of Braaten and Hammer [15].

5. More precisely, defining the total relative angular momentum of the 3 particles by $\vec{L} = (1/i)(\sum_{j=1}^{3} \vec{r}_j \times \vec{\boldsymbol{\nabla}}_{\vec{r}_j} - \vec{C} \times \vec{\boldsymbol{\nabla}}_{\vec{C}})$, we have $\vec{L} = (1/i)(\vec{r} \times \vec{\boldsymbol{\nabla}}_{\vec{r}} + \vec{\rho} \times \vec{\boldsymbol{\nabla}}_{\vec{\rho}})$ which implies $\vec{L}^2\,|\psi\rangle = l(l+1)\,|\psi\rangle$ and $L_z\,|\psi\rangle = m\,|\psi\rangle$.

with the boundary conditions

$$\varphi'(0) + \eta\ (-1)^l \frac{4}{\sqrt{3}}\ \varphi(\pi/3) = 0 \tag{3.28}$$

$$\varphi(\pi/2) = 0, \tag{3.29}$$

where

$$\eta = \begin{cases} +2 & \text{for bosons} \\ -1 & \text{for fermions.} \end{cases} \tag{3.30}$$

Boundary condition (3.29) means that ψ is finite for $\rho = 0$, and Eq. (3.28) expresses the Bethe-Peierls boundary condition Eq. (3.18).
In order for s to be uniquely determined by s^2, we take the convention

$$\begin{cases} s \in [0; +\infty) & \text{if } s^2 \in [0; +\infty) \\ s \in i \cdot [0; +\infty) & \text{if } s^2 \in (-\infty; 0]. \end{cases} \tag{3.31}$$

The solution of Eqs. (3.27,3.29) is [6] :

$$\varphi(\alpha) = \frac{1}{2i} \left\{ \left[i^l \sum_{k=0}^{l} \frac{(-l)_k (l+1)_k}{k!\ 2^k} \frac{(1-s)_l}{(1-s)_k} (1+i\tan\alpha)^k e^{is(\frac{\pi}{2}-\alpha)} \right] \right. \tag{3.32}$$

$$\left. - \left[(-i)^l \sum_{k=0}^{l} \frac{(-l)_k (l+1)_k}{k!\ 2^k} \frac{(1-s)_l}{(1-s)_k} (1-i\tan\alpha)^k e^{-is(\frac{\pi}{2}-\alpha)} \right] \right\}$$

where the Pochhammer symbol is defined by

$$(x)_n \equiv x(x+1)\dots(x+n-1) \text{ and } (x)_0 \equiv 1. \tag{3.33}$$

Here we have chosen the phase of $\varphi(\alpha)$ such that φ is real when s is real.
In particular,

$$l = 0 \ \Rightarrow\ \varphi(\alpha) = \sin\left[s\left(\frac{\pi}{2} - \alpha\right)\right] \tag{3.34}$$

$$\text{and thus if } s \in i\mathbb{R} : \varphi(\alpha) = i \sinh\left[|s| \left(\frac{\pi}{2} - \alpha\right)\right], \tag{3.35}$$

$$l = 1 \ \Rightarrow\ \varphi(\alpha) = -s\cos\left[s\left(\frac{\pi}{2} - \alpha\right)\right] + \tan\alpha \cdot \sin\left[s\left(\frac{\pi}{2} - \alpha\right)\right] \tag{3.36}$$

$$l = 2 \ \Rightarrow\ \varphi(\alpha) = -3s\tan\alpha \cdot \cos\left[s\left(\frac{\pi}{2} - \alpha\right)\right] \tag{3.37}$$

$$+ \left(1 - s^2 + 3\tan^2\alpha\right) \sin\left[s\left(\frac{\pi}{2} - \alpha\right)\right]. \tag{3.38}$$

Inserting Eq. (3.32) into the boundary condition Eq. (3.28) gives the transcendental equation for s :

$$\left[i^l \sum_{k=0}^{l} \frac{(-l)_k (l+1)_k}{k!} \frac{(1-s)_l}{(1-s)_k} \left(2^{-k} i (k-s) e^{is\frac{\pi}{2}} + \eta (-1)^l \frac{4}{\sqrt{3}} e^{i\frac{\pi}{6}(2k+s)} \right) \right]$$

$$- \left[(-i)^l \sum_{k=0}^{l} \frac{(-l)_k (l+1)_k}{k!} \frac{(1-s)_l}{(1-s)_k} \left(2^{-k} (-i) (k-s) e^{-is\frac{\pi}{2}} + \eta (-1)^l \frac{4}{\sqrt{3}} e^{-i\frac{\pi}{6}(2k+s)} \right) \right]$$

$$= 0. \tag{3.39}$$

6. For an expression in terms of the hypergeometric function ${}_2F_1$, see [86, 87].

3 fermions		
l	n	$s_{l,n}$
0	0	2.166221977
	1	5.127352163
	2	7.114476303
	3	8.832247757
1	0	1.772724267
	1	4.358249309
	2	5.716434034
	3	8.053186622
2	0	3.104976920
	1	4.795405385
	2	7.238828843
	3	8.837105068
3	0	3.959308833
	1	6.127419552
	2	7.816290593
	3	10.172447785

3 bosons		
l	n	$s_{l,n}$
0	0	$i \cdot 1.0062378251$
	1	4.465294619
	2	6.818360913
	3	9.324685319
1	0	2.863799435
	1	6.462200440
	2	7.852831918
	3	9.822928538
2	0	2.823341917
	1	5.508249355
	2	6.449306509
	3	9.272652269
3	0	4.090404751
	1	5.771443207
	2	8.406560584
	3	9.607381634

TABLE 3.1 – The transcendental numbers $s_{l,n}$ obtained by numerical solution of Eq. (3.39).

This equation has some spurious integer solutions ($l = 0, s = 2$ and $l = 1, s = 1$ for fermions ; $l = 0, s = 4$ and $l = 1, s = 3$ for bosons) which must be eliminated because they lead to a vanishing wavefunction ψ.
For $l = 0$, Eq. (3.39) reduces to :

$$-s\cos\left(s\frac{\pi}{2}\right) + \eta\frac{4}{\sqrt{3}}\sin\left(s\frac{\pi}{6}\right) = 0. \tag{3.40}$$

Eq. (3.39) is readily solved numerically : for each l, the solutions form an infinite sequence $(s_{l,n})_{n\geq 0}$, see Table 3.1 and Fig. 3.2. An expected fact which we proved analytically in Article III is that all solutions $s_{l,n}$ are real, except for bosons in the $l = 0$ channel, where a single purely imaginary solution exists,

$$s_{l=0,n=0} \equiv s_0 \simeq i \times 1.00624, \tag{3.41}$$

the well known Efimov solution.

3.1.d Hyperradial problem

The hyperradial problem writes :

$$-F''(R) - \frac{1}{R}F'(R) + \left(\frac{s^2}{R^2} + \omega^2 R^2\right)F(R) = 2EF(R). \tag{3.42}$$

We recall that the allowed values of s are given by the hyperangular problem discussed above. Eq. (3.42) can be interpreted as Schrödinger's equation for a fictitious particle of mass unity moving in two dimensions in the effective potential $(s^2/R^2 + \omega^2 R^2)/2$, the hyperradius R being interpreted as the distance of the fictious particle from the origin, and the hyperradial part $F(R)$ of the 3-body wavefunction being interpreted as the wavefunction of the fictitious particle. A detailed discussion of this problem is given in Appendix B page 65, which we summarize here. The key point is that one

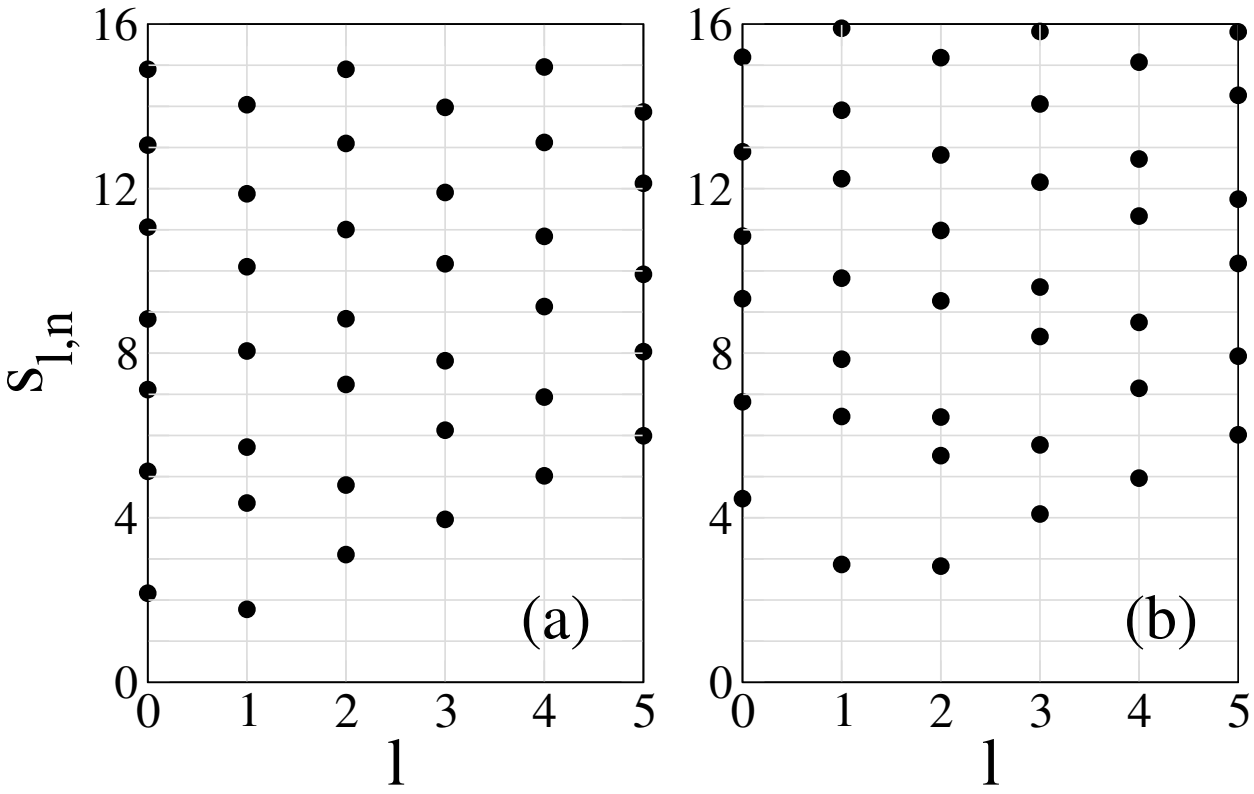

FIGURE 3.2 – The constants $s_{l,n}$ for (a) 3 equal mass fermions and (b) 3 bosons, obtained by numerical solution of the transcendental equation Eq. (3.39). We have not represented the $s_{l=0,n=0}$ solution for bosons, which is purely imaginary.

has to chose a boundary condition for $R \to 0$ in order for the hyperradial problem to be hermitian [for the scalar product $\{\,|\,\}$ defined in Eq. (3.57)], i. e. for the 3-body problem to be hermitian [for the scalar product $\langle\,|\,\rangle$ defined in Eq. (3.53)].[7] These boundary conditions strongly depends on the sign of s^2, i. e. on the repulsive or attractive nature of the effective potential s^2/R^2 (as shown in the Table p. 70).

We first consider the trapped case ($\omega = 1$).

Universal channels : $s^2 \geq 0$. In this case we simply take the boundary condition that $F(R)$ is bounded for $R \to 0$:

$$F(R) \underset{R\to 0}{=} O(1). \tag{3.43}$$

This choice corresponds physically to the absence of N-body resonance (see Chapter 2 p. 43). The eigenfunctions are then given by

$$F(R) = R^s e^{-\frac{R^2}{2}} L_q^{(s)}(R^2) \tag{3.44}$$

where $L_q^{(\cdot)}$ is the generalized Laguerre polynomial of degree $q \in \mathbb{N}$. The resulting spectrum for the relative motion of the 3 particles is

$$E = s + 1 + 2q. \tag{3.45}$$

The quantum number q leads to a semi-infinite ladder structure of the spectrum with a regular spacing 2 (see Fig. 3.3).
Eq. (3.45) was first obtained for the lowest $l = 0$ bosonic universal state ($q = 0$,$n = 1$) by Jonsell, Heiselberg and Pethick [69], and for the lowest $l = 0$ and $l = 1$ fermionic states by Tan [59]. In the N-body case, Eqs. (3.44,3.45) remain true for universal states, but the values of s are not known analytically (Article I, [31, 59]).

Efimovian channel : $s^2 < 0$. This case occurs only for bosons in the $l = n = 0$ channel where $s = s_0$ is imaginary[8]. In this case, all solutions of the Schrödinger equation are bounded and oscillate more and more rapidly when $R \to 0$. In order to obtain a hermitian problem with a discrete spectrum, one has to impose the boundary condition (Appendix B, [79, 78, 62]) :

$$\exists A/\ F(R) \underset{R\to 0}{\sim} A\ \mathrm{Im}\left[\left(\frac{R}{R_t}\right)^s\right], \tag{3.46}$$

where R_t is an additional 3-body parameter. An equivalent form is :

$$\exists A'/\ F(R) \underset{R\to 0}{\sim} A'\ \sin\left[|s| \ln\left(\frac{R}{R_t}\right)\right]. \tag{3.47}$$

For the resulting efimovian states, the hyperradial wavefunction is

$$F(R) = R^{-1}\, W_{E/2,s/2}(R^2) \tag{3.48}$$

where W is a Whittaker function [76, 75], and the spectrum is given by the implicit equation

$$\arg\Gamma\left[\frac{1+s-E}{2}\right] = -|s| \ln R_t + \arg\Gamma(1+s) \bmod \pi, \tag{3.49}$$

7. Since we are interested in eigenstates of the zero-range model which are the zero-range limits of eigenstates of finite-range models, we naturally assume hermiticity for the scalar product $\langle\,|\,\rangle$.

8. If one considers unequal masses it can also occur for fermions [74, 88].

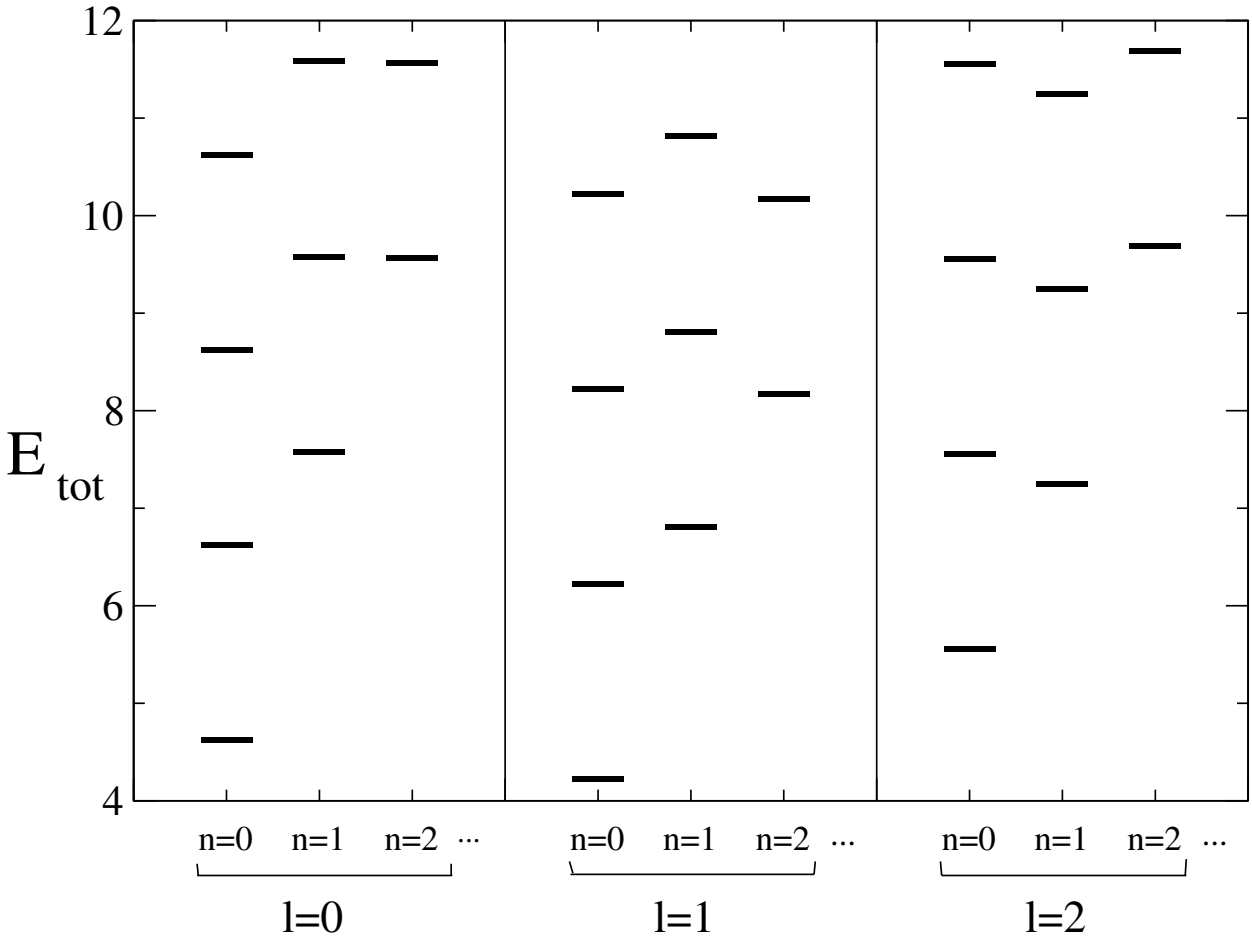

FIGURE 3.3 – The spectrum for 3 fermions (in units of $\hbar\omega$) is formed of ladders with energy steps $2 : E = s_{l,n} + 1 + 2q, q \in \mathbb{N}$. Here we assume that the center of mass is in its ground state so that the total energy is $E_{\text{tot}} = E + 3/2$. l is the total angular momentum of the system. The values of s are known by numerical solution of the transcendental equation Eq. (3.39), cf. Tab. 3.1 and Fig. 3.2. The ground state has an angular momentum $l = 1$ and an energy $E_{\text{tot}} \simeq 4.27$. The eigenstates in common with the non-interacting problem (Sec. 3.1.e) are not represented.

as first obtained by Jonsell *et al.* [69]. The solutions form a discrete series, which is unbounded from below, and can be labeled by a quantum number $q \in \mathbb{Z}$.

The resulting bosonic spectrum is represented in Fig. 3.4.

Let us now recall the solution of the free space problem ($\omega = 0$) at negative energy. For $s^2 > 0$ there are no such solutions, but for $s^2 < 0$ there is the well-known series of Efimov 3-body bound states [16, 26]. Their energies form the geometric series

$$E_q = -\frac{2}{R_t^2} \exp\left(q\frac{2\pi}{|s|} + \frac{2}{|s|}\arg\Gamma(1+s) \right), \ q \in \mathbb{Z} \tag{3.50}$$

and their hyperradial wavefunction is

$$F(R) = K_s(R\sqrt{2|E|}) \tag{3.51}$$

where K is a Bessel function.

In the limit $E \to -\infty$, the spectrum of the efimovian states in the trap approaches the one of the Efimov trimers in free space, as expected.

When Minlos and Faddeev discovered that the spectrum of Efimov states is unbounded from below in the zero-range model [63], their opinion was that this result "somewhat discredits" the model, "since probably only semibounded energy operators are of interest in nonrelativistic quantum mechanics" [64]. In our opinion, the unboundedness of the spectrum in the zero-range limit is rather an unavoidable consequence of the Thomas effect and of the limit cycle behavior (see Sec. 2.4).

3.1.e Eigenstates in common with the non-interacting problem

Up to now, we have obtained eigenstates by using Efimov's Ansatz. But this Ansatz does not capture all eigenstates of the problem. Indeed, it gives eigenstates which satisfy the Bethe-Peierls boundary condition Eq. (3.16) with a *nonzero* function A, i. e. the wavefunction diverges when particles 1 and 2 approach each other. Therefore we call these states the $A \neq 0$ states.

But there are also eigenstates of the problem whose wavefunction *vanishes* when two particles are at the same point ; these are also eigenstates of the noninteracting case. We call these states the $A = 0$ states. An example is the Laughlin state of the Fractional Quantum Hall Effect [89] :

$$\psi = e^{-\sum_{i=1}^{3} r_i^2/2} \prod_{1\leq n<m\leq 3} [(x_n + iy_n) - (x_m + iy_m)]^{|\eta|} . \tag{3.52}$$

The spectrum of these $A = 0$ states is of course included in the spectrum of the non-interacting problem ($\frac{9}{2} + \mathbb{N}$ for bosons, $\frac{11}{2} + \mathbb{N}$ for fermions). In the limit of high energies $E_{\text{tot}} \gg \hbar\omega$, there exists $A = 0$ states for any E belonging to the non-interacting spectrum, and there are much more $A = 0$ states than $A \neq 0$ states, as we will see in Sec. 3.3.d.

3.2 Overlaps

We define the scalar product :[9]

$$\langle \psi | \psi' \rangle \equiv \int d\vec{r} d\vec{\rho}\, \psi(\vec{r}, \vec{\rho})^* \psi'(\vec{r}, \vec{\rho}). \tag{3.53}$$

9. This scalar product is simply related to the usual scalar product by [Appendix A, Section 3] : $\int d\vec{r}_1 d\vec{r}_2 d\vec{r}_3 \left(\psi(\vec{r}, \vec{\rho})\psi_{\text{CM}}(\vec{C})\right)^* \left(\psi'(\vec{r}, \vec{\rho})\psi'_{\text{CM}}(\vec{C})\right) = \langle\psi|\psi'\rangle \int d\vec{C}\psi_{\text{CM}}(\vec{C})^*\psi'_{\text{CM}}(\vec{C}) \left(\frac{\sqrt{3}}{2}\right)^3$.

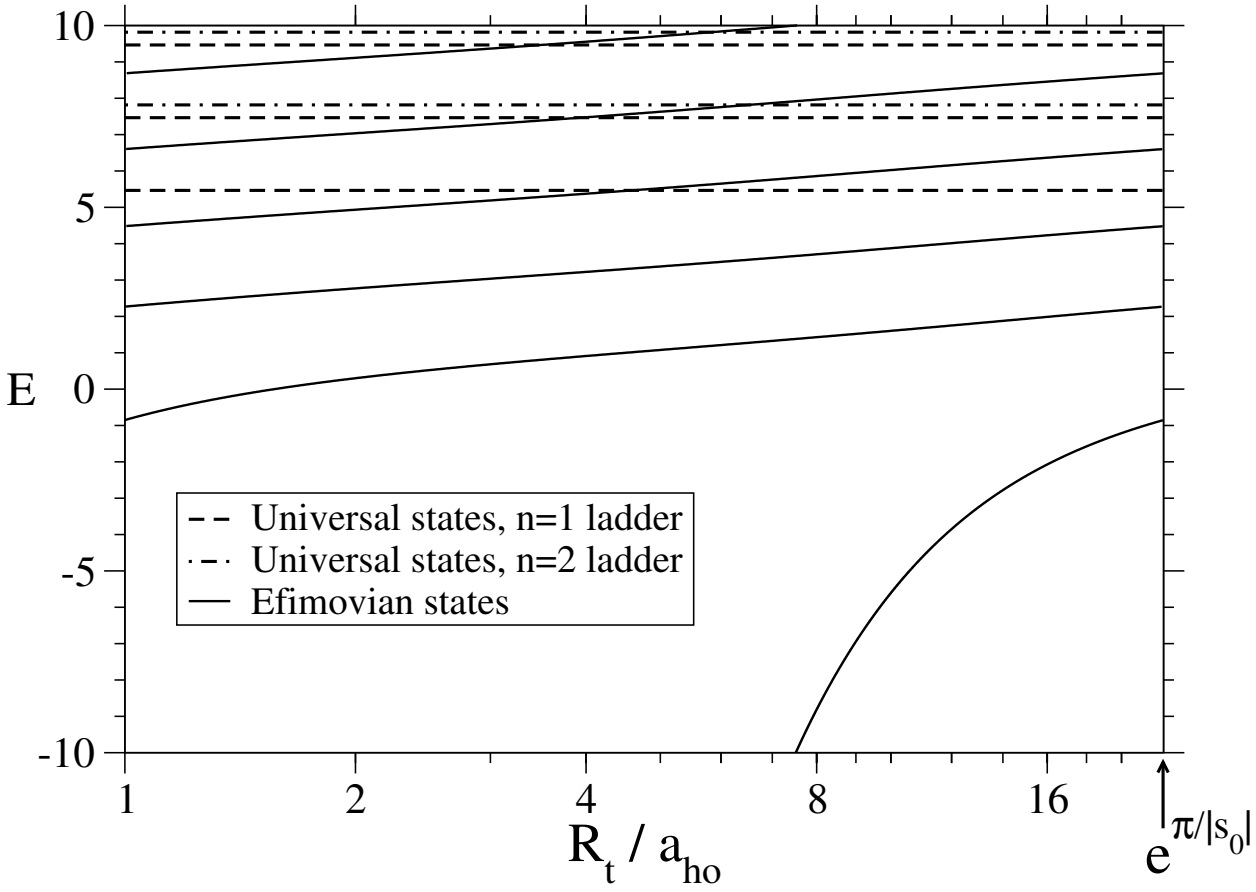

FIGURE 3.4 – Spectrum of 3 trapped bosons for the zero-range model, in units of $\hbar\omega$. The efimovian states depend on the 3-body parameter R_t. The universal states do not depend on R_t and are grouped in ladders of regular spacing 2. [We did not represent the universal eigenstates of non-zero total angular momentum and the eigenstates in common with the non-interacting problem (Sec. 3.1.e).]

In terms of hyperspherical coordinates we have :

$$\langle\psi|\psi'\rangle = \int_0^\infty dR\, R^5 \int d\vec{\Omega}\, \psi(R,\vec{\Omega})^* \psi'(R,\vec{\Omega}) \tag{3.54}$$

where

$$\int d\vec{\Omega}\, f(\vec{\Omega}) \equiv 2\int_0^{\pi/2} d\alpha\, \sin^2(2\alpha) \int d\hat{r} \int d\hat{\rho}\, f(\alpha,\hat{r},\hat{\rho}\,), \tag{3.55}$$

$d\hat{r}$ and $d\hat{\rho}$ being the differential solid angles.

A useful property is :

$$\psi(R,\vec{\Omega}) = \frac{F(R)}{R^2}\phi(\vec{\Omega}) \text{ and } \psi'(R,\vec{\Omega}) = \frac{F'(R)}{R^2}\phi'(\vec{\Omega}) \;\Rightarrow \langle\psi|\psi'\rangle = \{F|F'\}(\phi|\phi') \tag{3.56}$$

where

$$\{F|F'\} \equiv \int_0^\infty dR\, R\, F(R)^* F'(R) \tag{3.57}$$

$$(\phi|\phi') \equiv \int d\vec{\Omega}\, \phi(\vec{\Omega})^* \phi'(\vec{\Omega}). \tag{3.58}$$

3.2.a Normalisation of eigenstates

Let $|\psi\rangle$ denote an $A \neq 0$ eigenstate of the trapped problem or an Efimov bound state of the free space problem. We have :

$$\langle\psi|\psi\rangle = \{F|F\}(\phi|\phi). \tag{3.59}$$

The hyperradial integrals $\{F|F\}$ are known [76] : for universal states, where $F(R)$ is given by Eq. (3.44),

$$\{F|F\} = \frac{\Gamma(s+1+q)}{2\,q!}; \tag{3.60}$$

for efimovian states, where $F(R)$ is given by Eq. (3.48),

$$\{F|F\} = \frac{\pi \cdot \mathrm{Im}\,\psi\left(\frac{1-E+s}{2}\right)}{\sinh(|s|\pi)\cdot\left|\Gamma\left(\frac{1-E+s}{2}\right)\right|^2}; \tag{3.61}$$

and for Efimov states in free space, where $F(R)$ is given by Eq. (3.51),

$$\{F|F\} = \frac{\pi|s|}{4|E|\sinh(\pi|s|)}. \tag{3.62}$$

The calculation of the hyperangular integral $(\phi|\phi)$ is more involved. Using a change of variables due to Efimov (Appendix B in [90]) we obtain, for a total angular momentum $l = 0$:

$$(\phi|\phi) = -(1+|\eta|)\frac{4\pi}{s}\sin\left(s^*\frac{\pi}{2}\right)\left\{\cos\left(s\frac{\pi}{2}\right) - s\frac{\pi}{2}\sin\left(s\frac{\pi}{2}\right) - \eta\frac{2\pi}{3\sqrt{3}}\cos\left(s\frac{\pi}{6}\right)\right\}. \tag{3.63}$$

3.2.b Overlap between eigenstates and hermiticity

It is interesting to check that the overlap between two different eigenstates is zero, i. e. that the zero-range model is hermitian. We thus consider two $A \neq 0$ eigenstates $|\psi_{s,q}\rangle$ and $|\psi_{s',q'}\rangle$, with $(s,q) \neq (s',q')$. Since the wavefunctions have a separable form

$$\psi_{s,q} = \frac{F_{s,q}(R)}{R^2}\,\phi_s(\vec{\Omega}) \tag{3.64}$$

$$\psi_{s',q'} = \frac{F_{s',q'}(R)}{R^2}\,\phi_{s'}(\vec{\Omega}), \tag{3.65}$$

their overlap factorizes as

$$\langle \psi_{s,q}|\psi_{s',q'}\rangle = \{F_{s,q}|F_{s',q'}\}(\phi_s|\phi_{s'}). \tag{3.66}$$

Now there are two cases. First, if $s = s'$, then $q \neq q'$ and the hyperradial overlap $\{F_{s,q}|F_{s,q'}\}$ vanishes, because the hyperradial problem is hermitian, as a consequence of the boundary conditions for $R \to 0$. Second, if $s \neq s'$, the hyperangular overlap $(\phi_s|\phi_{s'})$ should vanish. In the case where both states have a zero angular momentum, we have checked that this is true, by using again Efimov's change of variables and the fact that s and s' solve the transcendental equation (3.40).

3.2.c Overlap with the non-interacting ground-state and completeness

Finally we consider the overlap between an $A \neq 0$ eigenstate $|\psi_{s,q}\rangle$ of angular momentum $l = 0$ and the non-interacting ground state ψ_0. This will be useful in order to check the completeness of the family of eigenstates $|\psi_{s,q}\rangle$, and also for the experimental considerations of Secs. 6.3, 6.4.

Restricting to bosons, the non-interacting ground state is $\Phi_0 \propto \exp(-\sum_{i=1}^{3} {r_i}^2/2)$, which gives, after separation of the center of mass, the unnormalized wavefunction :

$$\psi_0 = e^{-\frac{R^2}{2}}. \tag{3.67}$$

We consider the overlap :

$$P(s,q) \equiv \frac{|\langle \psi_{s,q}|\psi_0\rangle|^2}{\langle \psi_{s,q}|\psi_{s,q}\rangle\,\langle \psi_0|\psi_0\rangle}. \tag{3.68}$$

Setting

$$F_0(R) \equiv R^2\, e^{-\frac{R^2}{2}} \tag{3.69}$$

$$\phi_0(\vec{\Omega}) \equiv 1, \tag{3.70}$$

we have

$$\psi_0 = \frac{F_0(R)}{R^2}\phi_0(\vec{\Omega}), \tag{3.71}$$

and thus from Eq. (3.56) :

$$P(s,q) = \frac{|\{F_{s,q}|F_0\}|^2}{\{F_{s,q}|F_{s,q}\}\{F_0|F_0\}}\,P(s) \tag{3.72}$$

where

$$P(s) \equiv \frac{|(\phi_s|\phi_0)|^2}{(\phi_s|\phi_s)(\phi_0|\phi_0)}. \tag{3.73}$$

Since for any s, the hyperradial problem is self-adjoint and its eigenstates $(F_{s,q})_q$ form a complete family, we have

$$P(s) = \sum_q P(s,q). \tag{3.74}$$

Performing the straightforward calculation of $(\phi_0|\phi_0)$ and $(\phi_s|\phi_0)$, and using the expression (3.63) of $(\phi_s|\phi_s)$, we obtain :

$$P(s) = \frac{96\, s \sin(s\pi/2)}{\pi(s^2-4)^2\left[-\cos\left(s\frac{\pi}{2}\right) + s\frac{\pi}{2}\sin\left(s\frac{\pi}{2}\right) + \frac{4\pi}{3\sqrt{3}}\cos\left(s\frac{\pi}{6}\right)\right]}. \tag{3.75}$$

If the $A \neq 0$ states, together with the $A = 0$ states, form a complete family of eigenstates, which is the case assuming that the zero-range model is self-adjoint and that we did not miss any eigenstate, then we have the closure relation $\sum_{s,q} P(s,q) = 1$, i. e. :

$$\sum_s P(s) = 1. \tag{3.76}$$

Indeed, the $A \neq 0$ states of angular momentum $l = 0$ are the only unitary eigenstates with a non-zero overlap with ψ_0 : the $A \neq 0$ states of angular momentum $l \neq 0$ are orthogonal to ψ_0 because they are in a different eigenspace of the total angular momentum, and the $A = 0$ states are orthogonal to ψ_0 because they are in a different eigenspace of the non-interacting Hamitonian.

We checked analytically that Eq. (3.76) indeed holds, using Eq. (3.75) and the residue theorem [10]. This is a strong indication that the zero-range model is indeed self-adjoint.

Finally we note in view of Sec. 6.3 that

$$P(s, q=0) = \frac{\Gamma\left(\frac{s}{2}+2\right)^2}{2\,\Gamma(s+1)}\, P(s), \tag{3.77}$$

as follows from $\{F_{s,q=0}|F_0\} = \Gamma(s/2+2)/2$, $\{F_0|F_0\} = 1$, and $\{F_{s,0}|F_{s,0}\} = \Gamma(s+1)/2$ [Eq. (3.60)].

3.3 High energy limit

In this Section we discuss the spectrum at high energies. We will treat separately the three types of eigenstates, and then compare their density of states.

3.3.a Efimovian states

The energies of the efimovian states are the solutions $(E_q)_{q\in\mathbb{Z}}$ of Eq. (3.49). Using Stirling's formula we get

$$E_q \underset{q\to+\infty}{=} 2q + \frac{1}{\pi}\left[|s|\ln(qR_t^2) - 2\arg\Gamma(1+s)\right] + \frac{|s|^2}{2\pi^2}\frac{\ln q}{q} + O\left(\frac{1}{q}\right) \tag{3.78}$$

and thus the level spacing

$$E_{q+1} - E_q \underset{q\to+\infty}{\to} 2. \tag{3.79}$$

10. More precisely we define the function $f(z) = z\sin(z\pi/2)/\{(4-z^2)^2[z\cos(z\pi/2) - 8/\sqrt{3}\cdot\sin(z\pi/6)]\}$, which has simple poles for $z = \pm s$ and $z = \pm 2$, and apply the residue theorem to the integral $\oint_{\mathcal{C}} f(z)\,dz$ which tends to 0 when the integration contour $\mathcal{C}$ tends to infinity.

3.3.b Universal $A \neq 0$ states : asymptotics of s for high quantum numbers

The energies of the universal $A \neq 0$ states are directly related to the transcendental numbers s trough Eq. (3.45). Thus we have to study the behavior of s in the limit $s \gg 1$. It appears clearly on Fig. 3.2 page 85 that $s_{l,n}$ gets close to an integer value $\overline{s}_{l,n}$ as soon as l or n increases, with

$$\overline{s}_{l,n} = l + 1 + 2n \qquad \text{for } l \geq |\eta| \tag{3.80}$$

$$\overline{s}_{l,n} = 2n - l + (2\eta + 11)/3 \qquad \text{for } l < |\eta|. \tag{3.81}$$

This gives nearly integer values for E which differ from the non-interacting values ; for example for $l = 0$, Eqs. (3.81,3.45) imply that E is nearly an even integer, while E is odd in the non-interacting case. This holds within the zero-range model, in other words we have taken the zero-range limit before the high energy limit. [11]

To check Eqs. (3.80,3.81) analytically, the transcendental equation is not useful. We rather applied semi-classical WKB techniques to the problem (3.27,3.28,3.29), and obtained [12] :

$$s_{l,0} - \overline{s}_{l,0} \underset{l\to\infty}{\sim} \eta(-1)^{l+1} 2^{1-l} / \sqrt{3\pi l} \tag{3.82}$$

$$s_{l,n} - \overline{s}_{l,n} \underset{n\to\infty}{\sim} \eta \cos\left[\frac{\pi}{3}(l+1-n)\right] \frac{(-1)^{l+n+1} 4}{\pi\sqrt{3}\, n} \tag{3.83}$$

$$\max_n |s_{l,n} - \overline{s}_{l,n}| \underset{l\to\infty}{\sim} |\eta| \frac{4\, Ai_{\max}}{3^{7/12}\, \pi^{1/2}}\ l^{-5/6} \tag{3.84}$$

with $Ai_{\max} \simeq 0.5357$ the maximum of the Airy function.

3.3.c $A = 0$ states

In this Section we consider an arbitrary number N of particles following arbitrary statistics (e. g. N bosons), in space dimension d, trapped in an isotropic harmonic potential of frequency $\omega = 1$. Let us call $\mathcal{H}_{A=0}(E_{\rm tot})$ the space generated by the $A = 0$ states of energy $E_{\rm tot}$, and $\mathcal{H}_{\rm ideal}(E_{\rm tot})$ the space generated by the non-interacting eigenstates of energy $E_{\rm tot}$. To be explicit, we have :

$$\mathcal{H}_{A=0}(E_{\rm tot}) = \{\psi \in \mathcal{H}_{\rm ideal}(E_{\rm tot}) / \forall i \neq j,\ [\vec{r}_i = \vec{r}_j \Rightarrow \psi(\vec{r}_1, \dots, \vec{r}_N) = 0]\}. \tag{3.85}$$

We shall prove that

$$\frac{\dim \mathcal{H}_{A=0}(E_{\rm tot})}{\dim \mathcal{H}_{\rm ideal}(E_{\rm tot})} \underset{E_{\rm tot}\to\infty}{=} 1 - O\left({E_{\rm tot}}^{1-d}\right), \tag{3.86}$$

which implies that for $d \geq 2$ the number of $A = 0$ states becomes very close to the total number of non-interacting eigenstates. We take the limit $E_{\rm tot} \to \infty$ keeping N fixed, which is simply the classical limit in the non-interacting case [91].

To prove Eq. (3.86), we consider the operator

$$\hat{T} : \mathcal{H}_{\rm ideal}(E_{\rm tot}) \longrightarrow \left[L^2(\mathbb{R}^{d(N-1)})\right]^{\frac{N(N-1)}{2}} \tag{3.87}$$

$$\psi \longmapsto (\psi_{12}, \psi_{13}, \dots) \tag{3.88}$$

11. For a model with a finite but small range $0 < b \ll a_{\rm ho}$ and an infinite scattering length, the spectrum is close to the one of the zero-range model for energies $E \ll \hbar^2/(mb^2)$. For very high energies $E \gg \hbar^2/(mb^2)$, we rather expect to recover the non-interacting spectrum.

12. For (3.82) we used $\partial_{s^2}\varphi'(0) = \int_0^{\pi/2} \varphi^2(\alpha)$ where φ solves (3.27,3.28) with the normalization $\varphi(0) = 1$.

where

$$\psi_{12}(\vec{r}_1,\dots\vec{r}_{N-1}) = \psi(\vec{r}_1,\vec{r}_1,\vec{r}_2,\dots,\vec{r}_N) \quad (3.89)$$
$$\psi_{13}(\vec{r}_1,\dots\vec{r}_{N-1}) = \psi(\vec{r}_1,\vec{r}_2,\vec{r}_1,\vec{r}_3,\dots,\vec{r}_N) \quad (3.90)$$

and so on. Clearly, its kernel is $\mathrm{Ker}\,\hat{T} = \mathcal{H}_{A=0}(E_{\rm tot})$. Thus the rank theorem writes :

$$\dim \mathcal{H}_{A=0}(E_{\rm tot}) = \dim \mathcal{H}_{\rm ideal}(E_{\rm tot}) - \dim\,\mathrm{Im}\,\hat{T}. \quad (3.91)$$

Now one can easily show using the expression of the non-interacting unsymmetrized eigenstates in terms of Hermite polynomials that : [13]

$$\dim\,\mathrm{Im}\,\hat{T} \leq \frac{N(N-1)}{2}\left(E_{\rm tot} - \frac{dN}{2} + 1\right)^{d(N-1)} = O\left({E_{\rm tot}}^{d(N-1)}\right). \quad (3.92)$$

On the other hand, for distinguishable particles one finds

$$\dim \mathcal{H}_{\rm ideal}^{\rm distinguishable}(E_{\rm tot}) = \binom{E_{\rm tot}+\frac{dN}{2}-1}{dN-1} \underset{E_{\rm tot}\to\infty}{\sim} \frac{{E_{\rm tot}}^{dN-1}}{(dN-1)!} \quad (3.93)$$

so that for arbitrary statistics

$$\dim \mathcal{H}_{\rm ideal}(E_{\rm tot}) \underset{E_{\rm tot}\to\infty}{\sim} C{E_{\rm tot}}^{dN-1} \quad (3.94)$$

where C depends on N, d and on the statistics.

The result Eq. (3.86) then follows from Eqs. (3.91,3.92,3.94).

3.3.d Density of states

In this Section we study the density of 3-body eigenstates in the high energy limit.

Efimovian states : It follows from Eq. (3.79) that the density of efimovian states

$$\rho_{\rm efimovian}(E_{\rm tot}) \underset{E_{\rm tot}\to\infty}{\longrightarrow} \frac{1}{2}. \quad (3.95)$$

Universal $A \neq 0$ states : Using Eq. (3.80) we get for the number of universal $A \neq 0$ states of energy smaller than $E_{\rm tot}$:

$$\Omega_{A\neq0,\rm univ}(E_{\rm tot}) \underset{E_{\rm tot}\to\infty}{\sim} \#\{(\vec{n}_{\rm CM},n,q,l,m) \in \mathbb{N}^7/|m|\leq l \text{ and } \sum_{i=1}^{3} n_{{\rm CM},i} + \bar{s}_{l,n} + 2q \leq E_{\rm tot}\}$$
$$\underset{E_{\rm tot}\to\infty}{\sim} \frac{{E_{\rm tot}}^7}{10080} \quad (3.96)$$

and thus

$$\rho_{A\neq0,\rm univ}(E_{\rm tot}) = \frac{d\Omega_{A\neq0,\rm univ}}{dE_{\rm tot}} \underset{E_{\rm tot}\to\infty}{\sim} \frac{{E_{\rm tot}}^6}{1440}. \quad (3.97)$$

13. Indeed, $\mathrm{Im}\,\hat{T}$ is the direct sum of $N(N-1)/2$ spaces, all of which have the same dimension. Moreover, ψ_{12} contains a product of $d(N-1)$ coordinates, each of which is raised to a power at most $E_{\rm tot} - dN/2$.

This is much larger than $\rho_{\text{efimovian}}(E_{\text{tot}})$, so that

$$\rho_{A\neq 0}(E_{\text{tot}}) \underset{E_{\text{tot}}\to\infty}{\sim} \rho_{A\neq 0,\text{univ}}(E_{\text{tot}}). \tag{3.98}$$

But according to Eq. (3.94), this is still much smaller than the density of non-interacting eigenstates : [14]

$$\frac{\rho_{A\neq 0}(E_{\text{tot}})}{\rho_{\text{ideal}}(E_{\text{tot}})} \underset{E_{\text{tot}}\to\infty}{=} O\left({E_{\text{tot}}}^{-2}\right). \tag{3.99}$$

$A = 0$ **states :** We can rewrite Eq. (3.86) as

$$\frac{\rho_{A=0}(E_{\text{tot}})}{\rho_{\text{ideal}}(E_{\text{tot}})} \underset{E_{\text{tot}}\to\infty}{=} 1 - O\left({E_{\text{tot}}}^{-2}\right), \tag{3.100}$$

i. e. the density of $A = 0$ states is asymptotically as high as the density of non-interacting eigenstates.

In summary, the interactions become negligible in the high energy limit, which is a rather natural result. However, the way this happens is quite peculiar : most eigenstates are common to the non-interacting problem, while there is a fraction $O(1/{E_{\text{tot}}}^2)$ of truly interacting ($A \neq 0$) eigenstates with almost integer energies.

4 Deviations from the exactly solvable case

The exactly solvable case considered in the previous Section is of course an idealization of real experiments. In this Section, we consider situations which slightly deviate from the exactly solvable case.

4.1 Finite scattering length

Firstly, we consider the case where the scattering length a is large but not infinite. We still use the zero-range model, but with a non-zero value of the coefficient $1/a$ in the Bethe-Peierls boundary condition Eq. (3.3). The center of mass remains separable so that we only consider the relative motion. To first order in $1/a$, the correction to the energy is determined by the derivative $(\partial E/\partial(1/a))_{a=\infty}$, which is related to the function $A(\vec{\rho}) = \lim_{r\to 0}(r\,\psi(\vec{r},\vec{\rho}))$ by :

$$\left.\frac{\partial E}{\partial(1/a)}\right|_{a=\infty} = -4\pi(1+|\eta|)\frac{\int d\vec{\rho}\,|A(\vec{\rho})|^2}{\langle\psi|\psi\rangle}. \tag{3.101}$$

For universal states, this relation is contained in the work of Tan [92, 93]. Here we point out that it also holds in presence of the Efimov effect, provided the derivative with respect to $1/a$ is taken for a fixed 3-body parameter R_t. This result can be shown by adapting the approach used by Efimov in [90]. [15]

Using the expressions of the previous Section for the wavefunctions and their normalisation, we get, restricting to $l = 0$:

$$\left.\frac{\partial E}{\partial(1/a)}\right|_{a=\infty} = C_s\,C_F \tag{3.102}$$

14. There is an error in Eq. (16) of Article III. The right hand side should be : $O((\hbar\omega/E)^2)$.

15. In [90], Efimov treats the effective range as a perturbation, but one can make a similar reasoning and treat $1/a$ as a perturbation.

where

$$C_s \equiv \frac{\sqrt{2}s\sin\left(s\frac{\pi}{2}\right)}{\cos\left(s\frac{\pi}{2}\right) - s\frac{\pi}{2}\sin\left(s\frac{\pi}{2}\right) - \eta\frac{2\pi}{3\sqrt{3}}\cos\left(s\frac{\pi}{6}\right)} \tag{3.103}$$

and

$$C_F \equiv \frac{\{F|1/R|F\}}{\{F|F\}}. \tag{3.104}$$

The value of C_F depends on the considered state :

Efimov states : For Efimov trimers in free space, using Eq. (3.62) and Mathematica, we get :

$$C_F = \sqrt{-E}\frac{\pi}{\sqrt{2}s}\tan(\pi s). \tag{3.105}$$

Thus

$$\left.\frac{\partial E}{\partial(1/a)}\right|_{a=\infty} = C\sqrt{-E} \tag{3.106}$$

with

$$C = \frac{\pi\tan(s\pi)\sin\left(s\frac{\pi}{2}\right)}{\cos\left(s\frac{\pi}{2}\right) - s\frac{\pi}{2}\sin\left(s\frac{\pi}{2}\right) - \frac{4\pi}{3\sqrt{3}}\cos\left(s\frac{\pi}{6}\right)} = -2.1127\ldots, \tag{3.107}$$

in agreement with the value $C = -2.11$ obtained numerically in [15].

Universal states : Restricting to states which are at the bottom of a ladder (i. e. $q = 0$) we have :

$$C_F = \frac{\Gamma(s+1/2)}{\Gamma(s+1)}. \tag{3.108}$$

For the lowest fermionic $l = 0$ state, this gives $(\partial E/\partial(1/a))_{a=\infty} \simeq -1.1980$. This agrees with the value $-1.19(2)$ which we extracted from the numerical solution of a short-range model presented by J. von Stecher *et al.* in Fig. 4a of [3], where the error bar comes from our simple way of extracting the derivative from the numerical data of von Stecher *et al.*.

Efimovian states : For completeness we also consider efimovian states in the trap, and we get [94] :

$$C_F = \frac{-\sqrt{\pi}}{\mathrm{Im}\psi\left(\frac{1-E+s}{2}\right)}\mathrm{Im}\left[\frac{\Gamma\left(s+\frac{1}{2}\right)\Gamma\left(\frac{1-E+s}{2}\right)}{\Gamma(s+1)\,\Gamma\left(\frac{2-E+s}{2}\right)}\right. \tag{3.109}$$

$$\left. {}_3F_2\left(\frac{1}{2}, s+\frac{1}{2}, \frac{1-E+s}{2}; 1+s, \frac{2-E+s}{2}; 1\right)\right] \tag{3.110}$$

where ${}_3F_2$ is an extended hypergeometric function.

4.2 Finite range

We turn to the effect of a finite range of the interaction. To this end, we use a modified version of the zero-range model, the so-called effective range model, which has two parameters, the scattering length a and a finite *effective* range r_e. This model is well known in the context of nuclear physics ([90, 15] and refs. therein) and of cold atoms [70, 95, 96, 71, 97, 32, 72, 98]. It is sometimes called "energy-dependent pseudopotential" because for 2 particles, if the center of mass is separable, it

can be obtained from the zero-range pseudopotential model by replacing a in the Bethe-Peierls boundary condition by an energy-dependent scattering length $a_{\rm eff}(E)$ given by

$$\frac{1}{a_{\rm eff}(E)} = \frac{1}{a} - \frac{r_e}{2}E, \tag{3.111}$$

where E is the energy of the relative motion of the 2 particles.

Let us briefly discuss the case of 2 distinguishable particles in an isotropic harmonic trap, with $a = \infty$. For the zero-range model, the ground state energy $E_{\rm ZR}$ is $\hbar\omega$ below the non-interacting value, $E_{\rm ZR} = 2\hbar\omega$ ([33] ; Chap. 6, Sec. 1, p. 144). Now, let us assume that the 2 particles interact via an attractive square-well potential of width b [Eq. (3.5)] of depth such that $a = \infty$ [Eq. (3.6)] ; we call $E(b)$ the ground state energy with this square-well interaction, which can easily be calculated numerically (Chap. 6, Sec. 3, p. 146). As expected we get $E(b) \underset{b\to 0}{\longrightarrow} E_{\rm ZR}$. Moreover, the finite-range correction is linear in b, $E(b) - E_{\rm ZR} \underset{b\to 0}{\sim} C\,b$, and the factor C agrees with the prediction of the effective range model (Chap. 6, Fig. 6.1, p. 148). More generally we thus expect that the effective range model gives the correct prediction for the first order finite-range correction to the spectrum for 2 particles.

We now return to 3 particles, where the effective range model is defined by the non-interacting Schrödinger equation for the relative motion Eq. (3.17) when none of the particle positions coincide, and by the boundary condition :

$$\frac{\partial}{\partial r}(r\psi)|_{r=0,\vec{\rho}} = -\left(\frac{1}{a} + \frac{r_e}{2}\frac{\partial^2}{\partial r^2}\right)(r\psi)|_{r=0,\vec{\rho}}. \tag{3.112}$$

For $r_e = 0$ this reduces to the Bethe-Peierls boundary condition Eq. (3.18).

Exact non-perturbative results within the effective range model for 3 bosons in free space were obtained numerically [70] and analytically [72] in the case $r_e < 0$, where the model describes a narrow Feshbach resonance [70, 32, 72, 99]. In the case $r_e > 0$ the effective range model has some pathologies such as a spurious deep 2-body bound state, which has a negative norm for the scalar product of [71] (see also [98]). However, no pathology appears as long as r_e is treated perturbatively [90].

In the following we come back to $a = \infty$. Following Efimov [90] we treat r_e perturbatively to compute the first order correction δE to the energy. For a bosonic universal state of angular momentum $l = 0$, we obtain :

$$\delta E = r_e\, 3\pi\sqrt{2}\,\frac{\varphi(0)^2(s^2-1/2)}{(\phi|\phi)}\,\frac{\{F|1/R^3|F\}}{\{F|F\}}. \tag{3.113}$$

Restricting to states which are at the bottom of a ladder, i. e. with a quantum number $q = 0$, and using the results of Section 3, we obtain :

$$\delta E = r_e \frac{\Gamma(s-1/2)}{\Gamma(s+1)}\,\frac{s(s^2-1/2)\sin(s\pi/2)}{2\sqrt{2}\left[-\cos(s\pi/2) + s\pi/2\cdot\sin(s\pi/2) + 4\pi/(3\sqrt{3})\cdot\cos(s\pi/6)\right]}. \tag{3.114}$$

For the lowest universal state ($s = s_{l=0,n=1} = 4.46529\ldots$) this gives

$$\delta E = r_e \cdot 1.0525\ldots. \tag{3.115}$$

This result agrees with the numerical solution of a finite-range model, the separable potential of Sec. 4.3, as shown in Fig. 3.5. More precisely, setting $E = A + B\cdot r_e + \ldots$, the analytical prediction

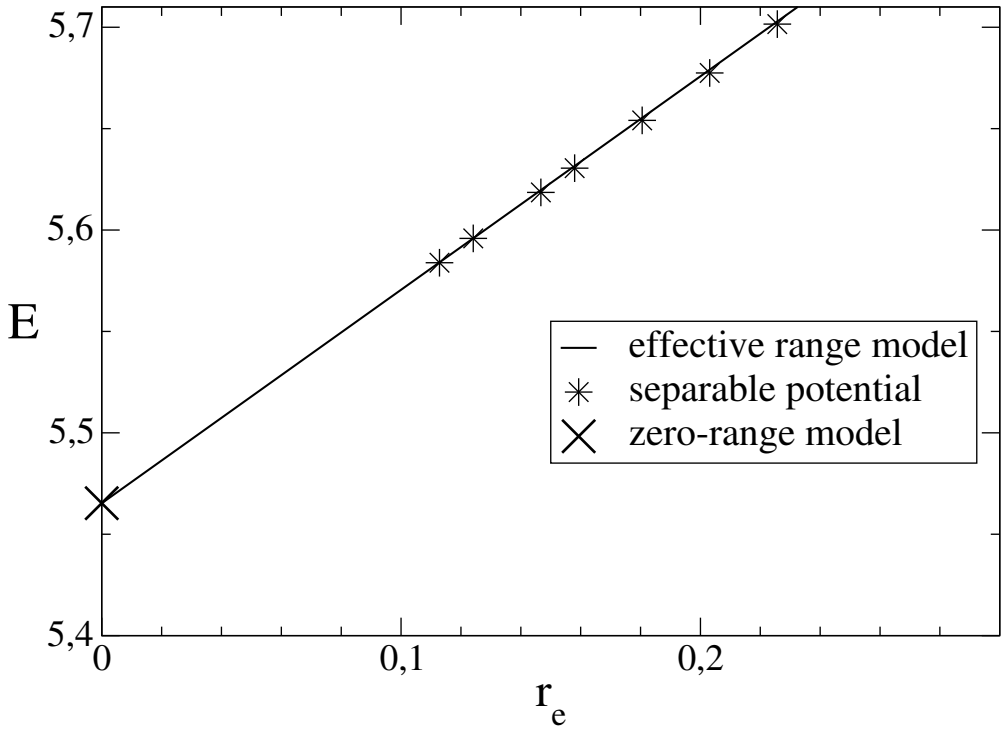

FIGURE 3.5 – Energy E (in units of $\hbar\omega$) as a function of effective range r_e (in units of $\sqrt{\hbar/(m\omega)}$) for the lowest universal eigenstate of 3 trapped bosons at $a = \infty$ with zero total angular momentum. The numerical solution of the separable potential model (stars) agrees to first order in r_e with the analytical prediction of the effective range model (solid line), which by definition coincides for $r_e = 0$ with the zero-range model ($\times$). For the separable potential, the effective range is related to the range b by $r_e = 4b/\sqrt{\pi}$ [1].

of the effective-range model is $A = s + 1 = 5.4653\ldots$ and $B = 1.0525\ldots$; while a linear fit of the numerical results for the separable potential model gives $A \simeq 5.466$ and $B \simeq 1.04$.

This indicates that the first order effective range corrections to universal states are model-independent, and are exactly given by the effective range model.

4.3 Numerical solution for a finite range model

The separable potential is a finite-range interaction for which the 3-body problem is comparatively simple to solve numerically. The separable potential is defined by the following two-body interaction Hamiltonian :

$$\langle \vec{r}_i, \vec{r}_j | V_{ij} | \vec{r}_i{}', \vec{r}_j{}' \rangle = g_0 \; \zeta(r_{ij}) \, \zeta(r'_{ij}) \, \delta^3(\vec{R}_{ij} - \vec{R}_{ij}{}') \tag{3.116}$$

where $r_{ij} = \|\vec{r}_j - \vec{r}_i\|$, $\vec{R}_{ij} = (\vec{r}_i + \vec{r}_j)/2$, and we take for ζ a normalized Gaussian of range b :

$$\zeta(r) = e^{-\frac{r^2}{2\,b^2}} \; (2\pi b^2)^{-3/2}. \tag{3.117}$$

To have an infinite scattering length, we take

$$g_0 = -4\pi^{3/2} b. \tag{3.118}$$

The resulting Hamiltonian for the 3-body problem writes, after separating out the center of mass :

$$H_{\rm sep} = H_0 + V_{12} + V_{13} + V_{23} \tag{3.119}$$

where the non-interacting Hamiltonian is

$$H_0 = -(\Delta_{\vec{r}} + \Delta_{\vec{\rho}}) + \omega^2 \frac{r^2+\rho^2}{4}. \tag{3.120}$$

This model was used in [1, 81] to predict 3-body spectra for ^{85}Rb and ^{133}Cs, by choosing b to reproduce known 2-body low-energy properties. In this work we use this model to study corrections to the zero-range model, which will be particularly important in Section 5.

Since our numerical method to solve this problem differs from the method of Stoll and Köhler [1], we describe it in Appendix C. The key point is that Schrödinger's equation

$$H_{\rm sep}|\psi\rangle = E|\psi\rangle \tag{3.121}$$

can be reduced to an integral equation with one variable, whose kernel we compute and diagonalize numerically.

Let us first discuss the obtained energies $(E_n^{\rm sep})_{n\geq 1}$ of the 3-body bound states in free space. One expects [16, 67, 15] that this spectrum of the separable potential becomes identical to the spectrum of the zero-range model Eq. (3.50) in the zero-range limit, i. e. for $|E| \ll \hbar^2/(mb^2)$, the 3-body parameter being given by $R_t = c\,b$, where c is a dimensionless constant. This implies :

$$\frac{E_n}{E_{n+1}} \underset{n\to\infty}{\longrightarrow} e^{2\pi/|s_0|} \simeq 515.04. \tag{3.122}$$

For the separable potential, we numerically obtain :

$$\frac{E_1^{\rm sep}}{E_2^{\rm sep}} \simeq 548, \tag{3.123}$$

$$\frac{E_2^{\rm sep}}{E_3^{\rm sep}} \simeq 516. \tag{3.124}$$

Thus the limit Eq. (3.122) is already reached to a good approximation for $n = 2$.[16] We can thus assume, to a good approximation, that $E_3^{\rm sep}$ belongs to the spectrum of the zero-range model Eq. (3.50), which implies :

$$R_t \simeq 3.60\, b\, e^{n\pi/|s_0|}, \tag{3.125}$$

where $n \in \mathbb{Z}$ is arbitrary.[17]

For the trapped case, our numerical results were shown on Fig. 3.5 for the lowest $l = 0$ bosonic universal state. The energy $E(b)$ varies almost linearly with b (i. e. with r_e), and is in good agreement with the zero-range model after a linear extrapolation $b \to 0$. Moreover, the slope of the numerical results agrees with the analytical prediction of the effective range model, as we have seen in Sec. 4.2.

For the efimovian states, we can compare the separable potential to the zero-range model, by taking the relation between R_t and b obtained in free space [Eq. (3.125)]. The agreement between the two models is very good, particularly for the smaller value of $b/a_{\rm ho}$, see Fig. 3.6, where the numerical calculations for the separable potential are the ones of Stoll and Köhler [1]. This confirms

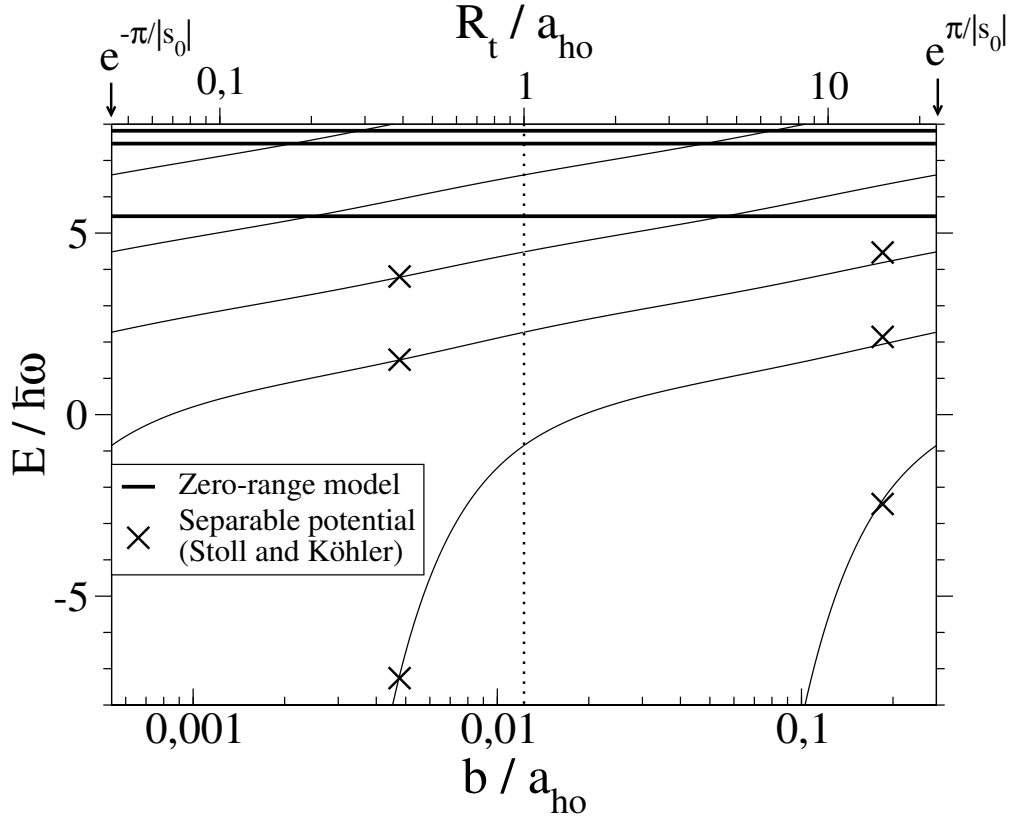

FIGURE 3.6 – Spectrum at $a = \infty$ for 3 trapped bosons of zero angular momentum. Lines : analytical solution of the zero-range model, where the efimovian states depend on the 3-body parameter R_t (thin lines) while the universal states don't (thick lines). Crosses : some eigenvalues of the separable potential model, calculated numerically by Stoll and Köhler [1], as a function of the range b. The relation between R_t and b is $R_t \simeq 3.60\, b$ [Eq. (3.125)]. The two models agree in the zero-range limit $b \ll a_{\rm ho}$. This confirms that the spectrum of the separable potential model has a limit cycle.

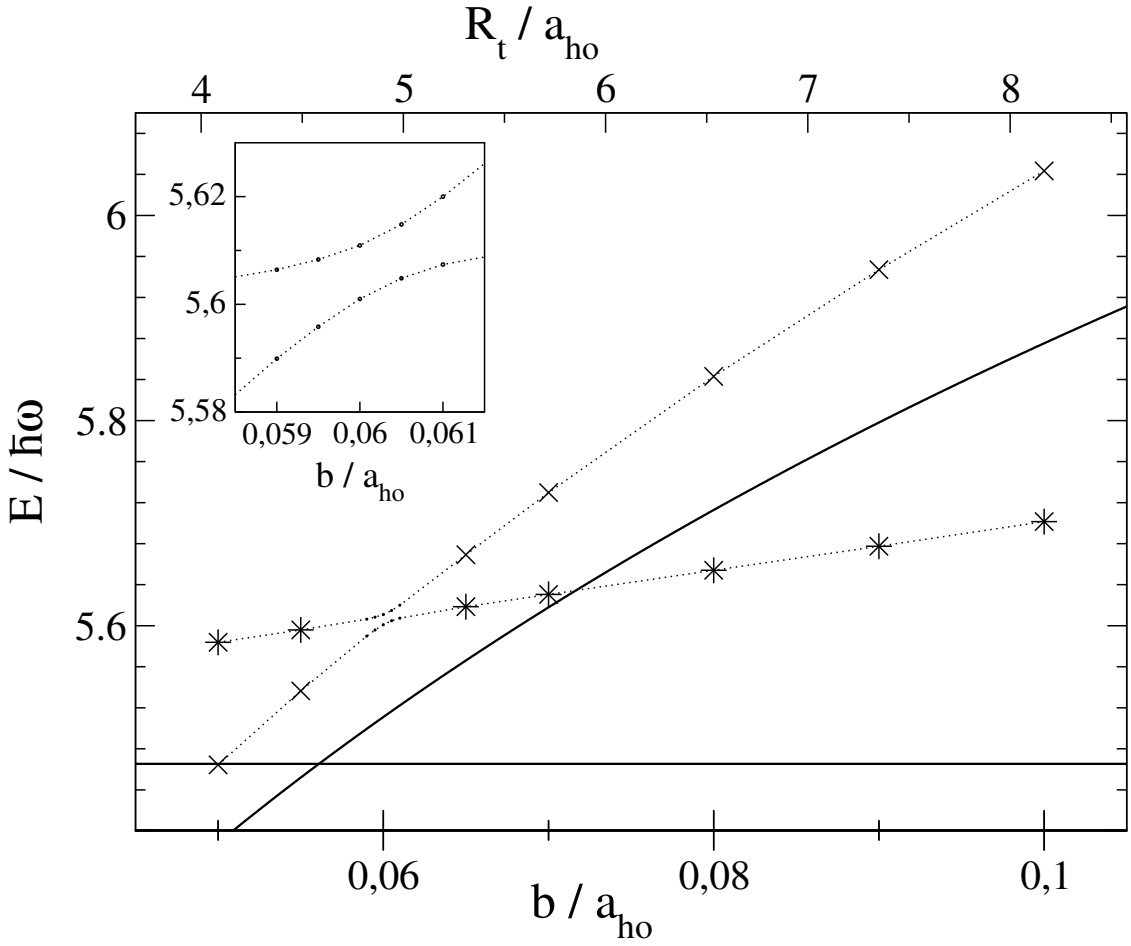

FIGURE 3.7 – Within the zero-range model, there is a crossing between universal and efimovian states (solid lines). This becomes an *avoided* crossing for the separable potential model (dotted lines). [Moreover there is a small shift between the two models due to finite-range corrections ; for the universal state, this correction agrees with the effective range model as shown in Fig. 3.5, the stars on Fig. 3.5 representing the same universal states as on the present Figure.]

that the two models indeed coincide in the zero-range limit, in the sense of a limit cycle, as discussed in Sec. 2.4.

In the zero-range model, there are crossings between universal and efimovian states as a function of $R_t/a_{\rm ho}$. For the separable potential, these crossings become *avoided* crossings as a function of $b/a_{\rm ho}$, as we show in Fig. 3.7. [18] As we shall see in Sec. 5.3, this can be interpreted as a coupling between universal and efimovian states due to the finite range of interactions, and this coupling strongly affects the lifetime of universal states.

16. Even for $n = 1$, the value Eq. (3.123) is surprisingly close to the limit Eq. (3.122). This is related to the fact that, for the separable potential, the dimensionless ground state binding energy $|E_1^{\rm sep}|/[\hbar^2/(mb^2)] = 0.090475$ is quite small compared to 1, i. e. the ground state is quite weakly bound.

17. There is a misprint in footnote [29] of Article III, which should read : $\ln(R_t/\sigma) \simeq 4.40 \ mod \ \pi/|s_0|$.

18. Avoided crossings also occur for 3 bosons in a box (L. Pricoupenko, private communication).

5 Lifetime

Interaction potentials between alkali metal atoms have many deep 2-body bound states [38, 15, 26], and 3 atoms can recombine to form a deeply bound dimer and an atom, which typically fly out of the trap. To fix ideas, let us consider the following simplified model. We assume that the interaction is given by the square-well potential of range b [Eq. (3.5)], with a depth V_0 adjusted to the value where the *second* 2-body bound state appears [i. e. $V_0 = (3\pi/2)^2\hbar^2/(mb^2)$], so that the scattering length is infinite *and* there exists a deeply bound dimer of binding energy $\propto \hbar^2/(mb^2)$. Moreover, we assume that the trapping potential is cut off at a depth U_0 :

$$U(r) = \min\left(\frac{1}{2}m\omega^2 r^2, U_0\right). \tag{3.126}$$

In principle one could then compute the quasi-discrete states of this model and their decay rates Γ. Doing this for a more realistic interaction than the square-well would allow to predict Γ without any free parameter, in the spirit of the *ab initio* free-space calculations of [81, 100, 101, 102, 103]. Here we rather consider the limit

$$\hbar\omega \ll U_0 \ll \frac{\hbar^2}{mb^2}, \tag{3.127}$$

where universal model-independent results can be expected. Eq. (3.127) is motivated by the picture that the trap depth is very large compared to the energy $\sim \hbar\omega$ of 3 trapped atoms, but very small compared to the kinetic energy $\sim \hbar^2/(mb^2)$ of atom-dimer states.

Before going into details, let us make a simple observation. Since all 3 atoms have to approach each other to small distances $\sim b$ in order to recombine, the loss rate is determined by the magnitude of the initial wavefunction at small hyperradius. For universal states, the probability to reach a small hyperradius R is suppressed, because of the *repulsive* effective potential in the hyperradial problem (s^2/R^2 with $s^2 > 0$) ; thus we can expect that the loss rate is small. For efimovian states, the effective potential is *attractive* ($-|s_0|^2/R^2$) ; thus we can expect that the loss rate is larger.

5.1 Lifetime of Efimov states and efimovian states, *à la* Braaten-Hammer

To calculate the loss rate of efimovian states, we use the approach of Braaten and Hammer (BH) [104, 105, 15, 26], where one keeps the zero-range model defined by the Schrödinger equation (3.17) and the Bethe-Peierls boundary condition (3.18), but one introduces an inelasticity parameter η_* into the boundary condition at short hyperradius in the efimovian channel :

$$\exists A/\ F(R) \underset{R\to 0}{\sim} A\left[e^{-\eta_*}\left(\frac{R}{R_t}\right)^s - e^{\eta_*}\left(\frac{R}{R_t}\right)^{-s}\right]. \tag{3.128}$$

For $\eta_* = 0$ this reduces to the usual boundary condition of the zero-range model [Eq. (3.46)]. For $\eta_* > 0$ this imposes that the flux of the outgoing wave R^s is smaller than the flux of the ingoing wave R^{-s} by a factor $e^{-4\eta_*}$, which modelizes the 3-body losses taking place when the 3 particles are close to each other, i. e. at small R.

Thus there is still separability in hyperspherical coordinates. In the efimovian channel the hyperradial Schrödinger equation (3.42) is now supplemented by the modified boundary condition Eq. (3.128) and the energy E becomes complex. The decay rate is then given by

$$\Gamma = -2\,\mathrm{Im}\,E. \tag{3.129}$$

For Efimov trimers in free space, the BH approach gives [104] :

$$\Gamma \simeq \frac{4\eta_*}{|s|}|E|, \tag{3.130}$$

provided that $\eta_* \ll 1$.

In the trapped case ($\omega = 1$) we find that the hyperradial wavefunctions are still given by Eq. (3.48) but with a complex energy E given by the modified implicit equation :

$$\frac{\Gamma\left(\frac{1+s-E}{2}\right)}{\Gamma\left(\frac{1-s-E}{2}\right)} = \frac{\Gamma(1+s)}{\Gamma(1-s)} e^{-2\eta_*} {R_t}^{-2s}. \tag{3.131}$$

In the limit $\eta_* \ll 1$ of small losses, this implies that E is approximately real, with

$$\Gamma \simeq \frac{4\eta_*}{\mathrm{Im}\,\psi\left(\frac{1+s-E}{2}\right)} \tag{3.132}$$

where ψ is the digamma function.
For $E \to -\infty$, Eq. (3.132) reduces to the free space result Eq. (3.130), as expected ; while for $E \to +\infty$ it gives $\Gamma \to 4\eta_*/\pi$ so that the "quality factor" $E/\Gamma \to \pi E/(4\eta_*) \ggg 1$.

In the limit $\eta_* \gg 1$ of large losses, the boundary condition Eq. (3.128) becomes purely absorbing and independent of the 3-body parameter R_t. The spectrum given by Eq. (3.131) has the universal limit

$$E \underset{\eta_* \to \infty}{\longrightarrow} 1 - s + 2q, \ q \in \mathbb{N} \tag{3.133}$$

so that

$$\Gamma \underset{\eta_* \to \infty}{\longrightarrow} 2|s|. \tag{3.134}$$

This surprising result has some amusing consequences : any superposition of efimovian states decays with this same universal rate ; and highly excited states ($\mathrm{Re}\, E \gg 1$) still have a high quality factor $\mathrm{Re}\, E/\Gamma \gg 1$.
The wavefunctions become

$$F(R) \underset{\eta_* \to \infty}{\longrightarrow} R^{-s} e^{-\frac{R^2}{2}} L_q^{(-s)}(R^2) \tag{3.135}$$

up to a normalization factor.
Formally, the spectrum Eq. (3.133) and the wavefunctions Eq. (3.135) are identical to the case of certain N-body resonances (Chap. 2, footnote 43 in Article I) except that s is imaginary here.

Finally, we note that within the BH approach, universal states are strictly identical to the case of the zero-range model without losses, so that the lifetime of universal states is infinite. This indicates that the lifetime of universal states tends to infinity in the limit (3.127).

5.2 Lifetime of universal states, *à la* Petrov-Salomon-Shlyapnikov

In order to study more precisely the lifetime of universal states, we start with an approach which is a transposition to the trapped case of the method used by Petrov, Salomon and Shlyapnikov to study the formation rate of deep dimers in the free space case relevant to the homogeneous gas [23, 106, 24]. We will refer to this approach as the PSS approach. [19] Similar ideas are present in the work of Kagan, Svistunov and Shlyapnikov on the lifetime of weakly interacting Bose-Einstein

19. We thank D. Petrov and G. Shlyapnikov for very useful discussions about this approach.

condensates [107]. The PSS approach predicts that in the limit Eq. (3.127), the loss rate has the asymptotic behavior :

$$\Gamma \sim K \frac{\hbar}{m b^2} P(R < b), \tag{3.136}$$

where $P(R < b)$ is the probability, calculated within the zero-range model, that the hyperradius is smaller than b ; and K is a dimensionless number which depends on the detailed shape of the interactions, but is independent of ω, b, and U_0. We note that K also depends on the considered state through the quantum numbers n,l,m. [20] [21]

We give a simple derivation of the PSS approach in Chapter 7, in the easier situation where only one pair of particles interacts resonantly. For free space collisions, the results of the PSS approach were recovered using a different approach in [108].

One can apply the PSS approach to Efimov states and efimovian states, and one recovers the results of the BH approach for $\eta_* \ll 1$, Eqs. (3.130,3.132). [22] It is not surprising that the PSS approach is restricted to $\eta_* \ll 1$, since it is based on wavefunctions which are unperturbed by the recombination process [106]. Thus, for efimovian states, the PSS approach is equivalent to the small-η_* limit of the BH approach.

For universal states, we have seen that the BH approach predicts a vanishing Γ. The PSS approach allows to go further and to predict *how* Γ tends to zero in the limit Eq. (3.127). Inserting the hyperradial wavefunction (3.44) and its normalization (3.60) into Eq. (3.136), we get :

$$\Gamma \sim \omega \left(\frac{b}{a_{\rm ho}}\right)^{2s} \binom{q+s}{q} \frac{K}{\Gamma(s+2)}. \tag{3.137}$$

Since s is real and strictly positive, this implies that $\Gamma/\omega \to 0$ for $b/a_{\rm ho} \to 0$, in accordance with the prediction of the BH approach.

As we shall see in the next Subsection, Eq. (3.137) breaks down for bosons in the $l = 0$ subspace, because for a finite range b, the universal states become coupled to the efimovian states, which leads to an additional contribution to the loss rate. Similarly, Eq. (3.137) may break down as soon as $s = s_{l,n}$ with $n \geq 1$, because for a finite range b the $s_{l,n}$ channel becomes coupled to the less long-lived $s_{l,n=0}$ channel, which leads to a contribution to Γ which dominates over the contribution already included in Eq. (3.137), unless the coupling is small enough. [23]

5.3 Influence of efimovian states on the lifetime of universal states

To study the combined effect of a finite-range interaction and losses, we consider the effective Hamiltonian

$$H_{\rm eff} = H_{\rm sep} + H_{\rm loss} \tag{3.138}$$

where $H_{\rm sep}$ is the Hamiltonian of the separable potential [defined in Eqs. (3.116,3.117,3.118,3.119,3.120) p. 98], and

$$H_{\rm loss} = -i B_3 \frac{\hbar^2 b^4}{12m} \int \left[\hat{\psi}^\dagger(\vec{r})\right]^3 \left[\hat{\psi}\ (\vec{r})\right]^3 d\vec{r}. \tag{3.139}$$

20. K does not depend on the quantum number q, because the 3-body wavefunction at $R \lesssim b$ is independent of q up to a normalisation factor.

21. Values of K could in principle be extracted from experiments such as [21, 22, 24].

22. The link between the parameter η_* of the BH approach and the parameter $K(l = n = 0)$ of the PSS approach for the Efimov channel is : $\eta_*/K(l = n = 0) = \int_0^1 \sin^2\left[|s| \ln(x\,c)\right] x\,dx\ /|s|$ where $c = b/R_t$ is a model-dependent constant. This is obtained by injecting into into Eq. (3.136) the expression of $F(R)$ Eq. (3.48), its normalisation Eq. (3.61) and its $R \to 0$ asymptotic behavior (Eq. (B.33) page 69).

23. This caveat does not affect the calculations of Petrov, Salomon and Shlyapnikov [23, 106, 24], where $n \neq 0$ channels do not play any role.

We will refer to $H_{\rm eff}$ as the separable-potential-based model. [24] A similar modelisation of 3-body losses was used e. g. in [109]. In first quantization we have, assuming that the center of mass motion is in a given eigenstate :

$$H_{\rm loss} = -iB_3 \frac{\hbar^2 b^4}{2m} |\vec{0},\vec{0}\rangle\langle\vec{0},\vec{0}| \tag{3.140}$$

where $|\vec{0},\vec{0}\rangle \equiv |\vec{r}=\vec{0},\vec{\rho}=\vec{0}\rangle$.

The dimensionless parameter B_3 characterizes the strength of the 3-body losses, in a similar way than the parameters η_* in the BH approach, and the parameters K in the PSS approach. In order to make quantitative predictions, these parameters must be determined from experimentally measured 3-body observables. [25] For Cesium atoms near the $-11\,G$ Feshbach resonance, by comparing the 3-body loss rate coefficient in a non-condensed cold homogeneous gas predicted by the separable-potential-based model to the experimental data from Innsbruck [2], we obtain $B_3 \simeq 25$ and $b \simeq 6.5\,\text{nm}$ (see Appendix D). With these parameters, the results we will present can be applied to 3 trapped Cesium atoms, sufficiently close to the $-11\,G$ Feshbach resonance to have $|a| \gg a_{\rm ho}$, in the hyperfine state used in [2]. [26] Our results can also be applied to other Feshbach resonances and other atomic species, but the value of B_3 is then unknown.

We focus on the region shown in Fig. 3.7 p. 101, where the lowest $l=0$ universal state meets an efimovian state. We restrict to the subspace generated by the these two eigenstates of the separable potential Hamiltonian $H_{\rm sep}$, i. e. to the two branches represented by dotted lines in Fig. 3.7. In this basis, hereafter denoted by $(|\psi_1\rangle, |\psi_2\rangle)$, the matrix of $H_{\rm sep}$ writes :

$$\text{Mat}_{(|\psi_1\rangle,|\psi_2\rangle)}\left(H_{\rm sep}\right) = \begin{pmatrix} E_1 & 0 \\ 0 & E_2 \end{pmatrix}, \tag{3.141}$$

and the matrix of $H_{\rm loss}$ is

$$\text{Mat}_{(|\psi_1\rangle,|\psi_2\rangle)}\left(H_{\rm loss}\right) = -\frac{i\hbar}{2} \begin{pmatrix} \Gamma_1 & \sqrt{\Gamma_1\Gamma_2} \\ \sqrt{\Gamma_1\Gamma_2} & \Gamma_2 \end{pmatrix} \tag{3.142}$$

with

$$\Gamma_j = B_3 \frac{\hbar b^4}{m} \left|\psi_j(\vec{0},\vec{0}\,)\right|^2, \quad j=1,2. \tag{3.143}$$

We numerically calculate the E_j's and Γ_j's, as described in Appendix C. We then deduce the complex eigenvalues E of the restriction to $(|\psi_1\rangle, |\psi_2\rangle)$ of $H_{\rm eff} = H_{\rm sep} + H_{\rm loss}$. [27] The loss rates Γ are then given by

$$E = \text{Re}\, E - \frac{i\hbar}{2}\Gamma. \tag{3.144}$$

Let us first compare the loss rate of the efimovian state obtained by the present approach to the one predicted by the BH approach of Section 5.1. We consider the case of Cesium, where we have $B_3 \simeq 25$ (see App. D), and in the BH approach we have $\eta_* \simeq 0.06$ ([2], App. D). We again use the relation (3.125) between the 3-body parameter R_t and the range b. As shown in Fig. 3.8, the agreement is reasonable. The discrepancy can be attributed to the uncertainty on the parameters B_3 and η_*, which is due to finite-range effects in the experiment [2] (see also Appendix D).

24. $H_{\rm loss}$ is an effective low energy Hamiltonian. Only its restriction to a low energy subspace of $H_{\rm sep}$ has a meaning.

25. Alternatively, they could be fitted to numerical calculations such as [100, 81].

26. Experimentally, going to negative magnetic fields may be problematic because the concerned hyperfine state is then no longer the ground state, so that 2-body losses become energetically allowed.

27. $H_{\rm loss}$ also couples the states $|\psi_1\rangle$ and $|\psi_2\rangle$ to the other $l=0$ eigenstates of the separable potential, but we shall neglect this coupling, because we stay sufficiently close to the crossing, so that the energy separation to these other states is $\gtrsim 2\hbar\omega$, while we restrict to values of B_3 which are sufficiently small to have loss rates much smaller than $\hbar\omega$.

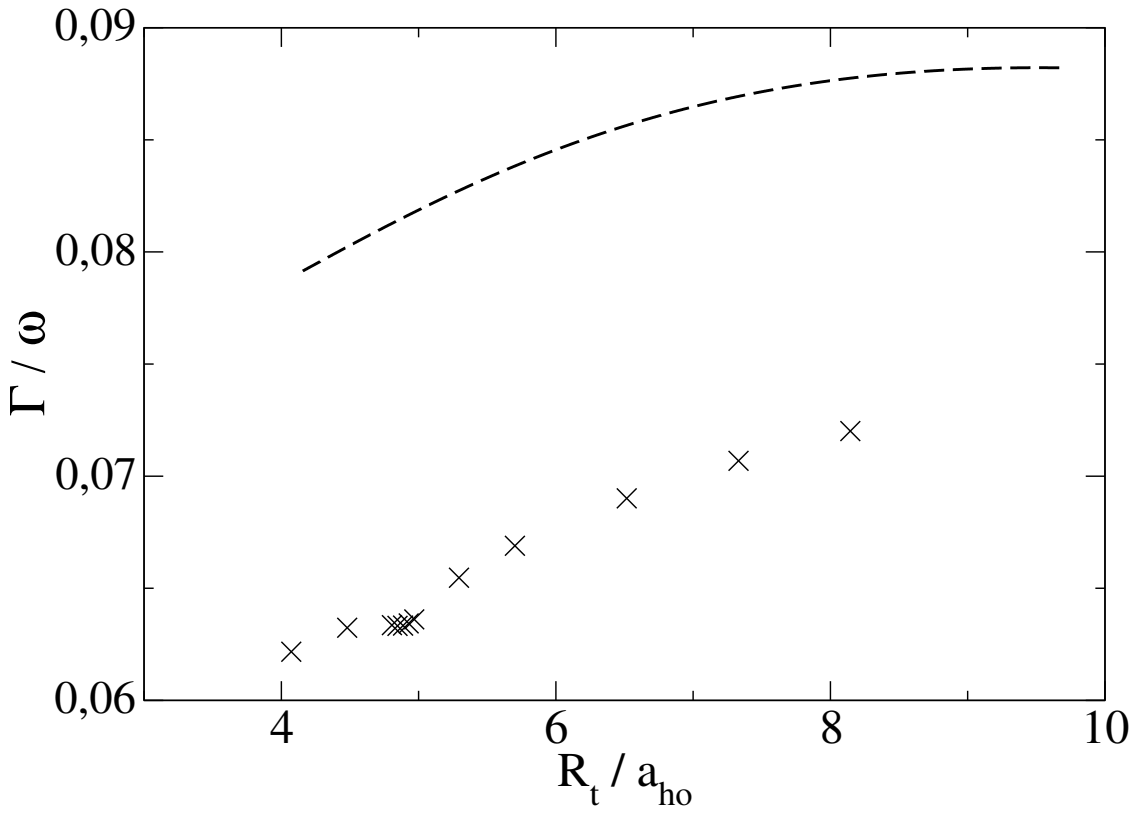

FIGURE 3.8 – Loss rate of the efimovian state as a function of the 3-body parameter. Dashed line : analytical prediction of the zero-range Braaten-Hammer approach [Eq. (3.131) p. 103], with the parameter $\eta_* = 0.06$ extracted from the Cesium experiment [2]. Crosses : numerical result of the separable-potential-base effective Hamiltonian, with the parameter $B_3 = 25$ extracted from the same experiment.

We now study the loss rate of the universal state. Our numerical results are shown on Fig. 3.9. It clearly appears that there are two different regimes :

— For small B_3, $H_{\rm loss}$ can be treated in non-degenerate first order perturbation theory. The eigenstates of $H_{\rm eff}$ are close to the eigenstates $|\psi_1\rangle$ and $|\psi_2\rangle$ of $H_{\rm sep}$. The real parts of the eigenenergies of $H_{\rm eff}$ are close to the eigenenergies of $H_{\rm sep}$, which have an *avoided* crossing, where the universal eigenstate of $H_{\rm eff}$ turns into efimovian and vice-versa. The loss rates are close to $\langle\psi_j|H_{\rm loss}|\psi_j\rangle = \Gamma_j$, which cross.

— To understand the regime of larger B_3 we introduce the eigenbasis of the restriction of $H_{\rm loss}$. Let $|u\rangle$ be the linear combination of $|\psi_1\rangle$ and $|\psi_2\rangle$ whose wavefunction vanishes at the origin : $H_{\rm loss}|u\rangle = 0$. Let $|e\rangle$ be the other eigenstate of $H_{\rm loss}$.[28] In the basis $(|e\rangle, |u\rangle)$ the matrix of $H_{\rm loss}$ can be written as :

$$\mathrm{Mat}_{(|e\rangle,|u\rangle)}\left(H_{\rm loss}\right) = -\frac{i\hbar}{2}\begin{pmatrix} \Gamma_e^0 & 0 \\ 0 & 0 \end{pmatrix}. \tag{3.145}$$

We expect that $|u\rangle$ (resp. $|e\rangle$) is close to the universal (resp. efimovian) state predicted by the zero-range model, even on the avoided crossing where the eigenstates of $H_{\rm sep}$ are superpositions of universal and efimovian state. We then write the matrix of $H_{\rm sep}$ in the basis $(|e\rangle, |u\rangle)$ as :

$$\mathrm{Mat}_{(|e\rangle,|u\rangle)}\left(H_{\rm sep}\right) = \begin{pmatrix} E_e^0 & w \\ w & E_u^0 \end{pmatrix}. \tag{3.146}$$

The diagonal matrix elements E_e^0 and E_u^0 simply cross (Fig. 3.10), as was expected since the energies of the zero-range model cross. The off-diagonal element w can be interpreted physically as the coupling between universal and efimovian states due to the finite range of the interaction. Note that $|u\rangle$, $|e\rangle$, w, E_e^0 and E_u^0 are independent of B_3.[29] Fig. 3.11 shows that $w \ll \hbar\omega$, as expected ; it also shows that w is nearly proportional to b, an interesting and yet unexplained property.

In the new basis, the matrix of the effective Hamiltonian writes

$$\mathrm{Mat}_{(|e\rangle,|u\rangle)}\left(H_{\rm eff}\right) = \begin{pmatrix} E_e^0 - i\hbar\Gamma_e^0/2 & w \\ w & E_u^0 \end{pmatrix}. \tag{3.147}$$

If B_3 is large enough to have $w \ll \Gamma_e^0$, we can treat w perturbatively, even on the crossing where $E_e^0 = E_u^0$. The eigenstates of $H_{\rm eff}$ are then close to $|u\rangle$ and $|e\rangle$, and the loss rate of the universal state is, within second-order perturbation theory :

$$\Gamma_u \simeq \Gamma_e^0 \frac{w^2}{(E_u^0 - E_e^0)^2 + (\hbar\Gamma_e^0/2)^2} \ll \Gamma_e^0. \tag{3.148}$$

The loss rate of the efimovian state is only slightly perturbed by the coupling :

$$\Gamma_e \simeq \Gamma_e^0, \tag{3.149}$$

more precisely $\Gamma_e \simeq \Gamma_e^0 - \Gamma_u$.

Eq. (3.148) shows that when Γ_e^0 increases, i. e. when B_3 increases, Γ_u paradoxically *decreases*. This is because the efimovian state becomes more separated from the universal state in the complex energy plane. A similar effect occurs in the context of atom-photon interactions, when an atomic ground state is coupled via a weak laser field to an atomic excited state [110].

28. $|u\rangle$ and $|e\rangle$ are orthogonal since $H_{\rm loss}$ is antihermitian [Eq. (3.142)].

29. We have $w = \left|\psi_1(\vec{0},\vec{0})\psi_2(\vec{0},\vec{0})\left(E_1 - E_2\right)/[\psi_1(\vec{0},\vec{0})^2 + \psi_2(\vec{0},\vec{0})^2]\right|$, where we chose the relative phase of $|e\rangle$ and $|u\rangle$ in such a way that $w > 0$.

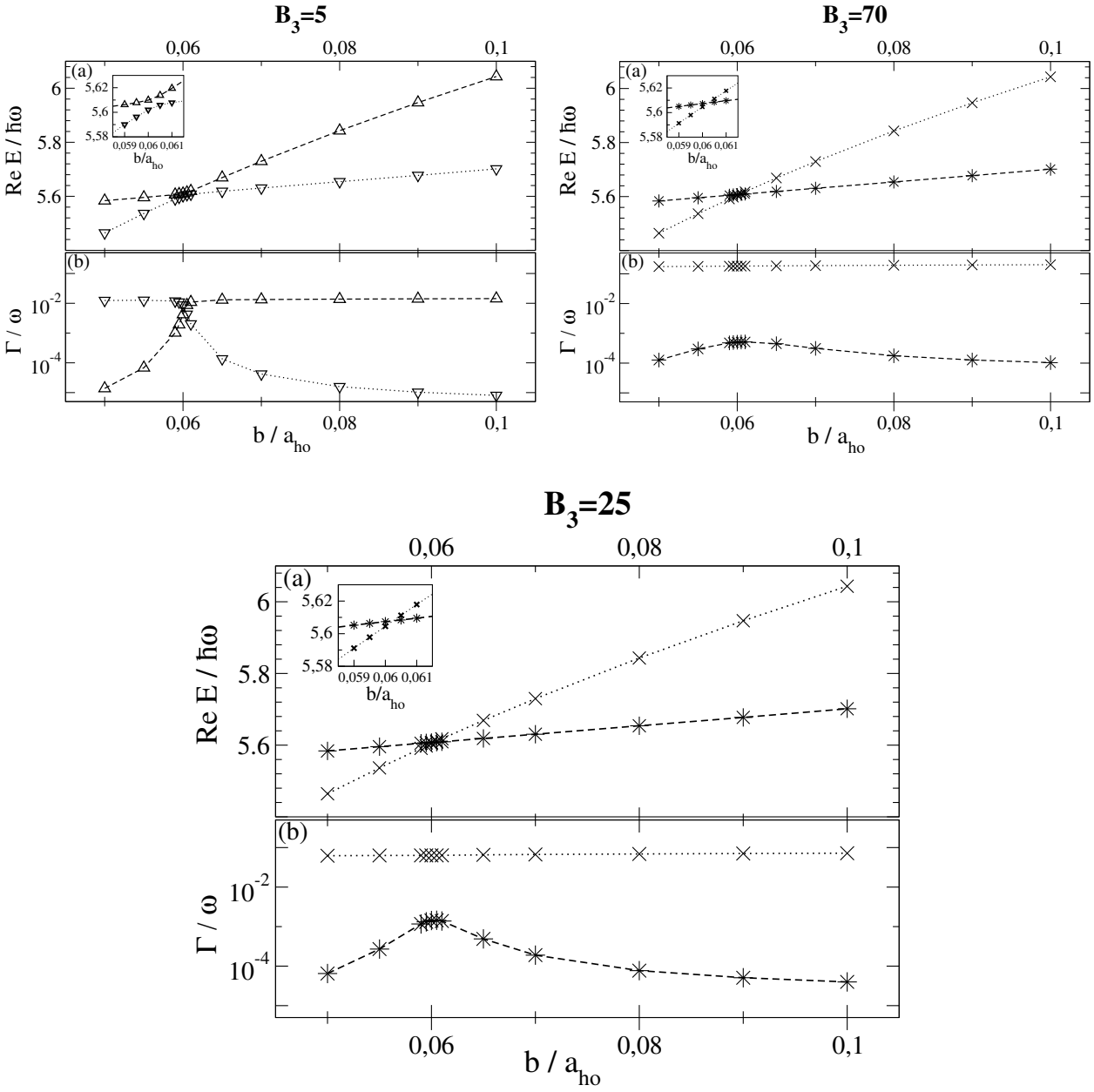

FIGURE 3.9 – Eigenvalues E of the separable-potential-based model H_{eff} : (a) Real part $\mathrm{Re}\,E$ and (b) loss rate $\Gamma = -2\,\mathrm{Im}\,E/\hbar$, as a function of the potential range b, for three different values of the coefficient B_3 which characterizes the strength of the 3-body losses [Eqs. (3.138,3.139)]. The insets are magnifications around the crossing or avoided crossing. For $B_3 = 70$ and $B_3 = 25$, the energies of the universal states ($*$) and of the efimovian states ($\times$) form two separated branches in the complex plane, whose real parts cross, and whose imaginary parts remain well separated. For $B_3 = 5$, there is an *avoided* crossing for $\mathrm{Re}\,E$, where the universal states turns into an efimovian state and vice versa. The value $B_3 = 25$ corresponds to the -11 G Feshbach resonance for Cesium. The loss rate of the universal state is always much smaller than ω ; and even much smaller than the loss rate of the efimovian state, except close to the avoided crossing occurring for $B_3 = 5$. For $B_3 = 25$ and $B_3 = 70$, the decay rate of the efimovian state Γ_e is much larger than the coupling $w/\hbar$ between efimovian and universal states, while for $B_3 = 5$ we have $\Gamma_e \lesssim w/\hbar$.

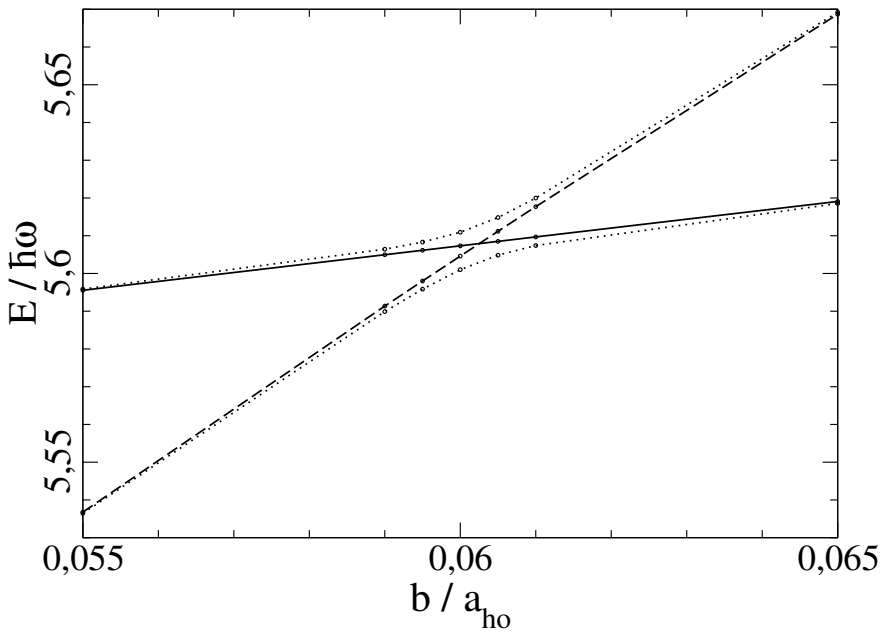

FIGURE 3.10 – The diagonal matrix elements $E_e^0 = \langle e|H_{\rm sep}|e\rangle$ (dashed line) and $E_u^0 = \langle u|H_{\rm sep}|u\rangle$ (continuous line) of $H_{\rm sep}$ simply cross, while the eigenvalues E_1 and E_2 of $H_{\rm sep}$ have an avoided crossing (dotted lines).

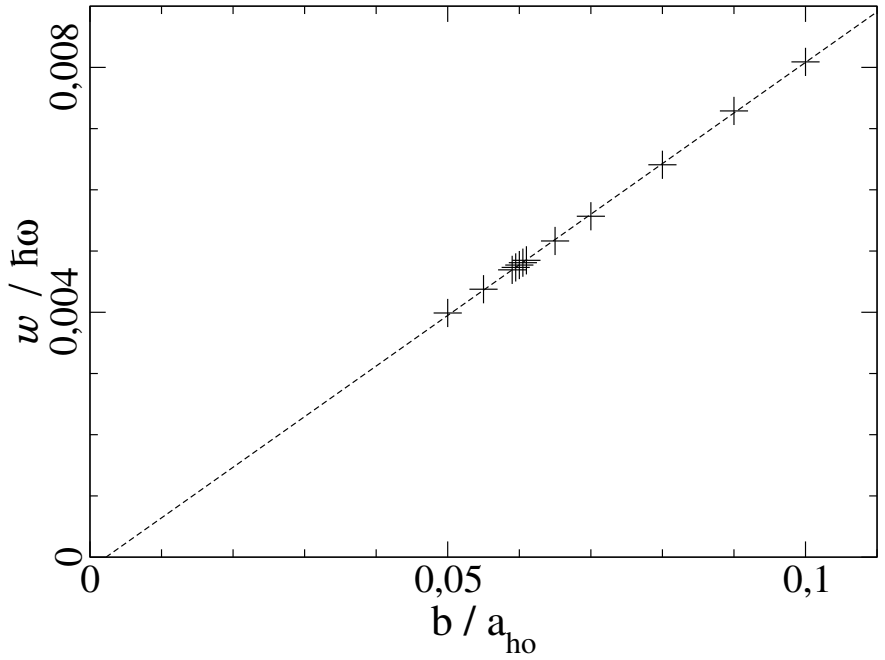

FIGURE 3.11 – Coupling $w = \langle u|H_{\rm sep}|e\rangle$ between universal and efimovian state. Remarkably, w is nearly proportional to the range b. The dashed line is a linear fit to the data $[w/(\hbar\omega) = 0.08266\,(b/a_{\rm ho}) - 0.000185]$.

The basis $(|e\rangle, |u\rangle)$ is also useful in the small-B_3 regime where $\hbar\Gamma_e^0 \lesssim w$, if one is sufficiently far from the crossing to have $w \ll |E_e^0 - E_u^0|$. Indeed, the matrix of $H_{\rm sep}$ is then nearly diagonal in this basis [Eq. (3.146)], so that one of the eigenvectors of $H_{\rm sep}$, say $|\psi_1\rangle$, is close to $|u\rangle$:

$$|\psi_1\rangle \simeq |u\rangle + \frac{w}{E_u^0 - E_e^0}|e\rangle. \tag{3.150}$$

Since we have $\hbar\Gamma_e^0 \ll |E_u^0 - E_e^0|$, $H_{\rm loss}$ is a small perturbation and

$$\Gamma_u \simeq -\frac{2}{\hbar}{\rm Im}\,\langle\psi_1|H_{\rm loss}|\psi_1\rangle, \tag{3.151}$$

so that from Eq. (3.150) :

$$\Gamma_u \simeq \Gamma_e^0 \left(\frac{w}{E_u^0 - E_e^0}\right)^2. \tag{3.152}$$

This result can also be obtained from the relation (3.136) used in the PSS approach, provided the probability $P(R < b)$ is calculated using the eigenstate *of the separable potential model*, which is contaminated by the efimovian state [Eq. (3.150)]. If instead we use the universal eigenstate of the zero-range model as in Section 5.2, i. e. we neglect the contamination by the efimovian state, then we get $\Gamma_u^{\rm ZR}/\omega = (b/a_{\rm ho})^{2s}\, K/\Gamma(s+2)$ [Eq. (3.137)] with $2s = 2s_{l=0,n=1} \simeq 9$ [Table 3.1 p. 84], which is in general underestimated. For example, for $b/a_{\rm ho} = 0.1$ we get $\Gamma_u^{\rm ZR}/\omega \simeq K \cdot 4 \cdot 10^{-12}$; assuming that K is not abnormally much larger than 1, this is much smaller than the value $\Gamma_u/\omega \simeq 4 \cdot 10^{-5}$ obtained in this Section for Cesium ($B_3 = 25$ in Fig. 3.9).

It seems likely that the relation

$$w/(\hbar\omega) \simeq C\,(b/a_{\rm ho}) \tag{3.153}$$

holds for any model, but the coefficient C is clearly model-dependent. Therefore, we do not known to which extent the separable potential predicts accurately the value of w and Γ_u for Cesium. We thus make an estimate of Γ_u which is independent of C. We distinguish two regimes :

— *Regime 1 :* If $w \ll \max\left(|E_e^0 - E_u^0|, \hbar\Gamma_e^0/2\right)$, the coupling can be treated perturbatively so that Eqs. (3.148,3.149) hold. Moreover, both $\hbar\Gamma_e^0$ and $(E_u^0 - E_e^0)$ are much smaller than $\hbar\omega$, under the assumptions we have already made (footnote 27 p. 105). Using also Eq. (3.153) we get

$$\Gamma_e\, C^2 \left(\frac{b}{a_{\rm ho}}\right)^2 < \Gamma_u \simeq \Gamma_e \frac{(C\hbar\omega)^2}{(E_u^0 - E_e^0)^2 + (\hbar\Gamma_e^0/2)^2}\left(\frac{b}{a_{\rm ho}}\right)^2 \ll \Gamma_e \ll \omega. \tag{3.154}$$

— *Regime 2 :* $w \gg \max\left(|E_e^0 - E_u^0|, \hbar\Gamma_e^0/2\right)$, which means that one is very close to the crossing ($w \gg |E_e^0 - E_u^0|$) and that the loss rate of the efimovian state is very small ($w \gg \hbar\Gamma_e^0/2$). Then, off-diagonal matrix elements of $H_{\rm eff}$ dominate over the diagonal ones [Eq. (3.147)], both eigenvectors of $H_{\rm eff}$ are equal weight superpositions of $|e\rangle$ and $|u\rangle$, and both loss rates are $\simeq \Gamma_e^0/2$.

Thus Γ_u is typically much larger than the prediction $\Gamma_u \propto \omega(b/a_{\rm ho})^{2s}$ of Eq. (3.137). However, Γ_u remains much smaller than Γ_e, except in the rather unusual Regime 2.

So far we have only considered the vicinity of the crossing, i. e. values of b which are on the order of $0.06\, a_{\rm ho}$. What can we expect for smaller b ? According to the limit cycle scenario, a second crossing occurs at $b \simeq 0.06/e^{\pi/|s_0|} \simeq 0.06/22.7$. For values of b which are intermediate between the two crossings, the two level approximation we used so far will break down, and one has to take into account the couplings of the universal state to *several* efimovian states. However, we expect that in the zero-range limit, all couplings tend to zero, so that the universal state's loss rate tends to zero. On the contrary, the efimovian state's loss rate should not tend to zero, but have a limit cycle given by the BH approach.

6 Experimental aspects

Let us first give a numerical value for the lifetime of the $l = 0$ universal state in Cesium. In Sec. 5.3 we obtained $\Gamma/\omega \simeq 4 \cdot 10^{-5}$ for $b/a_{\rm ho} = 0.1$ (see Fig. 3.9, $B_3 = 25$). Since $b = 6.5\,{\rm nm}$ (App. D), this corresponds to $a_{\rm ho} = 65\,{\rm nm}$, which gives a lifetime as long as $\tau = \Gamma^{-1} \simeq 0.2\,{\rm s}$. This gives hope to be able to observe bosonic universal states.

6.1 Zero-range limit

Let us first discuss to which extent the zero effective range limit $|r_e| \ll a_{\rm ho}$, which is a key assumption in this Chapter, can be realized in typical experiments.

The harmonic oscillator length $a_{\rm ho}$, for a cubic optical lattice of depth V_0, is

$$a_{\rm ho} = \frac{\lambda}{2\pi (V_0/E_r)^{1/4}}$$

where E_r is the recoil energy [11]. The lasers used in experiments typically have a wavelength on the order of $\lambda = 1\mu{\rm m}$. For $V_0/E_r = 40$ (resp. $V_0/E_r = 100$) this gives $a_{\rm ho} = 63\,{\rm nm}$ (resp. $a_{\rm ho} = 50\,{\rm nm}$).

To evaluate the effective range r_e, we distinguish between broad and narrow resonances. Let us define

$$r_e^b \equiv \left(\frac{mC_6}{\hbar^2}\right)^{1/4} \frac{\Gamma(1/4)^2}{3\pi} \tag{3.155}$$

where C_6 is such that the open-channel interaction potential is $\simeq -C_6/r^6$ at large r ; and

$$r_e^n \equiv -\frac{2\hbar^2}{m \cdot a_{\rm bg} \cdot \Delta B \cdot \partial E_{\rm res}/\partial B} < 0, \tag{3.156}$$

where $a_{\rm bg}$, ΔB and $\partial E_{\rm res}/\partial B$ are respectively the background scattering length, the width of the Feshbach resonance and the magnetic moment difference between the closed channel and the open channel. We shall refer to a Feshbach resonance as being broad if $r_e^b \gg |r_e^n|$, and narrow if $r_e^b \ll |r_e^n|$. [30] We will consider several known Feshbach resonances for various bosonic atoms.

— For a narrow resonance, one expects that the effective range is $r_e \simeq r_e^n$ [70, 32]. For the 1007 G resonance in ^{87}Rb (resp. the 907 G resonance in ^{23}Na) this gives $r_e = -64\,{\rm nm}$ (resp. $r_e = -52\,{\rm nm}$) [70]. Thus the zero-range limit is typically *not* reached for a narrow Feshbach resonance in a usual optical lattice. The zero-range limit can be reached if the lattice is created by a CO_2 laser, as in [111], where $\lambda = 11\,\mu{\rm m}$ so that $a_{\rm ho} \sim 500\,{\rm nm}$.

— For a broad resonance, one can expect [112] that the effective range is given by the single-channel result, which for a potential with a large C_6 is given by [113, 114] : $r_e = r_e^b$. For ^{85}Rb (resp. ^{133}Cs) we have $C_6 = 4703(9)$ a. u. [115] (resp. $C_6 = 6890(35)$ a.u. [116]) so that for the broad resonances which are known for these atoms [38], $r_e = 12.1\,{\rm nm}$ (resp. $r_e = 14.9\,{\rm nm}$). For $a_{\rm ho} = 50\,{\rm nm}$, this gives small but non-negligible effective-range corrections : for the lowest $l = 0$ universal state, Eq. (3.115) gives $\delta E = 0.255\,\hbar\omega$ (resp. $\delta E = 0.314\,\hbar\omega$). For Cesium, reaching the $-11\,{\rm G}$ resonance may be problematic (footnote 26 p. 105), but a promising alternative is the resonance predicted at 800 G [81].

The 720 G resonance in ^{7}Li is between broad and narrow. Coupled-channel calculations give $r_e \sim 0.5\,{\rm nm}$ at resonance [31]. For $a_{\rm ho} \sim 50\,{\rm nm}$, this is deep in the zero-range limit, and gives an effective range correction as small as $\delta E \sim \hbar\omega/100$.

30. The terminology used in [38] is entrance-channel dominated and close-channel dominated.
31. S. Kokkelmans, private communication.

It might also become possible to tune r_e using an electric field [117], which would allow to reach the zero-range limit much more easily, and even to tune the 3-body parameter.

6.2 Feasibility of a harmonic trapping

We have assumed that the optical lattice is deep enough for the trapping potential at the bottom of each site to be nearly harmonic. It would be interesting to calculate the anharmonic corrections (as was done in Article V for $N = 2$ particles). Indeed, since an anharmonic trapping potential couples hyperradius and hyperangles, it is a coupling mechanism between universal and efimovian state which might determine the lifetime of universal states. Here we only give a simple estimate of how deep the lattice has to be for the harmonic approximation to be reasonable. From the virial theorem for a universal state (Article I), the potential energy per particle for the motion along the x direction, divided by the lattice depth, is given by :

$$\frac{\langle \frac{1}{2} m\omega^2 x^2 \rangle}{V_0} = \frac{E/(\hbar\omega)}{9\sqrt{V_0/E_r}}. \tag{3.157}$$

If this ratio reaches 1 then the particle can easily escape for the lattice site and the harmonic approximation does not make any sense. For the lowest $l = 0$ state, this ratio is 0.12 for $V_0/E_r = 40$, 0.08 for $V_0/E_r = 100$, and 0.02 for $V_0/E_r = 1000$. Thus the harmonic approximation seems reasonably good in the first two cases, and very good in the third case. If one wants to increase V_0/E_r without too much laser power, one can decrease the detuning, provided the spontaneous emission time remains larger than the time during which one wishes to observe the universal state.

6.3 Sudden change of the scattering length

How can one prepare and observe bosonic universal states ? A simple procedure, which avoids problems associated with the short lifetime of the efimovian states, is to start from a weakly-interacting regime $|a| \ll a_{\rm ho}$, where the lifetime is long [32]. For example one may start from the weakly-interacting ground state, i. e. from a Mott state with 3 atoms per site (see e. g. [118]). Then, if one would slowly ramp the magnetic field to the Feshbach resonance, one would stay in the ground state, which is short-lived since the 3 atoms are at distances $\sim b$. We thus rather propose to jump rapidly to $a = \infty$ (i. e. $|a| \gg a_{\rm ho}$). Assuming that the jumping time is short enough, the wavefunction does not change during the jump, and its evolution after the jump is simply obtained by expanding the non-interacting ground state onto the eigenstates of the unitary 3-body problem. Thus the probability of ending up in the universal state of quantum numbers $l = 0$, n and q is the squared overlap $P(s_{l=0,n}, q)$ introduced in Sec. 3.2.c. The total probability of ending up in an efimovian state $P(s_{0,0}) = \sum_{q\in\mathbb{Z}} P(s_{0,0}, q)$ is given by the analytic expression Eq. (3.75), whose numerical value is $0.826\ldots$. The total probability of ending up in a universal state is thus $1 - P(s_{0,0}) = 0.174\ldots$, a value dominated by the contribution $P(s_{l=0,n=1}, q = 0) = 0.105\ldots$ [Eq. (3.77)] of the lowest $l = 0$ universal state. After a waiting time much longer than the lifetime of efimovian states and much shorter than the lifetime of universal states, the fraction of remaining atoms (within the lattice sites which were initially occupied by 3 atoms) is thus $\simeq 0.174$.

32. For the bosonic non-interacting ground state, the hyperradial wavefunction is the one of a universal state [Eq. (3.44)] with $s = 2$, and thus the loss rate predicted by the PSS approach Eq. (3.137) is $\Gamma \propto \omega(b/a_{\rm ho})^4$.

6.4 Radiofrequency spectroscopy

Radiofrequency (RF) spectroscopy is a powerful experimental method which was already used to study the 2-body problem with resonant interactions, at the sites of a deep optical lattice which are occupied by 2 atoms ([29, 119, 30], Article V). Extending these experiments to lattice sites occupied by 3 atoms would allow to compare accurately the experimental spectrum to the analytical prediction of the zero-range model (Sec. 3.1). This would be a serious check of the fundamental hypothesis that atoms near a Feshbach resonance are described by the universal zero-range theory. Universality was checked in the many-body case for fermions by comparing theoretical [39, 40, 42, 43] and experimental [44, 45, 46, 47, 48] results for the ground-state energy, but a much higher accuracy may be reached in the 3-body case. Theoretically, universality of the 3-body problem was tested for single-channel models (Sec. 2.4), and for a two-channel model in free space in the particular case of narrow resonances [99, 72]. For a more accurate comparison, one can include the corrections due to the finite effective range (Sec. 3.1 and 6.1). A further improvement of this method is to perform RF *association* ([30], Article V), where the initial state is a combination of hyperfine states with weak interatomic interactions and a small loss rate, and the final state is the strongly interacting state of interest. This could even allow to measure the energies E of efimovian states, provided $|E|$ is much larger than the loss rate Γ, the widths of the RF spectra being determined by Γ. The coupling between initial and final state induced by the RF wave is proportional their wavefunction overlap (see Article V, Sec. IV), and this overlap was calculated in Sections 3.2.c and 6.3.

We note that RF association may even be useful to create Efimov trimers from a homogeneous gas.

6.5 Non-zero angular momentum states

Among the bosonic universal states, the ones with an angular momentum $l \geq 1$ are particularly long-lived, because they are not coupled to the efimovian states by the finite-range interaction. Moreover the odd-l states remain decoupled from the efimovian states for any trapping potential which is symmetric with respect to the origin. The lowest $l = 1$ universal state is thus an excellent candidate for experiments. However, it is not as straightforward to reach experimentally as the $l = 0$ states. For example, one can start from a weakly interacting *excited* state with $l = 1$, and then use the method of Sec. 6.3 or 6.4. Weakly interacting excited states have been prepared by two-photon Raman process [120], and by adiabatically turning off a superlattice [121].

7 Conclusions and outlook

The exact solution of the unitary 3-body problem allowed us to obtain several physical results, concerning the high-energy limit, the effective range corrections, and the loss rate. For efimovian states, the loss rate can be expressed analytically using the approach of Braaten and Hammer. For universal states, we expect that the loss rate Γ_u tends to zero in the zero-range limit. For some universal states, the asymptotic behavior of Γ_u can be predicted by combining the zero-range model with the approach of Petrov, Salomon and Shlyapnikov. But for bosonic universal states of zero angular momentum, one cannot use the zero-range model to predict Γ_u, because these states become coupled to efimovian states as soon as the interactions have a finite range b. For a separable potential model, we numerically found that the coupling varies linearly with b : it would be interesting to understand this property analytically. Another open question is whether the coupling is a model-indepent function of e. g. the effective range and the 3-body parameter.

Another way of obtaining more accurate predictions for the coupling and Γ_u would be to use finite-range models which are more realistic than the separable potential : the effective-range model for a narrow Feshbach resonance (see Sec. 4.2), or more elaborated two-channel models [100, 81]. An easier task is to extend the numerical study presented here to smaller values of the range, where, according to the limit cycle scenario, the universal state will cross another efimovian state : in this case, will the coupling again be proportional to b ? Will the slope C be modified ? We also plan to compute the coupling induced by a finite scattering length and by a small anisotropy of the trap : this can be done within the zero-range model, and is experimentally relevant.

A more fundamental open problem is the existence of interacting universal states for $N \geq 4$ bosons.

Appendix C

Numerical method for the separable interaction

In this Appendix, we describe in some detail our method for solving the 3-body problem for the separable interaction defined in Eqs. (3.116,3.117,3.119,3.120).

1 Discrete states

In this Section we consider eigenstates which belong to the discrete spectrum : trimers in free space, or eigenstates in a trap. We restrict to an infinite scattering length, so that the coupling constant g_0 is given by Eq. (3.118).

We first reduce Schrödinger's equation

$$H_{\rm sep}|\psi\rangle = E|\psi\rangle \tag{C.1}$$

to the integral equation :

$$|f\rangle = g_0 \left(\langle\zeta| \otimes \mathbf{1}\right) \left(1 + \eta P_{13}\right) G_0(E) \left(|\zeta\rangle \otimes |f\rangle\right), \tag{C.2}$$

where $|f\rangle$ and $|\psi\rangle$ are related through

$$|f\rangle = g_0 \left(\langle\zeta| \otimes \mathbf{1}\right) |\psi\rangle \tag{C.3}$$

$$|\psi\rangle = (1 + \hat{Q}) G_0(E) \left(|\zeta\rangle \otimes |f\rangle\right). \tag{C.4}$$

Here we have assumed that E does not belong to the spectrum of H_0, so that one can define $G_0(E) \equiv (E - H_0)^{-1}$; the notation $|\phi\rangle = |\phi_1\rangle \otimes |\phi_2\rangle$ means that $\langle\vec{r},\vec{\rho}\,|\phi\rangle = \langle\vec{r}\,|\phi_1\rangle\langle\vec{\rho}\,|\phi_2\rangle$; $\hat{Q}$ and η are defined in Eqs. (3.26,3.30) ; and $\mathbf{1}$ stands for the identity matrix, for example Eq. (C.3) means that $\langle\vec{\rho}\,|f\rangle = g_0(\langle\zeta| \otimes \langle\vec{\rho}\,|)|\psi\rangle = g_0 \int d\vec{r}\langle\zeta|\vec{r}\,\rangle\langle\vec{r},\vec{\rho}\,|\psi\rangle$.

In what follows we restrict to zero total angular momentum, so that $|f\rangle$ is isotropic, and we shall reduce Eq. (C.2) to an integral equation with one variable.

1.1 Trimers in free space

The calculation in free space ($\omega = 0$) is rather straightforward. We use the plane-wave basis

$$\langle\vec{\rho}\,|\vec{\kappa}\rangle = \frac{e^{i\vec{\kappa}\cdot\vec{\rho}}}{(2\pi)^{3/2}}. \tag{C.5}$$

Defining

$$g(\kappa) = \kappa \langle \vec{\kappa} | f \rangle, \tag{C.6}$$

and taking units in which $b = 1$, Eq. (C.2) can be reduced to :

$$\begin{aligned} 0 &= -\frac{\sqrt{3\pi}}{2\,b} g(\kappa) + \int_0^\infty d\kappa' \left[\frac{\kappa'}{\kappa} e^{\kappa^2\, b^2} g(\kappa) + 2 e^{(\kappa^2+\kappa'^2) b^2/2} g(\kappa') \right] \\ &\cdot \left\{ E_1 \left[\left(-E + \frac{4}{3}(\kappa^2 + \kappa'^2 - \kappa\kappa') \right) b^2 \right] - E_1 \left[\left(-E + \frac{4}{3}(\kappa^2 + \kappa'^2 + \kappa\kappa') \right) b^2 \right] \right\} e^{-E\, b^2} \end{aligned} \tag{C.7}$$

where E_1 is the exponential integral

$$E_1(x) \equiv \int_1^\infty e^{-tx} t^{-1} dt. \tag{C.8}$$

We then discretise the variables κ and κ'. Because of the log-periodic oscillations of the wavefunctions of excited Efimov trimers [given by Eq. (3.47) in the zero-range limit], it is convenient to use a logarithmic grid. The kernel of Eq. (C.7) then becomes a matrix, which has one vanishing eigenvalue when Eq. (C.7) has a solution, i. e. when E belongs to the spectrum of the 3-body problem. We look for these values of E by dichotomy. A property which is useful for this is that the eigenvalues are increasing functions of E. This property also holds in the trapped case, and can be shown using the Hellmann-Feynman theorem [1].

Our results for the first bound states are :

$$E_1^{\rm sep} = -0.090475 \frac{\hbar^2}{m b^2} \tag{C.9}$$

$$E_2^{\rm sep} = -1.6506 \cdot 10^{-4}\, \frac{\hbar^2}{m b^2} \tag{C.10}$$

$$E_3^{\rm sep} = -3.199 \cdot 10^{-7}\, \frac{\hbar^2}{m b^2}. \tag{C.11}$$

For $E_3^{\rm sep}$ we have used a grid of 12800 steps between $\kappa_{\rm min} = 10^{-7}$ and $\kappa_{\rm max} = 3$.

1.2 Eigenstates in a trap

In the trapped case ($\omega = 1$), the calculation is more involved. We work in position space, and define

$$g(\rho) = \rho \langle \vec{\rho} | f \rangle. \tag{C.12}$$

Then, Eq. (C.2) reduces to the integral equation of one variable

$$g(\rho) = \int_0^\infty d\rho' K_E(\rho, \rho') g(\rho') \tag{C.13}$$

with the kernel

$$K_E(\rho, \rho') = g_0 4\pi \rho \rho' \overline{(\langle \zeta | \otimes \langle \vec{\rho} |)\,(1 + \eta P_{13}) G_0(E) (|\zeta\rangle \otimes |\vec{\rho'}\rangle)} \tag{C.14}$$

where the bar stands for the average over the directions of $\vec{\rho}$ and $\vec{\rho'}$. To calculate the kernel K_E, we use the fact that $G_0(E)$ is the Fourier transform of the Feynman propagator :

$$\langle \vec{X} | G_0(E) | \vec{X}' \rangle = -i \int_0^\infty dt \langle \vec{X} | e^{-iH_0 t} | \vec{X}' \rangle e^{i(E + i0^+)t} \tag{C.15}$$

1. Rewriting Eq. (C.2) as $|f\rangle = L(E)|f\rangle$, the eigenvalue equation writes $L(E)|f\rangle = \lambda(E)|f\rangle$, and since the operator $L(E)$ is real symmetric we can apply the Hellmann-Feynman theorem, which gives $d\lambda/dE = \langle f | dL/dE | f \rangle / \langle f | f \rangle = -[g_0/(1+|\eta|)] \| G_0(E)(1+Q)(|\zeta\rangle \otimes |f\rangle) \|^2 / \langle f | f \rangle > 0$.

where $|\vec{X}\rangle = |\vec{r},\vec{\rho}\rangle$ and $|\vec{X}'\rangle = |\vec{r'},\vec{\rho'}\rangle$. The well-known properties of the Feynman propagator of the harmonic oscillator (see e. g. [122]) imply :

$$\begin{aligned}\langle\vec{X}|G_0(E)|\vec{X}'\rangle &= \frac{-1}{2^6\pi^3\sin(\pi E)} \\ &\quad \mathrm{Im}\left[\int_0^\pi dt \frac{e^{iE(t-\pi)}}{|\sin t|^3}\exp\left\{i\left(\frac{X^2+X'^2}{4\tan t}-\frac{\vec{X}\cdot\vec{X}'}{2\sin t}\right)\right\}\right]. \qquad \text{(C.16)}\end{aligned}$$

We then insert the identities $\langle\zeta| = \int d\vec{r}\langle\zeta|\vec{r}\rangle\langle\vec{r}|$ and $|\zeta\rangle = \int d\vec{r'}|\vec{r'}\rangle\langle\vec{r'}|\zeta\rangle$ into Eq. (C.14). Using Eq. (C.16), the integrals over $\vec{r}$ and $\vec{r'}$ are gaussian and can be evaluated. We then integrate over the directions of $\vec{\rho}$ and $\vec{\rho'}$, and obtain :

$$K_E(\rho,\rho') = \frac{g_0}{\pi^2\cos(\pi E/2)}\mathrm{Re}\left[\frac{e^{-i\pi E/2}}{2i}\left(I_1+\frac{\eta}{2}I_2\right)\right] \qquad \text{(C.17)}$$

where

$$I_i \equiv \sum_{\epsilon=\pm1}\epsilon\, I_i^\epsilon \qquad \text{(C.18)}$$

and

$$\begin{aligned}I_1^\epsilon &\equiv \int_0^{\pi/2} dt e^{itE}\exp\left[i\left(\frac{\rho^2+\rho'^2}{4\tan t}+\epsilon\frac{\rho\rho'}{2\sin t}\right)\right] \\ &\quad \frac{\sin t}{\left(y(t)^2+b^4\right)^{3/2}}, \qquad \text{(C.19)} \\ I_2^\epsilon &\equiv 4\int_0^{\pi/2} dt \frac{e^{iEt}\sin t}{\left(y(t)^2+b^4/4\right)^{1/2}\left(y(t)^2+b^4\right)} \\ &\quad \exp\left[i\frac{\rho^2+\rho'^2}{4\tan t}+\frac{-3y(t)b^2(\rho^2+\rho'^2)/4+\epsilon i\left(y(t)^2+b^4\right)\rho\rho'}{\sin t\left(4y(t)^2+b^4\right)}\right], \qquad \text{(C.20)} \\ y(t) &\equiv 2\sin t - ib^2\cos t. \qquad \text{(C.21)}\end{aligned}$$

We calculate the integrals I_i^ϵ numerically for each (ρ,ρ'). These integrals are wildly oscillating, with an amplitude diverging as $1/\sqrt{t}$ for $t\to 0$ in the case of I_1^ϵ. We thus use *ad hoc* integration schemes for which we estimate the discretisation error. More precisely, we first make the change of variables $\tau = \tan(t/2)$ to get rid of the trigonometric functions. We then split the integration interval $0<\tau<1$ in two parts :

— For $b^2<\tau<1$, we make the change of variables $x=1/t$, write the integrand as $A(x)\exp[iB(x)]$, and split the integration interval $1<x<1/b^2$ into slices $(x,x+\Delta x)$ with Δx proportional to x.

— For $0<\tau<b^2$, we use slices $(\tau,\tau+\Delta\tau)$ with a uniform $\Delta\tau$. In the case of I_1^ϵ we write the integrand as $A(\tau)\exp[iC/\tau]/\sqrt{\tau}$. In the case of I_2^ϵ we write the integrand as $A(\tau)\exp[iB(\tau)]$.

The functions A and B differ in each of the above cases. They depend on ρ and ρ', and so does C. Then, on each slice, we quadratize the functions $A(x)$ and $B(x)$ and evaluate the resulting integral analytically. We also estimate the error on each slice due to the quadratisation, and choose the number of slices in order to obtain a fixed maximal total error.

For the calculations of Article III and of Chap. 3, we have restricted the variables ρ and ρ' in the integral equation Eq. (C.13) to the interval $[0;7.5]$, we used a uniform discretisation with $N=1000,1500,2000$ steps, and we extrapolated the results to $N\to\infty$.

We then have to find the values of E which belong to the 3-body spectrum, i. e. for which the integral equation Eq. (C.13) has a solution, i. e. for which one of the eigenvalues of the discretised version of the kernel $K_E(\rho,\rho')$ reaches one. We first do this by dichotomy, using the fact that the eigenvalues are increasing functions of E (see footnote 1 p. 116). We then improve the accuracy using Newton's method, the derivatives with respect to E of the eigenvalues being expressible in terms of $\partial K_E(\rho,\rho')/\partial E$ using the Hellmann-Feynman theorem. We compute $\partial K_E(\rho,\rho')/\partial E$ using the same method than for $K_E(\rho,\rho')$.

For the lifetime calculations, we first need to normalise the wavefunctions to $\langle\psi|\psi\rangle = 1$. For this we use the expression :

$$\langle\psi|\psi\rangle = -\frac{4\pi}{g_0}(1+|\eta|)\int_0^\infty d\rho\int_0^\infty d\rho'\frac{\partial K_E(\rho,\rho')}{\partial E}g(\rho)g(\rho'). \tag{C.22}$$

We then compute $\psi(\vec{0},\vec{0}\,)$ which, using Eq. (C.4), is given by :

$$\psi(\vec{0},\vec{0}\,) = \frac{-3\,\Gamma[(3-E)/2]}{\pi^{5/2}b^3}\int_0^\infty dr\int_0^\infty d\rho \tag{C.23}$$

$$\frac{r^2\rho}{(r^2+\rho^2)^{3/2}}W_{E/2,1}\left(\frac{r^2+\rho^2}{2}\right)e^{-r^2/(2b^2)}g(\rho) \tag{C.24}$$

where W is a Whittaker function.

2 Zero-energy scattering state

For Appendix D, we also need to calculate $\psi(\vec{0},\vec{0}\,)$ where ψ is now the zero-energy scattering state, and where the scattering length a is now finite and negative. The coupling constant is then given by :

$$\frac{1}{g_0} = \frac{1}{4\pi a} - \frac{1}{4\pi^{3/2}b}. \tag{C.25}$$

An outgoing scattering state $|\psi\rangle$ of energy E is given by the Lippman-Schwinger equation

$$|\psi\rangle = |\psi_0\rangle + G_0(E+iO^+)(V_{12}+V_{13}+V_{23})|\psi\rangle \tag{C.26}$$

where $|\psi_0\rangle$ is the incident wave. Since we restrict to $E=0$, $|\psi_0\rangle$ is constant, and we take the normalisation :

$$\psi_0(\vec{r},\vec{\rho}\,) = 1. \tag{C.27}$$

Defining $|f\rangle$ as previously by Eq. (C.3), we get the relation :

$$|\psi\rangle = |\psi_0\rangle + (1+\hat{Q})G_0(E+i0^+)\left(|\zeta\rangle\otimes|f\rangle\right), \tag{C.28}$$

leading to an integral equation which now contains a source term :

$$\frac{1}{g_0}|f\rangle = (2\pi)^{3/2}|\vec{\kappa}=\vec{0}\rangle + \left(\langle\zeta|\otimes\mathbf{1}\right)(1+\eta P_{13})\,G_0(E)\left(|\zeta\rangle\otimes|f\rangle\right). \tag{C.29}$$

Here we have kept the definition of the plane wave $|\vec{\kappa}\rangle$ given by Eq. (C.5), so that

$$\langle\vec{\rho}|\vec{\kappa}=\vec{0}\rangle = 1/(2\pi)^{3/2}.$$

The solution of Eq. (C.29) is

$$\langle\vec{\kappa}|f\rangle = A(2\pi)^{3/2}\delta^3(\vec{\kappa}) + \frac{u(\kappa)}{\kappa^2}, \tag{C.30}$$

where

$$A = 4\pi a \tag{C.31}$$

and $u(\kappa)$ has no singularity (for $a < 0$), and solves :

$$\begin{aligned} -a\sqrt{\frac{2^5}{3\pi}}e^{-5\kappa^2/6} &= \frac{1}{g_0}u(\kappa) + \frac{1}{2\sqrt{3}\pi^2}\int_0^\infty d\kappa' \left[\frac{\kappa'}{\kappa}e^{\kappa^2}u(\kappa) + 2\frac{\kappa}{\kappa'}e^{(\kappa^2+\kappa'^2)/2}u(\kappa')\right]\cdot \\ &\quad \left[E_1\left(-E + \frac{4}{3}(\kappa^2 + \kappa'^2 - \kappa\kappa')\right) - E_1\left(-E + \frac{4}{3}(\kappa^2 + \kappa'^2 + \kappa\kappa')\right)\right] e^{-E}. \end{aligned} \tag{C.32}$$

We solve this equation by discretising κ and κ' on a logarithmic grid and by inverting numerically the operator appearing on the right hand side. We tested the numerical results by checking the exact relation :

$$\lim_{\kappa\to 0} u(\kappa) = -16\sqrt{\frac{2\pi}{3}}\, a^2. \tag{C.33}$$

Finally, we get the desired $\psi(\vec{0}, \vec{0}\,)$ from the relation

$$\psi(\vec{0}, \vec{0}\,) = 1 - \frac{3}{\sqrt{2\pi^5}}\left[2\pi^2 a + \int_0^\infty dk \int_0^\infty d\kappa \frac{k^2 e^{-k^2/2}u(\kappa)}{k^2 + \kappa^2}\right], \tag{C.34}$$

which follows from Eq. (C.28).

Appendix D

Loss rate from a homogeneous Bose gas

In this Appendix, we calculate the formation rate of deeply bound dimers in a homogeneous Bose gas using the separable-potential-based model introduced in Eqs. (3.139,3.138) p. 104. We then compare the result of the calculation to the experimental data of [2] on a non-condensed gas of ^{133}Cs atoms for negative scattering lengths a near the $-11\,G$ Feshbach resonance. This allows us to determine the value of the two parameters of our effective Hamiltonian for this Feshbach resonance, which is useful for Chap. 3, Sec. 5.3.

We first consider the zero-energy scattering state $\psi_{\rm scat}$, with the normalisation

$$\psi_{\rm scat}(\vec{r},\vec{\rho}\,) \underset{r,\rho\to\infty}{\longrightarrow} 1, \tag{D.1}$$

and we calculate $\psi_{\rm scat}(\vec{0},\vec{0}\,)$ as described in Appendix C, Section 2. The loss rate coefficient from a non-condensed weakly interacting gas at low temperatures is then given by :

$$L_3^{\rm NC} = 3B_3\frac{\hbar b^4}{m}\left|\psi_{\rm scat}(\vec{0},\vec{0}\,)\right|^2. \tag{D.2}$$

This relation can be justified as follows. For N particles in a volume V, one has in general :

$$\dot{N} = -L_3\frac{N(N-1)(N-2)}{V^2}. \tag{D.3}$$

Now consider the case of a weakly interacting "Bose-Einstein condensate" of $N=3$ particles at temperature $T=0$ in a large box of volume V much larger than $|a|^3$ and than b^3. The normalized wavefunction is, after separation of the center of mass :

$$\psi_{\rm box}(\vec{r},\vec{\rho}\,) \simeq \frac{1}{V}\psi_{\rm scat}(\vec{r},\vec{\rho}\,). \tag{D.4}$$

Moreover, for the separable-potential-based model [Eqs. (3.139,3.138,3.140) p. 104], the loss rate is

$$\Gamma = -\frac{\dot{N}}{N} = -\frac{2}{\hbar}{\rm Im}\langle\psi_{\rm box}|H_{\rm loss}|\psi_{\rm box}\rangle = B_3\frac{\hbar b^4}{m}\left|\psi_{\rm box}(\vec{0},\vec{0}\,)\right|^2 \tag{D.5}$$

where we have treated the loss term $H_{\rm loss}$ in first order perturbation theory. Combining this with Eqs. (D.3,D.4) gives :

$$L_3^{\rm BEC}(T=0) = B_3\frac{\hbar b^4}{2m}\left|\psi_{\rm scat}(\vec{0},\vec{0}\,)\right|^2. \tag{D.6}$$

The result Eq. (D.2) then follows from the relation [107] :

$$L_3^{\rm NC} = 3!\; L_3^{\rm BEC}(T=0). \tag{D.7}$$

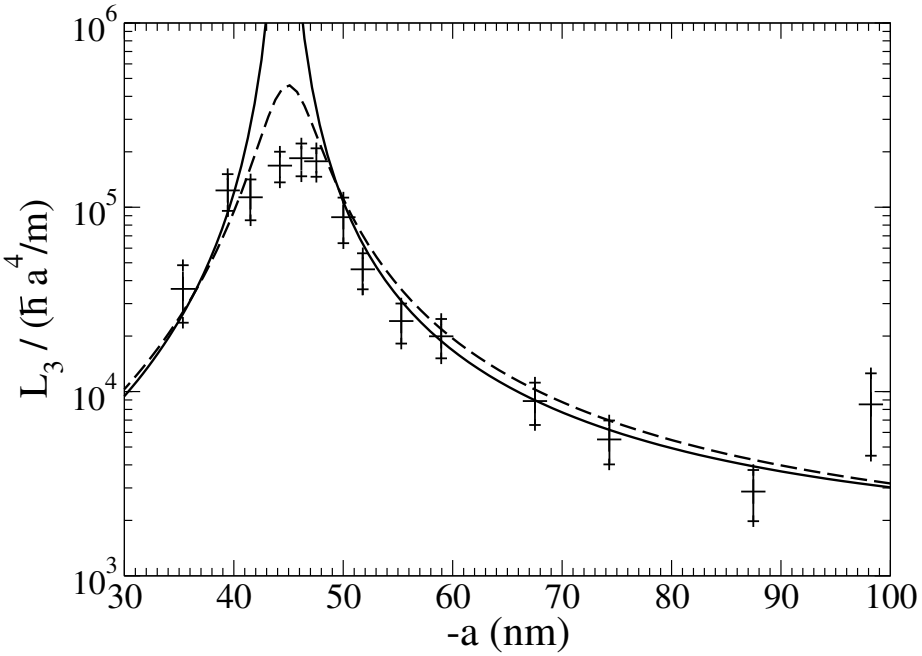

FIGURE D.1 – Loss rate coefficient L_3 in a non-condensed Cesium gas for negative scattering lengths a near the -11 G Feshbach resonance. Crosses : experimental data from Innsbruck [2]. Dashed line : formula of Braaten and Hammer [105], Eq. (D.8), with the parameters adjusted as in [2] to $\eta_* = 0.06$ and $a'_* = -850$ Bohr radii in order to fit the experimental data. Continuous line : separable-potential-based model (see text), with the parameters adjusted to $b = 6.5\,\text{nm}$ and $B_3 = 25$ to fit the experimental data.

This relation holds under the assumptions that $|a|$ and the range of interactions are much smaller than the interparticle distance and than the thermal de Broglie wavelength of the non-condensed gas ; these assumptions are rather well satisfied in the experiment [2]. We note that one can justify the above steps using the master equation formalism of [123].

The result is shown as a solid line in Figs. D.1 and D.2, with the parameters $b = 6.5\,\text{nm}$ and $B_3 = 25$ chosen in order to fit the experimental data. Our result diverges at the values of a where there is a trimer of vanishing energy. These unphysical divergences are due to the fact that we have treated H_{loss} perturbatively. These divergences are replaced by peaks in the experiment, and also in the non-perturabtive theory of Braaten and Hammer which predicts [105] :

$$L_3^{\text{NC}} = 3\frac{\hbar a^4}{m} 4590 \frac{\sinh(2\eta_*)}{\sin^2[|s_0|\ln(a/a'_*)] + \sinh^2(\eta_*)}. \tag{D.8}$$

The parameter η_* characterizes the loss mechanism (see [105, 26] and Chap. 3, Sec. 5.1 p. 102). The parameter a'_* gives the positions of the peaks and is directly related to the 3-body parameter. [1] The fit of Eq. (D.8) on the experimental data was performed in [2] and gives $\eta_* = 0.06(1)$ and $a'_* = -850(20)$ Bohr radii. The resulting curve is the dashed line in Figs. D.1 and D.2.

1. The relation between a'_* and the 3-body parameter κ_* of Braaten and Hammer is [26] : $a'_* \simeq -1.6/\kappa_*$. For the relation between κ_* and our 3-body parameter R_t, see the footnote on page 79.

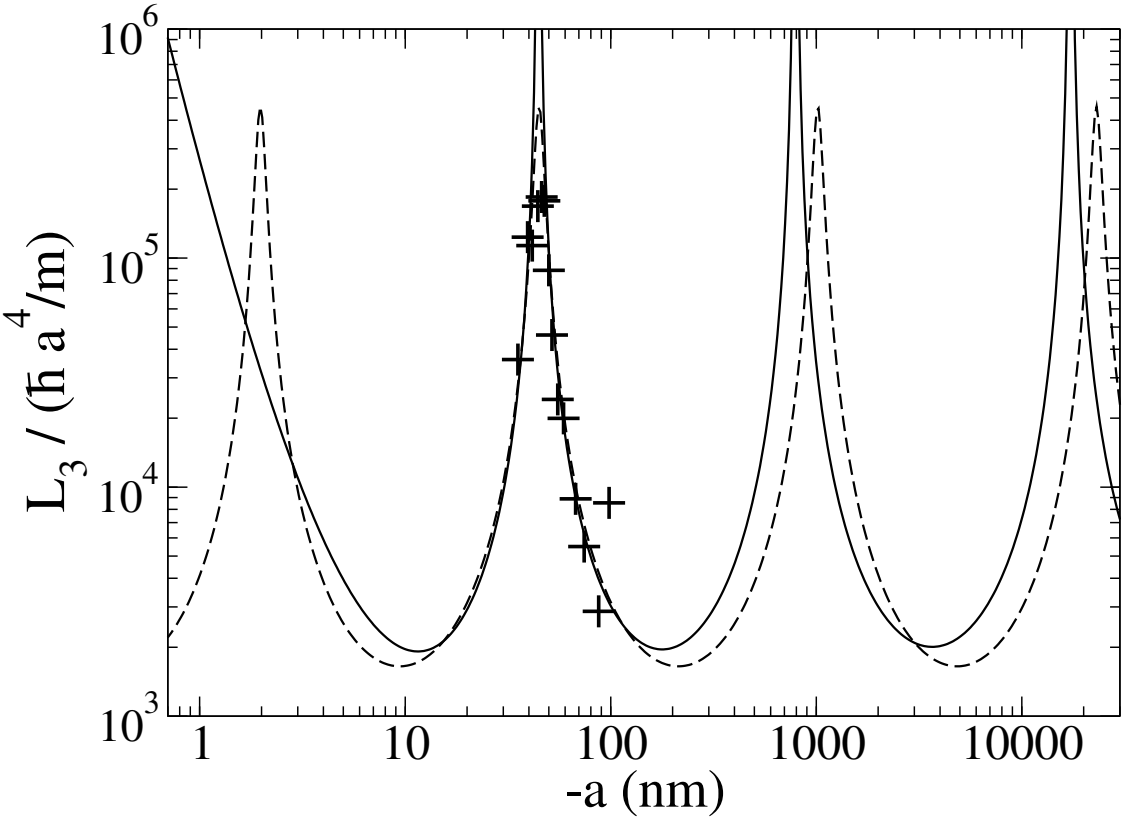

FIGURE D.2 – Same as Fig. D.1 on a broader range of variation for a.

We note that if one starts with a theoretical model which, more realistically than our effective Hamiltonian, explicitly contains one or several deep dimer states, as was done in [81, 100], then Equation (D.8) is expected to become exact in the limit where $|a|$ is much larger than all scales associated to the 2-body problem such as the van der Waals length, and where $|a|$ is much smaller than the interparticle distance so that the gas remains weakly interacting. The parameters η_* and a'_* depend on short-range details of the considered theoretical model.

Let us compare our results to Eq. (D.8). Fig. D.2 shows that at large values of $|a|$, where other peaks occur when *excited* trimers of the separable-potential-based model have a vanishing energy, there is some shift between the two curves. This is due to the fact that, around the first peak, where the fits on experimental data were done, the separable-potential-based model has not yet fully reached the asymptotic regime, where L_3/a^4 becomes a log-periodic function of $|a|$ in accordance with Eq. (D.8). This is directly related to the fact that the trimer which forms at the position of the first peak is the ground trimer. If we follow this trimer until $a = \infty$, we obtain a state which is not extremely weakly bound [its binding energy is $\simeq 0.1\,\hbar^2/(mb^2)$ for the separable potential], and is thus not extremely accurately described by the zero-range theory used by Efimov ; accordingly, the ratio between the binding energies of the ground trimer state and the first excited trimer state [$\simeq 548$, see Eq. (3.123) p. 99] does not fully match the asymptotic universal value predicted by Efimov for the ratio between successive highly excited states [$e^{2\pi/|s_0|} \simeq 515.04$].

Another manifestation of the same effect is that, for the value $a'_* = -850(20)$ Bohr radii (coming from the fit of Eq. (D.8) on the experiment) our 3-body parameter is $R_t = 29\,\text{nm}$ (see the footnote on page 121) ; while the value $b = 6.5\,\text{nm}$ (coming from the fit of our results on the experiment) together with the relation $R_t \simeq 3.60\,b$ [Eq. (3.125) p. 99] give $R_t = 23$ nm. This uncertainty on R_t is again due to the fact that the experiment was not carried out extremely deep in the large-$|a|$ regime where all models become equivalent. We note that there is no guarantee that the prediction of the separable-potential-based model for L_3 is more accurate than the prediction Eq. (D.8) of the zero-range theory. The separable-potential-based model really becomes useful for the discussion on the lifetime of universal states in a trap (Chap. 3, Sec. 5.3).

Partie 3 : Description hydrodynamique du gaz unitaire

Dans cette Partie, nous considérons le gaz unitaire piégé dans la limite où le nombre de particules est grand.

Au Chapitre 4, nous utilisons la version indépendante du temps de l'hydrodynamique, aussi appelée approximation de densité locale, pour déterminer le comportement asymptotique de l'énergie de l'état fondamental, et donc de l'exposant s introduit dans la Partie 1.

Au Chapitre 5, nous reprenons une relation trouvée dans la Partie 1 sur les fluctuations de la taille du gaz, et nous l'interprétons très simplement en terme d'excitation thermique du mode hydrodynamique de respiration.

L'Article IV sur les gaz de fermions en rotation est un travail de Giulia Tonini et Yvan Castin, auquel j'ai contribué au sujet des modes propres hydrodynamiques dans le cas tridimensionnel, ainsi que du diagramme de stabilité correspondant.

Chapitre 4

Approximation de densité locale

Dans la limite $N \to \infty$, on s'attend à ce que l'énergie et le profil de densité de l'état fondamental soient donnés par l'hydrostatique, où le gaz est localement approximé par un gaz homogène de densité $\rho(\vec{r})$, ce qui conduit à la fonctionnelle énergie :

$$E[\rho] = \int d\vec{r}\, [e(\vec{r}) + \rho(\vec{r})U(\vec{r})] \tag{4.1}$$

où

$$U(r) = \frac{1}{2} m\omega^2\, r^2 \tag{4.2}$$

et $e(\vec{r})$ est l'énergie volumique du gaz unitaire homogène, qui est proportionnelle à celle du gaz parfait

$$e(\vec{r}) = \eta\, e_{\text{parfait}}(\vec{r}), \tag{4.3}$$

avec $\eta \simeq 0.45$ dans le cas équilibré en spin (cf. [42] et Chap. 0, p. 20).

Pour déterminer l'état fondamental, on introduit le potentiel chimique μ et on minimise le grand potentiel

$$\Omega[\rho] = E[\rho] - \mu\, N[\rho] \tag{4.4}$$

avec

$$N[\rho] = \int d\vec{r}\, \rho(\vec{r}). \tag{4.5}$$

On obtient le résultat bien connu :

$$E_0 = \sqrt{\eta}\frac{(3N)^{4/3}}{4}\hbar\omega. \tag{4.6}$$

Rappelons que nous avons montré au Chap. 1 que la fonction d'onde de l'état fondamental dans le piège est de la forme

$$\Phi(\vec{r}_1, \ldots, \vec{r}_N) = R^{s-\frac{3N-5}{2}}\, e^{-\frac{1}{2}\left(\frac{R}{a_{\text{ho}}}\right)^2} \phi(\vec{\Omega})\, e^{-\frac{3}{2}\left(\frac{C}{a_{\text{ho}}}\right)^2}, \tag{4.7}$$

où R est l'hyperrayon, $\vec{\Omega}$ sont les hyperangles, $\vec{C}$ est la position du centre de masse, et l'exposant s est relié à l'énergie par

$$E_0 = \left(s + \frac{5}{2}\right)\hbar\omega. \tag{4.8}$$

L'énergie obtenue dans l'approximation de densité locale (4.6) permet donc d'obtenir le comportement asymptotique de s :

$$s \underset{N\to\infty}{\sim} \sqrt{\eta}\,\frac{(3N)^{4/3}}{4}. \tag{4.9}$$

Ceci a déjà été remarqué dans [59, 28]. Il est amusant de constater qu'il ait fallu passer par le gaz *piégé* pour obtenir simplement ce résultat. En effet, s est relié à la fonction d'onde d'énergie nulle *dans l'espace libre* Ψ par le fait que pour tout λ,

$$\Psi(\lambda\vec{r}_1,\ldots,\lambda\vec{r}_N) = \lambda^{s-\frac{3N-5}{2}}\,\Psi(\vec{r}_1,\ldots,\vec{r}_N). \tag{4.10}$$

On s'attend d'ailleurs à ce que cette dernière propriété soit vraie asymptotiquement dans la limite $\lambda \to 0$ pour la fonction d'onde de tout état propre du gaz *homogène* [59].

Chapter 5

Thermal fluctuations of the unitary gas' breathing mode

In this short Chapter we consider the two-component unitary Fermi gas in an isotropic harmonic trap. We restrict to the regime of low temperatures and large particle numbers :

$$\hbar\omega \ll k_B\,T \ll k_B\,T_F \tag{5.1}$$

where $k_B\,T_F = (3N)^{1/3}\,\hbar\omega$ is the Fermi temperature of the trapped gas in the absence of interactions. We consider the variance $\mathrm{Var}(H_{\rm trap}) = \langle (H_{\rm trap})^2\rangle - \langle H_{\rm trap}\rangle^2$ of the trapping potential energy

$$H_{\rm trap} = \sum_{i=1}^{N} U(r_i) \tag{5.2}$$

with

$$U(r) = \frac{1}{2} m\omega^2\, r^2. \tag{5.3}$$

We will show that :

$$\mathrm{Var}(H_{\rm trap}) \simeq \frac{k_B\,T\,E_0}{4} \tag{5.4}$$

where E_0 is the ground state energy. Then, we will interpret this relation in terms of thermal fluctuations of the hydrodynamic breathing mode. Finally, we will discuss whether Eq. (5.4) can be used experimentally to measure T.

To justify Eq. (5.4), we start from the exact relation

$$4\,\mathrm{Var}(H_{\rm trap}) = \langle H\rangle \hbar\omega\,\mathrm{cotanh}\left(\frac{\hbar\omega}{k_B T}\right) + \mathrm{Var}(H), \tag{5.5}$$

which directly follows from Eqs. (42,43) of Article I [i. e. Eqs. (1.61,1.62) p. 42 in Chap. 1]. For $\hbar\omega \ll k_B T$ we have $\mathrm{cotanh}\left(\frac{\hbar\omega}{k_B T}\right) \simeq \frac{k_B T}{\hbar\omega}$. Moreover, $\mathrm{Var}(H) = k_B\,T^2\,C$ where $C = d\langle H\rangle/dT$ is the specific heat. Thus :

$$4\,\mathrm{Var}(H_{\rm trap}) \simeq k_B\,T\,[\langle H\rangle + T\,C]\,. \tag{5.6}$$

We assume that $\langle H\rangle$ is a sufficiently regular function of T/T_F in order to have $\langle H\rangle \simeq E_0 \gg T\,C$ for $T \ll T_F$. This gives Eq. (5.4).

We now give a simple physical interpretation of Eq. (5.4). According to zero-temperature superfluid hydrodynamics, the trapped gas has several collective modes (see e. g. Article IV or [124]).

One of them is the breathing mode, where the density is simply rescaled by a factor λ with respect to its equilibrium value :

$$\rho_\lambda(\vec{r}) = \rho_{\rm eq}(\vec{r}/\lambda)/\lambda^3. \tag{5.7}$$

At non-zero but small temperature, this mode is thermally excited, which gives rise to fluctuations in the trapping potential energy. We can describe this using the energy functional $E_{\rm hydro}[\rho, \vec{v}]$ of the hydrodynamic theory ; for small fluctuations around equilibrium one finds that velocity fluctuations are decoupled from density fluctuations to leading order. Moreover the trapping potential energy does not depend on the velocity. Thus the velocity does not play any role and we only need to consider the energy functional

$$E[\rho] = E_{\rm trap}[\rho] + E_{\rm int}[\rho] \tag{5.8}$$

where the trapping potential energy is

$$E_{\rm trap}[\rho] = \int d\vec{r}\, \rho(\vec{r})\, U(\vec{r}), \tag{5.9}$$

and the internal (kinetic + interaction) energy is

$$E_{\rm int}[\rho] = \int d\vec{r}\, e\left(\rho(\vec{r})\right), \tag{5.10}$$

$e(\rho)$ being the energy of the homogeneous gas per unit volume. The equilibrium density $\rho_{\rm eq}(\vec{r})$ is obtained by minimizing $E[\rho] - \mu\, N$ (this is also called local-density approximation). One easily shows that

$$E_{\rm trap}[\rho_\lambda] = \lambda^2\, E_{\rm trap}[\rho_{\rm eq}], \tag{5.11}$$

and, using the relation $e(\rho) \propto \rho^{5/3}$, that

$$E_{\rm int}[\rho_\lambda] = \frac{1}{\lambda^2}\, E_{\rm int}[\rho_{\rm eq}]. \tag{5.12}$$

For a weak excitation of the breathing mode, we can set $\lambda = 1+\delta\lambda$ with $|\delta\lambda| \ll 1$. Since $E[\rho_\lambda] - E[\rho_{\rm eq}]$ must vanish to first order in $\delta\lambda$, one gets the virial theorem [60] [1] :

$$E_{\rm trap}[\rho_{\rm eq}] = E_{\rm int}[\rho_{\rm eq}] = E[\rho_{\rm eq}]/2. \tag{5.13}$$

To first order in $\delta\lambda$, Eq. (5.11) becomes

$$E_{\rm trap}[\rho_\lambda] \simeq E[\rho_{\rm eq}]\, \left(\frac{1}{2} + \delta\lambda\right), \tag{5.14}$$

so that

$$\mathrm{Var}(E_{\rm trap}) \simeq E[\rho_{\rm eq}]^2\, \langle \delta\lambda^2 \rangle. \tag{5.15}$$

Expanding Eqs. (5.11,5.12) to second order in $\delta\lambda$ gives :

$$E[\rho_\lambda] = E[\rho_{\rm eq}]\, (1 + 2\, \delta\lambda^2). \tag{5.16}$$

Thus the probability distribution of $\delta\lambda$

$$P(\delta\lambda) \propto e^{-\beta\, E[\rho_\lambda]} \tag{5.17}$$

1. Eqs. (5.11,5.12,5.13) are even exact beyond the local-density approximation [see Eq. (29) in Article I, or Eq. (1.61) p. 41 in Chap. 1].

is a gaussian of variance

$$\langle \delta\lambda^2 \rangle = \frac{1}{4\beta\, E[\rho_{\rm eq}]}. \tag{5.18}$$

Eqs. (5.15,5.18) give the desired Eq. (5.4). We obtained this without taking into account the other collective modes. We thus expect that the total contribution of the other modes to the variance of $E_{\rm trap}$ is zero.

Can one use Eq. (5.4) experimentally to measure T ? [2] This would require to measure $H_{\rm trap}$ with a relative sensitivity better than

$$\frac{\sqrt{{\rm Var}(H_{\rm trap})}}{\langle H_{\rm trap}\rangle} \sim \sqrt{\frac{T}{N\,T_F}}, \tag{5.19}$$

which does not look easy. One also needs to have sufficiently small fluctuations of the number of atoms.

2. We thank J. Thomas for this question.

Article IV

Formation of a vortex lattice in a rotating BCS Fermi gas

Eur. Phys. J. D (2006)
DOI: 10.1140/epjd/e2006-00110-7

THE EUROPEAN PHYSICAL JOURNAL D

Formation of a vortex lattice in a rotating BCS Fermi gas

G. Tonini[1], F. Werner[2], and Y. Castin[2,a]

[1] Dipartimento di fisica, Università di Firenze, Firenze, Italy
[2] Laboratoire Kastler Brossel, École Normale Supérieure, 24 rue Lhomond, 75231 Paris Cedex 05, France

Received 25 April 2005 / Received in final form 13 February 2006
Published online 18 May 2006 –

Abstract. We investigate theoretically the formation of a vortex lattice in a superfluid two-spin component Fermi gas in a rotating harmonic trap, in a BCS-type regime of condensed non-bosonic pairs. Our analytical solution of the superfluid hydrodynamic equations, both for the 2D BCS equation of state and for the 3D unitary quantum gas, predicts that the vortex free gas is subject to a dynamic instability for fast enough rotation. With a numerical solution of the full time dependent BCS equations in a 2D model, we confirm the existence of this dynamic instability and we show that it leads to the formation of a regular pattern of quantum vortices in the gas.

PACS. 03.75.Kk Dynamic properties of condensates; collective and hydrodynamic excitations, superfluid flow – 03.75.Lm Tunneling, Josephson effect, Bose-Einstein condensates in periodic potentials, solitons, vortices, and topological excitations – 03.75.Ss Degenerate Fermi gases

The field of trapped ultracold fermionic atomic gases is presently making rapid progress: thanks to the possibility of controlling at will the strength of the s-wave interaction between two different spin components by the technique of the Feshbach resonance [1,2], it is possible to investigate the cross-over [3] between the weakly interacting BCS regime (case of a small and negative scattering length) and the Bose-Einstein condensation of dimers (case of small and positive scattering length), including the strongly interacting regime and even the unitary quantum gas (infinite scattering length). The interaction energy of the gas was measured on both sides of the Feshbach resonance [2]; on the side of the resonance with a positive scattering length, Bose-Einstein condensation of dimers was observed [4]; on the side of the resonance with a negative scattering length, a condensation of pairs was revealed in the strongly interacting regime by a fast ramping of the magnetic field across the Feshbach resonance [5]. Also, the presence of a gap in the excitation spectrum was observed [6], for an excitation consisting in transferring atoms to an initially empty atomic internal state, as initially suggested by [7], revealing pairing.

Are there evidences of superfluidity in these fermionic gases? It was initially proposed [8] to reveal superfluidity by detecting an hydrodynamic behavior in the expansion of the gas after a switching-off of the trapping potential. Such an hydrodynamic behavior was indeed observed [1] but it was then realized that this can occur not only in the superfluid phase, but also in the normal phase in the so-called hydrodynamic regime, that is when the mean free path of atoms is smaller than the size of the cloud, a condition easy to fulfill close to a Feshbach resonance. The general experimental trend is now to try to detect superfluidity via an hydrodynamic behavior that has no counterpart in the normal phase [9]. A natural candidate to reveal superfluidity is therefore the detection of quantum vortex lattices in the rotating trapped Fermi gases: the superfluid velocity field, defined as the gradient of the phase of the order parameter, is irrotational everywhere, except on singularities corresponding to the vortex lines, so that a superfluid may respond to rotation by the formation of a vortex lattice [10]; on the contrary, a rotating hydrodynamic normal gas is expected to acquire the velocity field of solid-body rotation and should not exhibit a regular vortex lattice in steady state.

Steady state properties of vortices in a rotating Fermi gas described by BCS theory have already been the subject of several studies, for a single vortex configuration [11] and more recently for a vortex lattice configuration [10]. In this paper, we study the issue of the time dependent formation of the lattice in a rotating Fermi gas, by solving the time dependent BCS equations. A central point of the paper is to identify possible nucleation mechanisms of the vortices that could show up in a real experiment.

This problem was addressed a few years ago for rotating Bose gases. The expected nucleation mechanism was the Landau mechanism, corresponding to the apparition of negative energy surface modes for the gas in the rotating frame, for a rotation frequency above a minimal value; these negative energy modes can then be populated

[a] e-mail: yvan.castin@lkb.ens.fr

thermally, leading to the entrance of one or several vortices from the outside part of the trapped cloud [12,13]. The first experimental observation of a vortex lattice in a rotating Bose-Einstein condensate revealed however a nucleation frequency different from the one of the thermal Landau mechanism [14] and was suggested later on to be due to a dynamic instability of hydrodynamic nature triggered by the rotating harmonic trap [15], which was then submitted to experimental tests [16,17]. The discovered mechanism of dynamic instability was checked, by a numerical solution of the purely conservative time dependent Gross-Pitaevskii equation, to lead to turbulence [18] and to the formation of a vortex lattice [19]. The Landau mechanism was also observed in the simulations of [19] in presence of an initial non-condensed cloud set into rotation by the stirrer.

We now transpose the dynamic instability scenario to the case of a two spin component Fermi gas, initially at zero temperature and stirred by a rotating harmonic trapping potential of slowly increasing rotation speed, as described in Section 1. Does the hydrodynamic instability phenomenon occur also in the fermionic case, and does it lead to the entrance of vortices in the gas and to the subsequent formation of a vortex lattice? We first address this problem analytically, in Section 2, by solving exactly the time dependent two-dimensional hydrodynamic equations and by performing a linear stability analysis: very similarly to the bosonic case, we find that a dynamic instability can occur above some minimal rotation speed. We also extend this conclusion to the 3D unitary quantum gas. Then we test this prediction by a numerical solution of the time dependent BCS equations on a two-dimensional lattice model, in Section 3: this confirms that the dynamic instability can take place and leads to the entrance of vortices in the gas, which are then seen to arrange in a regular pattern at long evolution times.

1 Our model

We consider a gas of fermionic particles of mass m, with equally populated two spin states $\uparrow$ and $\downarrow$, trapped in a harmonic potential and initially at zero temperature. The particles with opposite spin have a s-wave interaction with a negligible range interaction potential, characterized by the scattering length a_{3D}, whereas the particles in the same spin state do not interact.

We shall be concerned mainly by the limit of a 2D Fermi gas. In this case, the trapping potential is very strong along z-axis so that the quantum of oscillation along z, that is $\hbar\omega_z$, where ω_z is the oscillation frequency along z, is much larger than both the mean oscillation energy in the $(x-y)$-plane and the interaction energy per particle, so that the gas is dynamically frozen along z in the ground state of the corresponding harmonic oscillator. In this geometry, the two-body interaction can be characterized by the 2D scattering length a_{2D} which was calculated as a function of the 3D scattering length in [20]. We recall that a_{2D} is always strictly positive and the 2D two-body problem in free space exhibits a bound state, that is a dimer, of spatial radius a_{2D}. For the 2D gas to have universal many-body interaction properties, characterized by a_{2D} only, one requires that the spatial extension $(\hbar/m\omega_z)^{1/2}$ of the ground state of the harmonic oscillator along z is smaller than a_{2D} [21], so that e.g. the dimer binding energy is smaller than $\hbar\omega_z$. The weakly attractive Fermi gas limit corresponds in 2D to $\rho a_{2D}^2 \to +\infty$ and the condensation of preformed dimers to $\rho a_{2D}^2 \to 0$ [22], where ρ is the 2D density of the gas.

In the $(x-y)$-plane, the zero temperature 2D gas is initially harmonically trapped in the non-rotating, anisotropic potential

$$U(\mathbf{r}) = \frac{1}{2}m\omega^2\left[(1-\epsilon)x^2 + (1+\epsilon)y^2\right] \qquad (1)$$

where $\mathbf{r} = (x, y)$ and $\epsilon > 0$ measures the anisotropy of the trapping potential. Then one gradually sets the trapping potential into rotation around z-axis with an instantaneous rotation frequency $\Omega(t)$, until it reaches a maximal value Ω to which it then remains equal. The question is to study the resulting evolution of the gas and predict the possible formation and subsequent crystallization of quantum vortices.

We shall consider this question within the approximate frame of the BCS theory, in a rather strongly interacting regime but closer to the weakly interacting BCS limit than to the BEC limit, which is most relevant for the present 3D experimental investigations: the chemical potential μ of the 2D gas is supposed to be positive, excluding the regime of Bose-Einstein condensation of the dimers, and the parameter $k_F a_{2D}$, where the Fermi momentum is defined as $\hbar^2 k_F^2/2m = \mu$, is larger than unity but not extremely larger than unity: we shall take $k_F a_{2D} = 4$ in the numerical simulations. In this relatively strongly interacting regime, we of course do not expect the BCS theory to be 100% quantitative.

In the hydrodynamic approach to come, one simply needs the equation of state of the gas, that is the expression of the chemical potential μ_0 of a spatially uniform zero temperature gas as a function of the total density $\rho = \rho_\uparrow + \rho_\downarrow = 2\rho_\uparrow$ and of the scattering length. In 2D, this equation of state was calculated with the BCS approach in [22]:

$$\mu_0[\rho] = \frac{\pi\hbar^2\rho}{m} - E_0/2 \qquad (2)$$

where E_0 is the binding energy of the dimer in free space,

$$E_0 = \frac{4\hbar^2}{m a_{2D}^2 e^{2\gamma}} \qquad (3)$$

and $\gamma = 0.57721\ldots$ is Euler's constant. Similarly, the gap for the zero temperature homogeneous BCS gas is related to the density by [22]

$$\Delta_0[\rho] = \left(E_0\frac{2\pi\hbar^2\rho}{m}\right)^{1/2}. \qquad (4)$$

We shall also consider analytically the 3D unitary quantum gas ($a_{3D} = \infty$) where the equation of state is known to be exactly of the form $\mu_0[\rho] \propto \hbar^2\rho^{2/3}/m$.

In the numerical solution of the 2D time dependent BCS equations to come, one needs an explicit microscopic model. We have chosen a square lattice model with an on-site interaction between opposite spin particles corresponding to a coupling constant g_0 so that the second quantized grand canonical Hamiltonian reads at the initial time

$$H = \sum_{\mathbf{k},\sigma} \left(\frac{\hbar^2 k^2}{2m} - \mu \right) c^\dagger_{\mathbf{k},\sigma} c_{\mathbf{k},\sigma} + \sum_{\mathbf{r},\sigma} l^2 \, U(\mathbf{r}) \psi^\dagger_\sigma(\mathbf{r}) \psi_\sigma(\mathbf{r}) + g_0 \sum_{\mathbf{r}} l^2 \, \psi^\dagger_\uparrow(\mathbf{r}) \psi^\dagger_\downarrow(\mathbf{r}) \psi_\downarrow(\mathbf{r}) \psi_\uparrow(\mathbf{r}) \quad (5)$$

where l is the grid spacing. In the numerics a quantization volume is introduced, in the form of a square box of size L with periodic boundary conditions, L being an integer multiple of l. The sum over $\mathbf{r}$ then runs over the $(L/l)^2$ points of the lattice. A plane wave on the lattice has wavevector components k_x and k_y having a meaning modulo $2\pi/l$ so that the wavevector $\mathbf{k}$ is restricted to the first Brillouin zone $D = [-\pi/l, \pi/l[^2$. The operator $c_{\mathbf{k},\sigma}$ annihilates a particle of wavevector $\mathbf{k}$ and spin state $\sigma = \uparrow$ or $\downarrow$, and obeys the usual fermionic anticommutation relations, such as

$$\{c_{\mathbf{k},\sigma}, c^\dagger_{\mathbf{k}',\sigma'}\} = \delta_{\mathbf{k},\mathbf{k}'} \delta_{\sigma,\sigma'}. \quad (6)$$

The discrete field operator $\psi_\sigma(\mathbf{r})$ is proportional to the annihilation operator of a particle at the lattice node $\mathbf{r}$ in the spin state σ in such a way that it obeys the anticommutation relations

$$\{\psi_\sigma(\mathbf{r}), \psi^\dagger_{\sigma'}(\mathbf{r}')\} = l^{-2} \, \delta_{\mathbf{r},\mathbf{r}'} \delta_{\sigma,\sigma'}. \quad (7)$$

The coupling constant g_0 is adjusted so that the 2D scattering length of two particles on the infinite lattice is exactly a_{2D} [23,24]:

$$\frac{1}{g_0} = \frac{m}{2\pi\hbar^2} \left[\log\left(\frac{l}{\pi a_{2D}} \right) - \gamma + \frac{2G}{\pi} \right] \quad (8)$$

where $G = 0.91596\ldots$ is Catalan's constant. In the limit $a_{2D} \to +\infty$, for a fixed density ρ and a fixed 'range' l of the interaction potential, one finds $g_0 \to 0^-$: we recover the fact that the limit $k_F a_{2D} \gg 1$ corresponds to a weakly attractive Fermi gas.

At later times, the Hamiltonian is written in the frame rotating at frequency $\Omega(t)$, to eliminate the time dependence of the trapping potential; this adds an extra term to the Hamiltonian,

$$H_{\rm rot} = -\Omega(t) \sum_{\mathbf{r},\sigma} l^2 \psi^\dagger_\sigma(\mathbf{r}) \left(L_z \psi_\sigma \right)(\mathbf{r}) \quad (9)$$

where the matrix L_z on the lattice represents the angular momentum operator along z, $xp_y - yp_x$. The square box defining the periodic boundary conditions is supposed to be fixed in the rotating frame, so that it rotates in the lab frame: this may be useful in practice to ensure that truncation effects due to the finite size of this box in the numerics do not arrest the rotation of the gas.

This lattice model is expected to reproduce a continuous model with harmonic trapping and zero range interaction potential in the limit of an infinite quantization volume ($L \gg$ spatial radius of the cloud) and in the limit of a vanishing grid size $l \to 0$ ($l \ll a_{2D}, k_F^{-1}$). In this limit g_0 is negative, leading to an attractive interaction, so that pairing can take place in the lattice model. In this limit, we have checked that BCS theory for the lattice model gives the same equation of state as equation (2) [25].

2 Solution to the superfluid hydrodynamic equations

In the hydrodynamic theory of a pure superfluid with no vortex, one introduces two fields, the total spatial density of the gas, $\rho(\mathbf{r}, t)$, and the phase of the so-called order parameter, $2S(\mathbf{r}, t)/\hbar$. In the BCS theory for the lattice model, the order parameter is simply

$$\Delta(\mathbf{r}, t) \equiv -g_0 \langle \psi_\uparrow(\mathbf{r}, t) \psi_\downarrow(\mathbf{r}, t) \rangle \equiv |\Delta| e^{2iS/\hbar} \quad (10)$$

which has a finite limit when $l \to 0$. The superfluid velocity field in the lab frame is then defined as

$$\mathbf{v} = \frac{\mathbf{grad}\, S}{m}. \quad (11)$$

In the rotating frame, the hydrodynamic equations read

$$\partial_t \rho = -\mathrm{div}\, [\rho \, (\mathbf{v} - \mathbf{\Omega}(t) \times \mathbf{r})] \quad (12)$$

$$-\partial_t S = \frac{1}{2} m v^2 + U(\mathbf{r}) + \mu_0[\rho(\mathbf{r}, t)] - \mu - m(\mathbf{\Omega}(t) \times \mathbf{r}) \cdot \mathbf{v} \quad (13)$$

where $\mathbf{\Omega}(t) = \Omega(t)\hat{\mathbf{z}}$ and $\hat{\mathbf{z}}$ is the unit vector along the rotation axis z. The first equation is simply the continuity equation in the rotating frame, including the fact that the velocity field in the rotating frame differs from the one in the lab frame by the solid body rotational term. When one takes the gradient of the second equation, one recovers Euler's equation for a superfluid. These superfluid equations are expected to be correct for a slowly varying density and phase, both in space (as compared to the size of a BCS pair) and in time (as compared to $\hbar/|\Delta|$) [26]. For a harmonically trapped system with a quantum of oscillation $\hbar\omega$, the slow spatial variation condition requires a gap parameter $|\Delta| \gg \hbar\omega$: in the present paper, considering the rather strongly interacting regime $1 \lesssim k_F a_{2D}$, the gap is of the order of the Fermi energy, which is much larger than $\hbar\omega$, so that there is slow spatial variation as long as no vortex enters the cloud. The gap is then much larger than $\hbar$ over the ramping time of the trap rotation, so that the expected condition of slow time variation is also satisfied. In Appendix A we present a simple but systematic derivation of these superfluid hydrodynamic equations starting from the time dependent BCS theory and using a semi-classical expansion. Surprisingly, for the case of slow ramping times and rather fast rotations considered in this paper, with Ω of the order of ω, our simple derivation requires an extra validity condition, in general more

stringent than $|\Delta| \gg \hbar\omega$: the quantum of oscillation $\hbar\omega$ should be smaller than $|\Delta|^2/\mu$, a condition also satisfied in our simulations.

We shall assume here that the rotation frequency is ramped up very slowly so that the density and the phase adiabatically follow a sequence of vortex free stationary states. The strategy then closely follows the one already developed in the bosonic case [15]: one solves analytically the corresponding stationary hydrodynamic equations, then one performs a linear stability analysis of the stationary solution. The apparition of a dynamic instability suggests that the system may evolve far away from the stationary branch; that this dynamic instability results in the entrance of vortices will be checked by the numerical simulations of Section 3.

In the stationary regime, for a fixed rotation frequency Ω, one sets $\partial_t \rho = 0$ in equation (12) and $-\partial_t S = 0$ in equation (13) [28]. We first consider the 2D case and we replace μ_0 by the equation of state equation (2): apart from an additive constant, μ_0 is proportional to the density, as was the case for the weakly interacting condensate of bosons [15], so that the calculations for the superfluid fermions are formally the same, if one replaces the coupling constant g of the bosons by $\pi\hbar^2/m$. Since the properties of the bosons do not depend on the value of g up to a scaling on the density [15], the results for the bosons can be directly transposed. Following [29], we take the ansatz for the phase:

$$S(\mathbf{r}) = m\omega\beta xy \tag{14}$$

which is applicable for a harmonic trapping potential U. When inserted in equation (13), this leads to an inverted parabola for the density profile, resulting in an elliptic boundary for the density of the cloud. Upon insertion of the density profile in the continuity equation, one recovers the cubic equation of [29]:

$$\beta^3 + \left(1 - 2\frac{\Omega^2}{\omega^2}\right)\beta - \epsilon\frac{\Omega}{\omega} = 0. \tag{15}$$

This equation has one real root for Ω below some ϵ dependent bifurcation value $\Omega_{\rm bif}(\epsilon)$, and has three real roots for $\Omega > \Omega_{\rm bif}(\epsilon)$. In the considered stirring procedure, the system starts with $\beta = 0$ and follows adiabatically the so-called upper branch of solution, corresponding to increasing values of β. In Figure 1, we have plotted β as a function of Ω/ω on this branch, for the value of the asymmetry parameter in the simulations of the next section, $\epsilon = 0.1$. When β takes appreciable values, the cloud significantly deforms itself in real space, becoming broader along x-axis than along y-axis, even for an arbitrarily weak trap anisotropy ϵ.

From the studies of the bosonic case [15] it is known that the significantly deformed clouds can become dynamically unstable. We recall briefly the calculation procedure: one introduces initially arbitrarily small deviations $\delta\rho$ and δS of the density and the phase from their stationary values; one then linearizes the hydrodynamic

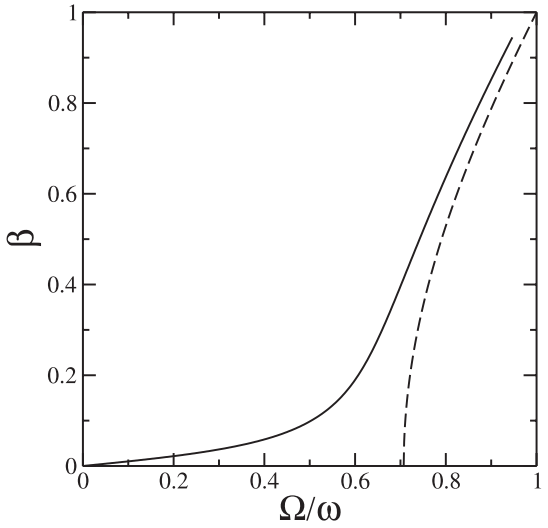

Fig. 1. The upper branch of solution for the phase parameter β of the hydrodynamic approach for a stationary vortex free BCS state in the rotating frame, as a function of the rotation frequency. Solid line: the trap anisotropy is $\epsilon = 0.1$. Dashed line: $\epsilon = 0$.

equations (12) and (13) to get

$$\frac{D\,\delta\rho}{Dt} = -\mathrm{div}\left(\rho\frac{\mathbf{grad}\,\delta S}{m}\right) \tag{16}$$

$$\frac{D\,\delta S}{Dt} = -\frac{\pi\hbar^2}{m}\,\delta\rho \tag{17}$$

where $D/Dt \equiv \partial_t + (\mathbf{v} - \mathbf{\Omega} \times \mathbf{r}) \cdot \mathbf{grad}$ and where we used the fact that the Laplacian of $S(\mathbf{r}) \propto xy$ vanishes. One then calculates the eigenmodes of the linearized equations, setting $\partial_t \to -i\nu$ where ν is the eigenfrequency of the mode. As an ansatz for $\delta\rho(\mathbf{r})$ and $\delta S(\mathbf{r})$, one takes polynomials of arbitrary total degree n in the variables x and y. One can indeed check that the subspace of polynomials of degree $\leq n$ is stable, since the stationary values ρ and S are quadratic functions of x and y. This turns the linearized partial differential equations into a finite size linear system whose eigenvalues can be calculated numerically. Complex eigenfrequencies, when obtained, lead to a non-zero Lyapunov exponent $\lambda \equiv \mathrm{Im}\,\nu$, which reveals a dynamical instability when $\lambda > 0$.

In Figure 2 we plot the stability diagram of the upper branch stationary solution in the plane (Ω, ϵ), for various total degrees n of the polynomial ansatz. Each degree contributes to this diagram in the form of a crescent, touching the horizontal axis ($\epsilon = 0$) with a broad basis on the right side and a very narrow tongue on the left side [30]. For the low value $\epsilon = 0.1$ considered in the numerical simulations of this paper, the Lyapunov exponents in the tongues are rather small, so that significant instability exponents are found only in the broad bases: for increasing Ω, the first encountered significant instability corresponds to a degree $n = 3$: for $\epsilon = 0$, the corresponding minimal value of Ω/ω is $[(183 + 36\sqrt{30})/599]^{1/2} = 0.79667\ldots$ [32]. This is apparent in Figure 3, where we plot the Lyapunov

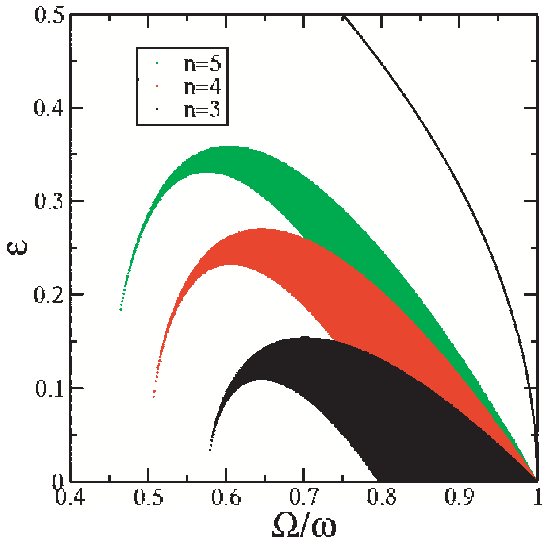

Fig. 2. (Color online) For the upper branch of solution for the phase parameter, in 2D: dark areas: instability domain in the $\Omega - \epsilon$ plane for degrees n equal to 3, 4 and 5 (crescents from bottom to top). There is no dynamical instability for $n \leq 2$. Solid line: border $\Omega^2 = (1-\epsilon)\omega$ of the branch existence domain.

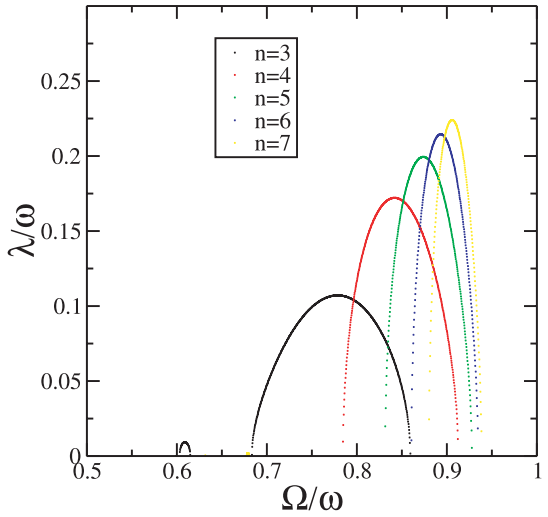

Fig. 3. (Color online) For the upper branch of solution for the phase parameter in 2D: Lyapunov exponent of the dynamic instability for degrees n from 3 to 7, as a function of the rotation frequency. The trap anisotropy is $\epsilon = 0.1$.

exponent as a function of Ω/ω for various degrees n and for $\epsilon = 0.1$.

Extension to the unitary quantum gas in 3D: in practice, the experiments are mainly performed in 3D, so that we generalize the previous hydrodynamic calculation to a 3D case where the exact equation of state is known: the so-called unitary regime, where the 3D s-wave scattering length between opposite spin fermions is infinite. Because of the universality of the unitary quantum gas, the equation of state of the gas is indeed a power law

$$\mu_0[\rho] = A\rho^\gamma \tag{18}$$

where the exponent $\gamma = 2/3$ and where the factor A is proportional to $\hbar^2/m$, with a proportionality constant recently calculated with fixed node Monte Carlo methods [33,34] and measured in recent experiments by Grimm [35] and by Salomon [4].

For such a non-linear equation of state, one seems to have lost the underlying structure of the hydrodynamic equations allowing a quadratic ansatz for ρ and S, and a polynomial ansatz for $\delta\rho$ and δS. Fortunately, this structure can be restored by using as a new variable $R(\mathbf{r},t) \equiv \rho^\gamma(\mathbf{r},t)$. One then gets effective hydrodynamic equations with a linear equation of state:

$$\partial_t R = -\gamma R \,\mathrm{div}\,\mathbf{v} - (\mathbf{v} - \mathbf{\Omega}(t)\times\mathbf{r})\cdot\mathbf{grad}\,R \tag{19}$$

$$-\partial_t S = \frac{1}{2}mv^2 + U_{3D}(\mathbf{r}) + A\,R(\mathbf{r}) - \mu - m(\mathbf{\Omega}(t)\times\mathbf{r})\cdot\mathbf{v}, \tag{20}$$

where the 3D trapping potential is

$$U_{3D}(\mathbf{r}) = \frac{1}{2}m\omega^2\left[(1-\epsilon)x^2 + (1+\epsilon)y^2\right] + \frac{1}{2}m\omega_z^2 z^2. \tag{21}$$

One then recycles the previous approach, with the usual quadratic ansatz for the steady state values of R and S. In particular the same cubic equation for β as in equation (15) is obtained. Linearizing the effective hydrodynamic equations around the steady state, one gets

$$\frac{D\,\delta R}{Dt} = -\gamma R\frac{\Delta_{\mathbf{r}}\delta S}{m} - \frac{1}{m}\,\mathbf{grad}\,\delta S\cdot\mathbf{grad}\,R \tag{22}$$

$$\frac{D\,\delta S}{Dt} = -A\,\delta R, \tag{23}$$

where we used the fact that S has a vanishing Laplacian. This system of partial different equations can be solved by a polynomial ansatz for δS and δR. This generalizes to the rotating case the ansatz of [36].

In Figure 4 we have plotted the stability diagram of the upper branch stationary solution in the plane (Ω, ϵ) for the 3D unitary quantum gas, for a trapping potential with $\omega_z = 0.4\omega$. The 3D nature of the problem makes the structure of the instability domain more involved that in 2D. This also appears in Figure 5, giving the Lyapunov exponents as a function of Ω for a fixed trap anisotropy in the $x-y$ plane, $\epsilon = 0.022$. In the limit of a cigar shaped potential, $\omega_z \ll \omega$, the structure is on the contrary close to the 2D one, as some of the eigenmodes for δR and δS almost factorize in a function of x, y and a function of z.

3 Numerical solution of the 2D time dependent BCS equations

We recall briefly the BCS equations for our two-component lattice model, in the case of equal populations

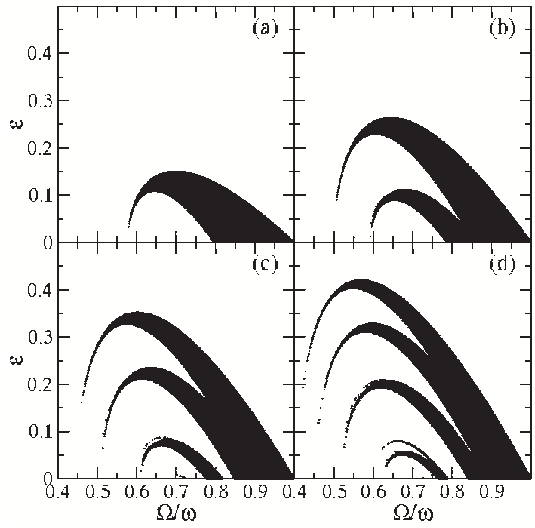

Fig. 4. Case of the 3D unitary quantum gas with $\omega_z = 0.4\omega$, for the upper branch of solution for the phase parameter: dark areas: instability domain in the $\Omega - \epsilon$ plane for degrees (a) $n = 3$, (b) $n = 4$, (c) $n = 5$ and (d) $n = 6$. There is no dynamical instability for $n \leq 2$.

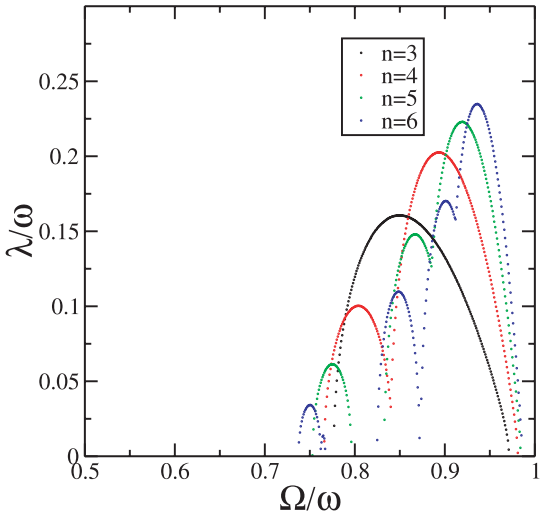

Fig. 5. (Color online) Case of the 3D unitary quantum gas with $\omega_z = 0.4\omega$, for the upper branch of solution for the phase parameter: Maximal Lyapunov exponent of the dynamic instability for degrees n from 3 to 6, as a function of the rotation frequency. The trap anisotropy is $\epsilon = 0.022$.

of the two spin states. In the non-rotating case, the many-body ground state of the Hamiltonian is approximated variationally in the zero temperature BCS theory by a so-called quasiparticle vacuum [37], that is the vacuum state of annihilation operators of elementary excitations, $b_{s,\sigma}$ (where $\sigma =\uparrow$ or $\downarrow$). By energy minimization, one finds that the $b_{s,\sigma}$ are such that

$$\psi_\uparrow(\mathbf{r}) = \sum_s \left[b_{s,\uparrow} u_s(\mathbf{r}) - b^\dagger_{s,\downarrow} v^*_s(\mathbf{r}) \right] \tag{24}$$

$$\psi_\downarrow(\mathbf{r}) = \sum_s \left[b_{s,\downarrow} u_s(\mathbf{r}) + b^\dagger_{s,\uparrow} v^*_s(\mathbf{r}) \right] \tag{25}$$

where the u's and v's are all the eigenvectors of the following Hermitian system with positive energies $E_s > 0$:

$$E_s \begin{pmatrix} u_s \\ v_s \end{pmatrix} = \begin{pmatrix} h_0 & \Delta \\ \Delta^* & -h_0^* \end{pmatrix} \begin{pmatrix} u_s \\ v_s \end{pmatrix} \tag{26}$$

and normalized so that

$$l^2 \sum_{\mathbf{r}} \left[|u_s(\mathbf{r})|^2 + |v_s(\mathbf{r})|^2 \right] = 1. \tag{27}$$

In the eigensystem, Δ is the position dependent gap parameter defined in equation (10) and the matrix h_0 represents on the lattice the single particle kinetic energy plus chemical potential plus harmonic potential energy terms. When the modal decompositions equations (24, 25) are inserted in equation (10), one gets

$$\Delta(\mathbf{r}) = -g_0 \sum_s u_s(\mathbf{r}) v^*_s(\mathbf{r}). \tag{28}$$

The density profile of the gas is given by

$$\rho(\mathbf{r}) = 2\langle \psi^\dagger_\uparrow(\mathbf{r}) \psi_\uparrow(\mathbf{r}) \rangle = 2 \sum_s |v_s(\mathbf{r})|^2. \tag{29}$$

These equations actually belong to the zero temperature Hartree-Fock-Bogoliubov formalism for fermions and are derived in Section 7.4b of [37]. Note that we have omitted the Hartree-Fock mean field term [38].

To solve numerically the 2D self-consistent stationary BCS equations, we have used the following iterative algorithm: one starts with an initial guess for the position dependence of the gap parameter (we used the local density approximation, taking advantage of the fact that the equation of state Eq. (2) and the value of the gap Eq. (4) within BCS theory are known analytically in 2D), then one calculates the u's and v's by diagonalization of the Hermitian matrix in equation (26), one calculates the corresponding $\Delta(\mathbf{r})$ using equation (28), and one iterates until convergence.

Once the stationary BCS state is calculated, one moves to the solution of the 2D time dependent BCS equations, to calculate the dynamics in the rotating trap. What we call here time dependent BCS theory is the time-dependent Hartree-Fock-Bogoliubov formalism for fermions, in the form of a variational calculation with a time dependent quasiparticle vacuum $|\phi(t)\rangle$, as detailed in Section 9.5 of [37]. At time t, the modal expansions equations (24, 25) still hold for $\psi_\uparrow(\mathbf{r})$ and $\psi_\downarrow(\mathbf{r})$, except that the operators $b_{s,\sigma}$ (where $\sigma =\uparrow$ or $\downarrow$) and the mode functions are now time dependent. The variational state

vector $|\phi(t)\rangle$ is the vacuum of all the operators $b_{s,\sigma}(t)$. The mode functions evolve according to

$$i\hbar\partial_t \begin{pmatrix} u_s \\ v_s \end{pmatrix} = \begin{pmatrix} h_0 & \Delta \\ \Delta^* & -h_0^* \end{pmatrix} \begin{pmatrix} u_s \\ v_s \end{pmatrix} \qquad (30)$$

where h_0 now includes the rotational term $-\Omega(t)L_z$ in addition to the kinetic energy, the chemical potential and the trapping potential. The gap function Δ is still given by equation (28) and is now time dependent as the mode functions are. Note that equation (30) corresponds to the first of equations (9.63b) in Section 9.5 of [37], up to a global complex conjugation. To be complete, we give the expression of the time dependent quasiparticle annihilation operators:

$$b_{s,\uparrow}(t) = l^2 \sum_{\mathbf{r}} u_s^*(\mathbf{r},t)\psi_\uparrow(\mathbf{r}) + v_s^*(\mathbf{r},t)\psi_\downarrow^\dagger(\mathbf{r}) \qquad (31)$$

$$b_{s,\downarrow}(t) = l^2 \sum_{\mathbf{r}} u_s^*(\mathbf{r},t)\psi_\downarrow(\mathbf{r}) - v_s^*(\mathbf{r},t)\psi_\uparrow^\dagger(\mathbf{r}). \qquad (32)$$

We also recall that this time-dependent formalism contains not only pair-breaking excitations, but also implicitly collective modes of the gas, as can be shown by a linearization of these equations around a steady-state solution, see Section 10.2 in [37], and as also shown by the fact that hydrodynamic equations may be derived from them as done in Appendix A. The numerical simulations to come therefore include excitations of these collective modes, when the numerical solution deviates from a stationary state.

We have integrated numerically equation (30). The usual FFT split technique, which exactly preserves the orthonormal nature of the u's and v's, is actually not satisfactory because it assumes that the gap function remains constant in time during one time step, which breaks the self-consistency of the equations and leads to a violation of the conservation of the mean number of particles. We therefore used an improved splitting method detailed in Appendix B.

In all the simulations that we present in this paper, the trap anisotropy is $\epsilon = 0.1$, the chemical potential of the initial state of the gas is fixed to $\mu = 8\hbar\omega$; setting $\mu = \hbar^2 k_F^2/2m$, the 2D scattering length is fixed to the value $a_{2D} = (\hbar/m\omega)^{1/2} \equiv a_{\rm ho}$ such that $k_F a_{2D} = 4$; the rotation frequency is turned on with the following law

$$\Omega(t) = \Omega \sin^2\left(\frac{\pi t}{2\tau}\right) \quad \text{for} \quad 0 \le t \le \tau \qquad (33)$$

with a ramping time $\tau = 160\omega^{-1}$ much larger than the oscillation period of the atoms in the trap. For $t > \tau$, the rotation frequency remains equal to Ω. The presence of vortices is detected by calculating the winding number of the phase of the gap parameter around each plaquette of the grid. We also calculate the total angular momentum of the gas. In all the simulations, we evolve the system for a total time of $1000\,\omega^{-1}$. The grid sizes are 64×64 so as to avoid truncation effects [40]. The CPU time for a single realization exceeds one month on a bi-processor AMD Opteron workstation, so that we have considered only two values of the rotation frequency.

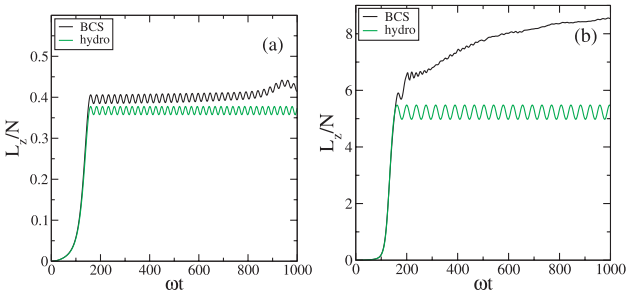

Fig. 6. Angular momentum per particle in the gas, in units of $\hbar$, as a function of time, for a final rotation frequency (a) $\Omega = 0.6\omega$ and (b) $\Omega = 0.8\omega$. Black curves: numerical simulations of the 2D time dependent BCS equations on a 64×64 grid. Green curves (color online): time dependent superfluid hydrodynamic theory of Section 2 [solution of Eqs. (12, 13) with a time dependent quadratic ansatz].

For $\Omega = 0.6\omega$, the cloud remains almost round and no entry of vortices is observed, in agreement with the fact that hydrodynamic theory predicts a small value of the β parameter (see Fig. 1) and the absence of dynamic instability (see Fig. 3). The total angular momentum of the gas experiences small amplitude oscillations, due to the non perfect adiabaticity of the branching of the trap rotation. Remarkably, the time dependent hydrodynamic theory very well reproduces these oscillations, see Figure 6a.

For $\Omega = 0.8\omega$ the dynamics is very different from the previous one. The shape of the cloud strongly elongates and deforms. Then strong turbulence sets in, at $t \simeq 200\omega^{-1}$: while the cloud anisotropy reduces, the density profile becomes irregular, not only close the cloud boundary but also in the cloud center; one observes a quick entrance of disordered vortices in the cloud at time $t \simeq 210\omega^{-1}$: several anti-vortices reach the high density regions of the cloud. After some evolution time, the density profile recovers a smooth and elliptic shape, the anti-vortices are expelled from the cloud and the vortex positions slowly relax to form a 22 vortex 'lattice' at times $\sim 500\omega^{-1}$. At time $t \sim 700\omega^{-1}$ two extra vortices join the group to form a regular 24 vortex pattern that remains essentially stationary till the end of the simulation, apart from small rearrangements of the vortex positions. Selected images of the movie are shown in Figure 7. The time evolution of the total angular momentum of the gas in shown in Figure 6b: as expected, the exact numerical result strongly deviates from the hydrodynamic prediction, except in the early stage of the evolution.

To briefly address the experimental observability of the vortex pattern, we also show in Figure 8 a cut of the particle density (directly measurable in an experiment) and of the gap parameter (not directly accessible experimentally) for the numerical simulation with $\Omega = 0.8\omega$ at a time when the vortex lattice is crystallized, this in parallel to an isocontour of the magnitude of the gap parameter: vortices embedded in high density regions result in dips

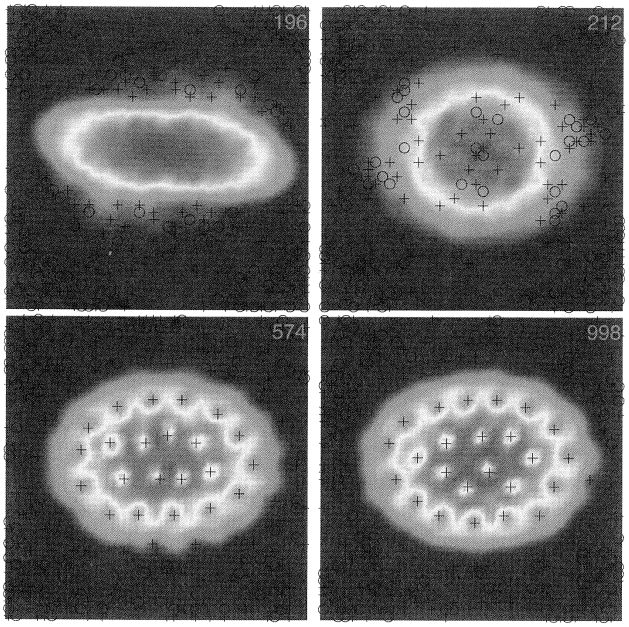

Fig. 7. (Color online) For the numerical simulation of the 2D time dependent BCS equations, density plots of the density of the trapped gas at selected times (in units of ω^{-1}), for a final rotation frequency $\Omega = 0.8\omega$. The trap anisotropy was $\epsilon = 0.1$ and the 2D scattering length $a_{2D} = \sqrt{\hbar/m\omega}$, and $\mu = 8\hbar\omega$ in the initial state. The spatial width of the simulation is truncated in the figure to about 70% of its value. Crosses: positive charge vortices. Circles: negative charge vortices. From top to bottom and from left to right: $t = 196\omega^{-1}$: a turbulent, elongated cloud is formed; $t = 212\omega^{-1}$: the cloud is round again, and includes a disordered mixture of vortices and anti-vortices; $t = 574\omega^{-1}$: the vortices crystallize in a quasi-stationary pattern; $t = 998\omega^{-1}$: the entrance of two extra vortices, and slow and small shifts of the vortex positions have taken place with respect to the previous density plot.

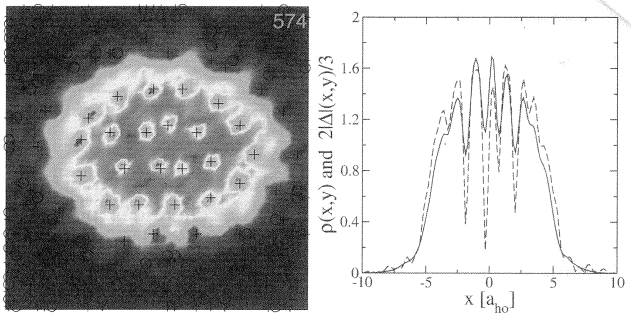

Fig. 8. (Color online) At time $t = 574\omega^{-1}$ of the numerical simulation for $\Omega = 0.8\omega$. Left panel: isocontours of the modulus of the gap parameter, showing the presence of a vortex lattice; the x and y coordinates run from $-10a_{\rm ho}$ to $+10a_{\rm ho}$ in the simulation but this left panel figure is truncated to a position interval approximately $-7a_{\rm ho}$ to $+7a_{\rm ho}$. Right panel: on the line $y = -0.627a_{\rm ho}$, x dependence of the density ρ (solid line, in units of $a_{\rm ho}^{-2}$) and of the modulus of the gap parameter (dashed line, in units of $\hbar\omega$). The gap parameter was multiplied by 2/3 for clarity. A Fourier interpolation technique was used in the right panel to map the 64×64 simulation grid onto a 128×128 grid.

in the density profile, with a contrast on the order here of 30%.

4 Conclusion

We have investigated a relevant problem for the present experiments on two-spin component interacting Fermi gases, the possibility to form a vortex lattice by slow ramping of the rotation frequency of the harmonic trap containing the particles. The observation of such a vortex lattice in steady state would be a very convincing evidence of superfluidity [39].

For a 2D model based on the BCS theory, and for the 3D unitary quantum gas, we predict analytically, with the superfluid hydrodynamic equations, that the gas experiences a dynamic instability when the final rotation frequency is above some minimal value Ω_u that we have calculated. This dynamic instability is very similar to the one discovered for a rotating Bose-Einstein condensate of bosonic atoms, where it was shown to lead to the vortex lattice formation.

To see if this dynamic instability leads to the formation of vortices also in the case of the Fermi gases, we have solved numerically the full 2D time-dependent BCS equations, for a trap anisotropy $\epsilon = 0.1$ and an initially zero temperature gas. For a final rotation frequency Ω above the predicted Ω_u, we see turbulence and the subsequent fast entry of vortices. We conclude that the dynamic instability can indeed result in a vortex lattice formation. The apparent irreversibility and energy dissipation that this seems to imply may be surprising at first sight, since the equations of motion that we integrated are purely conservative. The clue is probably the same as in the bosonic counterpart of these simulations [19]: the spatial noise produced in the turbulent phase populates many eigenmodes (including collective modes) of the system, and the subsequent non-linear evolution leads to effective thermalization of the modes.

For $\Omega < \Omega_u$ but for Ω larger than what we estimated to be the Landau rotation frequency (above which the vortex free superfluid is no longer a local minimum of energy in the rotating frame), $\Omega_L \sim 0.3\omega$ for the parameters of this paper [40], the simulation with $\Omega = 0.6\omega$ remarkably does not show the entrance of vortices after a time of $1000\omega^{-1}$. In a real experiment, however, the gas is initially at a finite temperature. Provided that long enough evolution times are available, we then expect the Landau mechanism to occur, if the small (but finite) normal component of the gas is set into rotation by the stirrer together with the vortex-free superfluid component. It would therefore be interesting to perform finite temperature simulations, generalizing to fermions the bosonic finite temperature simulations of [19].

We acknowledge useful discussions with C. Salomon, F. Chevy and A. Sinatra. One of us (G.T.) acknowledges financial support from the European Union (Marie Curie training site program QPAF). Laboratoire Kastler Brossel is a Unité de Recherche de l'École Normale Supérieure et de l'Université Paris 6, associée au CNRS.

Appendix A: Simple derivation of the hydrodynamic equations from BCS theory for a vortex-free gas

We show here that the time dependent hydrodynamic equations (12) and (13) can be formally derived for a vortex free gas from the time dependent BCS equations by using the lowest order semi-classical approximation and an adiabatic approximation for the resulting time dependent equations. As in the remaining part of the paper, we consider here the regime where the chemical potential is positive and larger than the binding energy E_0.

The general validity condition of a semi-classical approximation is that the coherence length of the gas should be much smaller than the typical length scales of variation of the applied potentials. Two coherence lengths appear for a zero temperature BCS Fermi gas: the inverse Fermi wave-vector, k_F^{-1}, associated to the correlation function $\langle\psi_\uparrow^\dagger(\mathbf{r})\psi_\uparrow(\mathbf{r'})\rangle$, and the pair size, $l_{\rm BCS}\sim\hbar^2k_F/m|\Delta|$, associated to the correlation function $\langle\psi_\uparrow(\mathbf{r})\psi_\downarrow(\mathbf{r'})\rangle$. A first typical length scale of variation of the matrix elements in equation (30) comes from the position dependence of $|\Delta|$: in the absence of rotation, we assume that this is the Thomas-Fermi radius $R_{\rm TF}$ of the gas, defined as $\hbar^2k_F^2/2m=m\omega^2R_{\rm TF}^2/2$. This assumes that the scale of variation of the modulus of the gap is the same as the one of the density; the adiabatic approximation to come will result in a $|\Delta|$ related to the density by equation (4), which justifies the assumption. Necessary validity conditions of a semi-classical approximation are then:

$$k_F^{-1}, l_{\rm BCS}\ll R_{\rm TF}. \tag{A.1}$$

In the BCS regime regime, $k_F^{-1}<l_{\rm BCS}$; for an isotropic harmonic trap, one then finds that the condition (A.1) is equivalent to

$$|\Delta|\gg\hbar\omega, \tag{A.2}$$

where ω is the atomic oscillation frequency [26].

In the rotating case, however, this is not the whole story, as the phase of Δ can also become position dependent. As we shall see, the phase of Δ in this paper may vary as $m\omega xy/\hbar$: when this quantity varies by $\sim2\pi$, Δ changes completely; this introduces a length scale $\sim2\pi\hbar/(m\omega R_{\rm TF})\sim1/k_F$, making a semi-classical approximation hopeless. We eliminate this problem by performing a gauge transform of the u's and v's:

$$\tilde u_s(\mathbf{r},t)\equiv u_s(\mathbf{r},t)e^{-iS(\mathbf{r},t)/\hbar} \tag{A.3}$$

$$\tilde v_s(\mathbf{r},t)\equiv v_s(\mathbf{r},t)e^{+iS(\mathbf{r},t)/\hbar} \tag{A.4}$$

where the phase is defined in equation (10). The time dependent BCS equations are modified as follows:

$$i\hbar\partial_t\begin{pmatrix}\tilde u_s\\ \tilde v_s\end{pmatrix}=\begin{pmatrix}\tilde h_0 & |\Delta|\\ |\Delta| & -\tilde h_0^*\end{pmatrix}\begin{pmatrix}\tilde u_s\\ \tilde v_s\end{pmatrix}\equiv\hat L\begin{pmatrix}\tilde u_s\\ \tilde v_s\end{pmatrix} \tag{A.5}$$

where the gauge transformed Hamiltonian is

$$\tilde h_0=e^{-iS/\hbar}h_0e^{+iS/\hbar}+\partial_tS. \tag{A.6}$$

Let us review relevant observables in the gauge transformed representation. First the gap equation is modified as

$$|\Delta|=-g_0\sum_s\tilde u_s\tilde v_s^*. \tag{A.7}$$

Then the mean total density reads

$$\rho=2\sum_s\tilde v_s\tilde v_s^*. \tag{A.8}$$

Last, we introduce the total matter current $\mathbf{j}(\mathbf{r},t)$, that obeys by definition

$$\partial_t\rho+\mathrm{div}\,\mathbf{j}=0. \tag{A.9}$$

In the rotating frame, in a many-body state invariant by exchange of the spin states $\uparrow$ and $\downarrow$, it is very generally given by

$$\mathbf{j}=\frac{\hbar}{im}\left(\langle\psi_\uparrow^\dagger\mathbf{grad}\,\psi_\uparrow\rangle-\text{c.c.}\right)-\rho\,\mathbf{\Omega}\times\mathbf{r}. \tag{A.10}$$

Within BCS theory, this gives

$$\mathbf{j}=\rho\,(\mathbf{v}-\mathbf{\Omega}\times\mathbf{r})+\frac{i\hbar}{m}\sum_s\left[\tilde v_s^*\,\mathbf{grad}\,\tilde v_s-\tilde v_s\,\mathbf{grad}\,\tilde v_s^*\right], \tag{A.11}$$

where the velocity field $\mathbf{v}$ is defined as $\mathbf{grad}\,S/m$. Note that the continuity equation (A.9) remains true for the BCS theory [37].

To calculate the two key quantities (A.8) and (A.11), it is sufficient to know the following one-body density operator for a fictitious particle of spin 1/2,

$$\sigma=\begin{pmatrix}\sigma_{\uparrow\uparrow} & \sigma_{\uparrow\downarrow}\\ \sigma_{\downarrow\uparrow} & \sigma_{\downarrow\downarrow}\end{pmatrix}\equiv\sum_s\begin{pmatrix}|\tilde u_s\rangle\langle\tilde u_s| & |\tilde u_s\rangle\langle\tilde v_s|\\ |\tilde v_s\rangle\langle\tilde u_s| & |\tilde v_s\rangle\langle\tilde v_s|\end{pmatrix}. \tag{A.12}$$

To prepare for the semi-classical approximation we introduce the Wigner representation of σ [41]:

$$W(\mathbf{r},\mathbf{p},t)=\mathrm{Wigner}\{\sigma\}\equiv\int\frac{d^d\mathbf{x}}{(2\pi\hbar)^d}\langle\mathbf{r}-\mathbf{x}/2|\sigma|\mathbf{r}+\mathbf{x}/2\rangle e^{i\mathbf{p}\cdot\mathbf{x}/\hbar} \tag{A.13}$$

where d is the dimension of space. The key observables have then the exact expressions:

$$\rho(\mathbf{r},t)=2\int d^d\mathbf{p}\,W_{\downarrow\downarrow}(\mathbf{r},\mathbf{p},t) \tag{A.14}$$

$$|\Delta|(\mathbf{r},t)=-g_0\int d^d\mathbf{p}\,W_{\uparrow\downarrow}(\mathbf{r},\mathbf{p},t) \tag{A.15}$$

$$\mathbf{j}(\mathbf{r},t)=\rho\,(\mathbf{v}-\mathbf{\Omega}\times\mathbf{r})-\frac{2}{m}\int d^d\mathbf{p}\,\mathbf{p}\,W_{\downarrow\downarrow}(\mathbf{r},\mathbf{p},t). \tag{A.16}$$

The semi-classical expansion then consists e.g. in

$$\text{Wigner}\{V(\hat{\mathbf{r}})\sigma\} = [V(\mathbf{r}) + \frac{i\hbar}{2}\partial_{\mathbf{r}}V\cdot\partial_{\mathbf{p}} + \ldots]W(\mathbf{r},\mathbf{p},t). \tag{A.17}$$

The successive terms we called zeroth order, first order, etc., in the semi-classical approximation.

We write the equations of motion (A.5) up to zeroth order in the semi-classical approximation:

$$i\hbar\partial_t W(\mathbf{r},\mathbf{p},t)|^{(0)} = [L_0(\mathbf{r},\mathbf{p},t), W(\mathbf{r},\mathbf{p},t)] \tag{A.18}$$

where the matrix L_0 is equal to

$$L_0(\mathbf{r},\mathbf{p},t) = \begin{pmatrix} \frac{p^2}{2m} - \mu_{\text{eff}}(\mathbf{r},t) & |\Delta|(\mathbf{r},t) \\ |\Delta|(\mathbf{r},t) & -\frac{p^2}{2m} + \mu_{\text{eff}}(\mathbf{r},t) \end{pmatrix}. \tag{A.19}$$

We have introduced the position and time dependent function,

$$\mu_{\text{eff}}(\mathbf{r},t) \equiv \mu - U(\mathbf{r},t) - \frac{1}{2}mv^2 + m\mathbf{v}\cdot(\mathbf{\Omega}\times\mathbf{r}) - \partial_t S(\mathbf{r},t), \tag{A.20}$$

that may be called effective chemical potential for reasons that will become clear later.

At time $t = 0$, the gas is at zero temperature. By introducing the spectral decomposition of $\hat{L}(t=0)$ one can then check that

$$\sigma(t=0) = \theta[\hat{L}(t=0)] \tag{A.21}$$

where $\theta(x)$ is the Heaviside function. Since $L_0(t=0)$ is the classical limit of the operator $\hat{L}(t=0)$, the leading order semi-classical approximation for the corresponding Wigner function is, in a standard way, given by

$$W(\mathbf{r},\mathbf{p},t=0) \simeq \frac{1}{(2\pi\hbar)^d}\,\theta[L_0(\mathbf{r},\mathbf{p},t=0)] \tag{A.22}$$

that is each two by two matrix W is proportional to a pure state $|\psi\rangle\langle\psi|$ with

$$|\psi(\mathbf{r},\mathbf{p},t=0)\rangle = \begin{pmatrix} U_0(\mathbf{r},\mathbf{p}) \\ V_0(\mathbf{r},\mathbf{p}) \end{pmatrix} \tag{A.23}$$

where (U_0, V_0) is the eigenvector of $L_0(\mathbf{r},\mathbf{p},t=0)$ of positive energy and normalized to unity. At time t, according to the zeroth order evolution equation (A.18), each two by two matrix W remains a pure state, with components U and V solving

$$i\hbar\partial_t \begin{pmatrix} U(\mathbf{r},\mathbf{p},t) \\ V(\mathbf{r},\mathbf{p},t) \end{pmatrix} = L_0(\mathbf{r},\mathbf{p},t) \begin{pmatrix} U(\mathbf{r},\mathbf{p},t) \\ V(\mathbf{r},\mathbf{p},t) \end{pmatrix}. \tag{A.24}$$

We then introduce the so-called adiabatic approximation: the vector (U,V), being initially an eigenstate of $L_0(\mathbf{r},\mathbf{p},t=0)$, will be an instantaneous eigenvector of $L_0(\mathbf{r},\mathbf{p},t)$ at all later times t. This approximation holds under the adiabaticity condition [42], detailed below, requiring that the energy difference between the two eigenvalues of $L_0(\mathbf{r},\mathbf{p},t)$ (divided by $\hbar$) be large enough. As this energy difference can be as small as the gap parameter, this will impose a minimal value to the gap, as we shall discuss later. In this adiabatic approximation, one can take

$$W(\mathbf{r},\mathbf{p},t) = \frac{1}{(2\pi\hbar)^d}\,\theta[L_0(\mathbf{r},\mathbf{p},t)] = \frac{1}{(2\pi\hbar)^d}\,|+\rangle\langle+| \tag{A.25}$$

where $|+(\mathbf{r},\mathbf{p},t)\rangle$, of real components $(U_{\text{inst}}, V_{\text{inst}})$, is the instantaneous eigenvector with positive eigenvalue of the matrix L_0 defined in equation (A.19). Its components are simply the amplitudes on the plane wave $\exp(i\mathbf{p}\cdot\mathbf{r}/\hbar)$ of the BCS mode functions of a spatially uniform BCS gas of chemical potential μ_{eff} and of gap parameter $|\Delta(\mathbf{r},t)|$. Using equations (A.14) and (A.15) with the approximate Wigner distribution (A.25), one further finds that this fictitious spatially uniform BCS gas is at equilibrium at zero temperature so that expressions (2) and (4) may be used. In particular, equation (2) gives

$$\mu_{\text{eff}}(\mathbf{r},t) = \mu_0[\rho(\mathbf{r},t)] \tag{A.26}$$

which leads, together with equation (A.20), to one of the time dependent hydrodynamic equations, the Euler-type one equation (13). Also, U_{inst} and V_{inst} are even functions of $\mathbf{p}$, so that the integral in the right hand side of equation (A.16) vanishes and equation (A.9) reduces to the hydrodynamic continuity equation (12). Under the adiabatic approximation, the superfluid hydrodynamic equations are thus derived.

We now discuss the validity of the adiabatic approximation. Without this approximation, the two by two matrix W has non-zero off-diagonal matrix elements $\langle+|W|-\rangle$ where $|-\rangle$ is the instantaneous eigenvector of equation (A.19) with a negative eigenvalue, that can be written $(V_{\text{inst}}, -U_{\text{inst}})$. Writing from equation (A.18) the equation of motion for $\langle+|W|-\rangle$, one indeed finds a coupling to the diagonal element $\langle+|W|+\rangle$ due to the non infinite ramping time of the rotation. This coupling can be calculated using the off-diagonal Hellman-Feynman theorem for real eigenvectors, and corresponds to a Rabi frequency

$$\frac{1}{2}\nu_{\text{time}} \equiv -\langle-|\partial_t|+\rangle = -\frac{1}{\epsilon_+ - \epsilon_-}\langle-|\,(\partial_t L_0)\,|+\rangle \tag{A.27}$$

where $\epsilon_\pm$ is the eigenenergy of $|\pm\rangle$ for the matrix L_0:

$$\epsilon_\pm = \pm\left[\left(p^2/(2m) - \mu_{\text{eff}}\right)^2 + |\Delta|^2\right]^{1/2}. \tag{A.28}$$

But this is not the whole story, as we have neglected the so-called motional couplings, that can also destroy adiabaticity. These motional couplings are due to the fact that $|+\rangle$ and $|-\rangle$ depends on $\mathbf{r},\mathbf{p}$ and that terms involving $\partial_{\mathbf{p}}W$ and $\partial_{\mathbf{r}}W$ will appear in the equation for W beyond the zeroth-order semi-classical approximation. Such non-adiabatic effects are well-known for the motion of a spin 1/2 particle in a static but spatially inhomogeneous magnetic field. In our problem, the first order term of the semi-classical expansion is actually simple to write:

$$\partial_t W|^{(1)} = \frac{1}{2}\left[\partial_{\mathbf{r}}L\cdot\partial_{\mathbf{p}}W - \partial_{\mathbf{p}}L\cdot\partial_{\mathbf{r}}W + \text{h.c.}\right]. \tag{A.29}$$

The matrix L corresponds to the classical limit of $\hat{L}(t)$:

$$L(\mathbf{r},\mathbf{p},t) = L_0(\mathbf{r},\mathbf{p},t) + \mathbf{p}\cdot(\mathbf{v}-\boldsymbol{\Omega}\times\mathbf{r})\ \mathrm{I}, \qquad (A.30)$$

where I is the 2×2 identity matrix. In the resulting equation of evolution of $\langle +|W|-\rangle$, taking $\langle +|W|+\rangle = 1/(2\pi\hbar)^d$ and $\langle -|W|-\rangle = 0$, a motional Rabi coupling to $\langle +|W|+\rangle$ now appears:

$$\frac{1}{2}\nu_{\mathrm{motion}} \equiv -\partial_{\mathbf{p}}\left[\mathbf{p}\cdot(\mathbf{v}-\boldsymbol{\Omega}\times\mathbf{r})\right]\cdot\langle -|\partial_{\mathbf{r}}|+\rangle + \partial_{\mathbf{r}}\left[\mathbf{p}\cdot(\mathbf{v}-\boldsymbol{\Omega}\times\mathbf{r})\right]\cdot\langle -|\partial_{\mathbf{p}}|+\rangle. \qquad (A.31)$$

Expressions similar to the one for $\langle -|\partial_t|+\rangle$ can be derived with the off-diagonal Hellman-Feynman theorem.

We now calculate the total Rabi frequency $\nu_{\mathrm{tot}} \equiv \nu_{\mathrm{time}}+\nu_{\mathrm{motion}}$ at the local Fermi surface, that is for a value of the momentum such that $p^2/2m = \mu_{\mathrm{eff}}(\mathbf{r},t)$. This is indeed at the Fermi surface that we expect the adiabaticity condition to be most stringent, as the energy difference $\epsilon_+ - \epsilon_-$ takes there its minimal value, equal to twice the gap $|\Delta(\mathbf{r},t)|$. Then $U_{\mathrm{inst}} = V_{\mathrm{inst}} = 1/\sqrt{2}$ and the expressions resulting from the Hellman-Feynman theorem are very simple:

$$\langle -|\partial_\lambda|+\rangle = -\frac{\partial_\lambda(\mu_{\mathrm{eff}} - p^2/2m)}{2|\Delta|}, \qquad (A.32)$$

where λ stands for t or for an arbitrary component of the vectors $\mathbf{r}$ or $\mathbf{p}$. We then get the condition for adiabaticity:

$$\frac{|\nu_{\mathrm{tot}}|}{2} = \frac{1}{2|\Delta|}\left|\frac{D\mu_{\mathrm{eff}}}{Dt} + \left(\frac{\mathbf{p}\cdot\partial_{\mathbf{r}}}{m}\right)^2 S\right| \ll 2|\Delta|/\hbar, \quad (A.33)$$

where $D/Dt = \partial_t + (\mathbf{v}-\boldsymbol{\Omega}\times\mathbf{r})\cdot\partial_{\mathbf{r}}$.

A fully explicit expression for ν_{tot} can be obtained using the hydrodynamic equations and taking the limit of a very long ramping time of the rotation, as is the case in our simulations, so that the hydrodynamic variables are close to a steady state and $S \simeq m\omega\beta(t)xy$. Using equation (A.26) and the continuity equation (12), one gets $D\mu_{\mathrm{eff}}/Dt = -\rho\mu_0'[\rho]\mathrm{div}\,\mathbf{v} \simeq 0$ so that one is left with

$$\frac{1}{2}\nu_{\mathrm{tot}} = \frac{\beta(t)\omega p_x p_y}{m|\Delta|}. \qquad (A.34)$$

The constraint $|\nu_{\mathrm{tot}}/2| \ll 2|\Delta|/\hbar$ then results in the condition in 2D:

$$\hbar\omega \ll 4E_0/|\beta(t)|, \qquad (A.35)$$

where E_0 is the dimer binding energy. To obtain equation (A.35) starting from equation (A.34), we have used the upper bound $|p_x p_y|/m \leq \mu_{\mathrm{eff}}(\mathbf{r},t)$ valid on the local Fermi surface $p^2/2m = \mu_{\mathrm{eff}}$, then we have used equations (2, 4) neglecting the additive E_0 term in the equation of state, which is valid in the considered regime $\mu \gg E_0$ over the major part of the density profile [26]. The resulting condition (A.35) is satisfied in our simulations as β is at most $\sim$0.64 (for $\Omega = 0.8\omega$) and we took $a_{2D} = (\hbar/m\omega)^{1/2}$, $\mu = 8\hbar\omega$ resulting in $E_0 \sim 1.3\hbar\omega$ and $\Delta \sim 4.7\hbar\omega$. Note that it is in general more stringent than the usual condition (A.2) but for the particular parameters of our simulations, it turns out to be roughly equivalent.

Appendix B: splitting technique conserving the mean number of particles

The standard splitting technique approximates the evolution due to equation (30) during a small time step dt by first evolving the (u_s, v_s) into (u_s', v_s') with the kinetic energy and rotational energy during dt, and then evolving the (u_s', v_s') with the $\mathbf{r}$-dependent part of two by two matrix of equation (30) during dt, for a *fixed* value of $\Delta(\mathbf{r},t) = -g_0\sum_s u_s'(\mathbf{r})v_s'^*(\mathbf{r})$. This exactly preserves the unitary of the full evolution, but the fact that a *fixed* value of Δ is taken during the second step of the evolution breaks the self-consistency between Δ and u_s, v_s so that the total number of particles, $N = 2\sum_s\langle v_s|v_s\rangle$, is conserved to first order in dt but not to all orders in dt. Numerically, for the time steps dt leading to a reasonable CPU time, one then observes strong deviations of this total number from its initial value. Note that such a problem does not arise for the time dependent Gross-Pitaevskii equation for bosons, for which conservation of unitary and number of particles is one and a same thing.

This problem for the BCS equations can be fixed by restoring the self-consistency for the evolution during dt associated to the $\mathbf{r}$-dependent part of the equation of evolution. That is one solves during dt:

$$i\hbar\partial_t\begin{pmatrix} u_s \\ v_s\end{pmatrix} = \begin{pmatrix} U(\mathbf{r})-\mu & \Delta(\mathbf{r},t) \\ \Delta^*(\mathbf{r},t) & \mu - U(\mathbf{r})\end{pmatrix}\begin{pmatrix} u_s \\ v_s\end{pmatrix} \qquad (B.1)$$

not for a fixed Δ but with the time dependent Δ given by the self-consistency condition (28). As a consequence, equation (B.1) written for all modes s is a set of nonlinearly coupled time dependent equations. Fortunately, they are purely local in $\mathbf{r}$, so that they can be solved analytically. One finds that $\Delta(\mathbf{r},t)$ varies as $e^{-i\lambda(\mathbf{r})t}$, where

$$\hbar\lambda(\mathbf{r}) = 2[U(\mathbf{r})-\mu] - g_0\sum_s\left[|v_s(\mathbf{r},t)|^2 - |u_s(\mathbf{r},t)|^2\right] \quad (B.2)$$

can be checked to be time independent for the local evolution (B.1). Then the system (B.1) is transformed into one with time independent coefficients (so readily integrable) by performing a time dependent gauge transform, $u_s(\mathbf{r},t) = U_s(\mathbf{r},t)e^{-i\lambda(\mathbf{r})t/2}$ and $v_s(\mathbf{r},t) = V_s(\mathbf{r},t)e^{+i\lambda(\mathbf{r})t/2}$.

References

1. K.M. O'Hara, S.L. Hemmer, M.E. Gehm, S.R Granade, J.E. Thomas, Science **298**, 2179 (2002)
2. T. Bourdel, J. Cubizolles, L. Khaykovich, K.M.F. Magalhães, S.J.J.M.F. Kokkelmans, G.V. Shlyapnikov, C. Salomon, Phys. Rev. Lett. **91**, 020402 (2003)
3. A.G. Leggett, J. Phys. (Paris) C **7**, 19 (1980); P. Nozières, S. Schmitt-Rink, J. Low Temp. Phys. **59**, 195 (1985); J.R. Engelbrecht, M. Randeria, C. Sá de Melo, Phys. Rev. B **55**, 15153 (1997)
4. M. Greiner, C.A. Regal, D.S. Jin, Nature **426**, 537 (2003); S. Jochim, M. Bartenstein, A. Altmeyer, G. Hendl,

S. Riedl, C. Chin, J. Hecker Denschlag, R. Grimm, Science **302**, 2101 (2003); M.W. Zwierlein, C.A. Stan, C.H. Schunck, S.M.F. Raupach, S. Gupta, Z. Hadzibabic, W. Ketterle, Phys. Rev. Lett. **91**, 250401 (2003); T. Bourdel, L. Khaykovich, J. Cubizolles, J. Zhang, F. Chevy, M. Teichmann, L. Tarruell, S.J.J.M.F. Kokkelmans, C. Salomon, Phys. Rev. Lett. **93**, 050401 (2004)

5. C.A. Regal, M. Greiner, D.S. Jin, Phys. Rev. Lett. **92**, 040403 (2004); M.W. Zwierlein, C.A. Stan, C. H. Schunck, S.M.F. Raupach, A.J. Kerman, W. Ketterle, Phys. Rev. Lett. **92**, 120403 (2004)
6. C. Chin, M. Bartenstein, A. Altmeyer, S. Riedl, S. Jochim, J. Hecker Denschlag, R. Grimm, Science **305**, 1128 (2004)
7. P. Törmä, P. Zoller, Phys. Rev. Lett. **85**, 487 (2000)
8. C. Menotti, P. Pedri, S. Stringari, Phys. Rev. Lett. **89**, 250402 (2002)
9. M. Cozzini, S. Stringari, Phys. Rev. Lett. **91**, 070401 (2003)
10. D.L. Feder, Phys. Rev. Lett. **93**, 200406 (2004)
11. N. Nygaard, G.M. Bruun, C.W. Clark, D.L. Feder, Phys. Rev. Lett. **90**, 210402 (2003)
12. T. Isoshima, K. Machida, Phys. Rev. A **60**, 3313 (1999)
13. F. Dalfovo, S. Stringari, Phys. Rev. A **63**, 011601(R) (2000)
14. K.W. Madison, F. Chevy, W. Wohlleben, J. Dalibard, Phys. Rev. Lett. **84**, 806 (2000)
15. S. Sinha, Y. Castin, Phys. Rev. Lett. **87**, 190402 (2001)
16. K. Madison, F. Chevy, V. Bretin, J. Dalibard, Phys. Rev. Lett. **86**, 4443 (2001)
17. E. Hodby, G. Hechenblaikner, S.A. Hopkins, O.M. Maragò, C.J. Foot, Phys. Rev. Lett. **88**, 010405 (2002)
18. D.L. Feder, A.A. Svidzinsky, A.L. Fetter, C.W. Clark, Phys. Rev. Lett. **86**, 564 (2001)
19. C. Lobo, A. Sinatra, Y. Castin, Phys. Rev. Lett. **92**, 020403 (2004)
20. D.S. Petrov, M. Holzmann, G. Shlyapnikov, Phys. Rev. Lett. **84**, 2551 (2000); D.S. Petrov, G.V. Shlyapnikov, Phys. Rev. A **64**, 012706 (2001); G. Shlyapnikov, J. Phys. IV France **116**, 89 (2004)
21. L. Pricoupenko, M. Olshanii, `arXiv:cond-mat/0205210`
22. M. Randeria, J. Duan, L. Shieh, Phys. Rev. B **41**, 327 (1990)
23. C. Mora, Y. Castin, Phys. Rev. A **67**, 053615 (2003)
24. Y. Castin, J. Phys. IV France **116**, 89 (2004)
25. G. Tonini, "Study of Ultracold Fermi gases: crystalline LOFF phase and nucleation of vortices", Ph.D. thesis of the University of Florence (Italy)
26. At the border of the atomic cloud, the gap parameter assumes very small values, which locally (but not globally) invalidates the hydrodynamic approximation. Such a failure of hydrodynamics close to the boundaries of a trapped gas is well-known for Bose condensates [27]. Moreover, hydrodynamics will fail when turbulence develops and vortices enter the cloud, since hydrodynamics does not include properly short length scale variations of $|\Delta|$. For all these reasons, we have performed numerical simulations of the full time dependent BCS theory, as presented in this paper
27. S. Stringari, Phys. Rev. Lett. **77**, 2360 (1996)
28. We note that the chemical potential μ is a function of the rotation frequency Ω, since we are here in a system with a fixed total number of particles. We do not need here the explicit expression for μ
29. A. Recati, F. Zambelli, S. Stringari, Phys. Rev. Lett. **86**, 377 (2001)
30. In this figure, it is not apparent that the very narrow tongues actually touch the $\epsilon = 0$ axis; but this can be shown analytically, and the contact points are $\Omega = \omega/\sqrt{n}$, which is the value of the rotation frequency ensuring the resonance of the rotating anisotropy with the surface mode of frequency $\sqrt{n}\omega$ in the lab frame [31]. Note also that the degrees $n = 6$ and $n = 7$ (not shown in the figure) have each an additional instability zone, however with very low values of the Lyapunov exponent ($\sim 0.01\omega$) so of little physical relevance. We have not explored $n \geq 8$
31. S. Sinha, private communication
32. This value is obtained from the following result: the boundaries of the crescent of degree $n = 3$ can be parametrized as $\epsilon = \pm z_0(-z_0^2 + 2\Omega^2 - 1)/\Omega$ where z_0 is a root of the degree 5 polynomial $P(z) = 3z^5 + 19\Omega z^4 + (6 - 13\Omega^2)z^3 + (26\Omega - 25\Omega^3)z^2 + (3 + 3\Omega^4 - 10\Omega^2)z + 3\Omega^5 - 22\Omega^3 + 7\Omega$, Ω being expressed in units of ω
33. J. Carlson, S.-Y. Chang, V.R. Pandharipande, K.E. Schmidt, Phys. Rev. Lett. **91**, 050401 (2003)
34. G.E. Astrakharchik, J. Boronat, J. Casulleras, S. Giorgini, Phys. Rev. Lett. **93**, 200404 (2004)
35. M. Bartenstein, A. Altmeyer, S. Riedl, S. Jochim, C. Chin, J. Hecker Denschlag, R. Grimm, Phys. Rev. Lett. **92**, 120401 (2004)
36. M. Amoruso, I. Meccoli, A. Minguzzi, M.P. Tosi, Eur. Phys. J. D **7**, 441 (1999)
37. J.-P. Blaizot, G. Ripka, *Quantum Theory of Finite Systems* (The MIT Press, Cambridge, Massachusetts, 1986)
38. The mean field term is simply $g_0\rho/2$. It tends to zero in the limit of a grid spacing l tending to zero, both in the 3D and 2D BCS theories. In 2D however, this convergence is only logarithmic so it can never be achieved in a practical numerical calculation. Keeping this mean field term introduces a spurious dependence on l in the BCS equation of state. This, as we have checked numerically, leads to a spurious dependence on l of the density profile and the gap parameter for a stationary gas in the trap in the BCS approximation: we have therefore removed the mean field term. In an exact many-body solution of the lattice model, not relying on the Born approximation as the Hartree-Fock mean field term does, we do not expect such a slow convergence in the $l \to 0$ limit
39. Shortly after submission of this paper, the observation of a vortex lattice in a 3D superfluid Fermi gas was reported, see M.W. Zwierlein, J.R. Abo-Shaeer, A. Schirotzek, C.H. Schunck, W. Ketterle, Nature **435**, 1047 (2005)
40. G. Tonini, F. Werner, Y. Castin, `arXiv:cond-mat/0504612` version 2
41. E.P. Wigner, Phys. Rev. **40**, 749 (1932)
42. A. Messiah, in *Quantum Mechanics* (North Holland, 1961); Vol. II A.B. Migdal, in *Qualitative methods in Quantum Theory* (W.A. Benjamin, Massachusetts, 1977), p. 155

Partie 4 : Problème à 2 corps et expérience de Hambourg

Le Chapitre 6 traite du problème élémentaire mais fondamental de 2 particules à la limite unitaire dans un piège.

L'Article V concerne l'interprétation théorique d'une expérience menée à Hambourg, sur le problème à 2 corps dans un site d'un réseau optique profond. Il résulte d'une collaboration avec les théoriciens Frank Deuretzbacher, Kim Plassmeier et Daniela Pfannkuche, ainsi que les expérimentateurs Christian et Silke Ospelkaus, Kai Bongs et Klaus Sengstock.

Au Chapitre 7, nous effectuons le calcul complet du taux de perte dans une modélisation simple de la situation expérimentale de Hambourg, et nous vérifions que notre résultat est compatible avec l'approche de Petrov, Salomon et Shlyapnikov.

Au Chapitre 8, nous discutons dans quelle mesure la limite de portée nulle est réalisée dans l'expérience de Hambourg.

L'Appendice E est un petit calcul de physique atomique motivé par cette même expérience.

Chapitre 6

Problème à 2 corps dans un piège harmonique

Dans ce Chapitre, nous considérons 2 particules discernables de masse m, de positions $\vec{r}_1$, $\vec{r}_2$, dans un piège harmonique $U(r_i) = \frac{1}{2}m\omega^2 {r_i}^2$.

Dans la Section 1, nous rappelons la solution du problème pour une interaction décrite par le pseudopotentiel. Dans la Section 2, nous montrons que le pseudopotentiel est le seul modèle de portée nulle qui soit hermitien pour le produit scalaire usuel. Dans le Section 3 nous considérons un potentiel d'interaction en puits carré de portée b, et nous vérifions que le spectre converge vers celui du pseudopotentiel pour $b \to 0$. Dans la Section 4, nous étudions *comment* cette convergence se produit, et nous vérifions qu'elle est bien décrite par le modèle de la portée effective au premier ordre en b.

Le centre de masse étant séparable, nous considérons le mouvement relatif, d'énergie E, de fonction d'onde $\Psi(\vec{r})$, où $\vec{r} = \vec{r}_2 - \vec{r}_1$. Nous nous restreignons aux états invariants par rotation $[\Psi(\vec{r}) = \Psi(r)]$.

1 Pour le pseudopotentiel

Considérons que les 2 particules interagissent *via* le pseudopotentiel de longueur de diffusion a :

$$\begin{cases} \bullet \text{ Pour } \vec{r} \neq \vec{0} : \ \left[-\dfrac{\hbar^2}{2\mu}\Delta_{\vec{r}} + \dfrac{1}{2}\mu\omega^2\, r^2 \right] \Psi(\vec{r}) = E\, \Psi(\vec{r}) & (6.1) \\ \bullet \text{ Pour } r \to 0 : \ \text{il existe } A \text{ tel que } \Psi(\vec{r}) = A \cdot \left(\dfrac{1}{r} - \dfrac{1}{a} \right) + O(r), & (6.2) \end{cases}$$

où $\mu = m/2$ est la masse réduite.

Ce problème a été résolu par Busch *et al.* [33]. Nous pouvons aisément redériver la solution car il s'agit d'un cas particulier du problème étudié dans l'Appendice B. [1] On en déduit que pour

1. Le lien avec les notations de l'Appendice B est le suivant : $\vec{R} = \vec{r}$, $d = 3$, $C = 0$ et donc $s = 1/2$; et la condition aux limites de Bethe-Peierls (6.2) correspond à la condition aux limites de la 4^{eme} ligne du Tableau page 70, $F(R) =_{R\to 0} A \cdot [R^{-s} - \frac{\epsilon}{l^{2s}} R^s] + O(R^{-s+2})$, avec ϵ égal au signe de a et $l = |a|$.

$0 < |a| < \infty$ le spectre est donné par l'équation implicite :

$$\frac{a_{\rm rel}}{2a} = \frac{\Gamma\left(\frac{3}{4} - \frac{E}{2\hbar\omega}\right)}{\Gamma\left(\frac{1}{4} - \frac{E}{2\hbar\omega}\right)} \tag{6.3}$$

avec

$$a_{\rm rel} := \sqrt{\frac{\hbar}{\mu\omega}}, \tag{6.4}$$

et que les fonctions d'ondes sont :

$$\Psi(r) = \left(\frac{r}{a_{\rm rel}}\right)^{-3/2} W_{\frac{E}{2\hbar\omega},\frac{1}{4}}\left(\left(\frac{r}{a_{\rm rel}}\right)^2\right), \tag{6.5}$$

avec la normalisation :

$$\langle\Psi|\Psi\rangle = 2\pi^2 \frac{\psi\left(\frac{1+\frac{1}{2}-\frac{E}{\hbar\omega}}{2}\right) - \psi\left(\frac{1-\frac{1}{2}-\frac{E}{\hbar\omega}}{2}\right)}{\Gamma\left(\frac{1+\frac{1}{2}-\frac{E}{\hbar\omega}}{2}\right)\Gamma\left(\frac{1-\frac{1}{2}-\frac{E}{\hbar\omega}}{2}\right)} {a_{\rm rel}}^3 \tag{6.6}$$

où ψ est la fonction digamma.

Dans la limite $a \to 0^-$, la condition aux limites de Bethe-Peierls (6.2) devient

$$\exists A'/\ \Psi(r) \underset{r\to 0}{=} A' + O(r)$$

ce qui équivaut bien à l'absence d'interaction entre les particules, et on retrouve les résultats de l'oscillateur harmonique à 3 dimensions : [2]

$$E = \left(\frac{3}{2} + 2q\right)\hbar\omega,\ q \in \mathbb{N} \tag{6.7}$$

$$\Psi(r) = e^{-\left(\frac{r}{a_{\rm rel}}\right)^2/2} L_q^{(1/2)}\left(\left(\frac{r}{a_{\rm rel}}\right)^2\right) = e^{-\left(\frac{r}{a_{\rm rel}}\right)^2/2}\ \frac{a_{\rm rel}}{r}\ H_{2q+1}\left(\frac{r}{a_{\rm rel}}\right)\frac{(-1)^q}{q!\,2^{2q+1}}, \tag{6.8}$$

$$\langle\Psi|\Psi\rangle = 2\pi\frac{\Gamma(q+\frac{3}{2})}{q!}\,{a_{\rm rel}}^3 \tag{6.9}$$

Dans la limite $a \to 0^+$, il existe de plus un état dont l'énergie $E \sim -\hbar^2/(ma^2)$ est équivalente à celle du dimère dans l'espace libre.

À la limite unitaire $a = \infty$, on obtient [3] :

$$E = \left(\frac{1}{2} + 2q\right)\hbar\omega,\ q \in \mathbb{N} \tag{6.10}$$

$$\Psi(r) = e^{-\left(\frac{r}{a_{\rm rel}}\right)^2/2}\ \frac{a_{\rm rel}}{r}\ L_q^{(-1/2)}\left(\left(\frac{r}{a_{\rm rel}}\right)^2\right), \tag{6.11}$$

$$\langle\Psi|\Psi\rangle = 2\pi\frac{\Gamma(q+\frac{1}{2})}{q!}\,{a_{\rm rel}}^3. \tag{6.12}$$

2. Cf. 2$^{\rm eme}$ ligne du Tableau page 70.
3. Cf. 3$^{\rm eme}$ ligne du Tableau page 70.

2 Unicité du pseudopotentiel

Dans le cas présent, on peut vérifier (cf. Appendice B, Section 2) que pour le produit scalaire usuel :

— Le pseudopotentiel est hermitien.

— L'équation de Schrödinger (6.1) ne définit un problème hermitien pour le produit scalaire usuel *que* si l'on impose une condition aux limites de Bethe-Peierls (6.2).

Le pseudopotentiel est donc le seul modèle de portée nulle qui soit hermitien pour le produit scalaire usuel. [4]

3 Pour une interaction en puits carré

Pour un potentiel d'interaction $V(r)$, l'équation de Schrödinger décrivant le mouvement relatif est :

$$\left[-\frac{\hbar^2}{2\mu}\Delta_{\vec{r}} + V(r) + \frac{1}{2}\mu\omega^2 r^2\right]\Psi(\vec{r}) = E\,\Psi(\vec{r}). \tag{6.13}$$

Prenons une interaction en puits carré de profondeur V_0 :

$$V(r) \;= \begin{cases} -V_0 & \text{si } r < b \\ 0 & \text{si } r > b. \end{cases} \tag{6.14}$$

De même que dans le Chapitre B, Section 1, ramenons-nous à deux dimensions en posant

$$\Psi(r) = r^{-1/2}F(r). \tag{6.15}$$

On peut prendre $\hbar = \mu = \omega = 1$. Pour $r > b$, la fonction d'onde étant bornée à l'infini, on obtient :

$$F_>(r) = \frac{1}{r}\; W_{\frac{E}{2},\frac{1}{4}}(r^2). \tag{6.16}$$

Pour $r < b$, la fonction d'onde $\Psi(r)$ étant convergente pour $R \to 0$, on obtient :

$$F_<(r) = \frac{1}{r}\; M_{\frac{E+V_0}{2},\frac{1}{4}}(r^2). \tag{6.17}$$

Dans ces 2 dernières équations, W et M sont des fonctions de Whittaker [75], et nous n'avons pas normalisé les fonctions d'ondes.

À la limite unitaire ($a = \infty$), il faut prendre $V_0 = \frac{\hbar^2}{2\mu b^2}\left(\frac{\pi}{2}\right)^2$.

Finalement, nous obtenons le spectre en résolvant numériquement l'équation

$$\frac{F_<'(b)}{F_<(b)} = \frac{F_>'(b)}{F_>(b)}. \tag{6.18}$$

Le calcul précédent s'inspire de [125]. [5]

Dans la limite $b \to 0$, le spectre obtenu pour le modèle du puits carré converge vers le résultat obtenu analytiquement pour le pseudopotentiel, comme on le constate Figure 4 page 17.

4. Le modèle de la portée effective, utilisé dans la Section 4, n'est hermitien que pour un produit scalaire *modifié* [71].

5. Je remercie Pietro Massignan pour nos discussions sur ce sujet.

4 Correction de portée finie

Il est possible de pousser le calcul analytique un ordre plus loin, et de calculer la correction par rapport au pseudopotentiel au premier ordre en b. Pour cela, nous utilisons le modèle de la portée effective. Ce modèle est parfois appelé "pseudopotentiel dépendant de l'énergie", car il s'obtient en remplaçant, dans la condition aux limites de Bethe-Peierls (6.2), la longueur de diffusion a par une longueur de diffusion effective dépendante de l'énergie $a_{\text{eff}}(E)$, définie par :

$$\frac{1}{a_{\text{eff}}(E)} = \frac{1}{a} - \frac{1}{2}\frac{Em}{\hbar^2} r_e, \tag{6.19}$$

où r_e est la portée effective. Pour ce modèle, l'amplitude de diffusion [définie par l'éq. (3) page 13] vaut :

$$f_k = \frac{-1}{1/a + ik - k^2 r_e/2}, \tag{6.20}$$

de sorte que r_e est bien la portée effective au sens habituel de la théorie de la diffusion. Pour plus de précisions sur le modèle de la portée effective, voir Chap. 3, Section 4.2 page 96.

Pour comparer le résultat du puits carré à la prédiction du modèle de la porté effective, on utilise le fait bien connu que pour une interaction en puits carré de longueur de diffusion infinie, la portée effective vaut $r_e = b$ [32].

Pour obtenir le spectre dans le modèle de la portée effetive, il suffit de remplacer a par $a_{\text{eff}}(E)$ dans l'éq. (6.3) donnant le spectre du pseudopotentiel. Au premier ordre en r_e on en déduit que

$$\frac{E}{\hbar\omega} = E_0 + B\,\frac{r_e}{a_{\text{ho}}} + \dots \tag{6.21}$$

où $a_{\text{ho}} = \sqrt{\hbar/(m\omega)}$, E_0 est l'énergie pour $r_e = 0$ (i. e. pour le pseudopotentiel) et

$$B = -\frac{E_0}{\sqrt{2}\, f'(E_0)} \tag{6.22}$$

avec

$$f(x) \equiv 2\frac{\Gamma(-x/2 + 3/4)}{\Gamma(-x/2 + 1/4)}. \tag{6.23}$$

Numériquement, pour l'état fondamental ($E_0 = 1/2$), cela donne $B = 0.19947\dots$, en accord avec la valeur $B = 0.19955$ obtenue par un ajustement linéaire des résultats obtenus numériquement pour le puits carré dans l'intervalle $0 < b < 0.001$, cf. Fig. 6.1. Pour le premier état excité de moment cinétique nul ($E_0 = 5/2$), le modèle de la portée effective donne $B = 0.4987\dots$, et l'ajustement des résultats du puits carré donne $B = 0.4988$.

Ces résultat numériques laissent supposer que le modèle de portée effective coincide exactement, au premier ordre en r_e (i. e. en b), avec le modèle en puits carré, et plus généralement avec tout modèle de portée finie.

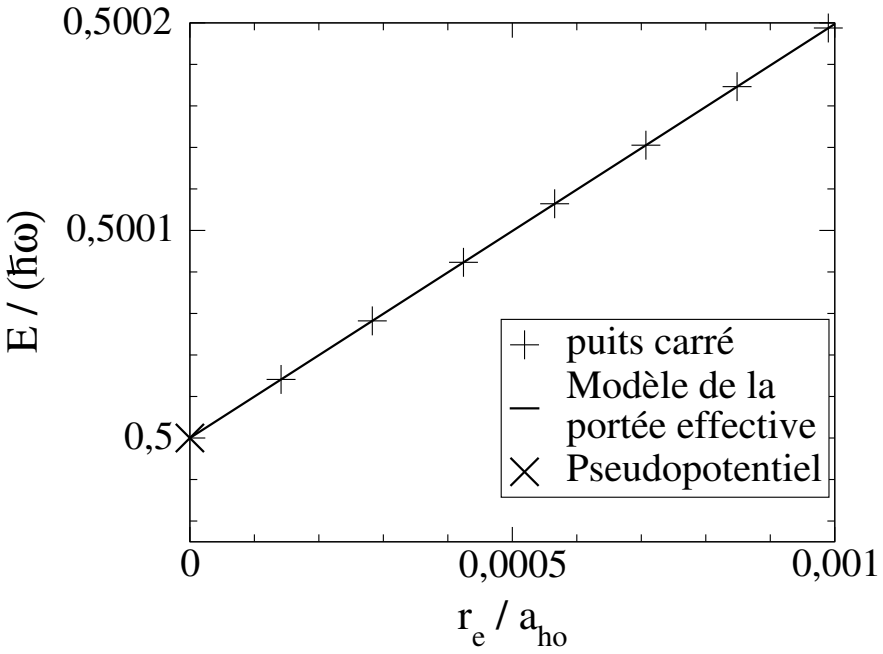

FIGURE 6.1 – Énergie E du mouvement relatif pour l'état fondamental à 2 corps dans un piège harmonique, pour une longueur de diffusion infinie, en fonction de la portée effective r_e des interactions. Le résultat obtenu numériquement pour une interaction en puits carré (+) est en très bon accord, au premier ordre en r_e, avec la prédiction analytique du modèle de la portée effective (ligne droite), qui coincide pour $r_e = 0$ avec la valeur $E/(\hbar\omega) = 1/2$ du pseudopotentiel ($\times$). [$a_{\rm ho} = \sqrt{\hbar/(m\omega)}$.]

Article V

Heteronuclear molecules in an optical lattice : theory and experiment

PHYSICAL REVIEW A **77**, 032726 (2008)

Heteronuclear molecules in an optical lattice: Theory and experiment

F. Deuretzbacher, K. Plassmeier, and D. Pfannkuche
I. Institut für Theoretische Physik, Universität Hamburg, Jungiusstrasse 9, 20355 Hamburg, Germany

F. Werner
Laboratoire Kastler Brossel, ENS, UPMC, CNRS, 24 rue Lhomond, 75231 Paris Cedex 05, France

C. Ospelkaus, S. Ospelkaus, and K. Sengstock
Institut für Laserphysik, Universität Hamburg, Luruper Chaussee 149, 22761 Hamburg, Germany

K. Bongs
Institut für Laserphysik, Universität Hamburg, Luruper Chaussee 149, 22761 Hamburg, Germany
and Midlands Centre for Ultracold Atoms, School of Physics and Astronomy, University of Birmingham, Edgbaston, Birmingham B15 2TT, United Kingdom

(Received 12 March 2007; published 31 March 2008)

We study properties of two different atoms at a single optical lattice site at a heteronuclear atomic Feshbach resonance. We calculate the energy spectrum, the efficiency of rf association, and the lifetime as a function of magnetic field and compare the results with the experimental data obtained for ^{40}K and ^{87}Rb [C. Ospelkaus *et al.*, Phys. Rev. Lett. **97**, 120402 (2006)]. We treat the interaction in terms of a regularized δ function pseudopotential and consider the general case of particles with different trap frequencies, where the usual approach of separating center-of-mass and relative motion fails. We develop an exact diagonalization approach to the coupling between center-of-mass and relative motion and numerically determine the spectrum of the system. At the same time, our approach allows us to treat the anharmonicity of the lattice potential exactly. Within the pseudopotential model, the center of the Feshbach resonance can be precisely determined from the experimental data.

DOI: 10.1103/PhysRevA.77.032726 PACS number(s): 34.20.Cf, 34.50.−s, 37.10.De, 03.75.Kk

INTRODUCTION

Motivated by the intriguing perspectives of heteronuclear molecule formation, observation of charge-density waves [1], boson-induced fermionic superfluidity [2–4] in optical lattices [5], and supersolids [6], Fermi-Bose mixtures have recently attracted lots of attention. An important step in this direction was the simultaneous trapping of bosons and fermions in a three-dimensional (3D) optical lattice [7,8]. Recently, even heteronuclear molecules [9,10] were created by means of a magnetic field Feshbach resonance in combination with rf association [9].

In interpreting the experimental results and for future extensions, it is essential to develop a detailed understanding of the interaction of two particles across the Feshbach resonance, taking into account the external confinement of the optical lattice in a consistent manner. In a seminal paper, Th. Busch *et al.* [11] have analytically solved the problem of two identical atoms in a harmonic trap. This model has been compared to two-component Fermi gases in an optical lattice at a Feshbach resonance [12,13].

In this paper, we study the generalized case of two different atoms at an optical lattice site accounting for the anharmonic part of the potential. Both the fact that the two atoms feel different trap frequencies and the anharmonicity lead to a coupling of center-of-mass and relative motion of the two atoms resulting in deviations from the model in Ref. [11]. We model interactions between two cold atoms by a regularized δ function type interatomic pseudopotential. We discuss the solutions of the uncoupled problem and develop an exact diagonalization approach to the coupling term. In this very general approach, we find significant deviations from the identical particle scenario, the strongest effect being observed for repulsively interacting atoms with large mass ratios. We further discuss rf association as a method of determining the energy spectrum at a heteronuclear Feshbach resonance between ^{87}Rb and ^{40}K in a 3D optical lattice. We compare the theoretical energy spectrum to the experimental results [9] and discuss methods of precisely determining the Feshbach resonance center position based on this comparison. Finally we calculate the efficiency of rf association and the lifetime of heteronuclear ^{40}K-^{87}Rb molecules and find qualitative agreement with experimental results.

I. THEORETICAL MODEL

In order to model interactions within an atom pair, we consider an interatomic potential given by a regularized δ potential [14–17]. For two atoms of the same kind in an isotropic harmonic trap an analytic solution exists [11]. Here we consider two different atomic species which are confined at a single site of a 3D optical lattice. In this case the atoms experience different trapping frequencies and the confining potential has significant anharmonic features. We use the following Hamiltonian as a starting point

$$H = \sum_{i=1,2} \left[-\frac{\hbar^2}{2m_i}\Delta_i + \frac{1}{2}m_i\omega_i^2 r_i^2 \right] + \frac{2\pi\hbar^2 a_s}{\mu}\delta(\vec{r})\frac{\partial}{\partial r}r + V_{\mathrm{corr}}(\vec{r}_1,\vec{r}_2). \quad (1)$$

Here m_1 and m_2 are the masses of the two atoms, ω_i

$=\sqrt{2V_i k^2/m_i}$ are the trapping frequencies obtained using the harmonic approximation to the trapping potential, k is the wave number and V_i is the depth of the lattice felt by atom i, a_s is the scattering length, $\mu=m_1\cdot m_2/M$ the reduced mass, $M=m_1+m_2$ the total mass, $\vec{r}=\vec{r}_1-\vec{r}_2$ the relative position, and $r=|\vec{r}_1-\vec{r}_2|$ is the distance between the atoms. V_{corr} contains the anharmonic corrections which are necessary to accurately approximate the potential of one lattice site given by

$$V_{\text{lattice}} = V^{(x)}_{\text{lattice}} + V^{(y)}_{\text{lattice}} + V^{(z)}_{\text{lattice}} \tag{2}$$

with

$$V^{(x)}_{\text{lattice}} = \sum_{i=1,2} V_i \sin^2(kx_i) \approx \sum_{i=1,2} \left[V_i k^2 x_i^2 - \frac{V_i k^4}{3} x_i^4 + \cdots \right] \tag{3}$$

and similar expressions for $V^{(y)}_{\text{lattice}}$ and $V^{(z)}_{\text{lattice}}$. The first term of Eq. (3) gives rise to the harmonic approximation through $\omega_i=\sqrt{2V_i k^2/m_i}$, and the remainder gives rise to V_{corr}.

We introduce relative and center-of-mass coordinates $\vec{r}=\vec{r}_1-\vec{r}_2$ and $\vec{R}=(m_1\vec{r}_1+m_2\vec{r}_2)/M$ and define the corresponding frequencies

$$\omega_{\text{c.m.}} := \sqrt{\frac{m_1\omega_1^2 + m_2\omega_2^2}{m_1+m_2}}, \tag{4}$$

$$\omega_{\text{rel}} := \sqrt{\frac{m_2\omega_1^2 + m_1\omega_2^2}{m_1+m_2}}, \tag{5}$$

$$\Delta\omega := \sqrt{\omega_1^2 - \omega_2^2}. \tag{6}$$

The transformed Hamiltonian consists of three contributions: one center-of-mass harmonic oscillator Hamiltonian $H_{\text{c.m.}}$, one term for the relative motion H_{rel} containing a harmonic oscillator term and the contact interaction, and one last term H_{couple} grouping together all terms which couple relative and center-of-mass motion and which arise from the different trap frequencies and the anharmonic corrections

$$\begin{aligned} H &= -\frac{\hbar^2}{2M}\Delta_{\text{c.m.}} + \frac{1}{2}M\omega_{\text{c.m.}}^2 R^2 - \frac{\hbar^2}{2\mu}\Delta_{\text{rel}} + \frac{1}{2}\mu\omega_{\text{rel}}^2 r^2 \\ &\quad + \frac{2\pi\hbar^2 a_s}{\mu}\delta(\vec{r})\frac{\partial}{\partial r}r + \mu\Delta\omega^2\vec{r}\cdot\vec{R} + V_{\text{corr}}(\vec{R},\vec{r}) \\ &=: H_{\text{c.m.}} + H_{\text{rel}} + H_{\text{couple}}. \end{aligned} \tag{7}$$

Let us first neglect the coupling terms H_{couple}. In this case, the problem separates into relative and center-of-mass motion, with the center-of-mass motion given by harmonic oscillator wave functions. The Hamiltonian of the relative motion H_{rel} is solved analytically in Ref. [11] and leads to the energy structure

$$2\frac{\Gamma[-E_{\text{rel}}/(2\hbar\omega_{\text{rel}}) + 3/4]}{\Gamma[-E_{\text{rel}}/(2\hbar\omega_{\text{rel}}) + 1/4]} = \frac{1}{(a_s/a_{\text{rel}})} \quad (l=0), \tag{8}$$

with $a_{\text{rel}}=\sqrt{\hbar/(\mu\omega_{\text{rel}})}$. Only $l=0$ states are considered here, since these are the only ones affected by the regularized δ potential. The rest of the spectrum consists of $l\neq 0$ harmonic oscillator states with an energy independent of a_s. The corresponding eigenfunctions are given by

$$\phi(r;\nu) = \frac{A}{a_{\text{rel}}^{3/2}}\Gamma(-\nu)U\left(-\nu,\frac{3}{2};(r/a_{\text{rel}})^2\right)e^{-(r/a_{\text{rel}})^2/2}. \tag{9}$$

A is a normalization constant which we determine numerically, $U(a,b;z)$ are the confluent hypergeometric functions and the noninteger indices ν are related to the energy by $E_{\text{rel}}=\hbar\omega_{\text{rel}}(2\nu+\frac{3}{2})$.

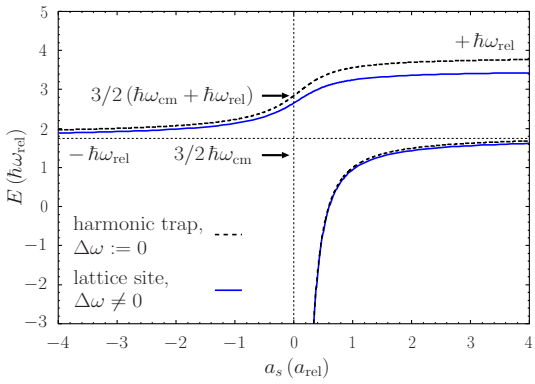

FIG. 1. (Color online) Energy eigenvalues of ^{40}K and ^{87}Rb as a function of scattering length without (black dashed line) and with coupling terms (blue solid line) due to anharmonicity and unequal trap frequencies in the lattice for parameters: $V_{\text{Rb}}=40.5E_{r,\text{Rb}}$, $V_{\text{K}}=0.86V_{\text{Rb}}$, and $\lambda=1030$ nm. The deviation between the idealized model and the full solution is substantial in particular for the upper branch.

The resulting energy spectrum is shown in Fig. 1 (black dashed line) for a center-of-mass energy of $\frac{3}{2}\hbar\omega_{\text{c.m.}}$. For vanishing interaction, the lowest harmonic oscillator state has an energy of $\frac{3}{2}(\hbar\omega_{\text{c.m.}}+\hbar\omega_{\text{rel}})$. For large positive values of a_s, it transforms into repulsively interacting atom pairs with a unitary positive "binding energy" of $+\hbar\omega_{\text{rel}}$. In a recent experiment with bosonic atoms in an optical lattice, such repulsively interacting atom pairs served as a starting point to create stable repulsively bound pairs [18]. For negative a_s, the aforementioned state transforms into attractively interacting atoms. In the unitary limit ($a_s\to-\infty$), these atoms acquire a binding energy of $-\hbar\omega_{\text{rel}}$. When the scattering length changes from large and negative to large and positive (as observed, e.g., at atomic Feshbach resonances), we enter the molecule part of the spectrum. In that part of the spectrum, the resulting two-body bound state is stable even in the absence of the external potential. As a_s becomes smaller and smaller again from above ($a_s\to+0$), the size of the molecule decreases proportionally to a_s, and the binding energy tends to $-\infty$.

As soon as we add the coupling term H_{couple} this treatment is no longer valid as center-of-mass and relative motion are no longer decoupled. In order to describe this problem in a consistent fashion, we have calculated the matrix of the complete Hamiltonian (7) using the eigenfunctions of $H_{\text{c.m.}}+H_{\text{rel}}$ and numerically obtained energy eigenvalues and eigenfunctions for the coupled problem by diagonalizing H.

The anharmonic corrections are treated as follows. Since $x_1=X+ax$ and $x_2=X-bx$ with $a:=m_2/M$ and $b:=m_1/M$, the x-dependent part of the anharmonic corrections $V_{\mathrm{corr}}^{(x)}$ transforms to

$$V_{\mathrm{corr}}^{(x)} = -\frac{V_1+V_2}{3}k^4X^4 - \frac{4(V_1a-V_2b)}{3}k^4xX^3 - 2(V_1a^2+V_2b^2)k^4x^2X^2 - \frac{4(V_1a^3-V_2b^3)}{3}k^4x^3X - \frac{V_1a^4+V_2b^4}{3}k^4x^4+\cdots . \quad (10)$$

Corresponding expressions are obtained for the y- and z-direction, $V_{\mathrm{corr}}^{(y)}$ and $V_{\mathrm{corr}}^{(z)}$. In the numerical implementation, we have tested for convergence with terms up to eighth order. We found that including eighth-order corrections improve the accuracy of the calculation by only $\approx 3\times 10^{-3}\hbar\omega_{\mathrm{rel}}$.

Our approach leads to the diagonalization of rather small Hamiltonian matrices as our main interest is the modification of the ground state and the repulsively interacting pair branch. The whole calculation has been done with MATHEMATICA. As basis we have chosen the states $|N,L,M,n,l,m\rangle$ with lowest principal quantum numbers $\Pi:=2N+L+2n+l=0,1,\ldots,\Pi_{\max}$, where N, L, M and n, l, m are the quantum numbers of the eigenfunctions of the rotationally symmetric harmonic oscillator of center-of-mass and relative motion, respectively. We typically used $\Pi_{\max}=7$ leading to a total number of 258 basis states. We have found that adding another level of the uncoupled problem to the basis set leads to additional changes in the energy smaller than $\approx 10^{-3}\hbar\omega_{\mathrm{rel}}$. Furthermore, we exploited the fact that the total angular momentum $L_z=\hbar(M+m)$ of the low-energy eigenfunctions is approximately conserved despite the cubic symmetry of the optical lattice. Again, we found that including $L_z\neq 0$ basis states lowers the energy by only $\approx 3\times 10^{-3}\hbar\omega_{\mathrm{rel}}$ [19].

Figure 1 shows the resulting energy spectrum (blue solid line) compared to the uncoupled solution (black dashed line), calculated for ^{40}K and ^{87}Rb with the experimental parameters of Ref. [9]: $V_{\mathrm{Rb}}=40.5E_{r,\mathrm{Rb}}$, $V_{\mathrm{K}}=0.86V_{\mathrm{Rb}}$, and $\lambda=1030$ nm. $E_{r,\mathrm{Rb}}=\hbar^2k^2/2m_{\mathrm{Rb}}$ is the ^{87}Rb recoil energy. In the case of heteronuclear atom pairs it is useful to express the lattice depth in units of $E_{r,\mathrm{rel}}=\hbar^2k^2/2\mu$, which is the kinetic energy given to a particle with reduced mass μ by a photon of momentum $\hbar k$. Then, $V_{\mathrm{Rb}}=40.5E_{r,\mathrm{Rb}}=12.6E_{r,\mathrm{rel}}$. As can be seen from the figure, the deviation between the idealized model, where the coupling term has been neglected, and the full solution is substantial. The difference is most pronounced in the repulsively interacting pair branch ($0.34\hbar\omega_{\mathrm{rel}}\approx 20\%$ of the level spacing) and becomes smaller as we enter the attractively interacting atom part of the spectrum. The molecular branch is relatively unaffected by the coupling term H_{couple}. This is natural because as we approach $a\to+0$, the role of the external confinement decreases since the molecule becomes smaller.

The influence of the coupling term H_{couple} is even stronger if we consider molecules with large mass ratios as in the case of ^{6}Li and ^{133}Cs, see Fig. 2. We have chosen the lattice parameters $V_{\mathrm{Li}}=V_{\mathrm{Cs}}=10E_{r,\mathrm{rel}}$ and $\lambda=1$ μm. Here the energy of the repulsively interacting atoms is lowered by up to $\approx 0.6\hbar\omega_{\mathrm{rel}}$.

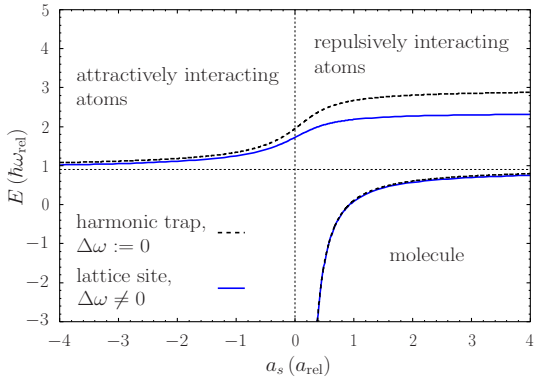

FIG. 2. (Color online) Low-energy spectrum of states with center-of-mass energy $3/2\hbar\omega_{\mathrm{c.m.}}$ for ^{6}Li and ^{133}Cs and lattice parameters $V_{\mathrm{Li}}=V_{\mathrm{Cs}}=10\hbar^2k^2/2\mu$ and $\lambda=1$ μm. The energy is much more lowered compared to the case of ^{40}K and ^{87}Rb. This is due to the large mass ratio of the ^{6}Li and ^{133}Cs atoms.

Table I shows the effect of the individual coupling terms, $H_{\Delta\omega}:=\mu\Delta\omega^2\vec{r}\cdot\vec{R}$ and V_{corr}, on to the energy of several atom pairs. The energies have been calculated for repulsively interacting atoms at $a_s=4a_{\mathrm{rel}}$ which is the largest scattering length shown in Figs. 1 and 2. All energies of Table I are given in units of the level spacing of the relative motion $\hbar\omega_{\mathrm{rel}}$. Adding the coupling term $H_{\Delta\omega}$ contributes up to 62% to the total change ΔE for ^{6}Li and ^{133}Cs. The strong influence of $H_{\Delta\omega}$ stems from the large mass ratio which results in extremely different trap frequencies ω_{Li} and ω_{Cs}. By contrast, the energy of ^{6}Li and ^{7}Li atoms is nearly not affected by $H_{\Delta\omega}$ since the trap frequencies are almost equal.

II. EXPERIMENTAL PROCEDURE

In the experiment, we have tested our theoretical approach by studying the energy spectrum of ^{40}K and ^{87}Rb

TABLE I. Influence of the individual coupling terms $H_{\Delta\omega}$ and V_{corr}, onto the total energy of several atom pairs. The energies are given in units of $\hbar\omega_{\mathrm{rel}}$. All values are calculated at $a_s=4a_{\mathrm{rel}}$ for lattice depths of $V_1=V_2=10E_{\mathrm{r,rel}}$ and a wavelength of $\lambda=1$ μm. $E_0:=E_{\mathrm{cm}}+E_{\mathrm{rel}}$ is the energy of the uncoupled Hamiltonian. Including $H_{\Delta\omega}$ into the Hamiltonian reduces the energy by $\Delta E_{\Delta\omega}$ and including $H_{\Delta\omega}+V_{\mathrm{corr}}$ reduces the energy further by ΔE_{corr}. The value in brackets is the percentage contribution of the individual coupling terms to the total change of the energy ΔE.

atom pair	E_0	$\Delta E_{\Delta\omega}$	ΔE_{corr}	ΔE
^{40}K and ^{87}Rb	3.74	−0.12(29%)	−0.27(71%)	−0.39
^{6}Li and ^{133}Cs	2.88	−0.35(62%)	−0.22(38%)	−0.57
^{6}Li and ^{87}Rb	2.99	−0.36(61%)	−0.22(39%)	−0.58
^{6}Li and ^{40}K	3.24	−0.31(58%)	−0.24(42%)	−0.55
^{6}Li and ^{7}Li	3.92	−0.01 (2%)	−0.29(98%)	−0.30

atom pairs at a single lattice site of a 3D optical lattice in the vicinity of a heteronuclear Feshbach resonance, allowing a_s to be tuned from strong attractive to repulsive interactions. Our experimental procedure for obtaining Fermi-Bose mixtures [20,21] in optical lattices has been discussed previously [7,9]. In our experiment, we obtain a mixture of ^{40}K atoms in the $|F=9/2,m_F=9/2\rangle$ state and ^{87}Rb in the $|F=2,m_F=2\rangle$ state by rf-induced sympathetic cooling in a magnetic trap. The mixture is transferred into a crossed optical dipole trap with final trap frequencies for ^{87}Rb of $2\pi 50$ Hz. In the optical dipole trap, ^{87}Rb atoms are transferred from $|2,2\rangle$ to $|1,1\rangle$ by a microwave sweep at 20 G and any remaining atoms in the upper hyperfine $|F=2,m_F\rangle$ states are removed by a resonant light pulse. Next, we transfer ^{40}K into the $|9/2,-7/2\rangle$ state by performing an rf sweep at the same magnetic field with almost 100% efficiency. With the mixture in the $^{87}\mathrm{Rb}|1,1\rangle\otimes{}^{40}\mathrm{K}|9/2,-7/2\rangle$ state, we ramp up the magnetic field to final field values at the Feshbach resonance occurring around 547 G [22–24]. Note that the state which we prepare is not Feshbach-resonant at the magnetic field values which we study, and that a final transfer of ^{40}K into the $|9/2,-9/2\rangle$ state is necessary to access the resonantly interacting state. This is precisely the transition which we use to measure the energy spectrum as outlined further below.

We ramp up a 3D optical lattice at a wavelength of 1030 nm, where the trapping potential for both species is related according to $V_{\mathrm{K}}=0.86V_{\mathrm{Rb}}$. Due to the different masses of the two species, the trapping frequencies are $\omega_{\mathrm{K}}=\sqrt{87/40\cdot 0.86}\omega_{\mathrm{Rb}}\simeq 1.4\omega_{\mathrm{Rb}}$ in the harmonic approximation. The optical lattice light is derived from a frequency stabilized 20W Yb:YAG disk laser with a 50 ms linewidth of 20 kHz. The lattice is formed by three retroreflected laser beams with orthogonal polarizations and a minimum detuning of 10 MHz between individual beams. In order to get a maximum of lattice sites occupied by one boson and one fermion, the best trade-off has been to limit the particle number at this stage to a few ten thousand.

In the optical lattice, we study the energy spectrum (binding energy) of two particles at a single lattice site by rf spectroscopy (association) of pairs of one ^{87}Rb and one ^{40}K atom (see Fig. 3). The idea for the measurement is to drive an rf transition between two atomic sublevels one of which is characterized by the presence of the Feshbach resonance and exhibits a large variation of the scattering length as a function of magnetic field according to [25]

$$a_s(B)=a_{\mathrm{bg}}\left(1-\frac{\Delta B}{B-B_0}\right), \tag{11}$$

where a_{bg} is the nonresonant background scattering length, ΔB the magnetic field width of the resonance, and B_0 the resonance center position. The other level involved in the rf transition is characterized by a nonresonant scattering length independent of magnetic field over the experimentally studied field range. We use the ^{40}K $|9/2,-7/2\rangle\rightarrow|9/2,-9/2\rangle$ transition where the Feshbach-resonant state is the final $|1,1\rangle\otimes|9/2,-9/2\rangle$ state.

A sample spectrum of this transition for the mixture in the optical lattice is shown in Fig. 3. The figure shows two peaks; one of them occurs at the frequency corresponding to the undisturbed ^{40}K $|9/2,-7/2\rangle\rightarrow|9/2,-9/2\rangle$ Zeeman transition frequency at lattice sites occupied by a single ^{40}K fermion. This peak is used for the calibration of the magnetic field across the Feshbach resonance using the Breit-Rabi formula for ^{40}K and the hyperfine parameters from Ref. [26]. For 57 measurements on 11 consecutive days, we find a mean deviation from the magnetic field calibration of 2.7 mG at magnetic fields around 547 G, corresponding to a field reproducibility of 5×10^{-6}. There is an additional uncertainty on the absolute value of the magnetic field due to the specified reference frequency source accuracy for the rf synthesizer of 1×10^{-5}, resulting in an uncertainty of the measured magnetic fields of 12 mG.

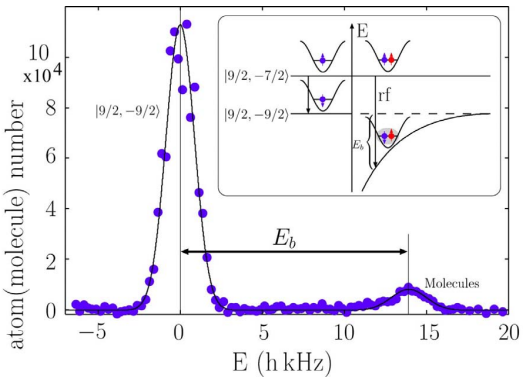

FIG. 3. (Color online) rf spectroscopy of ^{40}K-^{87}Rb in a 3D optical lattice on the $^{40}\mathrm{K}|9/2,-7/2\rangle\rightarrow|9/2,-9/2\rangle$ transition (see inset) at a lattice depth of $V_{\mathrm{Rb}}=27.5E_{r,\mathrm{Rb}}$ and a magnetic field of 547.13 G, where the interaction is attractive. The spectrum is plotted as a function of detuning from the undisturbed atomic resonance frequency and clearly shows the large atomic peak at zero detuning. The peak at 13.9 kHz is due to association of $|1,1\rangle\otimes|9/2,-7/2\rangle$ atom pairs into a bound state (figure from Ref. [9]).

The second peak at a positive detuning of 13.9 kHz is the result of interactions between ^{40}K and ^{87}Rb at a lattice site where one heteronuclear atom pair is present. There are two different energy shifts causing the observed separation of the peaks: One is the constant, small energy shift of the initial $|1,1\rangle\otimes|9/2,-7/2\rangle$ state which is independent of B, and the important, magnetic field sensitive collisional shift which stems from the strong Feshbach-resonant interactions in the $|1,1\rangle\otimes|9/2,-9/2\rangle$ final state. In the specific example, the negative energy shift (binding energy) of the final state increases the transition frequency as seen in Fig. 3. In order to perform spectroscopy on the aforementioned transition, we use pulses with a Gaussian amplitude envelope ($1/e^2$ full width of 400 μs and total pulse length of 800 μs), resulting in an rf $1/e^2$ half linewidth of 1.7 kHz. We choose the pulse power such as to achieve full transfer on the single atom transition, i.e., rf pulse parameters including power are identical for all magnetic fields. Not only for rf spectroscopy pulse generation, but also for evaporation and state transfer, we have used an advanced rf synthesizer [52] allowing precise control of frequency, amplitude and phase down to the 5 ns level and therefore the synthesis of in principle arbitrary pulse shapes.

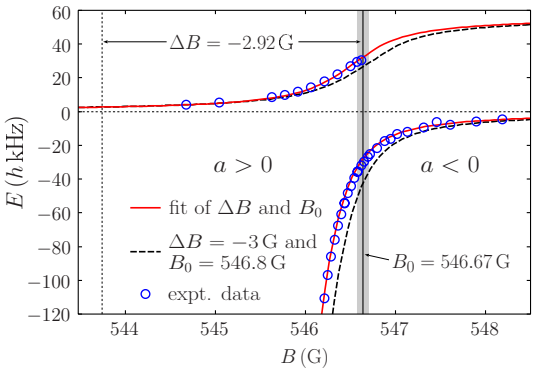

FIG. 4. (Color online) Experimentally observed energy spectrum together with theory without free parameters (black dashed line) and a least-squares fit for the resonance parameters B_0 and ΔB (red solid line). Experimental data from Ref. [9].

III. EXPERIMENTAL vs THEORETICAL SPECTRUM. RESONANCE POSITION

From rf spectra as in Fig. 3, we can determine the separation between the single atom and the two-particle ("molecular") peak with high precision (typical uncertainty of 250 Hz) and thus extract the binding energy up to a constant offset due to nonzero background scattering lengths. At the same time, the atomic peak provides us with a precise magnetic field calibration as described above. Spectra as in Fig. 3 have been recorded for magnetic field values across the whole resonance and yield the energy spectrum as a function of magnetic field.

Figure 4 shows the measured energy shift across the resonance at a lattice depth of $40.5E_{r,\mathrm{Rb}}$ as a function of magnetic field. The energy shift is obtained from Fig. 1 by subtracting the energy of the initial $^{87}\mathrm{Rb}|1,1\rangle \otimes {}^{40}\mathrm{K}|9/2,-7/2\rangle$ state $E_s = E - E(a_{-7/2} = -175a_0)$ [27]. In addition, Figs. 4 and 1 are connected through Eq. (11). One branch of the spectrum is characterized by the presence of a "positive" binding energy, the repulsively interacting pair branch. In Fig. 1, we have seen that this branch continuously transforms into attractively interacting atoms as a function of a_s. As a function of magnetic field, however, and as a result of Eq. (11), we observe this transition as a jump from the left-hand side of Fig. 4, where the interaction is weak and repulsive, to the right-hand side of Fig. 4, where the interaction is weak and attractive. Here, we find attractively interacting atoms which decay into free atom pairs if the external confinement of the optical lattice is removed.

Whereas in Fig. 1, the attractively interacting atoms branch and the molecule branch are only asymptotically equal in the limit $|a_s| \to \infty$, the singularity on resonance in Eq. (11) transforms this into a continuous crossover across the center of the resonance position as a function of magnetic field and as seen in Fig. 4. These molecules are stable even in the absence of the optical lattice potential.

In order to compare the numerically calculated energy spectrum $E(a_s)$ (blue solid line of Fig. 1) to the experimental data $E(B)$ of Fig. 4, we transform the scattering length a_s into the magnetic field strength B via Eq. (11). By using parameters from the literature: $a_{\mathrm{bg}} = -185a_0$, $\Delta B = -3$ G [28], and $B_0 = 546.8$ G [24], we obtain the black dashed curve in Fig. 4. As can be seen, the difference between the theoretical prediction and the experimental data can be overcome by a shift of the black dashed curve along the magnetic field axis. We attribute this shift to an insufficient knowledge of the resonance center position B_0.

We therefore fit our theoretical calculations to the experimental data in order to improve the estimate for the resonance center position B_0. As independent fit parameters we choose B_0 and ΔB, while a_{bg} is fixed. The latter parameter cannot be determined independently from the measurements due to its strong correlations with ΔB. This is due to the fact that in the vicinity of the resonance center position B_0 the first term of Eq. (11) is negligible so that only the product $a_{\mathrm{bg}}\Delta B$ can be determined precisely from the fit. We therefore set $a_{\mathrm{bg}} = -185a_0$ [28] and use ΔB and B_0 as free fit parameters, with the caveat that only the value obtained for B_0 is to be considered precise. In Fig. 4, the result of the least-squares fit is displayed as a red solid line. Note that the reliability of the fitting procedure sensitively depends on an accurate calculation of the energy spectrum $E(a_s)$ which includes an exact treatment of the anharmonicity and the different trap frequencies of the two atoms.

The least-squares fit results in the following values of the resonance parameters $\Delta B = -2.92$ G and $B_0 = 546.669$ G. The fit results in an uncertainty of 2 mG on B_0. The value of B_0 sensitively depends on the scattering length of the initial state $a_{-7/2}$. Assuming an uncertainty of $a_{-7/2}$ of 10% results in an uncertainty on B_0 of 20 mG. Another possible source of systematic uncertainties may be the lattice depth calibration. The lattice depth has been calibrated by parametric excitation from the first to the third band of the lattice and is estimated to have an uncertainty of 5%. Repeating the fit procedure with $\pm 5\%$ variations on the lattice depth calibration, we obtain a corresponding systematic uncertainty on B_0 of 7 mG. A third source of systematic uncertainties finally stems from the finite basis and an imprecise approximation of the lattice site potential. Here, we included corrections up to eighth order and generated basis states of the lowest eight energy levels of the uncoupled Hamiltonian. This improved the value of B_0 by 2 mG compared to a calculation with up to sixth order corrections and basis states of lowest seven energy levels. Adding the systematic uncertainty of the magnetic field calibration of 12 mG (see above), we finally obtain

$$B_0 = 546.669(24)_{\mathrm{syst}}(2)_{\mathrm{stat}}\ \mathrm{G} \tag{12}$$

under the assumption that the pseudopotential treatment is valid in the present experimental situation [14].

IV. EFFICIENCY OF rf ASSOCIATION

In a next step, we have analyzed the transfer efficiency of the rf association. The rf association process can be described theoretically by a Rabi model: The spin of the $^{40}\mathrm{K}$ atoms is flipped from $|9/2,-7/2\rangle$ to $|9/2,-9/2\rangle$ by applying a radio frequency. The atoms are initially in state $|1\rangle$:

$=(\Phi_i,0)$ and afterwards in state $|2\rangle:=(0,\Phi_f)$. In the rotating frame and by integrating out the spatial degrees of freedom we obtain the Hamiltonian

$$H_{\mathrm{rf}}=\frac{\hbar}{2}\begin{pmatrix}-\Delta\omega & \langle\Phi_i|\Phi_f\rangle\omega_1(t)\\ \langle\Phi_i|\Phi_f\rangle\omega_1(t) & +\Delta\omega\end{pmatrix}, \tag{13}$$

where $\Delta\omega:=\omega-\omega_0-\omega_b$ is the detuning, ω is the radio frequency, $\omega_0\propto B_0$ is proportional to the applied magnetic field, ω_b is proportional to the binding energy $E_b=\hbar\omega_b$, $\omega_1(t)$ is proportional to the amplitude of the oscillating magnetic field $B_1(t)$, and $\langle\Phi_i|\Phi_f\rangle$ is the overlap integral between the initial and final motional wave functions. As can be seen, the off-diagonal elements of Hamiltonian (13) are not only proportional to the rf amplitude $\omega_1(t)$, but also to the overlap integral $\langle\Phi_i|\Phi_f\rangle$. Therefore, the transfer probability between states $|1\rangle$ and $|2\rangle$ corresponds to Rabi flopping with a Rabi frequency reduced by the overlap integral of Φ_i and Φ_f compared to the pure atomic transition. Exactly on the molecular resonance, we have $\omega=\omega_0+\omega_b$ $(\rightarrow\Delta\omega=0)$. The on-resonant result for the theoretical transfer probability (efficiency) is thus given by

$$P_{1\rightarrow 2}=\sin^2\left[\frac{1}{2}\langle\Phi_i|\Phi_f\rangle\int_0^t\omega_1(t')dt'\right] \tag{14}$$

which is unity for a transfer between atomic states, where $\Phi_i=\Phi_f$, when setting the area under the $\omega_1(t)$ curve to $\int_0^t\omega_1(t')dt'=\pi$. For transfer into the molecular state, the theoretical probability decreases as a function of the wave function overlap integral since the molecular final orbital wave function becomes more and more dissimilar from the initial two-body atomic wave function.

In the experiment, the molecules were associated using rf pulses designed to induce a π pulse for the noninteracting atoms $\int_0^t\omega_1(t')dt'=\pi$. This π pulse has been kept fixed over the entire range of magnetic field values investigated. The experimental association efficiency is determined from the height of the molecular peak (see Fig. 3) as a function of magnetic field for constant pulse parameters and $\omega=\omega_0+\omega_b$ $(\rightarrow\Delta\omega=0)$ as in the theory above.

Figures 5(a) and 5(b) show a comparison between the conversion efficiency as extracted from the experimental data and the theoretical estimate from Eq. (14). Theory and experiment show the general trend of dropping association efficiency with increasing binding energy when the initial and final wave functions become more and more dissimilar. In this context, we define the experimental conversion efficiency as the ratio of the number of molecules created and the initial lattice sites which are occupied by exactly one K and one Rb atom. Note that only on these lattice sites molecules can be created. For the comparison of experimental and theoretical transfer efficiency, the experimental data have been scaled by a global factor to reproduce a conversion efficiency of 1 far off the Feshbach resonance where initial and final two-body wave function are equal. This is necessary, because the initial lattice sites occupied by one K and one Rb atom have not been determined experimentally.

While the experiments presented here were performed at constant rf pulse parameters, it should be possible from the above arguments to increase either pulse power or duration or both of the rf pulse to account for the reduced wave function overlap and thereby always obtain an efficiency of 1. In particular, it should be possible to drive Rabi oscillations between atoms and molecules in a very similar way as recently demonstrated [29]. The comparison also indicates that in the case of association efficiency a full quantitative agreement might require some more sophisticated treatment of the association process. This is in contrast to the analysis of binding energies and lifetimes (see below), where the good quantitiative agreement shows that here the δ interaction approximation captures the essential physics. Testing the Rabi oscillation hypothesis for molecules with rf might provide further insight.

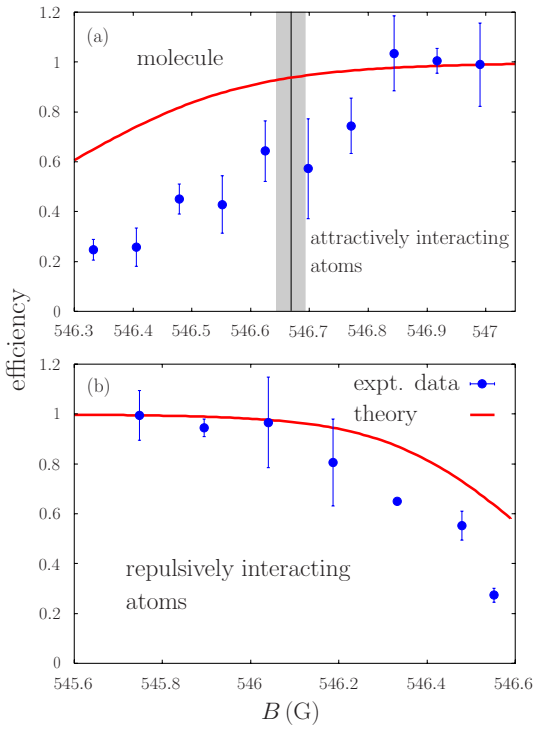

FIG. 5. (Color online) Transfer efficiency of rf association as observed in the experiment and estimated from a Rabi model, both for (a) attractively interacting atoms and molecules and for (b) repulsively interacting pairs. The experimental data contain a global factor which has been chosen such that the value of the outermost right (a) [left (b)] data point is one (see text). Experimental data of (a) from Ref. [9].

V. LIFETIME

Molecule formation at atomic Feshbach resonances results in dimers which are very weakly bound and may exhibit strong inelastic collisional losses. Experiments with molecules created from bosonic atoms showed very small lifetimes. As a result, these molecules can be brought into the quantum degenerate regime [30], but thermal equilibrium is generally difficult to achieve for molecules created from bosonic atoms because of the short lifetime.

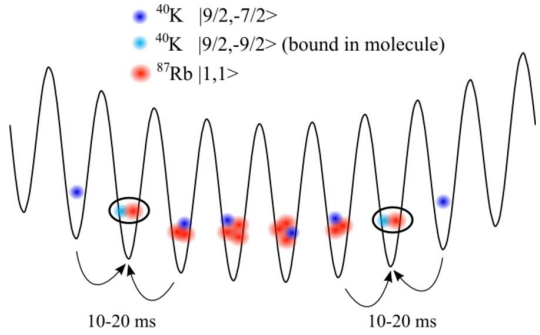

FIG. 6. (Color online) Sketch of expected lattice occupation. The arrows illustrate tunneling of remaining fermionic ^{40}K atoms to the "molecular" shell where they can undergo inelastic three-body collisions with a ^{40}K-^{87}Rb molecule.

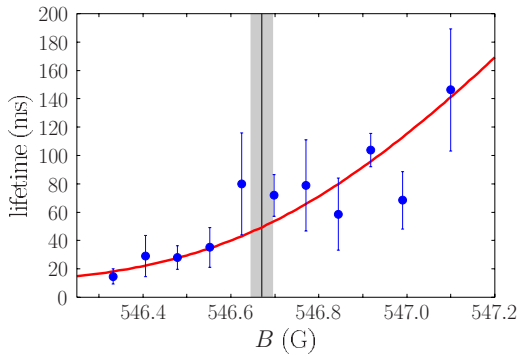

FIG. 7. (Color online) Lifetime of heteronuclear ^{40}K-^{87}Rb molecules in the optical lattice. The Lifetime is limited due to residual atoms which can tunnel to lattice sites with molecules and provoke inelastic three-body loss. The theoretical prediction uses the pseudopotential wave function and contains a global factor which was adjusted to the experimental data of Ref. [9].

In experiments with molecule creation from two-component Fermi gases [31], inelastic molecule-molecule and molecule-atom collisions are suppressed by the Pauli exclusion principle [32,33], resulting in remarkably long lifetimes between approximately 100 ms and even seconds, allowing Bose-Einstein condensation of Feshbach molecules [34] and the observation of BCS-BEC crossover physics [35–39]. The lifetime limitation for molecules created from bosonic atoms has been overcome by creating molecules in 3D optical lattices, where molecules are created at a single lattice site and isolated from inelastic collisions with residual atoms or other molecules [40].

For molecules created from Fermi-Bose mixtures, the situation is a little bit more complicated. As far as collisions between molecules are concerned, the fermionic character of the molecule should become more evident the deeper the molecule is bound, thus resulting in suppression of collisions [41].

As far as collisions with residual atoms are concerned, we expect inelastic collisions with fermionic atoms in the same spin state as the fermionic component of the molecule, i.e., in the $|9/2,-9/2\rangle$ state, to be suppressed due to the Pauli exclusion principle close to the resonance, when the "atomic" character of the molecule's constituents is still significant [32,33]. For collisions with bosonic atoms and fermionic atoms in a different internal state, we do not expect any Pauli-blocking enhanced lifetime, since the residual atom can in principle come arbitrarily near to the molecule's constituents.

In our situation, where the molecules are created through rf association, residual fermionic atoms remain in a different spin state, either in $|9/2,-7/2\rangle$ or $|9/2,-5/2\rangle$ (for the latter case, and for a description of the experimental procedure, see Ref. [9]). These residual fermionic atoms as well as the remaining bosonic atoms may therefore limit the stability of the molecular sample.

Molecule creation in the optical lattice introduces a second aspect concerning the lifetime: lattice occupation and tunneling probabilities. In Fig. 6, we have sketched the expected occupation in the optical lattice. Prior to molecule creation, we expect slightly less than unity filling for the fermionic component. As far as the bosons are concerned, we expect a central occupation number between 3 and 5, surrounded by shells of decreasing occupation number. In the rf association process, molecules are only created in the shell where we have one fermion and one boson per lattice site. In the outermost region of the lattice, we have lattice sites with only one fermion which are responsible for the "atomic" peak in the rf spectroscopy signal. After the rf association process in the "molecular" shell, bosons from neighboring sites as well as fermions remaining in a different spin state can tunnel to the "molecular" shell and provoke inelastic three-body loss. In our experimental situation, this is more probable for the remaining fermionic atoms, since they are lighter and have a smaller tunneling time (10 to 20 ms for the lattice depths discussed here). For the highest binding energies observed in the experiment, we find a limiting lifetime of 10 to 20 ms as seen in Fig. 7, which is consistent with the assumption that in this case, three-body loss is highly probable once tunneling of a distinguishable residual fermion has occurred. Still, for the more weakly bound molecules and in particular for attractively interacting atoms, we observe high lifetimes of 120 ms, raising the question of the magnetic field dependence of the lifetime.

We can understand this magnetic field dependence using the pseudopotential model by introducing a product wave function for the combined wave function of the resonantly interacting atom pair and a residual fermionic atom after tunneling to a molecular site. We write this three-body wave function as

$$\Phi(\vec{r},\vec{R},\vec{r}_3) := \Phi_{\mathrm{mol}}(\vec{r},\vec{R})\Phi_3(\vec{r}_3), \tag{15}$$

where Φ_{mol} is the result of the pseudopotential calculation for the molecule and Φ_3 is the ground-state wave function of the residual atom at the same lattice site. Note that this treatment assumes weak interactions between the residual atom and the molecule (the interaction between the residual atom and the molecule's constituents is on the order of the background scattering length). From solution (15) of the pseudo-

potential model, the dependence of the loss rate on the scattering length can be obtained close to the resonance [32]: the loss rate Γ is proportional to the probability $\mathcal{P}$ of finding the three atoms within a small sphere of radius σ, where they can undergo three-body recombination. This probability is expected to become larger for more deeply bound molecules, since two of the three atoms are already at a close distance. Up to a global factor, $\mathcal{P}$ is independent of the value chosen for σ, provided $\sigma \ll a_{\mathrm{rel}}$, and also $\sigma \ll a_s$ in the molecule regime. More quantitatively, we calculate this probability according to

$$\mathcal{P} = \int_{\substack{|\vec{r}|<\sigma \\ |\vec{r}_3-\vec{R}|<\sigma}} d\vec{r}d\vec{R}d\vec{r}_3 |\Phi(\vec{r},\vec{R},\vec{r}_3)|^2. \tag{16}$$

The magnetic field dependence of the loss rate is thus given through $\Gamma \propto \mathcal{P}$, and the lifetime is proportional to $1/\Gamma$. By using the wave functions (9) and the relation $|A|^2 \propto a_s^2 dE_{\mathrm{rel}}/da_s$ [11], we obtain

$$\mathcal{P} = C \frac{a_s}{\psi\left(-\frac{E_{\mathrm{rel}}}{2\hbar\omega_{\mathrm{rel}}}+\frac{3}{4}\right)-\psi\left(-\frac{E_{\mathrm{rel}}}{2\hbar\omega_{\mathrm{rel}}}+\frac{1}{4}\right)}, \tag{17}$$

where C is independent of a_s, and $\psi(x) \equiv \Gamma'(x)/\Gamma(x)$ is the digamma function. This result agrees with a numerical integration of Eq. (16) using the eigenfunctions of the complete Hamiltonian (7).

The lifetime obtained from the calculation is shown in Fig. 7 as a red solid line, scaled by a global factor to allow comparison to the experiment. As can be seen, the theoretical prediction explains the magnetic field dependence of the lifetime rather well. From an experimental point of view, we can therefore expect that removal of the remaining atoms using a resonant light pulse will significantly increase the lifetime of the molecules in the optical lattice.

CONCLUSIONS

To summarize, we have developed a pseudopotential approach to the scattering of unequally trapped atoms at a single site of an optical lattice including terms which couple center of mass and relative motion. We have compared the energy spectrum to experimental results for ^{40}K and ^{87}Rb atoms interacting at a heteronuclear Feshbach resonance in a 3D optical lattice. Within the pseudopotential model we have precisely determined the center position of the Feshbach resonance based on this comparison. The pseudopotential approach also allows us to understand the efficiency of rf association used to experimentally determine the energy spectrum, as well as the dependence of the molecular lifetime on magnetic field. The model developed in this paper enables a broad understanding of heteronuclear atom pairs in an optical lattice. We are aware of possible limitations of the pseudopotential model. It might be an interesting option to extend the method described here to energy dependent pseudopotentials [42–47] or multichannel models [43,48,49]. Finally, we note that the present rf association technique could be used to study the three-body problem at a triply occupied lattice site [50,51]. An advantage of this method with respect to the adiabatic magnetic field sweep proposed in [50] is that it is less sensitive to three-body losses, which are particularly important for Efimovian states [51].

ACKNOWLEDGMENTS

The authors would like to thank K. Rzażewski for his contributions in the initial discussion of possible extensions to Ref. [11]. We acknowledge discussions with Y. Castin, P. Julienne, Th. Köhler, P. Naidon, D. Petrov, and L. Pricoupenko on the pseudopotential models and on loss rates. We would like to thank A. Simoni for providing us with the closed channel magnetic moment at the Feshbach resonance and the scattering length in the initial state of the rf association. We acknowledge financial support by the Deutsche Forschungsgemeinschaft (SPP 1116).

[1] L. Mathey, D.-W. Wang, W. Hofstetter, M. D. Lukin, and E. Demler, Phys. Rev. Lett. **93**, 120404 (2004); E. Pazy and A. Vardi, Phys. Rev. A **72**, 033609 (2005); D.-W. Wang, M. D. Lukin, and E. Demler, *ibid.* **72**, 051604(R) (2005).
[2] L. Viverit, Phys. Rev. A **66**, 023605 (2002).
[3] M. J. Bijlsma, B. A. Heringa, and H. T. C. Stoof, Phys. Rev. A **61**, 053601 (2000).
[4] D. V. Efremov and L. Viverit, Phys. Rev. B **65**, 134519 (2002).
[5] F. Illuminati and A. Albus, Phys. Rev. Lett. **93**, 090406 (2004).
[6] H. P. Büchler and G. Blatter, Phys. Rev. Lett. **91**, 130404 (2003).
[7] S. Ospelkaus, C. Ospelkaus, O. Wille, M. Succo, P. Ernst, K. Sengstock, and K. Bongs, Phys. Rev. Lett. **96**, 180403 (2006).
[8] K. Günter, T. Stöferle, H. Moritz, M. Köhl, and T. Esslinger, Phys. Rev. Lett. **96**, 180402 (2006).
[9] C. Ospelkaus, S. Ospelkaus, L. Humbert, P. Ernst, K. Sengstock, and K. Bongs, Phys. Rev. Lett. **97**, 120402 (2006).
[10] S. B. Papp and C. E. Wieman, Phys. Rev. Lett. **97**, 180404 (2006).
[11] Th. Busch, B. G. Englert, K. Rzażewski, and M. Wilkens, Found. Phys. **28**, 549 (1998).
[12] T. Stöferle, H. Moritz, K. Günter, M. Köhl, and T. Esslinger, Phys. Rev. Lett. **96**, 030401 (2006).
[13] M. Köhl, K. Günter, T. Stöferle, H. Moritz, and T. Esslinger, J. Phys. B **39**, S47 (2006).
[14] We expect the pseudopotential model to be fairly accurate for the experimental parameters of Ref. [9]. Indeed, even for large scattering lengths, this model is expected to become exact in the zero-range limit [15], that is, when $1/k_{\mathrm{typ}} \gg \max(\beta_6, |r_e^0|)$. Here, k_{typ} is the typical wave number of the relative motion of the two atoms, $\beta_6 = (2\mu C_6/\hbar^2)^{1/4}$ is the van der Waals length scale, and $r_e^0 := -\hbar^2/\mu a_{\mathrm{bg}} \Delta B \partial E_{\mathrm{res}}/\partial B$, $\partial E_{\mathrm{res}}/\partial B$ being the

magnetic moment of the closed channel with respect to the two-atom open channel. For K-Rb in their ground state, $\beta_6 = 7.6$ nm [16]. Using $\partial E_{\rm res}/\partial B = k_B 144\ \mu$K/G [17], we get $r_e^0 = -4.6$ nm. It remains to estimate $k_{\rm typ}$. In the molecule regime, we have $1/k_{\rm typ} \sim a_s > 47$ nm. In the other regimes (attractively and repulsively interacting atoms), we have $1/k_{\rm typ} \sim a_{\rm rel}$. In the harmonic approximation for the experimental lattice depth $a_{\rm rel} = 103$ nm. Thus, the above inequality is fairly well satisfied.

[15] Y. Castin, e-print arXiv:cond-mat/0612613.

[16] A. Derevianko, J. F. Babb, and A. Dalgarno, Phys. Rev. A **63**, 052704 (2001).

[17] A. Simoni (private communication).

[18] K. Winkler, G. Thalhammer, F. Lang, R. Grimm, J. Hecker Denschlag, A. J. Daley, A. Kantian, H. P. Büchler, and P. Zoller, Nature (London) **441**, 853 (2006); A. J. Daley, A. Kantian, H. P. Büchler, P. Zoller, K. Winkler, G. Thalhammer, F. Lang, R. Grimm, and J. Hecker Denschlag, e-print arXiv:cond-mat/0608721v2.

[19] We note that we neglect many low-energy basis states $|N,L,0,0,0,0\rangle$ with $2N+L > \Pi_{\rm max}$ when the scattering length is small and positive $a_s \gtrsim 0$. These molecule states with highly excited center-of-mass energy have nevertheless low total energy since the energy of the relative motion is large and negative. We have included the states $|N,L,0,0,0,0\rangle$ with $2N+L \leq \Pi_{\rm max}$ to allow for the flattening of the center of mass wave function due to the anharmonicity of the lattice site potential. However, we have neglected the states with $2N+L > \Pi_{\rm max}$ since they are only weakly coupled to the states $|0,0,0,0,0,0\rangle$ (molecule) and $|0,0,0,n=1,0,0\rangle$ (repulsively interacting atoms of the decoupled problem). These matrix elements become even zero if $2N+L > p$ $(p=1,\ldots,8)$ since in this case the matrix elements $\langle 0,0,0,0,0,0|X^p|N,L,0,0,0,0\rangle$ and $\langle 0,0,0,1,0,0|X^p|N,L,0,0,0,0\rangle$ are exactly zero.

[20] C. Ospelkaus, S. Ospelkaus, K. Sengstock, and K. Bongs, Phys. Rev. Lett. **96**, 020401 (2006).

[21] S. Ospelkaus, C. Ospelkaus, R. Dinter, J. Fuchs, M. Nakat, K. Sengstock, and K. Bongs, J. Mod. Opt. **54**, 661 (2007).

[22] S. Inouye, J. Goldwin, M. L. Olsen, C. Ticknor, J. L. Bohn, and D. S. Jin, Phys. Rev. Lett. **93**, 183201 (2004).

[23] F. Ferlaino, C. D'Errico, G. Roati, M. Zaccanti, M. Inguscio, and G. Modugno, and A. Simoni, Phys. Rev. A **73**, 040702(R) (2006).

[24] S. Ospelkaus, C. Ospelkaus, L. Humbert, K. Sengstock, and K. Bongs, Phys. Rev. Lett. **97**, 120403 (2006).

[25] T. Köhler, K. Góral, and P. S. Julienne, Rev. Mod. Phys. **78**, 1311 (2006).

[26] E. Arimondo, M. Inguscio, and P. Violino, Rev. Mod. Phys. **49**, 31 (1977).

[27] For the scattering length in the initial ^{87}Rb$|1,1\rangle \otimes {}^{40}K|9/2, -7/2\rangle$ state in the considered magnetic field range $544\text{G} < B < 549$ G we take the value $-175a_0$ [A. Simoni (private communication)].

[28] M. Zaccanti, C. D'Errico, F. Ferlaino, G. Roati, M. Inguscio, and G. Modugno, Phys. Rev. A **74**, 041605(R) (2006).

[29] N. Syassen, D. M. Bauer, M. Lettner, D. Dietze, T. Volz, S. Dürr, and G. Rempe, Phys. Rev. Lett. **99**, 033201 (2007).

[30] K. Xu, T. Mukaiyama, J. R. Abo-Shaeer, J. K. Chin, D. E. Miller, and W. Ketterle, Phys. Rev. Lett. **91**, 210402 (2003); J. Herbig, T. Kraemer, M. Mark, T. Weber, C. Chin, H.-C. Nägerl, and R. Grimm, Science **301**, 1510 (2003).

[31] C. A. Regal, C. Ticknor, J. L. Bohn, and D. S. Jin, Nature (London) **424**, 47 (2003); J. Cubizolles, T. Bourdel, S. J. J. M. F. Kokkelmans, G. V. Shlyapnikov, and C. Salomon, Phys. Rev. Lett. **91**, 240401 (2003); K. E. Strecker, G. B. Partridge, and R. G. Hulet, *ibid.* **91**, 080406 (2003); S. Jochim, M. Bartenstein, A. Altmeyer, G. Hendl, C. Chin, J. Hecker Denschlag, and R. Grimm, *ibid.* **91**, 240402 (2003).

[32] D. S. Petrov, C. Salomon, and G. V. Shlyapnikov, Phys. Rev. Lett. **93**, 090404 (2004); Phys. Rev. A **71**, 012708 (2005).

[33] D. S. Petrov, C. Salomon, and G. V. Shlyapnikov, J. Phys. B **38**, S645 (2005).

[34] M. Greiner, C. A. Regal, and D. S. Jin, Nature (London) **426**, 537 (2003); M. W. Zwierlein, C. A. Stan, C. H. Schunck, S. M. F. Raupach, S. Gupta, Z. Hadzibabic, and W. Ketterle, Phys. Rev. Lett. **91**, 250401 (2003); S. Jochim, M. Bartenstein, A. Altmeyer, G. Hendl, S. Riedl, C. Chin, J. Hecker Denschlag, and R. Grimm, Science **302**, 2101 (2003).

[35] C. A. Regal, M. Greiner, and D. S. Jin, Phys. Rev. Lett. **92**, 040403 (2004).

[36] M. W. Zwierlein, C. A. Stan, C. H. Schunck, S. M. F. Raupach, A. J. Kerman, and W. Ketterle, Phys. Rev. Lett. **92**, 120403 (2004).

[37] M. Bartenstein, A. Altmeyer, S. Riedl, S. Jochim, C. Chin, J. Hecker Denschlag, and R. Grimm, Phys. Rev. Lett. **92**, 120401 (2004).

[38] T. Bourdel, L. Khaykovich, J. Cubizolles, J. Zhang, F. Chevy, M. Teichmann, L. Tarruell, S. J. J. M. F. Kokkelmans, and C. Salomon, Phys. Rev. Lett. **93**, 050401 (2004).

[39] J. Kinast, S. L. Hemmer, M. E. Gehm, A. Turlapov, and J. E. Thomas, Phys. Rev. Lett. **92**, 150402 (2004).

[40] G. Thalhammer, K. Winkler, F. Lang, S. Schmid, R. Grimm, and J. Hecker Denschlag, Phys. Rev. Lett. **96**, 050402 (2006); T. Volz, N. Syassen, D. M. Bauer, E. Hansis, S. Dürr, and G. Rempe, Nat. Phys. **2**, 692 (2006).

[41] C. A. Stan, M. W. Zwierlein, C. H. Schunck, S. M. F. Raupach, and W. Ketterle, Phys. Rev. Lett. **93**, 143001 (2004).

[42] D. Blume and C. H. Greene, Phys. Rev. A **65**, 043613 (2002).

[43] E. L. Bolda, E. Tiesinga, and P. S. Julienne, Phys. Rev. A **66**, 013403 (2002).

[44] Z. Idziaszek and T. Calarco, Phys. Rev. A **74**, 022712 (2006).

[45] D. S. Petrov, Phys. Rev. Lett. **93**, 143201 (2004).

[46] P. Naidon, E. Tiesinga, W. Mitchell, and P. Julienne, New J. Phys. **9**, 19 (2007), and references therein.

[47] For an equivalent energy-independent formulation of such a model, see L. Pricoupenko, Phys. Rev. A **73**, 012701 (2006).

[48] E. Tiesinga, C. J. Williams, F. H. Mies, and P. S. Julienne, Phys. Rev. A **61**, 063416 (2000).

[49] D. B. M. Dickerscheid and H. T. C. Stoof, Phys. Rev. A **72**, 053625 (2005); K. B. Gubbels, D. B. M. Dickerscheid, and H. T. C. Stoof, New J. Phys. **8**, 151 (2006), and references therein.

[50] M. Stoll and T. Köhler, Phys. Rev. A **72**, 022714 (2005).

[51] F. Werner and Y. Castin, Phys. Rev. Lett. **97**, 150401 (2006).

[52] VFG-150, a FPGA-driven fast versatile frequency generator, controlled via an USB2.0 interface and developed by Th. Hannemann in the group of C. Wunderlich, University of Siegen, Germany.

Chapter 7

Derivation of the Petrov-Salomon-Shlyapnikov approach for a simple model

In Article V, Section V, we used the approach of Petrov, Salomon and Shlyapnikov (PSS) to calculate the dependence on the scattering length a of the loss rate Γ due to recombination towards deeply bound dimers. In this Chapter, we use a simple microscopic model to justify this approach. As in the experimental situation of Article V, we consider 3 distinguishable particles in a harmonic trap, only the interaction between particles 1 and 2 being resonant with a large scattering length a, while the interactions with the third particle are weak. This will allow us to justify the PSS approach simply by using Fermi's golden rule. [1]

We assume that all particles are subject to the same harmonic trapping potential of frequency ω, which simplifies the discussion and allows to obtain an analytical result within the PSS approach. [2]

The non-interacting Hamiltonian is

$$\mathcal{H}_0 = \sum_{i=1}^{3} -\frac{\hbar^2}{2m_i}\Delta_{\vec{r}_i} + \frac{1}{2}m_i\omega^2\, {r_i}^2. \tag{7.1}$$

Defining the total mass

$$M = \sum_{i=1}^{3} m_i, \tag{7.2}$$

the center of mass coordinate is

$$\vec{C} = \frac{\sum_{i=1}^{3} m_i\, \vec{r}_i}{M}, \tag{7.3}$$

and the Jacobi coordinates are : [3]

$$\vec{r} = \vec{r}_2 - \vec{r}_1 \tag{7.4}$$

$$\vec{\rho} = \left(\vec{r}_3 - \frac{\vec{r}_1 + \vec{r}_2}{2}\right)\sqrt{\frac{(m_1+m_2)^2\, m_3}{m_1 m_2 M}}. \tag{7.5}$$

1. In the situation considered in Part 3 of this manuscript, where several pairs have resonant interactions, the PSS approach cannot be justified as easily.

2. In Article V, it was checked that the results for the lifetime almost do not change if one takes into account the anharmonicity and the fact that the trapping frequencies are not the same.

3. See Appendix A for the derivations, and Fig. 3.1 page 80 for a picture in the case of equal masses.

The non-interacting Hamiltonian becomes :

$$\mathcal{H}_0 = -\frac{\hbar^2}{2M}\Delta_{\vec{C}} + \frac{1}{2}M\omega^2\, C^2 - \frac{\hbar^2}{m}(\Delta_{\vec{r}} + \Delta_{\vec{\rho}}) + \frac{1}{4}m\omega^2(r^2+\rho^2) \tag{7.6}$$

where

$$m \equiv 2\frac{m_1 m_2}{m_1+m_2}. \tag{7.7}$$

1 Loss rate in the PSS approach

In this Section we review the calculation of the 3-body recombination rate within the PSS approach, and recover the result of Article V. We define the hyperradius :

$$R = \sqrt{\frac{r^2+\rho^2}{2}}, \tag{7.8}$$

which is small when all 3 particles are close. The PSS approach predicts a loss rate :

$$\Gamma_{\rm PSS} = K\frac{\hbar}{mb^2}P(R<b), \tag{7.9}$$

where b is the typical range of interactions; $P(R<b)$ is the probability, calculated within the zero-range model, that the hyperradius is smaller than b; and K is a dimensionless number which depends on the detailed shape of the interactions, but is independent of a and ω.[4] We shall always consider the zero-range limit, where all microscopic length scales $\sim b$ are much smaller than $|a|$ and than the harmonic oscillator length

$$a_{\rm ho} = \sqrt{\frac{\hbar}{m\omega}}, \tag{7.10}$$

more precisely

$$\frac{a_{\rm ho}}{b} \to \infty, \quad \frac{a_{\rm ho}}{a} \text{ fixed.} \tag{7.11}$$

In the zero-range limit, the predicted $\Gamma(a, a_{\rm ho})$ becomes independent of the definition of b, up to a multiplicative constant. For the trapping potential, we cannot take a harmonic potential extending to infinity, because we want the atoms to be able to escape after having recombined into the deep dimer. A trapping potential which qualitatively reproduces the experimental situation is a harmonic potential which is truncated :

$$U(r_i) = \min\left(\frac{1}{2}m_i\omega^2\, {r_i}^2, U_0\right), \tag{7.12}$$

with a height U_0 satisfying

$$\hbar\omega \ll U_0 \ll \frac{\hbar^2}{mb^2} \tag{7.13}$$

which means that the trap is so deep that it does not perturb the wavefunction of the initial state, and so shallow that the recombination products can escape easily. In the limits (7.11,7.13), the PSS approach is expected to give the *exact* asymptotic dependence of Γ on a and $a_{\rm ho}$, up to a global multiplicative constant. This also implies that Γ becomes independent of the particular choice (7.12) of how the trap was truncated.

4. In Article V we replaced $P(R<b)$ by $P(r<b; \|\vec{r}_3 - (\vec{r}_1+\vec{r}_2)/2\| < b)$ in Eq. (7.9). This simplifies the calculation but does not change the result in the $b \to 0$ limit, up to a global factor which can be absorbed by redefining K.

To calculate the asymptotic behavior of $P(R < b)$ in the limit $b \to 0$, we note that the eigenfunctions of the zero-range model can be written in the separable form

$$\Phi(\vec{r}_1, \vec{r}_2, \vec{r}_3) = \phi(\vec{r})\, \psi_\rho(\vec{\rho})\, \psi_{\rm CM}(\vec{C}). \tag{7.14}$$

The relative motion of particles 1 and 2 is then given by the Schrödinger equation

$$\left[-\frac{\hbar^2}{m} \Delta_{\vec{r}} + \frac{1}{4} m\omega^2\, r^2 \right] \phi(\vec{r}) = E\, \phi(\vec{r}), \tag{7.15}$$

together with the Bethe-Peierls boundary condition that there exists a constant A such that

$$\phi(\vec{r}) \underset{r\to 0}{=} A \cdot \left(\frac{1}{r} - \frac{1}{a} \right) + O(r). \tag{7.16}$$

The analytical solution of this problem is well-known [33], and was reviewed in Chapter 6 of this manuscript ; let us recall that the spectrum is given by

$$\frac{a_{\rm ho}}{\sqrt{2}\, a} = \frac{\Gamma\left(\frac{3}{4} - \frac{E}{2\hbar\omega}\right)}{\Gamma\left(\frac{1}{4} - \frac{E}{2\hbar\omega}\right)} \tag{7.17}$$

and that the wavefunctions are

$$\phi(r) = \frac{1}{\sqrt{2}\pi} \sqrt{\frac{\Gamma\left(\frac{3}{4} - \frac{E}{2\hbar\omega}\right)\, \Gamma\left(\frac{1}{4} - \frac{E}{2\hbar\omega}\right)}{\psi\left(\frac{3}{4} - \frac{E}{2\hbar\omega}\right) - \psi\left(\frac{1}{4} - \frac{E}{2\hbar\omega}\right)}} \frac{1}{r^{3/2}} W_{\frac{E}{2\hbar\omega}, \frac{1}{4}} \left(\frac{r^2}{2\, {a_{\rm ho}}^2} \right), \tag{7.18}$$

where W is a Whittaker function, ψ is the digamma function, and the normalisation is such that

$$\int d\vec{r} |\phi(\vec{r})|^2 = 1. \tag{7.19}$$

Using the asymptotic behavior of W for a small argument [Eq. (B.33) p. 69] one finds that the coefficient A appearing in the Bethe-Peierls boundary condition Eq. (7.16) is given by :

$$|A|^2 = \frac{a}{2\pi\, {a_{\rm ho}}^2} \frac{1}{\psi\left(\frac{3}{4} - \frac{E}{2\hbar\omega}\right) - \psi\left(\frac{1}{4} - \frac{E}{2\hbar\omega}\right)}. \tag{7.20}$$

This result can also be obtained very directly by using the relation [92, 93]

$$\frac{\partial E}{\partial (1/a)} = -\frac{4\pi\hbar^2}{m} |A|^2 \tag{7.21}$$

and Eq. (7.17).

Assuming that both the center of mass and particle 3 are in their ground state, we have :

$$\psi_\rho(\vec{\rho}) = e^{-\rho^2/(4\, {a_{\rm ho}}^2)} \left(\sqrt{2\pi}\, a_{\rm ho} \right)^{-3/2}, \tag{7.22}$$

where we the normalisation is such that

$$\int d\vec{\rho} |\psi_\rho(\vec{\rho})|^2 = 1. \tag{7.23}$$

The total energy of the 3 particles is then $E + 3\hbar\omega$.

We can now calculate

$$P(R<b) = \int d\vec{r} \int d\vec{\rho}\, |\phi(r)|^2\, |\psi_\rho(\rho)|^2\, \mathbf{1}_{\{R<b\}} \tag{7.24}$$

where $\mathbf{1}_{\{R<b\}}$ equals 1 if $R<b$ and 0 otherwise. Using Eqs. (7.16,7.22) we get :

$$P(R<b) \underset{b\to 0}{\sim} |A|^2 \frac{b^4}{{a_{\rm ho}}^3} \sqrt{2}\, \pi^{3/2}. \tag{7.25}$$

In conclusion,

$$\Gamma_{\rm PSS} = \frac{|A|^2}{{a_{\rm ho}}^3}\, K\, b^2\, \frac{\hbar}{m} \sqrt{2\pi^3}, \tag{7.26}$$

where $|A|^2$ is given by Eq. (7.20). This result is shown in Fig. 7 of Article V (page 156 in this manuscript), where the numerical value of $K\, b^2$ was adjusted to the experimental data.

2 Loss rate for a simple model

In this Section we use a simple microscopic model for which the loss rate can be obtained using Fermi's golden rule, without using the PSS approach. We will see that the result agrees with the one of the PSS approach. Our microscopic model is not fully realistic, but it contains all physical ingredients, so that one can expect that a fully realistic model would also agree with the PSS approach.

2.1 Our model

The interaction between particles i and j is described by a *finite* range potential $V_{ij}(r)$. For concreteness we assume that $V_{ij}(r)$ is a square-well interaction potential of range b :

$$V_{ij}(r) = -V_{ij,0}\, \mathbf{1}_{\{r<b\}} \tag{7.27}$$

where

$$\mathbf{1}_{\{r<b\}} \equiv \begin{cases} -V_{ij,0} & \text{if } r<b \\ 0 & \text{if } r>b. \end{cases} \tag{7.28}$$

We set $V_{12,0} = V_0$ and $V_{13,0} = V_{23,0} = V_0'$.

The depth V_0 is chosen to be close to the value V_0^∞ where the *second* 2-body bound state appears :

$$V_0 \simeq V_0^\infty = \left(\frac{3\pi}{2}\right)^2 \frac{\hbar^2}{mb^2}. \tag{7.29}$$

In this resonant regime, the potential $V_{12}(r)$ has a large scattering length

$$|a| \gg b, \tag{7.30}$$

and we have a one-to-one correspondence between a and V_0. This potential also supports one *deeply* bound state of energy E_d and wavefunction $\phi_d(r)$. The binding energy $|E_d|$ is on the order of $\hbar^2/(mb^2)$.

The interaction potential with particle 3 is assumed to be very weak :

$$|V_0'| \ll \frac{\hbar^2}{mb^2}, \tag{7.31}$$

so that the Born approximation is applicable and the scattering length is

$$a' \simeq \frac{m}{4\pi\hbar^2}\int d\vec{r}\, V_{13}(r) = -\frac{b^3\, V_0' m}{3\hbar^2}, \tag{7.32}$$

and thus

$$|a'| \ll b. \tag{7.33}$$

In the zero-range limit, the harmonic oscillator length

$$a_{\rm ho} = \sqrt{\frac{\hbar}{m\omega}} \tag{7.34}$$

is much larger than the range :

$$a_{\rm ho} \gg b. \tag{7.35}$$

For the trapping potential, we do not take the truncated harmonic potential of Eq. (7.12) because this potential is not convenient for calculating Γ. We rather take the trapping potential

$$H_{\rm trap} = \frac{1}{4}m\omega^2 r^2 + (1 - |\phi_d\rangle\langle\phi_d|) \otimes \left(\frac{1}{4}m\omega^2\rho^2\right), \tag{7.36}$$

which is less realistic but has the physically correct property that if particles 1 and 2 have formed the deep dimer $|\phi_d\rangle$, then this dimer and the third particle become free to fly away from each other. We thus expect that Γ coincides for both traps in the limit (7.13).

Our total Hamiltonian for the relative motion of the three particles reads :

$$H = -\frac{\hbar^2}{m}(\Delta_{\vec{r}} + \Delta_{\vec{\rho}}) + H_{\rm trap} + V_{12}(r_{12}) + V_{13}(r_{13}) + V_{23}(r_{23}). \tag{7.37}$$

2.2 The loss rate from Fermi's golden rule

We apply Fermi's golden rule to $H = H_0 + V$ with the unperturbed Hamiltonian

$$H_0 = -\frac{\hbar^2}{m}(\Delta_{\vec{r}} + \Delta_{\vec{\rho}}) + H_{\rm trap} + V_{12}(r_{12}) \tag{7.38}$$

and the perturbation

$$V = V_{13}(r_{13}) + V_{23}(r_{23}). \tag{7.39}$$

Our initial state is

$$\psi_i(\vec{r},\vec{\rho}) = \phi(r)\psi_\rho(\rho), \tag{7.40}$$

where $\psi_\rho(\rho)$ is still given by Eq. (7.22), and $\phi(r)$ satisfies

$$H_r\,\phi = E\,\phi, \tag{7.41}$$

H_r being the relative Hamiltonian between particles 1 and 2

$$H_r = -\frac{\hbar^2}{m}\Delta_{\vec{r}} + V_{12}(r) + \frac{1}{4}m\omega^2\, r^2. \tag{7.42}$$

The deep bound state $\phi_d(r)$ is almost unaffected by the trap and is very close to being the groundstate of H_r, as a consequence of Eq. (7.35). The *excited* eigenstates of H_r have energies which are close to the ones of the zero-range model, as a consequence of Eqs. (7.30,7.35). As in the experiment, we take for $\phi(r)$ the first excited state of H_r, whose energy E is close to the ground state energy $E_{\rm ZR}(a)$ of the zero-range model, and whose wavefunction $\phi(r)$ is close to the wavefunction $\phi_{\rm ZR}(r)$ of the zero-range model provided $r \gg b$.

Since $|\langle\phi_d|\phi\rangle| \ll 1$, we can neglect the term $|\phi_d\rangle\langle\phi_d|$ in the expression (7.36) of $H_{\rm trap}$, so that

$$H_0\psi_i \simeq E_i\psi_i \tag{7.43}$$

where

$$E_i = E + \frac{3}{2}\hbar\omega. \tag{7.44}$$

The final states belonging to the continuous spectrum of H_0 correspond to the deep dimer and the third atom flying away from each other :

$$\psi_{f,\vec{k}}(\vec{r},\vec{\rho}) = \phi_d(r)\, e^{i\vec{k}\cdot\vec{\rho}}/\sqrt{\mathcal{V}} \tag{7.45}$$

where $\mathcal{V}$ is a large quantization volume. We have

$$H_0\,\psi_{f,\vec{k}} = E_{f,\vec{k}}\,\psi_i \tag{7.46}$$

with

$$E_{f,\vec{k}} = E_d + \frac{\hbar^2\,k^2}{m}. \tag{7.47}$$

Since V is weak, we can apply Fermi's golden rule :

$$\Gamma = \frac{2\pi}{\hbar}\sum_{\vec{k}}\left|\langle\psi_{f,\vec{k}}|V|\psi_i\rangle\right|^2\ \delta(E_{f,\vec{k}} - E_i) \tag{7.48}$$

Defining a vector $\vec{k}_f$ of arbitrary direction satisfying

$$E_i = E_{f,\vec{k}_f}, \tag{7.49}$$

i. e.

$$E_i = E_d + \frac{\hbar^2\,{k_f}^2}{m}, \tag{7.50}$$

we get :

$$\Gamma = \frac{m}{2\pi\hbar^3}\,k_f\left|\int d\vec{r}\,d\vec{\rho}\ \phi_d(r)e^{-i\vec{k}_f\cdot\vec{\rho}}\ V(\vec{r},\vec{\rho})\,\psi_i(r,\rho)\right|^2. \tag{7.51}$$

Only values of r and ρ which are $\lesssim b$ contribute to this integral, because the wavefunction of the deep dimer $\phi_d(r)$ has an extension $\sim b$, and for $r \lesssim b$ the interaction term $V(\vec{r},\vec{\rho}) = V_{13}(r_{13}) + V_{23}(r_{23})$ is non-zero only if $\rho \lesssim b$. At these short distances we of course have

$$\psi_\rho(\rho) \underset{\rho\lesssim b}{\simeq} \psi_\rho(0). \tag{7.52}$$

Now we analyze the behavior of $\phi(r)$ at $r \lesssim b$ and relate it to the zero-range model's wavefunction, using the same reasoning than Petrov, Salomon and Shlyapnikov in [106, 24]. We expect that :

$$\phi(r) \underset{r\ll a_{\rm ho}}{\simeq} B\,\phi_0(r), \tag{7.53}$$

where B is a constant and $\phi_0(r)$ is the zero-energy scattering state :

$$\left(-\frac{\hbar^2}{m}\Delta_{\vec{r}} + V_{12}(r)\right)\phi_0(r) = 0, \tag{7.54}$$

normalized in such a way that

$$\phi_0(r) \underset{b\ll r}{\simeq} \frac{1}{r} - \frac{1}{a}. \tag{7.55}$$

Since $|a| \gg b \gtrsim r$ (i. e. $V_0 \simeq V_0^\infty$) we can replace $\phi_0(r)$ in Eq. (7.53) by the scattering state ϕ_0^∞ for $a = \infty$ (i. e. for a potential depth $V_0 = V_0^\infty$), which gives :

$$\phi(r) \underset{r\ll a_{\rm ho}}{\simeq} B\,\phi_0^\infty(r). \tag{7.56}$$

Eq. (7.55) becomes :

$$\phi_0^\infty(r) \underset{b\ll r}{\simeq} \frac{1}{r}. \tag{7.57}$$

As in Section 1, we define A as the coefficient of the $1/r$ divergence of the zero-range model's wavefunction :

$$\phi_{\rm ZR}(r) \underset{r\ll \min(a_{\rm ho},|a|)}{\simeq} \frac{A}{r}. \tag{7.58}$$

We recall that :

$$\phi(r) \underset{b\ll r}{\simeq} \phi_{\rm ZR}(r). \tag{7.59}$$

In the intermediate region $b \ll r \ll \min(a_{\rm ho}, |a|)$, Eqs. (7.56,7.57,7.58,7.59) all hold, so that $\phi(r) \simeq B/r \simeq A/r$. Thus

$$B \simeq A. \tag{7.60}$$

In conclusion, we can set

$$\psi_i(r,\rho) \simeq A\,\phi_0^\infty(r)\ \psi_\rho(0) \tag{7.61}$$

in Eq. (7.51), which gives :

$$\Gamma = \frac{|A|^2}{{a_{\rm ho}}^3}\,C \tag{7.62}$$

where

$$C = \frac{m\,k_f}{(2\pi)^{5/2}\hbar^3}\left|\int d\vec{r}\,d\vec{\rho}\ \phi_d(r)e^{-i\vec{k}_f\cdot\vec{\rho}}\ V(\vec{r},\vec{\rho})\,\phi_0^\infty(r)\right|^2 \tag{7.63}$$

is independent of a and ω. [5]

Thus we obtain the same dependence of Γ on a and $a_{\rm ho}$ than the prediction Eq. (7.26) of the PSS approach. We conclude that the PSS is indeed valid for our model.

Amusingly, we also find the expression for our model of the constant K, which enters as a parameter in the PSS approach :

$$K = \frac{m^2\,k_f}{8\pi^4\hbar^4\,b^2}\left|\int d\vec{r}\,d\vec{\rho}\ \phi_d(r)e^{-i\vec{k}_f\cdot\vec{\rho}}\ V(\vec{r},\vec{\rho})\,\phi_0^\infty(r)\right|^2. \tag{7.64}$$

From Eq. (7.32) and dimensional analysis, this implies that

$$K = D\left(\frac{a'}{b}\right)^2 \tag{7.65}$$

5. Eqs. (7.35,7.30) imply that we can neglect E in Eq. (7.50) so that k_f becomes independent of a and ω.

where D is a dimensionless constant which we do not calculate here. Thus $K \ll 1$, which is a peculiarity of our model where we assumed that $|a'| \ll b$.

For a more realistic interaction, this last condition is not satisfied, and one cannot simply apply Fermi's golden rule. However, we expect that the PSS approach remains valid, which explains that it is in good agreement with the experimental data.

Chapter 8

Applicability of the zero-range approximation to the Hamburg experiment

In this Chapter we discuss the validity of the pseudopotential model in the experimental situation considered in Article V. The Equations, Tables and Figures we refer to are the ones of Article V.

Following the discussion of [32], we expect the pseudopotential to give accurate results in the zero-range limit, that is when :

$$1/k_{\rm typ} \gg \max(\beta_6, |r_e^0|). \tag{8.1}$$

Here, $k_{\rm typ}$ is the typical wavevector of the relative motion of the two atoms, $\beta_6 = (2\mu C_6/\hbar^2)^{1/4}$ is the van der Waals length scale, and

$$r_e^0 := -\frac{\hbar^2}{\mu \cdot a_{\rm bg} \cdot \Delta B \cdot \partial E_{\rm res}/\partial B}, \tag{8.2}$$

$\partial E_{\rm res}/\partial B$ being the magnetic moment of the closed channel with respect to the open channel.

Before applying the predictions of the pseudopotential (e. g. the ones in Fig. 2 and Table I) to a particular experimental situation, one must check carefully whether Eq. (8.1) is satisfied. Note that Eq. (8.1) is more difficult to fulfill for resonances with a small width ΔB. For example, in [96], Eq. (8.1) is violated due to the large value $r_e^0 \simeq -52\,$nm [70] for the narrow 900 G resonance in Na, and the pseudopotential breaks down.

In the experiment, for K-Rb in their ground state, $\beta_6 = 7.6$ nm [126]. Using $\partial E_{\rm res}/\partial B = k_B \cdot 144\,\mu$K/G [1], we get $r_e^0 = -4.6\,$nm. It remains to estimate $1/k_{\rm typ}$. In the "real molecule" regime, we have $1/k_{\rm typ} \sim a > 47$ nm . In the other regimes (repulsively or attractively interacting atoms), we have $1/k_{\rm typ} \sim a_{\rm rel}$. In the harmonic approximation for the experimental lattice depth, $a_{\rm rel} = 103\,$nm. Thus, Eq.(8.1) is moderately well satisfied.

To estimate more quantitatively the error that we commit by using the pseudopotential model, we use the energy-dependent pseudopotential [95, 127, 70, 128, 97], which is defined by replacing a_s by an energy-dependent effective scattering length $a_{s,\rm eff}(E_{\rm rel})$ in the definition of the (usual) pseudopotential [see Eq.(1)]. In the effective-range approximation, i. e. to first order in $E_{\rm rel}$, the effective scattering length is :

$$\frac{1}{a_{s,\rm eff}(E_{\rm rel})} = \frac{1}{a_s} - \frac{\mu}{\hbar^2} E_{\rm rel} r_e, \tag{8.3}$$

1. A. Simoni, private communication.

where r_e is the effective range. In the following, we call effective range model the model resulting from the energy-dependent pseudopotential *and* from the effective-range approximation. This effective range model was used e. g. in [95, 70, 97, 98, 90]. The usual definition of the effective range model model assumes that the center-of-mass is separable, so that the energy of the relative motion $E_{\rm rel}$ is well-defined. For an equivalent energy-independent formulation of the effective range model, see [71]. The effective range model is expected to be exact to first order in r_e as we discuss in Sec. 4 of Chap. 6 and in Sec. 4.2 of Chap. 3.

Let us compare the predictions of the effective range model and of the pseudopotential for the relative motion of two particles in a harmonic trapping potential. The solution for the pseudopotential is given by Eq.(8). The solution for the effective range model [95, 127] is simply obtained by replacing a_s by $a_{s,\rm eff}(E_{\rm rel})$ in Eq.(8), $a_{s,\rm eff}(E_{\rm rel})$ being given by Eq.(8.3). If for a given eigenenergy of the relative motion $E_{\rm rel}$, the pseudopotential predicts a scattering length a_s ; then for the same $E_{\rm rel}$ the effective range model predicts a different scattering length $\tilde{a}_s$, such that :

$$\frac{a_{\rm rel}}{\tilde{a}_s} - \frac{a_{\rm rel}}{a_s} = \frac{r_e}{a_{\rm rel}} \frac{E_{\rm rel}}{\hbar\omega_{\rm rel}}. \tag{8.4}$$

Note that, for $|E_{\rm rel}|$ not much larger than $\hbar\omega_{\rm rel}$, the predictions of the two models become identical in the limit $|r_e| \ll a_{\rm rel}$. This remains true for a large scattering length, and is consistent with the expectation that the pseudopotential becomes exact in the zero-range limit [2].

Since our experimental situation is not deeply in this limit, and since the result for B_0 in Eq. (12) was obtained using the pseudopotential, there is an additional uncertainty $\delta B_{0,\rm model}$ on the value of B_0. To estimate it, we define an idealized "reality" where : i) the effective range model is exact ; ii) relative and CM motions are decoupled and the trap is harmonic, i.e. $H_{\rm couple} = 0$ in Eq. (7) ; iii) the relation between the "true" scattering length and B is given by the usual formula, Eq.(11), with the values of B_0, ΔB and $a_{\rm bg}$ given at the end of Sec. III. We then calculate "experimental data" which reproduce this "reality", for the same values of the binding energy than in the actual experiment [3]. Fitting these "data" to the pseudopotential's prediction Eq.(8) leads to a new value of the resonance position, which differs from the "true" one by some error $\delta B_{0,\rm model}$. For each value of $E_{\rm rel}$, the "true" scattering length $\tilde{a}_s$ and the pseudopotential's prediction a_s differ according to Eq.(8.4). It remains to estimate r_e. For single-channel potentials with a large C_6 [113, 114] :

$$r_e = \frac{\beta_6}{3}\left(\frac{\Gamma(1/4)^2}{\pi} - 4\frac{\beta_6}{a_s} + \frac{8\pi}{\Gamma(1/4)^2}\left(\frac{\beta_6}{a_s}\right)^2\right). \tag{8.5}$$

For a broad, entrance-channel dominated Feshbach resonance (i.e. for $|r_e^0| \ll \beta_6$), this formula is expected to remain fairly accurate. [4] In the narrow resonance limit ($|r_e^0| \gg \beta_6$), it is expected that $r_e \simeq r_e^0$, and that the effective range model becomes exact [70]. The resonance considered here is neither broad nor narrow, since we have $|r_e^0| \sim \beta_6$. Thus we are only able to estimate r_e. We simply assume that $|r_e|$ is at most 14 nm, the maximum of $|r_e^0|$ and of all values given by Eq.(8.5) for our values of a. The error $|\delta B_{0,\rm model}|$ is then maximized by setting $r_e E_{\rm rel} = \pm 14\,{\rm nm}\cdot|E_{\rm rel}|$ in Eq.(8.4), which gives :

$$\delta B_{0,\rm model} = \pm 40\,{\rm mG}. \tag{8.6}$$

Assuming for simplicity that B is uniformly distributed in an interval of half-width $|\delta B_{0,\rm model}|$, we get a variance of 23 mG, which is close to the systematic uncertainty of 24 mG already included in

2. In the weakly interacting regime $|a_s| \ll a_{\rm rel}$, it is sufficient to have $|r_e| \lesssim a_{\rm rel}$ (and $|E_{\rm rel}| \lesssim \hbar\omega_{\rm rel}$) in order to have $a_s \simeq \tilde{a}_s$.

3. For the scattering length in the initial $|1,1\rangle \otimes |9/2,-7/2\rangle$ state in the considered magnetic field range 544G $< B <$ 549G we take the value $-175\,a_0$ (A. Simoni, private communication).

4. P. Julienne, private communication. For the case of ^{6}Li near the 834G resonance, see Fig. 2 in [112].

Article V, Eq. (12). Adding up all variances finally gives a total standard uncertainty of 33 mG. This gives the slightly modified version of Eq. (12) :

$$B_0 = 546.67(3)\,\mathrm{G}. \tag{8.7}$$

Thus the pseudopotential is well suited to describe this experiment, since even our rather pessimistic estimate gives a model-induced uncertainty on the same order than the experimental uncertainties.

The model-induced uncertainty on B_0 could be reduced by redoing the calculation of Sec. I with a more realistic model than the pseudopotential, such as the effective range model. This would however require a precise knowledge of r_e. Other possible models include the energy-dependent pseudopotential without the effective-range approximation [127, 128], separable potential models [1], two-channel models [129, 130, 38], and multi-channel models [127, 96].

Appendice E

Dépendance en champ magnétique des états atomiques internes

1 Introduction

Dans l'Article V, l'accord entre théorie et expérience n'est pas très satisfaisant en ce qui concerne l'efficacité de l'association radiofréquence (Fig. 5 de l'article). Ceci m'a conduit à calculer la dépendance en champ magnétique du couplage de Rabi. Le résultat est que cette dépendance est bien négligeable, comme nous l'avions supposé dans l'article, et le relatif désaccord entre théorie et expérience doit être du à un autre effet. [1] Nous résumons ici ce calcul, qui consiste essentiellement à reproduire le calcul bien connu (mais rarement explicité dans la littérature) de Breit et Rabi concernant un atome alcalin dans l'état orbital électronique fondamental dans un champ magnétique extérieur.

2 États internes d'un alcalin

L'état interne d'un atome alcalin dans l'état orbital électronique fondamental est bien décrit par l'Hamiltonien hyperfin [131] :

$$H_{\rm hf} = \mathcal{A}\ \vec{I}\cdot\vec{S}, \tag{E.1}$$

où I est le spin nucléaire, S est le spin 1/2 électronique, et la constante $\mathcal{A}$ est en général déterminée expérimentalement (Tab. IX p. 67 dans [131]). En présence d'un champ magnétique externe $\vec{B}$, le Hamiltonien total devient

$$H = H_{\rm hf} + H_{\rm Z}, \tag{E.2}$$

où le Hamiltonien Zeeman est

$$H_{\rm Z} = -(\overrightarrow{M}_I + \overrightarrow{M}_S)\cdot\vec{B}, \tag{E.3}$$

les moments magnétiques nucléaire et électronique étant donnés par

$$\overrightarrow{M}_I = -g_I\mu_B\vec{I} \tag{E.4}$$

$$\overrightarrow{M}_S = -g_S\mu_B\vec{S}. \tag{E.5}$$

1. Un explication possible est l'inhomogénéité spatiale du réseau optique due au profil gaussien des faisceaux laser [120].

Ici nous prenons la convention que $\vec{I}$ et $\vec{S}$ sont sans dimension, par exemple

$$S_z \equiv \frac{1}{2}\begin{pmatrix} 1 & 0 \\ 0 & -1 \end{pmatrix}. \tag{E.6}$$

Le magnéton de Bohr est

$$\mu_B = \frac{\hbar|e|}{2m_e}, \tag{E.7}$$

dont la valeur actuelle donnée par le CODATA est

$$\mu_B/h = 13.99624604(35) \cdot 10^9 \text{ Hz T}^{-1}. \tag{E.8}$$

Les facteurs gyromagnétiques g_S et g_I dépendent de l'atome [131], on a $g_S \simeq 2$ et $g_I \lesssim 10^{-3}$.

Pour résoudre ce problème, on considère le spin total

$$\vec{F} = \vec{I} + \vec{S}, \tag{E.9}$$

dont les états propres $|f, m_F\rangle$ sont tels que

$$F^2|f, m_F\rangle = f(f+1)|f, m_F\rangle \tag{E.10}$$
$$F_z|f, m_F\rangle = m_F|f, m_F\rangle, \tag{E.11}$$

avec $|i - 1/2| \leq f \leq |i + 1/2|$ et $|m_F| \leq f$.

Définissant les états $\|m_I, m_S\rangle$ par

$$I_z\|m_I; m_S\rangle = m_I\|m_I; m_S\rangle \tag{E.12}$$
$$S_z\|m_I; m_S\rangle = m_S\|m_I; m_S\rangle, \tag{E.13}$$

où $|m_I| \leq i$ et $|m_S| \leq s = 1/2$, on montre que

$$\begin{aligned} |f = i + \frac{1}{2}, m_F\rangle &= \frac{\sqrt{i + \frac{1}{2} + m_F}\|m_F - \frac{1}{2}; \frac{1}{2}\rangle + \sqrt{i + \frac{1}{2} - m_F}\|m_F + \frac{1}{2}; -\frac{1}{2}\rangle}{\sqrt{2i+1}} \\ |f = i - \frac{1}{2}, m_F\rangle &= \frac{-\sqrt{i + \frac{1}{2} - m_F}\|m_F - \frac{1}{2}; \frac{1}{2}\rangle + \sqrt{i + \frac{1}{2} + m_F}\|m_F + \frac{1}{2}; -\frac{1}{2}\rangle}{\sqrt{2i+1}}. \end{aligned} \tag{E.14}$$

Pour $B = 0$, les états propres de $H = H_{\text{hf}}$ sont les états $|f, m_F\rangle$, et les énergies associées sont

$$E(f = i + \frac{1}{2}, m_F; B = 0) = \mathcal{A}\frac{i}{2} \tag{E.15}$$
$$E(f = i - \frac{1}{2}, m_F; B = 0) = -\mathcal{A}\frac{i+1}{2}. \tag{E.16}$$

Pour $B \neq 0$, on oriente l'axe z selon le vecteur $\vec{B}$, de sorte que m_F reste un bon nombre quantique. Par contre, f n'est plus un bon nombre quantique, mais on peut définir l'énergie propre $E(f, m_F; B)$ par continuité comme étant celle qui tend vers $E(f, m_F; B = 0)$ lorsque $B \to 0$. On diagonalise ensuite H dans chaque sous-espace propre $\mathcal{E}_{m_F}$ de F_z, en distinguant deux cas :

• Pour $m_F = \pm(i + 1/2)$, $\mathcal{E}_{m_F}$ est engendré par un seul vecteur,

$$|f = i + 1/2, m_F = \pm(i + 1/2)\rangle = \|\pm i; \pm 1/2\rangle, \tag{E.17}$$

d'énergie

$$E(f = i + 1/2, m_F = \pm(i + 1/2); B) = \mathcal{A}\frac{i}{2} \pm (\frac{1}{2}g_S + ig_I)\mu_B B. \tag{E.18}$$

• Pour $|m_F| \leq i - 1/2$, $\mathcal{E}_{m_F}$ est engendré par deux vecteurs, $|f = i + \frac{1}{2}, m_F\rangle$ et $|f = i - \frac{1}{2}, m_F\rangle$. La matrice 2×2 de H dans cette base se calcule à partir de l'éq. (E.14), et les énergies propres résultantes sont données par la formule de Breit-Rabi :

$$\begin{aligned} E(f = i \pm \frac{1}{2}, m_F; B) = -\frac{\mathcal{A}}{4} + \mu_B B g_I m_F \\ \pm\frac{1}{2}\sqrt{\left[\mathcal{A}\left(i + \frac{1}{2}\right)\right]^2 + 2\mathcal{A}\mu_B B(g_S - g_I)m_F + [\mu_B B(g_S - g_I)]^2} \end{aligned} \tag{E.19}$$

dans le cas $\mathcal{A} < 0$. Ces énergies sont par exemple représentées dans [132] p. 118 pour ^{40}K et dans l'Annexe B de [133] pour ^{6}Li et ^{7}Li. [2]

Les vecteurs propres associé $|f, m_F; B\rangle$ se calculent aisément, ce qui sera utile dans la Section suivante.

3 Dépendance en champ magnétique du couplage de Rabi dans l'expérience de Hambourg

Dans l'expérience d'association radiofréquence de l'Article V, on ajoute au champ magnétique constant

$$\vec{B} = B\vec{u}_z \tag{E.20}$$

permettant d'atteindre la résonance de Feshbach, un champ magnétique oscillant

$$\vec{B}_1(t) = b_1(t)\cos(\omega t)\vec{u}_x, \tag{E.21}$$

à une fréquence $\omega/(2\pi)$ d'environ 80 MHz correspondante à la transition $|f = 9/2, m_F = -7/2; B\rangle \rightarrow |f = 9/2, m_F = -9/2; B\rangle$ de l'atome ^{40}K. En traitant le champ oscillant en perturbation, et en tenant compte de la présence éventuelle d'un atome de ^{87}Rb, l'Hamiltonien interne (E.2,E.3) conduit à l'Hamiltonien effectif donné dans l'éq. (13) de l'Article V, avec un couplage de Rabi donné par

$$\omega_1(t) = \frac{\mu_B}{\hbar} b_1(t)\, F(B) \tag{E.22}$$

où

$$F(B) = \frac{1}{2}\langle f = \frac{9}{2}, m_F = -\frac{7}{2}; B|g_S S_+ + g_I I_+|f = \frac{9}{2}, m_F = -\frac{9}{2}; B\rangle. \tag{E.23}$$

Nous obtenons la fonction $F(B)$ à partir du calcul des vecteurs propres $|f, m_F; B\rangle$ décrit dans la Partie précédante. Pour ce faire, nous utilisons le fait que pour le ^{40}K on a [131] :

$$g_S = 2.00229421(24) \tag{E.24}$$
$$g_I = 0.000176490(34) \tag{E.25}$$
$$\mathcal{A}/\hbar = -285.7308(24)\ \text{MHz} \tag{E.26}$$
$$i = 4. \tag{E.27}$$

2. Notons qu'il existe deux petites imprécisions dans [133] : pour ^{7}Li on a $g_I = -1.182\,10^{-3}$ d'après [131], et il faut remplacer g_n par $-g_n$ dans les équations (B.2,B.3).

Le résultat est que la variation relative de $F(B)$ ne dépasse pas 1.5% dans le domaine de champ magnétiques $545.6\,G < B < 547\,G$ étudié dans l'Article V, et peut donc bien être négligée dans le calcul de l'efficacité de l'association radiofréquence. Cette faible variation est due au fait que la plage de B étudiée dans l'expérience est étroite, mais n'est pas due à l'existence d'un régime asymptotique pour $B \to \infty$, puisque la valeur $F(B \simeq 546\,\mathrm{G}) \simeq 0.15$ est encore bien supérieure à la valeur asymptotique $F(B \to \infty) = \sqrt{2}\,g_I \simeq 0.00025$. Cette faible valeur asymptotique est due au fait que dans la limite $B \to \infty$ (dite limite de Paschen-Back), on a $H \simeq H_Z$, les spins électroniques et nucléaires se découplent, et les états $|f = 9/2, m_F = -7/2; B\rangle$ et $|f = 9/2, m_F = -9/2; B\rangle$ ne diffèrent plus que par leur spin nucléaire, qui a un faible moment magnétique.

Partie 5 : Antiferromagnétisme dans un réseau optique

Cette Partie sort quelque peu du cadre de cette thèse, puisqu'il n'y est pas directement question d'atomes en interaction résonnante. Nous supposons ici que les atomes sont dans un réseau optique suffisamment peu profond pour que l'effet tunnel entre sites soit appréciable, et avec des interactions sur site suffisamment faibles pour que la description habituelle des états de basse énergie en terme du modèle de Hubbard soit applicable, comme discuté dans l'Article VI. Cela n'exclut pas l'utilisation d'une résonance de Feshbach pour contrôler la longueur de diffusion, mais cela suppose que l'on reste suffisamment loin de la résonance pour que la longueur de diffusion a reste faible par rapport à l'extension a_{ho} de l'état fondamental d'une particule dans un puits. Le régime considéré dans cette Partie est donc diamétralement opposé à celui considéré dans la Partie 2, où nous supposions que le réseau optique est suffisamment profond pour que l'effet tunnel entre sites soit négligeable, et nous nous placions sur une résonance de Feshbach pour atteindre la limite unitaire $|a| \gg a_{\mathrm{ho}}$, où la description habituelle en terme du modèle de Hubbard n'est plus applicable.

L'Article VI résulte d'un travail effectué avec Antoine Georges, Olivier Parcollet et Syed Hassan au cours de mon stage de DEA et poursuivi pendant ma première année de thèse. Il concerne le cas tridimensionnel.

Le Chapitre 9 concerne le cas bidimensionnel. Nous y utilisons simplement des résultats existants sur le modèle de Heisenberg pour discuter brièvement la possibilité d'observer des corrélations antiferromagnétiques.

Article VI

Interaction-induced adiabatic cooling and antiferromagnetism of cold fermions in optical lattices

PRL 95, 056401 (2005) PHYSICAL REVIEW LETTERS week ending 29 JULY 2005

Interaction-Induced Adiabatic Cooling and Antiferromagnetism of Cold Fermions in Optical Lattices

F. Werner,[1,2] O. Parcollet,[3] A. Georges,[2] and S. R. Hassan[2]
[1]*LKB, Ecole Normale Supérieure, 24 Rue Lhomond, 75231 Paris Cedex 05, France*
[2]*CPHT, Ecole Polytechnique, 91128 Palaiseau Cedex, France*
[3]*SPhT, CEA-Saclay, 91191 Gif sur Yvette Cedex, France*
(Received 31 March 2005; published 25 July 2005)

We propose an interaction-induced cooling mechanism for two-component cold fermions in an optical lattice. It is based on an increase of the spin entropy upon localization, an analogue of the Pomeranchuk effect in liquid helium 3. We discuss its application to the experimental realization of the antiferromagnetic phase. We illustrate our arguments with dynamical mean-field theory calculations.

DOI: 10.1103/PhysRevLett.95.056401 PACS numbers: 71.10.Fd, 03.75.Lm, 32.80.Pj, 71.30.+h

Cold atoms in optical lattices [1] offer a promising laboratory for the study of strongly correlated systems, bringing quantum optics to have bearing on key issues in condensed matter physics. Pioneering experiments on the Mott insulator to superfluid transition [2] have demonstrated the possibility [3] of probing quantum phase transitions between different ground states of these systems. Recently, great progress has been achieved on cold Fermi gases as well, resulting in the production of molecular condensates in trapped gases [4–7] and the first imaging of Fermi surfaces in a three-dimensional optical lattice [8]. Controllability is one of the most remarkable aspects of these systems, with the possibility of tuning both the tunneling amplitude between lattice sites (t) and the on-site interaction strength (U), by varying the depth of the optical lattice and by varying the interatomic scattering length thanks to Feshbach resonances.

In this Letter, we consider fermionic atoms with two hyperfine (''spin'') states in an optical lattice. When the lattice is deep and the scattering length is small (see below for a precise condition), a one-band Hubbard model is realized. The main physical effect studied in this Letter is the possibility of cooling down the system by increasing the interaction strength adiabatically. As described below, this is due to a higher degree of localization—and hence an increase in spin entropy—as U/t or the temperature is increased. This is a direct analogue of the Pomeranchuk effect in liquid helium 3. This mechanism relies on interactions and should be distinguished from the adiabatic cooling for noninteracting atoms in the lattice discussed in [9,10]. The second main goal of the present Letter is to study how this effect can be used in order to reach the phase with antiferromagnetic (AF) long-range order. For deep lattices (large U/t), the Néel temperature is expected to become very low, of the order of the magnetic superexchange $J_{\mathrm{AF}} = 4t^2/U$. Naively, it would seem that this requires extreme cooling of the gas. Here, we point out that the appropriate concept is actually the entropy along the antiferromagnetic critical line, and that at large U/t this quantity tends to *a finite constant* which depends only on the specific lattice. Hence, cooling the gas down to a temperature corresponding to this finite entropy per atom, and then following equal-entropy trajectories, should be enough to reach the magnetic phase. These physical observations are substantiated by theoretical calculations using, in particular, dynamical mean-field theory (DMFT) [11,12], an approach that has led to important progress on strongly correlated fermion systems in recent years.

We consider the one-band repulsive Hubbard model:

$$H = -\sum_{i,j,\sigma} t_{ij} c^{\dagger}_{i\sigma} c_{j\sigma} + U \sum_{i} n_{i\uparrow} n_{i\downarrow}, \qquad (1)$$

where i and j are site indices on the lattice, and $\sigma = \uparrow, \downarrow$ is a spin index associated with the two hyperfine states. The conditions under which two-component fermionic atoms in an optical lattice actually realize such a single-band lattice model will be discussed later. On an unfrustrated bipartite three-dimensional lattice (e.g., the cubic lattice), with hopping between nearest-neighbor sites $t_{ij} = t$, and for one particle per site on average (half filling), the physics of this model is rather well understood (see, e.g., [13]). For temperatures above the Néel critical temperature T_N, the system is a paramagnet with an increasing tendency to Mott localization as U/t is increased (the Mott gap becomes of order U at large U/t). For $T < T_N$, the antiferromagnetic phase (Fig. 1) displays a two-sublattice spin ordering and a doubling of the unit cell. At weak coupling (small U/t), this is a spin-density wave instability with a weak modulation of the sublattice magnetization. In this regime, T_N is exponentially small in t/U, as a simple Hartree mean-field theory suggests. At strong coupling (large U/t), the low-energy sector of the model is described by a Heisenberg exchange Hamiltonian $J_{\mathrm{AF}} \Sigma_{\langle ij \rangle} \vec{S}_i \cdot \vec{S}_j$, with $J_{\mathrm{AF}} = 4t^2/U$. In this Heisenberg limit, $T_N = \theta J_{\mathrm{AF}}$, with θ a numerical constant depending on the lattice ($\theta = 0.957$ for the cubic lattice [13]). These two regimes are connected by a smooth crossover (which is equivalent to the Bose-Einstein-condensation–BCS cross-

PRL 95, 056401 (2005) PHYSICAL REVIEW LETTERS week ending 29 JULY 2005

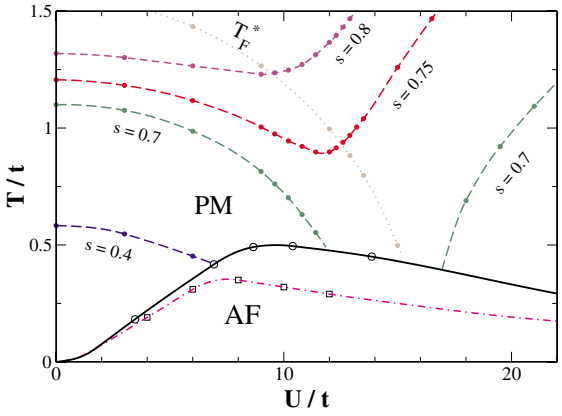

FIG. 1 (color online). Phase diagram of the half-filled Hubbard model on the cubic lattice: antiferromagnetic (AF) and paramagnetic (PM) phases. Transition temperature within DMFT approximation (solid curve, open circles) and QMC calculation of Ref. [13] (dot-dashed curve, squares). Dashed lines: isentropic curves ($s = 0.4$, 0.7, 0.75, 0.8), computed within DMFT. Dotted line: quasiparticle coherence scale $T_F^*(U)$. The DMFT results were obtained with QMC calculations (for T_N) and the IPT approximation [11] (for the isentropics). The transition curves are interpolations, continued at high U/t using the analytical expressions for the Heisenberg regime.

over at half filling). The Néel temperature displays a maximum at intermediate coupling, as a function of U/t. This is illustrated by Fig. 1, in which we display our calculation of T_N vs U/t, using the DMFT approximation on the cubic lattice and the quantum Monte Carlo (QMC) Hirsch-Fye algorithm. DMFT overestimates T_N by about 50% in the intermediate coupling regime, in comparison to the direct QMC calculations of Ref. [13] on the cubic lattice (also displayed in Fig. 1).

We now discuss how the entropy varies as the effective strength of the on-site interaction U/t is changed in the paramagnetic phase. Since all properties depend on the ratios T/t and U/t, we can consider that the hopping is fixed and that T and U are varied, or alternatively that both the temperature and coupling are measured in units of t, the natural unit of kinetic energy. Denoting by f and s the free energy and entropy per lattice site, respectively, one has $s = -\partial f/\partial T$ and $\partial f/\partial U = d$, with d the probability that a given site is doubly occupied: $d \equiv \langle n_{i\uparrow} n_{i\downarrow} \rangle$. We thus obtain

$$\frac{\partial s}{\partial U} = -\frac{\partial d}{\partial T}. \tag{2}$$

This equation can be used to discuss qualitatively the shape of the isentropic curves $T_i = T_i(U)$ in the (U, T) phase diagram, along which $s(T_i(U), U) = \text{const}$. Taking a derivative of this equation yields

$$c(T_i)\frac{\partial T_i}{\partial U} = T_i \frac{\partial d}{\partial T}\bigg|_{T=T_i}, \tag{3}$$

in which $c = T\partial s/\partial T$ is the specific heat per lattice site. Fortunately, the temperature dependence of the probability of double occupancy $d(T)$ has been studied in previous work by one of the authors [14,15] and others [16]. It was observed that, when U/t is not too large, the double occupancy first *decreases* as temperature is increased from $T = 0$ (indicating a higher degree of localization), and then turns around and grows again. This is shown in Fig. 2 using DMFT calculations. This apparently counterintuitive behavior is a direct analogue of the Pomeranchuk effect in liquid helium 3: Since the (spin) entropy is larger in a localized state than when the fermions form a Fermi liquid (in which $s \propto T$), it is favorable to increase the degree of localization upon heating. The minimum of $d(T)$ essentially coincides with the quasiparticle coherence scale $T_F^*(U)$, which is a rapidly decreasing function of U (Fig. 1). This phenomenon therefore applies only as long as $T_F^* > T_N$, and hence when U/t is not too large. For large U/t, Mott localization dominates for all temperatures $T < U$ and suppresses this effect. Since $\partial d/\partial T < 0$ for $T < T_F^*(U)$ while $\partial d/\partial T > 0$ for $T > T_F^*(U)$, Eq. (3) implies that the isentropic curves of the half-filled Hubbard model (for not too high values of the entropy) must have a negative slope at weak to intermediate coupling, before turning around at stronger coupling. In order to substantiate this behavior, inferred on rather general grounds, we have performed DMFT calculations of the isentropic curves, with results displayed in Fig. 1. The entropy $s(T)$ was calculated by integrating the internal energy per site $e(T)$ according to $s(T) = \ln 4 + e(T)/T - \int_T^\infty dT' e(T')/T'^2$, which follows from the thermodynamic relation $\partial_T e = T\partial_T s$. The DMFT equations were solved using the "iterated perturbation theory" (IPT) approximation [11] (using, for simplicity, a semicircular density of

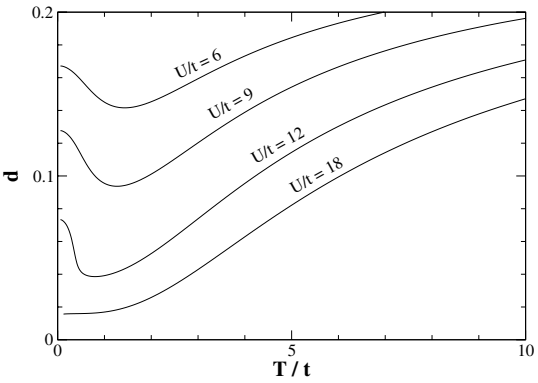

FIG. 2. Double occupancy $d = \langle n_{i\uparrow} n_{i\downarrow} \rangle$ as a function of temperature, for several values of U/t, calculated within DMFT (IPT). The initial decrease is the Pomeranchuk effect responsible for adiabatic cooling.

PRL 95, 056401 (2005) PHYSICAL REVIEW LETTERS week ending 29 JULY 2005

states), and the internal energy was calculated from the one-particle Green's function.

It is clear from the results of Fig. 1 that, starting from a low enough initial value of the entropy per site, adiabatic cooling can be achieved by either increasing U/t starting from a small value or decreasing U/t starting from a large value (the latter, however, requires one to cool down the gas while the lattice is already present). We emphasize that this cooling mechanism is an interaction-driven phenomenon: indeed, as U/t is increased, it allows one to lower the *reduced temperature* T/t, normalized to the natural scale for the Fermi energy in the presence of the lattice. Hence, cooling is not simply due to the tunneling amplitude t becoming smaller as the lattice is turned on. At weak coupling and low temperature, the cooling mechanism can be related to the effective mass of quasiparticles ($\propto 1/T_F^*$) becoming heavier as U/t is increased, due to Mott localization. Indeed, in this regime, the entropy is proportional to $T/T_F^*(U)$. Hence, conserving the entropy while increasing U/t adiabatically from $(U/t)_i$ to $(U/t)_f$ will reduce the final temperature in comparison to the initial one T_i according to $T_f/T_i = T_F^*(U_f)/T_F^*(U_i)$.

At this stage, let us briefly discuss the validity of the DMFT approach, extensively used in the present work. In this approach, the lattice model is mapped onto a single-site quantum problem coupled to a self-consistent effective medium. This is an approximation, which becomes exact only in the limit of infinite lattice coordination [11]. As a local approach, it underestimates the precursor antiferromagnetic correlations above T_N, which will in turn quench the entropy and ultimately play against the cooling mechanism very close to T_N. However, as long as the correlation length is not too large, a local approximation should be accurate. Indeed, the existence of a minimum in $d(T)$ has been confirmed by the calculations of Ref. [17] using a different method, for a three-dimensional lattice, suggesting that the cooling mechanism discussed here is a robust effect.

The isentropic curves in Fig. 1 suggest that interaction-induced adiabatic cooling could be used in order to reach the magnetically ordered phase. To explore this idea in more details, we focus on the entropy along the Néel critical boundary $s_N(U) \equiv s(T_N(U), U)$. At weak coupling (the spin-density wave regime), $s_N(U)$ is expected to be exponentially small. In contrast, in the opposite Heisenberg regime of large U/t, s_N will reach a finite value s_H, which is the entropy of the quantum Heisenberg model at its critical point. s_H is a pure number which depends only on the specific lattice of interest. Mean-field theory of the Heisenberg model yields $s_H = \ln 2$, but quantum fluctuations will reduce this number. We have performed a Schwinger boson calculation of this quantity, along the lines of [18,19], and found that this reduction is of the order of 50% on the cubic lattice. How does s_N evolve from weak to strong coupling? A rather general argument suggests that it should go through a maximum $s_{\max} > s_H$. In order to see this, we use again (2) and take a derivative of $s_N = s(T_N(U), U)$, which yields

$$\frac{ds_N}{dU} = \frac{c(T_N)}{T_N}\frac{dT_N}{dU} - \left.\frac{\partial d}{\partial T}\right|_{T=T_N}. \quad (4)$$

If only the first term was present on the right-hand side of this equation, it would imply that s_N is maximum exactly at the value of the coupling where T_N is maximum [note that $c(T_N)$ is finite ($\alpha < 0$) for the 3D Heisenberg model [20]]. However, in view of the above properties of the double occupancy, the second term on the right-hand side has a similar variation than the first one: it starts positive, and then changes sign at an intermediate coupling when $T_F^*(U) = T_N(U)$. These considerations suggest that $s_N(U)$ does reach a maximum value at intermediate coupling, in the same regime where T_N reaches a maximum. Hence, $s_N(U)$ has the general form sketched in Fig. 3. This figure can be viewed as a phase diagram of the half-filled Hubbard model, in which *entropy itself is used as a thermometer*, a very natural representation when addressing adiabatic cooling. Experimentally, one may first cool down the gas (in the absence of the optical lattice) to a temperature where the entropy per particle is lower than s_H (this corresponds to $T/T_F < s_H/\pi^2$ for a trapped ideal gas). Then, by branching on the optical lattice adiabatically, one could increase U/t until one particle per site is reached over most of the trap: this should allow one to reach the antiferromagnetic phase. Assuming that the time scale for adiabaticity is simply set by the hopping, we observe that typically $\hbar/t \sim 1$ ms.

Let us now discuss the conditions under which two-component fermions in an optical lattice are accurately described by the Hubbard Hamiltonian (1) (see also [1,3]). The many-body Hamiltonian is written in second-

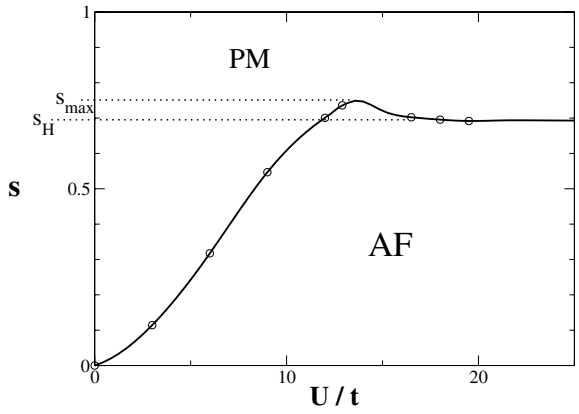

FIG. 3. Phase diagram as a function of entropy. The displayed curve results from a DMFT-IPT calculation (in which case $s_H = \ln 2$), but its shape is expected to be general (with s_H reduced by quantum fluctuations).

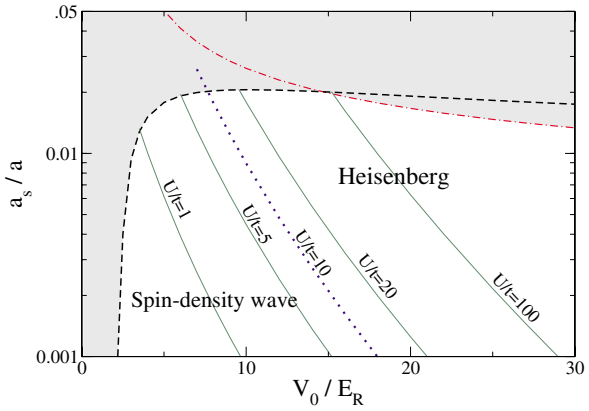

FIG. 4 (color online). Spin-density wave and Heisenberg regimes as a function of the depth of the periodic potential V_0 and the scattering length a_s. The crossover between these regimes is indicated by the dotted line ($U/t = 10$), where T_N/t is maximum (other contour lines are also indicated). In the shaded region, the one-band Hubbard description is no longer valid. Above the dashed line ($U/\Delta > 0.1$), other bands must be taken into account and the pseudopotential approximation fails. Above the dashed-dotted line, non-Hubbard interaction terms become sizeable ($t_d/t > 0.1$, see text).

quantized form using as single-particle basis functions the Wannier functions associated with the periodic potential $V_{\text{opt}}(\vec{r}) = V_0 \Sigma_{i=1}^{3} \sin^2(\pi x_i/a)$ (the lattice spacing is $a = \lambda/2$, with λ the wavelength of the laser). The interaction terms are obtained as matrix elements of the low-energy effective potential $V_{\text{int}}(\vec{r}_1 - \vec{r}_2) = \frac{4\pi\hbar^2 a_s}{m} \delta^3(\vec{r}_1 - \vec{r}_2)$, where a_s is the scattering length. In general, this results in a multiband model which, besides the on-site Hubbard interaction, involves also more complicated interaction terms such as nearest-neighbor interactions or density-assisted hopping terms of the form $t_d c_i^\dagger c_j n_i$, with i and j neighboring sites. By explicitly computing these terms, as well as the one-body part of the Hamiltonian, we examined under which conditions (i) the reduction to a one-band model is valid and (ii) these non-Hubbard interactions are negligible. This determines a domain in the $(V_0/E_R, a_s/a)$ plane (with $E_R = \hbar^2\pi^2/2ma^2$ the recoil energy), which is depicted in Fig. 4. Condition (i) requires, in particular, that the on-site Hubbard repulsion is smaller than the gap Δ between the first and the second band: $U \ll \Delta$. At large values of V_0/E_R, it can be shown that this is also the condition for our use of the pseudopotential approximation to be valid: $a_s \ll l_0$, with l_0 the spatial extension of the Wannier function of the first band. We found that the stricter condition of type (ii) originates from density-assisted hopping terms which should obey $t_d \ll t$. We also displayed in Fig. 4 some contour lines associated with a given value of U/t. The one associated with $U/t \approx 10$ can be taken as the approximate separatrix between the spin-density wave and Heisenberg antiferromagnetic regions. T_N/t is maximal along this line, and $T_N < 0.015E_R$ in the allowed region. Thus adiabatic cooling is important to reach the AF phase. Since V_0 and a_s are the two experimentally tunable parameters, Fig. 4 aims at summarizing useful information for such experimental investigations. The detection of the antiferromagnetic long-range order might be achieved by spin-selective Bragg spectroscopy in order to reveal the doubling of the unit cell. The two hyperfine states could be distinguished by their Zeeman splitting or by using polarized light. A different method, which has been recently proposed [21] and investigated experimentally [22], is to use quantum noise interferometry.

To summarize, in this Letter we propose an interaction-induced cooling mechanism for two-component cold fermions in an optical lattice. One possible application of this mechanism is in reaching the phase with antiferromagnetic long-range order.

We are grateful to C. Salomon and F. Chevy for encouragement and several discussions. We also thank S. Biermann, I. Bloch, Y. Castin, J. Dalibard, E. Demler, W. Krauth, F. Lechermann, L. Tarruell, and A.-M. Tremblay. We acknowledge the support of an AC-Nanosciences "Gaz quantiques" (Project No. 201), the IFCPAR (Project No. 2404-1), CNRS, and Ecole Polytechnique.

[1] D. Jaksch and P. Zoller, cond-mat/0410614.
[2] M. Greiner *et al.*, Nature (London) **415**, 39 (2002).
[3] D. Jaksch *et al.*, Phys. Rev. Lett. **81**, 3108 (1998).
[4] M. Greiner *et al.*, Nature (London) **426**, 537 (2003).
[5] S. Jochim *et al.*, Science **302**, 2101 (2003).
[6] M. W. Zwierlein *et al.*, Phys. Rev. Lett. **91**, 250401 (2003).
[7] T. Bourdel *et al.*, Phys. Rev. Lett. **93**, 050401 (2004).
[8] M. Köhl *et al.*, Phys. Rev. Lett. **94**, 080403 (2005).
[9] P. B. Blakie and A. Bezett, Phys. Rev. A **71**, 033616 (2005).
[10] W. Hofstetter *et al.*, Phys. Rev. Lett. **89**, 220407 (2002).
[11] A. Georges *et al.*, Rev. Mod. Phys. **68**, 13 (1996).
[12] A. Georges, in *Lectures on the Physics of Highly Correlated Electron Systems VIII*, edited by A. Avella and F. Mancini (American Institute of Physics, New York, 2004).
[13] R. Staudt *et al.*, Eur. Phys. J. B **17**, 411 (2000).
[14] A. Georges and W. Krauth, Phys. Rev. Lett. **69**, 1240 (1992).
[15] A. Georges and W. Krauth, Phys. Rev. B **48**, 7167 (1993).
[16] M. J. Rozenberg *et al.*, Phys. Rev. Lett. **83**, 3498 (1999).
[17] A.-M. Daré and G. Albinet, Phys. Rev. B **61**, 4567 (2000).
[18] D. Arovas and A. Auerbach, Phys. Rev. B **38**, 316 (1988).
[19] A. Auerbach, *Interacting Electrons and Quantum Magnetism* (Springer, New York, 1994).
[20] K. Chen *et al.*, Phys. Rev. B **48**, 3249 (1993).
[21] E. Altman *et al.*, Phys. Rev. A **70**, 013603 (2004).
[22] S. Fölling *et al.*, Nature (London) **434**, 481 (2005).

Chapter 9

Heisenberg model in 2 dimensions

This Chapter results from discussions with Prof. Alejandro Muramatsu.

1 Introduction

In this short Chapter, we consider the 2-dimensional antiferromagnetic Heisenberg model, which is the strong-coupling limit of the fermionic Hubbard model, and therefore relevant to experiments with cold fermionic atoms in optical lattices (see e. g. Article VI). The Heisenberg model could also be realized using bosonic atoms with two species or two internal states [134, 135]. We restrict to a cubic lattice. We shall use existing numerical results in order to obtain the relation $S(\xi)$ between entropy and correlation length. Entropy is conserved when the optical lattice depth or the scattering length is slowly changed (see e. g. [136] and Article VI). This allowed to measure entropy for a unitary gas, by going adiabatically to a weakly interacting regime where the temperature can be deduced from a time of flight image and where the relation between entropy and temperature is simple [48, 137]. The value of the entropy in a given situation gives a good indication of how hard experimentalists will have to cool in order to reach this situation. More generally, if the dependence of some measurable quantity on entropy is known, then this quantity can be used as "thermometer". Of course, entropy is only conserved if one can neglect the effects of evaporation and heating, which were studied in [138].

The spin structure factor, i. e. the Fourier transform of the spin-spin correlation function, is in principle measurable using the noise-correlation technique [139, 140, 141] or Bragg scattering [142], which makes the correlation length ξ experimentally relevant. If ξ becomes larger than the system size (the number of lattice sites occupied by an atom), then finite-size effects become important, and the system can be expected to behave as if it was antiferromagnetically ordered. This is similar to the physics of quasicondensates [143, 11].

2 Relation between entropy and correlation length

The Hamiltonian of the Heisenberg model is

$$H = J \sum_{\langle i,j \rangle} \vec{S}_i \cdot \vec{S}_j, \tag{9.1}$$

where $\vec{S}_i$ is the spin operator on site i, and each pair of nearest-neighbor sites is counted once in the sum. In the considered antiferromagnetic case, $J > 0$. We take units in which the Boltzmann

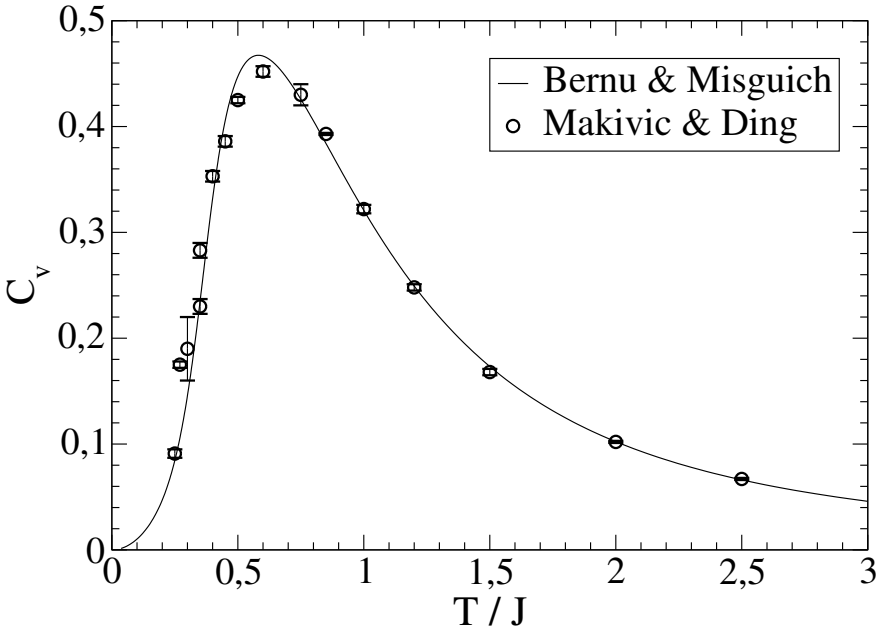

FIGURE 9.1 – Specific heat per spin. Continuous line : interpolation scheme of Bernu and Misguich [4]. Squares : QMC of Makivić and Ding [144].

constant k_B equals 1.

Bernu and Misguich have calculated the specific heat $C_V(T)$ using an interpolation scheme, which incorporates a value of the ground state energy coming from Quantum Monte-Carlo (QMC) simulations, the known properties that C_V is proportionnal to T^2 at low T and that $S(T \to \infty) = \ln 2$, and a high temperature series expansion [4]. There is no garantee that the interpolation method becomes exact in the limit where the order of the high-temperature expansion and of the Padé approximant used for the interpolation tends to infinity. However the results compare well with QMC calculations, as has been tested for several models [4]. In Fig. 9.1 we compare the result of Bernu and Misguich with the QMC of Makivić and Ding [144]. The error bars in the QMC have not been evaluated systematically for every point, but they increase at low T.

We then integrate the function $C_V(T)$ obtained by Bernu and Misguich to get the entropy per lattice site

$$S(T) = \int_0^T \frac{C_V(T')}{T'} dT', \tag{9.2}$$

and the result is plotted in Fig. 9.2.

The correlation length ξ can be defined in the limit of an infinite system by [144] :

$$\ln \left[(-1)^r \langle \vec{S}_{(0,0)} \cdot \vec{S}_{(r,0)} \rangle \right] \underset{r \to \infty}{\sim} -\frac{r}{\xi}. \tag{9.3}$$

The QMC of Makević and Ding is fitted very well by the formula :

$$\xi(T) = A e^{2\pi\rho_s/T} \tag{9.4}$$

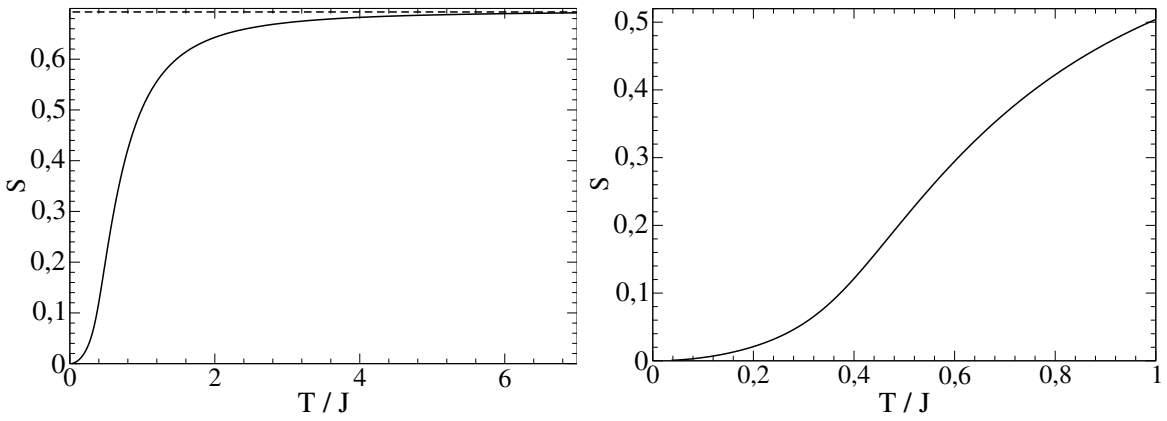

FIGURE 9.2 – Entropy per spin obtained by integrating the function $C_V(T)$ calculated by Bernu and Misguich [4]. In the left graph, the dashed line is $S(T \to \infty) = \ln 2$. The right graph is a zoom on the low temperature region.

in the region $1/4 < T/J < 1$ where the calculation was done, and the fit gives

$$A = 0.276(6) \tag{9.5}$$

$$\rho_s = [0.199(2)]J. \tag{9.6}$$

More recent accurate QMC calculations were performed by Kim and Troyer [145]. They find deviations from the fitting formula of Makević and Ding Eqs. (9.4,9.5,9.6), both at sufficiently high and at sufficiently low temperature. Eq. (9.4) is expected to be asymptotically exact for $T \to 0$, but the asymptotic regime is only reached for very small T, and the parameters A and ρ_s are not precisely given by Eqs. (9.5,9.6) [145]. However, we will restrict to the intermediate temperature range $0.25 \lesssim T/J \lesssim 0.6$ (where $2 \lesssim \xi \lesssim 40$), and we will stick for simplicity to the fitting formula of Makević and Ding Eqs. (9.4), which agrees quite well with the QMC data of Kim and Troyer in this temperature range, see Fig. 9.3.

By combining this $\xi(T)$ [Eqs. (9.4,9.5,9.6)] with the function $S(T)$ obtained above, we immediately get the function $S(\xi)$ shown in Fig. 9.4.

3 Discussion

In order to have a correlation length ξ larger than typical experimental system sizes, say $\xi \gtrsim 20$, one has to reach very low entropies, $S \lesssim 0.05$. This is one order of magnitude below the lowest value of the entropy measured in [137], $S \sim 0.6$. Thus it looks difficult to obtain antiferromagnetic order over the hole system in $2D$. The situation is more favorable in $3D$, where ξ diverges at the Néel temperature T_N, at an estimated entropy $S(T_N) \sim 0.3$ (Article VI). In $2D$, for $S = 0.3$, the correlation length is only $\xi \simeq 2$ (Fig. 9.4), which may be too small to be measurable via the spin structure factor.

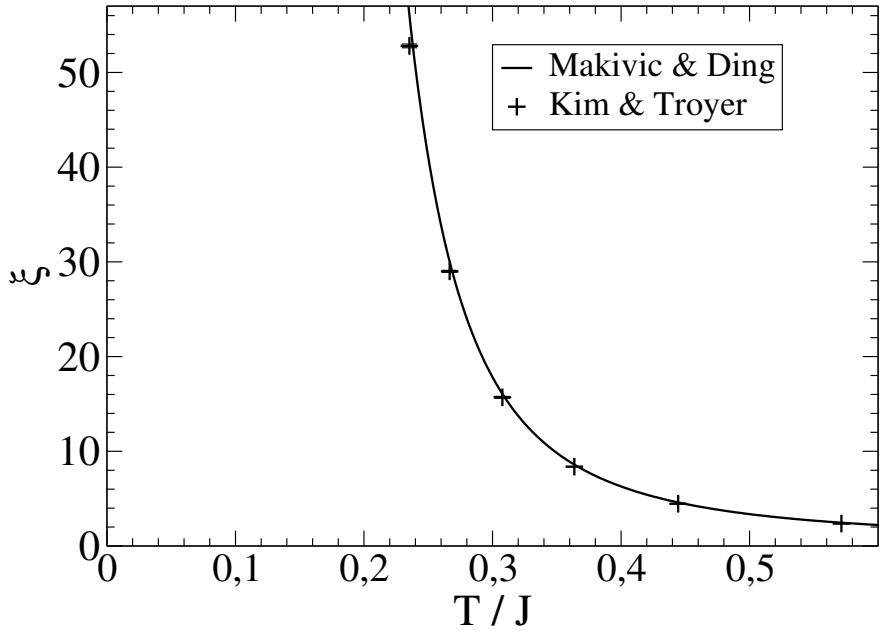

FIGURE 9.3 – Correlation length $\xi(T)$. Continuous line : simple fitting formula of Makivić and Ding. Crosses : QMC of Kim and Troyer [145].

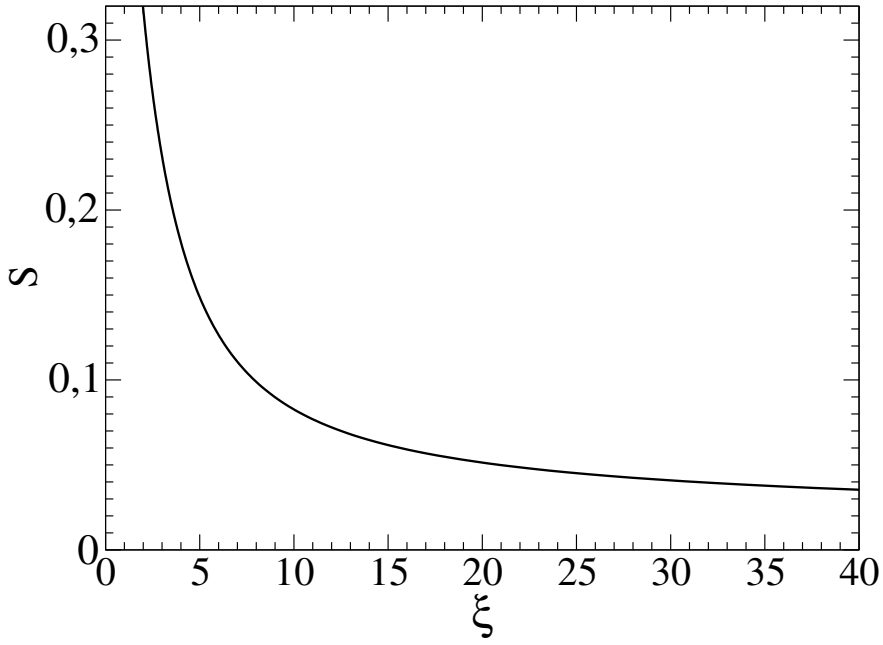

FIGURE 9.4 – Entropy per spin S as a function of the correlation length ξ.

Conclusion générale

La limite unitaire n'est pas seulement le point central de la transition BEC-BCS où les corrélations sont particulièrement fortes. C'est aussi le point où le gaz possède des propriétés exactes très simples.

Ces propriétés s'expriment naturellement en fonction de l'hyperrayon et des hyperangles. [1] Dans un piège isotrope, le problème à N corps se sépare en problème hyperradial et problème hyperangulaire.

On peut comparer ceci au problème d'une particule dans un potentiel isotrope, qui se sépare en problème radial et problème angulaire, les fonctions propres du problème angulaire étant les harmoniques sphériques. Le problème radial contient alors un potentiel effectif $\propto l(l+1)/r^2$, déterminé par le nombre quantique l provenant du problème angulaire.

Dans le cas du problème à N corps unitaire, le problème hyperradial contient un potentiel effectif $\propto s^2/R^2$, où R est l'hyperrayon, et s est un nombre réel provenant du problème hyperangulaire. Ceci nous a permis de résoudre le problème hyperradial. Le spectre du problème hyperradial coïncide avec celui du problème à N corps, et est constitué d'échelles dont les barreaux sont équidistants de $2\hbar\omega$. Les états propres d'une même échelle ont la même fonction d'onde hyperangulaire, et les fonctions d'onde hyperradiales ont une expression simple et fonction de s et du nombre quantique q qui numérote les barreaux. Ce nombre q a aussi le sens suivant : le gaz possède un mode collectif de respiration qui correspond à une simple oscillation de la taille du nuage, ce mode est bosonique, et q est le nombre de telles excitations bosoniques. Ce mode étant découplé des autres degrés de liberté du gaz, à savoir des hyperangles, on comprend qu'il puisse osciller sans s'amortir [31]. Ces propriétés sont liées à une symétrie dynamique $SO(2,1)$.

Pour 3 particules, le problème hyperradial a été résolu par Efimov. Nous en avons déduit la solution complète du problème à 3 corps. Pour 3 bosons, il existe une valeur de s imaginaire pure, qui conduit à un potentiel effectif $\propto -|s|^2/R^2$ qui attire les 3 particules vers le même point. Ceci implique l'existence des trimères d'Efimov, dont la fonction d'onde oscille avec un vecteur d'onde et une amplitude qui divergent dans la limite $R \to 0$ où les 3 particules sont proches, d'où un fort taux de pertes à 3 corps et la nécessité d'introduire un paramètre à 3 corps. Cependant, il existe aussi une infinité d'autres valeurs de s qui sont réelles, conduisant à des états propres dans le piège qui, de même que les états propres de 3 fermions, sont universels, et ont un faible taux de pertes.

La détermination de ce taux de pertes s'est révélée plus difficile que prévu. Nous avons montré numériquement qu'il est nécessaire de tenir compte des corrections dues à la portée finie des interactions, qui couplent les états universels aux états efimoviens. Cependant ce couplage doit tendre vers zéro dans la limite de portée nulle, et le taux de pertes reste généralement très faible. Ceci devrait permettre de stabiliser 3 atomes bosoniques à la limite unitaire aux nœuds d'un réseau optique profond.

Nous espérons obtenir des résultats plus généraux sur ce couplage et sur la durée de vie, en poussant plus loin notre étude analytique des déviations par rapport au cas exactement soluble dues à une portée non nulle des interactions, à une longueur de diffusion finie ou à une anisotropie

1. Rappelons que si l'on multiplie les coordonnées de toutes les particules par un même facteur, alors l'hyperrayon est multiplié par ce même facteur, et les hyperangles ne changent pas.

du piège. Nous comptons également généraliser l'étude des résonances à N corps présentée ici. Une autre voie est l'étude du problème à N corps unitaire dans un réseau optique profond, qui est directement relié aux problèmes à 2 et 3 corps dans un piège harmonique.

Bibliographie

[1] M. Stoll and T. Köhler, "Production of three-body Efimov molecules in an optical lattice", *Phys. Rev. A* **72**, 022714 (2005).

[2] T. Kraemer, M. Mark, P. Waldburger, J. G. Danzl, C. Chin, B. Engeser, A. D. Lange, K. Pilch, A. Jaakkola, H.-C. Naegerl and R. Grimm, "Evidence for Efimov quantum states in an ultracold gas of caesium atoms", *Nature* **440**, 315 (2006).

[3] J. von Stecher, C. H. Greene and D. Blume, "Energetics and Structural Properties of Trapped Two-Component Fermi Gases", *Phys. Rev. A* **77**, 043619 (2008).

[4] B. Bernu and G. Misguich, "Specific heat and high-temperature series of lattice models : interpolation scheme and examples on quantum spin systems in one and two dimensions", *Phys. Rev. B* **63**, 134409 (2001).

[5] E. Tiesinga, B. J. Verhaar and H. T. C. Stoof, "Threshold and resonance phenomena in ultracold ground-state collisions", *Phys. Rev. A* **47**, 4114–4122 (1993).

[6] S. Inouye, M. R. Andrews, J. Stenger, H.-J. Miesner, D. M. Stamper-Kurn and W. Ketterle, "Observation of Feshbach resonances in a Bose-Einstein condensate", *Nature* **392**, 151 (1998).

[7] K. M. O'Hara, S. L. Hemmer, M. E. Gehm, S. R. Granade and J. E. Thomas, "Observation of a Strongly Interacting Degenerate Fermi Gas of Atoms", *Science* **298**, 2179 (2002).

[8] C. A. Regal and D. S. Jin, "Measurement of Positive and Negative Scattering Lengths in a Fermi Gas of Atoms", *Phys. Rev. Lett.* **90**, 230404 (2003).

[9] T. Bourdel, J. Cubizolles, L. Khaykovich, K. M. F. Magalhaes, S. J. J. M. F. Kokkelmans, G. V. Shlyapnikov and C. Salomon, "Measurement of interactions energy near a Feshbach resonance in a ^{6}Li Fermi gas", *Phys. Rev. Lett.* **91**, 020402 (2003).

[10] *Proceedings of the International School of Physics "Enrico Fermi" on Ultra-Cold Fermi gases, edited by M. Inguscio, W. Ketterle and C. Salomon*, SIF, Bologna (2007).

[11] I. Bloch, J. Dalibard and W. Zwerger, "Many-Body Physics with Ultracold Gases", *Rev. Mod. Phys.* **80**, 885 (2008).

[12] S. Giorgini, L. P. Pitaevskii and S. Stringari, "Theory of ultracold Fermi gases", *Rev. Mod. Phys.* **80**, 1215 (2008).

[13] E. Wigner, "Über die Streuung von Neutronen an Protonen", *Zeits. f. Physik* **83**, 253 (1933).

[14] H. Bethe and R. Peierls, "Quantum Theory of the Diplon", *Proc. R. Soc. London, Ser. A* **148**, 146 (1935).

[15] E. Braaten and H.-W. Hammer, "Universality in few-body systems with large scattering length", *Physics Reports* **428**, 259 (2006).

[16] V. N. Efimov, "Weakly-bound states of three resonantly interating particles", *Yad. Fiz.* **12**, 1080 (1970), [Sov. J. Nucl. Phys. **12**, 589 (1971)].

[17] J. Stenger, S. Inouye, M. R. Andrews, H.-J. Miesner, D. M. Stamper-Kurn and W. Ketterle, "Strongly Enhanced Inelastic Collisions in a Bose-Einstein Condensate near Feshbach Resonances", *Phys. Rev. Lett.* **82**, 2422–2425 (1999).

[18] J. L. Roberts, N. R. Claussen, S. L. Cornish and C. E. Wieman, "Magnetic Field Dependence of Ultracold Inelastic Collisions near a Feshbach Resonance", *Phys. Rev. Lett.* **85**, 728–731 (2000).

[19] A. Marte, T. Volz, J. Schuster, S. Dürr, G. Rempe, E. G. M. van Kempen and B. J. Verhaar, "Feshbach Resonances in Rubidium 87 : Precision Measurement and Analysis", *Phys. Rev. Lett.* **89**, 283202 (2002).

[20] T. Weber, J. Herbig, M. Mark, H.-C. Nägerl and R. Grimm, "Three-Body Recombination at Large Scattering Lengths in an Ultracold Atomic Gas", *Phys. Rev. Lett.* **91**, 123201 (2003).

[21] C. A. Regal, M. Greiner and D. S. Jin, "Lifetime of Molecule-Atom Mixtures near a Feshbach Resonance in ^{40}K", *Phys. Rev. Lett.* **92**, 083201 (2004).

[22] T. Bourdel, L. Khaykovich, J. Cubizolles, J. Zhang, F. Chevy, M. Teichmann, L. Tarruell, S. J. J. M. F. Kokkelmans and C. Salomon, "Experimental Study of the BEC-BCS Crossover Region in Lithium 6", *Phys. Rev. Lett.* **93**, 050401 (2004).

[23] D. S. Petrov, C. Salomon and G. V. Shlyapnikov, "Weakly Bound Dimers of Fermionic Atoms", *Phys. Rev. Lett.* **93**, 090404 (2004).

[24] D. S. Petrov, C. Salomon and G. V. Shlyapnikov, "Diatomic molecules in ultracold Fermi gases - Novel composite bosons", *J. Phys. B* **38**, S645 (2005).

[25] S. B. Papp, J. M. Pino, R. J. Wild, S. Ronen, C. E. Wieman, D. S. Jin and E. A. Cornell, "Bragg spectroscopy of a strongly interacting ^{85}Rb Bose-Einstein condensate", *Phys. Rev. Lett.* **101**, 135301 (2008).

[26] E. Braaten and H.-W. Hammer, "Efimov Physics in Cold Atoms", *Ann. Phys.* **322**, 120 (2007).

[27] E. Braaten, H.-W. Hammer and T. Mehen, "The Dilute Bose-Einstein Condensate with Large Scattering Length", *Phys. Rev. Lett.* **88**, 040401 (2002).

[28] D. Blume, J. von Stecher and C. H. Greene, "Universal Properties of a Trapped Two-Component Fermi Gas at Unitarity", *Phys. Rev. Lett.* **99**, 233201 (2007).

[29] T. Stöferle, H. Moritz, K. Günter, M. Köhl and T. Esslinger, "Molecules of Fermionic Atoms in an Optical Lattice", *Phys. Rev. Lett.* **96**, 030401 (2006).

[30] C. Ospelkaus, S. Ospelkaus, L. Humbert, P. Ernst, K. Sengstock and K. Bongs, "Ultracold Heteronuclear Molecules in a 3D Optical Lattice", *Phys. Rev. Lett.* **97**, 120402 (2006).

[31] Y. Castin, "Exact scaling transform for a unitary quantum gas in a time dependent harmonic potential", *Comptes Rendus Physique* **5**, 407 (2004).

[32] Y. Castin, *in : Proceedings of the International School of Physics "Enrico Fermi" on Ultra-Cold Fermi gases, edited by M. Inguscio, W. Ketterle and C. Salomon*, SIF, Bologna (2007).

[33] T. Busch, B. G. Englert, K. Rzazewski and M. Wilkens, "Two Cold Atoms in a Harmonic Trap", *Found. Phys.* **28**, 549 (1998).

[34] S. Albeverio, F. Gesztesy, R. Hoegh-Krohn and H. Holden, *Solvable models in quantum mechanics*, Springer-Verlag, Berlin (1988).

[35] M. Jona-Lasinio, L. Pricoupenko and Y. Castin, "Three fully polarized fermions close to a p-wave Feshbach resonance", *Phys. Rev. A* **77**, 043611 (2008).

[36] M. Reed and B. Simon, *Methods of modern mathematical physics 1 : functional analysis*, Academic Press (1980).

[37] S. Y. Chang and G. F. Bertsch, "Unitary Fermi gas in a harmonic trap", *Phys. Rev. A* **76**, 021603 (2007).

[38] T. Köhler, K. Góral and P. S. Julienne, "Production of cold molecules via magnetically tunable Feshbach resonances", *Rev. Mod. Phys.* **78**, 1311 (2006).

[39] J. Carlson, S.-Y. Chang, V. R. Pandharipande and K. E. Schmidt, "Superfluid Fermi Gases with Large Scattering Length", *Phys. Rev. Lett.* **91**, 050401 (2003).

[40] G. E. Astrakharchik, J. Boronat, J. Casulleras and S. Giorgini, "Equation of State of a Fermi Gas in the BEC-BCS Crossover : A Quantum Monte Carlo Study", *Phys. Rev. Lett.* **93**, 200404 (2004).

[41] J. R. Engelbrecht, M. Randeria and C. A. R. Sá de Melo, "BCS to Bose crossover : Broken-symmetry state", *Phys. Rev. B* **55**, 15153–15156 (1997).

[42] O. Juillet, "Sign-free stochastic mean-field approach to strongly correlated phases of ultracold fermions", *New J. Phys.* **9**, 163 (2007).

[43] D. Lee, *Phys. Rev. B* **73**, 11511 (2006).

[44] M. Bartenstein, A. Altmeyer, S. Riedl, S. Jochim, R. Geursen, C. Chin, J. H. Denschlag and R. Grimm, *in Proceedings of the XIX International Conference on Atomic Physics (America Institute of Physics, Melville, NY, 2004) ; arXiv :cond-mat/0412712* .

[45] L. Tarruell, M. Teichmann, J. McKeever, T. Bourdel, J. Cubizolles, L. Khaykovich, J. Zhang, N. Navon, F. Chevy and C. Salomon, *Expansion of an ultra-cold lithium gas in the BEC-BCS crossover, in : Proceedings of the International School of Physics "Enrico Fermi" on Ultra-Cold Fermi gases, edited by M. Inguscio, W. Ketterle and C. Salomon*, SIF, Bologna (2007).

[46] J. Kinast, A. Turlapov, J. Thomas, Q. Chen, J. Stajic and K. Levin, "Heat Capacity of a Strongly Interacting Fermi Gas", *Science* **307**, 1296 (2005).

[47] G. B. Partridge, W. Li, R. I. Kamar, Y. Liao and R. G. Hulet, "Pairing and Phase Separation in a Polarized Fermi Gas", *Science* **311**, 503 (2006).

[48] J. T. Stewart, J. P. Gaebler, C. A. Regal and D. S. Jin, "Potential Energy of a 40 K Fermi Gas in the BCS-BEC Crossover", *Phys. Rev. Lett.* **97**, 220406 (2006).

[49] S. Y. Chang, V. R. Pandharipande, J. Carlson and K. E. Schmidt, "Quantum Monte Carlo studies of superfluid Fermi gases", *Phys. Rev. A* **70**, 043602 (2004).

[50] J. M. Blatt and V. F. Weisskopf, *Theoretical Nuclear Physics*, Wiley, New York (1952).

[51] B. M. Fregoso and G. Baym, *Phys. Rev. A* **73**, 043616 (2006).

[52] E. Burovski, N. Prokof'ev, B. Svistunov and M. Troyer, "Critical Temperature and Thermodynamics of Attractive Fermions at Unitarity", *Phys. Rev. Lett.* **96**, 160402 (2006).

[53] E. Burovski, N. Prokof'ev, B. Svistunov and M. Troyer, "Erratum : Critical Temperature and Thermodynamics of Attractive Fermions at Unitarity [Phys. Rev. Lett. **96**, 160402 (2006)]", *Phys. Rev. Lett.* **97**, 239902 (2006).

[54] E. Burovski, N. Prokof'ev, B. Svistunov and M. Troyer, "The Fermi-Hubbard model at unitarity", *New J. Phys.* **8**, 153 (2006).

[55] A. Bulgac, J. E. Drut and P. Magierski, "Spin 1/2 Fermions in the Unitary Regime : A Superfluid of a New Type", *Phys. Rev. Lett.* **96**, 090404 (2006).

[56] Y. Castin, *Simple theoretical tools for low dimension Bose gases*, Lecture notes of the 2003 Les Houches Spring School, Quantum Gases in Low Dimensions, Olshanii M., Perrin H., Pricoupenko L. Eds., J. Phys. IV France 116 (2004) 89-132.

[57] C. Mora and Y. Castin, "Extension of Bogoliubov theory to quasicondensates", *Phys. Rev. A* **67**, 053615 (2003).

[58] L. Pricoupenko and Y. Castin, "Three fermions in a box at the unitary limit : universality in a lattice model", *J. Phys. A* **40**, 12863 (2007).

[59] S. Tan, "Short Range Scaling Laws of Quantum Gases With Contact Interactions", *arXiv :cond-mat/0412764* .

[60] L. H. Thomas, "The Interaction Between a Neutron and a Proton and the Structure of ^{3}H", *Phys. Rev.* **47**, 903 (1935).

[61] R. L. Pease and H. Feshbach, "Binding Energy of the Triton", *Phys. Rev.* **81**, 142–143 (1951).

[62] G. S. Danilov, "On the three-body problem with short-range forces", *JETP* 40*, 498 (1961) [Sov. Phys. JETP* **13***, 349 (1961)]* .

[63] R. A. Minlos and L. D. Faddeev, "Comment on the problem of three particles with point interactions", *JETP* **41**, 1850 (1961) [*Sov. Phys. JETP* **14**, 1315 (1962)] .

[64] R. A. Minlos and L. D. Faddeev, "On the point interaction for a three-particle system in quantum mechanics", *DAN SSSR* **141**, 1335 (1961) [*Sov. Phys. Dokl.* **6**, 1072 (1962)] .

[65] R. D. Amado and J. V. Noble, *Phys. Lett* **35B**, 25 (1971).

[66] R. D. Amado and J. V. Noble, *Phys. Rev. D* **5**, 1992 (1972).

[67] S. Albeverio, R. Høegh-Krohn and T. T. Wu, "A class of exactly solvable three-body quantum mechanical problems and universal low energy behavior", *Phys. Lett. A* **83**, 105 (1981).

[68] S. Albeverio, S. N. Lakaev and Z. I. Muminov, *Ann. Henri Poincaré* **5**, 743 (2004).

[69] S. Jonsell, H. Heiselberg and C. J. Pethick, "Universal Behavior of the Energy of Trapped Few-Boson Systems with Large Scattering Length", *Phys. Rev. Lett.* **89**, 250401 (2002).

[70] D. S. Petrov, "Three-Boson Problem near a Narrow Feshbach Resonance", *Phys. Rev. Lett.* **93**, 143201 (2004).

[71] L. Pricoupenko, "Pseudopotential in resonant regimes", *Phys. Rev. A* **73**, 012701 (2006).

[72] A. O. Gogolin, C. Mora and R. Egger, "Analytical solution of the bosonic three-body problem", *Phys. Rev. Lett.* **100**, 140404 (2008).

[73] L. Pricoupenko, "Modeling Interactions for Resonant p-Wave Scattering", *Phys. Rev. Lett.* **96**, 050401 (2006).

[74] V. Efimov, "Energy levels of three resonantly interacting particles", *Nucl. Phys.* **A 210**, 157 (1973).

[75] M. Abramowitz and I. A. Stegun, *eds., Handbook of Mathematical Functions With Formulas, Graphs, and Mathematical Tables*, Applied Mathematics Series 55, National Bureau of Standards, Washington, DC (1970), ninth printing.

[76] I. S. Gradshteyn and I. M. Ryzhik, *Tables of integrals, series, and products*, Academic Press (1994), 5th Edition, A. Jeffrey, Editor.

[77] F. Werner and Y. Castin, "A unitary quantum gas in a harmonic trap : exact mapping to free space zero energy eigenstates and application to the three-body problem", *cond-mat/0507399v1* .

[78] K. M. Case, "Singular Potentials", *Phys. Rev.* **80**, 797 (1950).

[79] P. Morse and H. Feshbach, *Methods of Theoretical Physics*, tome II, Mc Graw-Hill (1953), p. 1665.

[80] L. D. Landau and E. M. Lifschitz, *Quantenmechanik*, Akademie-Verlag, Berlin (1985).

[81] M. D. Lee, T. Köhler and P. S. Julienne, "Excited Thomas-Efimov levels in ultracold gases", *Phys. Rev. A* **76**, 012720 (2007).

[82] G. V. Skorniakov and K. A. Ter-Martirosian, "Three Body Problem for Short Range Forces. I. Scattering of Low Energy Neutrons dy Deuterons", *JETP* **31**, 775 (1956) [*Sov. Phys. JETP* **4**, 648 (1957)] .

[83] B. Marcelis, S. J. J. M. F. Kokkelmans, G. V. Shlyapnikov and D. S. Petrov, "Collisional properties of weakly bound heteronuclear dimers", *Phys. Rev. A* **77**, 032707 (2008).

[84] Y. Alhassid, G. Bertsch and L. Fang, *arXiv :0706.4085v1* .

[85] I. Stetcu, B. R. Barrett, U. van Kolck and J. P. Vary, *Phys. Rev. A* **76**, 063613 (2007).

[86] G. Gasaneo and J. H. Macek, *J. Phys. B* **35**, 2239 (2002).

[87] M. C. Birse, "Renormalization-group analysis of repulsive three-body systems", *J. Phys. A* **39**, L49 (2006).

[88] D. S. Petrov, "Three-body problem in Fermi gases with short-range interparticle interaction", *Phys. Rev. A* **67**, 010703 (2003).

[89] R. B. Laughlin, *Phys. Rev. Lett.* **50**, 1395 (1983).

[90] V. Efimov, "Effective interaction of three resonantly interacting particles and the force range", *Phys. Rev. C* **47**, 1876 (1993).

[91] A. Comtet, P. Leboeuf and S. N. Majumdar, "Level Density of a Bose Gas and Extreme Value Statistics", *Phys. Rev. Lett.* **98**, 070404 (2007).

[92] S. Tan, "Large momentum part of fermions with large scattering length", *Ann. Phys.* **323**, 2971 (2008), arXiv :cond-mat/0508320.

[93] S. Tan, "Energetics of the a strongly correlated Fermi gas", *Ann. Phys.* **323**, 2952 (2008), arXiv :cond-mat/0505200.

[94] H. Bateman and A. Erdélyi, *Tables of integral transforms. Vol. II*, McGraw-Hill, New York (1954).

[95] D. Blume and C. H. Greene, *Phys. Rev. A* **65**, 043613 (2002).

[96] E. Tiesinga, C. J. Williams, F. H. Mies and P. S. Julienne, *Phys. Rev. A* **61**, 063416 (2002).

[97] P. Naidon, E. Tiesinga, W. Mitchell and P. Julienne, *New J. Phys.* **9**, 19 (2007), and references therein.

[98] E. Braaten, M. Kusonoki and D. Zhang, "Scattering Models for Ultracold Atoms", *Ann. Phys.* **323**, 1770 (2008).

[99] M. Jona-Lasinio and L. Pricoupenko, *in preparation* .

[100] G. Smirne, R. M. Godun, D. Cassettari, V. Boyer, C. J. Foot, T. Volz, N. Syassen, S. Dürr, G. Rempe, M. D. Lee, K. Góral and T. Köhler, "Collisional relaxation of Feshbach molecules and three-body recombination in ^{87}Rb Bose-Einstein condensates", *Phys. Rev. A* **75**, 020702 (2007).

[101] Y. Kagan, I. A. Vartan'yants and G. V. Shlyapnikov, *Zh. Eksp. Yeor. Fiz.* **81**, 1113 (1981) [*Sov. Phys. JETP* **54**, 590 (1981)] .

[102] L. P. H. de Goey, H. T. C. Stoof, B. J. Verhaar and W. Glöckle, "Role of three-body correlations in recombination of spin-polarized atomic hydrogen", *Phys. Rev. B* **38**, 646–658 (1988).

[103] H. T. C. Stoof, B. J. Verhaar, L. P. H. de Goey and W. Glöckle, "Resonances in recombination of atomic hydrogen due to long-range $H3$ molecular states", *Phys. Rev. B* **40**, 9176–9182 (1989).

[104] E. Braaten, H.-W. Hammer and M. Kusunoki, "Universal equation for Efimov states", *Phys. Rev. A* **67**, 022505 (2003).

[105] E. Braaten and H.-W. Hammer, "Enhanced dimer relaxation in an atomic and molecular Bose-Einstein condensate", *Phys. Rev. A* **70**, 042706 (2004).

[106] D. S. Petrov, C. Salomon and G. V. Shlyapnikov, "Scattering properties of weakly bound dimers of fermionic atoms", *Phys. Rev. A* **71**, 012708 (2005).

[107] Y. Kagan, B. V. Svistunov and G. V. Shlyapnikov, "Effect of Bose condensation on inelastic processes in gases", *JETP Lett.* **42**, 209 (1985).

[108] J. P. D'Incao and B. D. Esry, "Scattering Length Scaling Laws for Ultracold Three-Body Collisions", *Phys. Rev. Lett.* **94**, 213201 (2005).

[109] E. Braaten and H.-W. Hammer, "Three-Body Recombination into Deep Bound States in a Bose Gas with Large Scattering Length", *Phys. Rev. Lett.* **87**, 160407 (2001).

[110] C. Cohen-Tannoudji, J. Dupont-Roc and G. Grynberg, *Atom-Photon Interactions, C_I.3b*, Wiley, New York (1992).

[111] G. Cennini, C. Geckeler, G. Ritt and M. Weitz, "Interference of a variable number of coherent atomic sources", *Phys. Rev. A* **72**, 051601 (2005).

[112] C. Chin and P. S. Julienne, *Phys. Rev. A* **71**, 012713 (2005).

[113] B. Gao, *Phys. Rev. A* **58**, 4222 (1998).

[114] V. V. Flaumbaum, G. F. Gribakin and C. Harabati, *Phys. Rev. A* **59**, 1998 (1999).

[115] E. G. M. van Kempen, S. J. J. M. F. Kokkelmans, D. J. Heinzen and B. J. Verhaar, "Interisotope Determination of Ultracold Rubidium Interactions from Three High-Precision Experiments", *Phys. Rev. Lett.* **88**, 093201 (Feb 2002).

[116] P. J. Leo, C. J. Williams and P. S. Julienne, "Collision Properties of Ultracold $C133s$ Atoms", *Phys. Rev. Lett.* **85**, 2721–2724 (2000).

[117] B. Marcelis, B. Verhaar and S. Kokkelmans, "Total Control over Ultracold Interactions via Electric and Magnetic Fields", *Phys. Rev. Lett.* **100**, 153201 (2008).

[118] G. K. Campbell, J. Mun, M. Boyd, P. Medley, A. E. Leanhardt, L. Marcassa, D. E. Pritchard and W. Ketterle, "Imaging the Mott Insulator Shells By Using Atmoic Clock Shifts", *Science* **313**, 649 (2006).

[119] M. Köhl, K. Günter, T. Stöferle, H. Moritz and T. Esslinger, *J. Phys. B* **39**, S47 (2006).

[120] T. Müller, S. Fölling, A. Widera and I. Bloch, "State Preparation and Dynamics of Ultracold Atoms in Higher Lattice Orbitals", *Phys. Rev. Lett.* **99**, 200405 (2007).

[121] M. Anderlini, P. J. Lee, B. L. Brown, J. Sebby-Strabley, W. D. Phillips and J. V. Porto, "Controlled exchange interaction between pairs of neutral atoms in an optical lattice", *Nature* **448**, 452 (2007).

[122] G. Bruun, Y. Castin, R. Dum and K. Burnett, "BCS Theory for Trapped Ultracold Fermions", *Eur. Phys. J. D* **7**, 433 (1999).

[123] A. Sinatra and Y. Castin, *Eur. Phys. J. D* **4**, 247 (1998).

[124] S. Stringari, *in : Proceedings of the International School of Physics "Enrico Fermi" on Ultra-Cold Fermi gases, edited by M. Inguscio, W. Ketterle and C. Salomon*, SIF, Bologna (2007).

[125] A. Collin, P. Massignan and C. J. Pethick, "Energy-dependent effective interactions for dilute many-body systems", *Phys. Rev. A* **75**, 013615 (2007).

[126] A. Derevianko, J. F. Babb and A. Dalgarno, *Phys. Rev. A* **63**, 052704 (2001).

[127] E. L. Bolda, E. Tiesinga and P. S. Julienne, *Phys. Rev. A* **66**, 013403 (2002).

[128] Z. Idziaszek and T. Calarco, *Phys. Rev. A* **74**, 022712 (2006).

[129] D. Dickerscheid, U. A. Khawaja and H. S. D.van Oosten, *New J. Phys.* **8**, 151 (2006).

[130] R. B. Diener and T.-L. Ho, *Phys. Rev. Lett.* **96**, 010402 (2006).

[131] E. Arimondo, M. Inguscio and P. Violino, "Hyperfine structure in the alkali atoms", *Rev. Mod. Phys.* **49**, 31 (1977).

[132] C. Ospelkaus, *PhD Thesis*, Hamburg (2006).

[133] J. Cubizolles, *Thèse de Doctorat*, Université Paris VI (2004).

[134] E. Altman, W. Hofstetter, E. Demler and M. D. Lukin, "Phase diagram of two-component bosons on an optical lattice", *New J. Phys.* **5**, 113 (2003).

[135] S. Trotzky, P. Cheinet, S. Fölling, M. Feld, U. Schnorrberger, A. M. Rey, A. Polkovnikov, E. A. Demler, M. D. Lukin and I. Bloch, "Time-resolved Observation and Control of Superexchange Interactions with Ultracold Atoms in Optical Lattices", *Science* **319**, 295 (2008).

[136] L. D. Carr, G. V. Shlyapnikov and Y. Castin, "Achieving a BCS Transition in an Atomic Fermi Gas", *Phys. Rev. Lett.* **92**, 150404 (2004).

[137] L. Luo, B. Clancy, J. Joseph, J. Kinast and J. E. Thomas, "Measurement of the Entropy and Critical Temperature of a Strongly Interacting Fermi Gas", *Phys. Rev. Lett.* **98**, 080402 (2007).

[138] T. Gericke, F. Gerbier, A. Widera, S. Foelling, O. Mandel and I. Bloch, "Adiabatic loading of a Bose-Einstein condensate in a 3D optical lattice", *J. Mod. Opt.* **54**, 735 (2007).

[139] E. Altman, E. Demler and M. D. Lukin, "Probing many-body states of ultracold atoms via noise correlations", *Phys. Rev. A* **70**, 013603 (2004).

[140] S. Fölling, F. Gerbier, A. Widera, O. Mandel, T. Gericke and I. Bloch, "Spatial quantum noise interferometry in expanding ultracold atom clouds", *Nature* **434**, 481 (2005).

[141] T. Rom, T. Best, D. van Oosten, U. Schneider, S. Fölling, B. Paredes and I. Bloch, "Free fermion antibunching in a degenerate atomic Fermi gas released from an optical lattice", *Nature* **444**, 733 (2006).

[142] I. Carusotto, "Bragg scattering and the spin structure factor of two-component atomic gases", *J. Phys. B* **39**, S211 (2006).

[143] D. S. Petrov, M. Holzmann and G. V. Shlyapnikov, "Bose-Einstein Condensation in Quasi-2D Trapped Gases", *Phys. Rev. Lett.* **84**, 2551–2555 (2000).

[144] M. S. Makivić and H.-Q. Ding, "Two-dimensional spin-1/2 Heisenberg antierromagnet : A quantum Monte-Carlo study", *Phys. Rev. B* **43**, 3562 (1991).

[145] J.-K. Kim and M. Troyer, *Phys. Rev. Lett.* **80**, 2705 (1998).